Elucidating hepatic and pancreatic fate acquisition during early mouse development

INAUGURAL-DISSERTATION

to obtain the academic degree

Doctor rerum naturalium (Dr. rer. nat.)

submitted to the Department of Biology, Chemistry and Pharmacy

of Freie Universität Berlin

by

David Willnow

Berlin, 2018

Die vorliegende Arbeit wurde unter der Anleitung von Dr. Francesca M. Spagnoli am Max-Delbrück-Centrum für Molekulare Medizin (MDC) in Berlin-Buch von März 2016 bis Dezember 2018 angefertigt.

1. Gutachter: Dr. Francesca M. Spagnoli

2. Gutachter: Prof. Dr. Josef Köhrle

Disputation am: 02.05.2019

Selbstständigkeitserklärung

Ich erkläre gegenüber der Freien Universität Berlin, dass ich die vorliegende Dissertation selbstständig und ohne Benutzung anderer als der angegebenen Quellen und Hilfsmittel angefertigt habe.

Die vorliegende Arbeit ist frei von Plagiaten. Alle Ausführungen, die wörtlich oder inhaltlich aus anderen Schriften entnommen sind, habe ich als solche kenntlich gemacht.

Ich bestätige, dass ich meine Dissertation im Einvernehmen mit meiner Betreuerin in Teilen veröffentlicht habe.

Diese Arbeit wurde in gleicher oder ähnlicher Form noch bei keiner anderen Universität als Prüfungsleistung eingereicht.

Datum	Unterschrift

Table of contents

List of Figures

List of Tables

Summary

Liver and pancreas are derivatives of the endodermal germ layer that become specified around E8.5 in the mouse embryo. The pancreas arises from two distinct regions in the foregut, one dorsally, one ventrally located. Interestingly, the ventral pancreatic domain overlaps with the prospective hepatic endoderm and both organ rudiments develop in close proximity to one another throughout early development. Previous analyses suggested that liver and ventral pancreas arise from a common progenitor domain. However, this hypothesis had not been validated in mammalian embryos *in vivo*. In addition, the cellular and tissue dynamics defining hepatic and pancreatic lineage segregation from this presumed common progenitor domain remained elusive.

In this study, I applied complementary genetic lineage tracing approaches in mouse models to label early hepato-pancreatic progenitors and to follow their contribution to liver and pancreas *in vivo*. By employing a combination of unicolor and multicolor (Confetti) reporter systems, I traced the common origin of liver and ventral pancreas to a bipotent progenitor domain situated in the ventral foregut. In addition, I uncovered the surprising fact that ventral pancreatic cells retain the bipotent nature of these ventral foregut progenitors and contribute to the growing liver rudiment throughout early organogenesis. *In vivo* analyses of marker gene expression suggested that this progenitor population is characterized by the concurrent expression of the transcription factors Prox1, Pdx1, and Sox17. I substantiated these findings of pancreatic cell fate plasticity by detailed *in vivo* time course analyses of cell numbers and proliferation dynamics in the hepato-pancreatic organ system. Finally, I identified Robo-Slit signaling as an essential signaling pathway to maintain pancreatic identity and to prevent aberrant hepatic fate acquisition within the ventral pancreatic domain.

Taken together, by combining genetic lineage tracing and quantitative immunohistochemical analyses in genetic mouse models *in vivo*, I uncovered that ventral pancreatic cells display a hitherto unappreciated level of cell fate plasticity fundamental for proper development of ventral foregut derivatives.

Keywords: pancreas, liver, development, plasticity, lineage tracing, organogenesis

Zusammenfassung

Leber und Pankreas sind Derivate des endodermalen Keimblattes, die im Maus-Embryo zum Embryonalstadium (E) 8.5 spezifiziert werden. Der Pankreas entwickelt sich aus zwei unterschiedlichen Regionen im dorsalen und ventralen Vorderdarm. Interessanterweise überlappt die Domäne des ventralen Pankreas mit der des zukünftigen hepatischen Endoderms und beide Organanlagen entwickeln sich während ihrer frühen Ontogenese in unmittelbarer räumlicher Nähe zueinander. Frühere Studien gaben zu der Vermutung Anlass, dass Leber und Pankreas aus einer gemeinsamen Vorläuferzelldomäne hervorgehen. Allerdings wurde diese Hypothese nie durch *in vivo* Studien in Säugerembryonen belegt. Darüber hinaus gab es bisher auch keinerlei Erkenntnisse über die Dynamik zellulärer und gewebsspezifischer Prozesse, welche einer Aufspaltung pankreatischer und hepatischer Zellpopulationen aus einer mutmaßlichen gemeinsamen Vorläuferpopulation zu Grunde liegen könnten.

In der vorliegenden Arbeit habe ich verschiedene Ansätze zur Verfolgung der genetischen Abstammung (engl., genetic lineage tracing) hepato-pankreatischer Vorläuferzellen in Mausembryonen eingesetzt, um deren Beitrag zur Entwicklung der Organanlagen von Leber und Pankreas *in vivo* aufzuklären. Durch die Kombination einzel- und mehrfarbiger (Confetti) Reportersysteme gelang es mir, den gemeinsamen Ursprung von Leber und ventralem Pankreas tatsächlich auf eine bipotente Vorläuferzelldomäne im ventralen Vorderdarm zurückzuführen. Darüber hinaus kamen meine Studien zu dem überraschenden Ergebnis, dass Zellen des ventralen Pankreas die bipotenten Eigenschaften dieser Vorläuferzelldomäne beibehalten und dadurch befähigt sind, während der frühen Organogenese kontinuierlich zur wachsenden Leberanlage beizutragen. Weitere *in vivo* Analysen des Expressionsmusters bekannter Marker-Gene legten nahe, dass diese Vorläuferzellpopulation durch die gleichzeitige Expression der Transkriptionsfaktoren Prox1, Pdx1 und Sox17 charakterisiert ist. Meine Hypothese einer andauernden Plastizität der Zellen des ventralen Pankreas konnte ich durch detaillierte Analysen von Zellzahl und Proliferationsdynamik des hepato-pankreatischen Organsystems zu verschiedenen Zeitpunkten der Embryogenese bestätigen. Schließlich konnte ich auch noch die essentielle Bedeutung des Robo-Slit Signalweges für die

Aufrechterhaltung einer pankreatischen und die Verhinderung einer fehlerhaften hepatischen Zellidentität im ventralen Pankreas identifizieren.

Zusammengefasst haben meine Arbeiten gezeigt, dass Zellen des ventralen Pankreas eine bisher nicht gekannte und lang andauernde Plastizität für pankreatische und hepatische Differenzierung besitzen und dass diese Plastizität von zentraler Bedeutung für die Entwicklung der Organsysteme aus dem ventralen Vorderdarm ist.

Stichworte: Pankreas, Leber, Entwicklung, Plastizität, Abstammungsstudien, Organogenese

1. Introduction

Developmental biology encompasses the investigation of processes governing morphogenesis, growth, and differentiation of cells, tissues, and entire organisms. In the past, developmental biology has fundamentally shaped our understanding of basic concepts in molecular biology, genetics, physiology, and evolutionary biology. Recently, developmental biology also gained increasing importance in the context of biomedical research, especially for stem cell research and the development of cell-based therapies[1]. Advances in developmental biology provide insights into the developmental origin, gene expression profiles, and signaling pathways of a tissue or organ of interest. This knowledge provides us with the tools to reenact the development of tissues or organs *in vitro* and to implement regenerative therapies for treatment of degenerative diseases in patients[2,3].

Amongst the diseases showing promising approaches for regenerative therapies are those affecting the liver and pancreas[4], including chronic hepatitis and diabetes. A profound knowledge of processes governing hepatic and pancreatic development will greatly aid in the further improvement of cell-based therapies for these diseases. A unique aspect of liver and pancreas development is that both tissues share a developmental origin as they arise from a common progenitor domain[5–9]. This situation offers the exciting possibility of employing patient liver cells to be transdifferentiated into β-cells for the treatment of diabetes through cell-replacement therapy[4,10]. Although initial evidence for a bipotent hepato-pancreatic progenitor domain was suggested more than a decade ago[5,7,8], our precise knowledge about the nature of this cell population in mammals and the processes governing the segregation of hepatic and pancreatic fates remain elusive. Elucidating the dynamics of this divergent differentiation was the overall aim of my thesis project.

1.1 Physiology of liver and pancreas in health and disease

Liver and pancreas serve as essential regulators of systemic metabolism[11–14]. Millions of patients worldwide suffer from diseases affecting these organs, which are often life threatening and represent huge socio-economic burdens. In the following chapter, I will give a brief overview of the physiological relevance of liver and pancreas. I will describe the main diseases affecting these organs and introduce current approaches towards cell-based regenerative therapies for them.

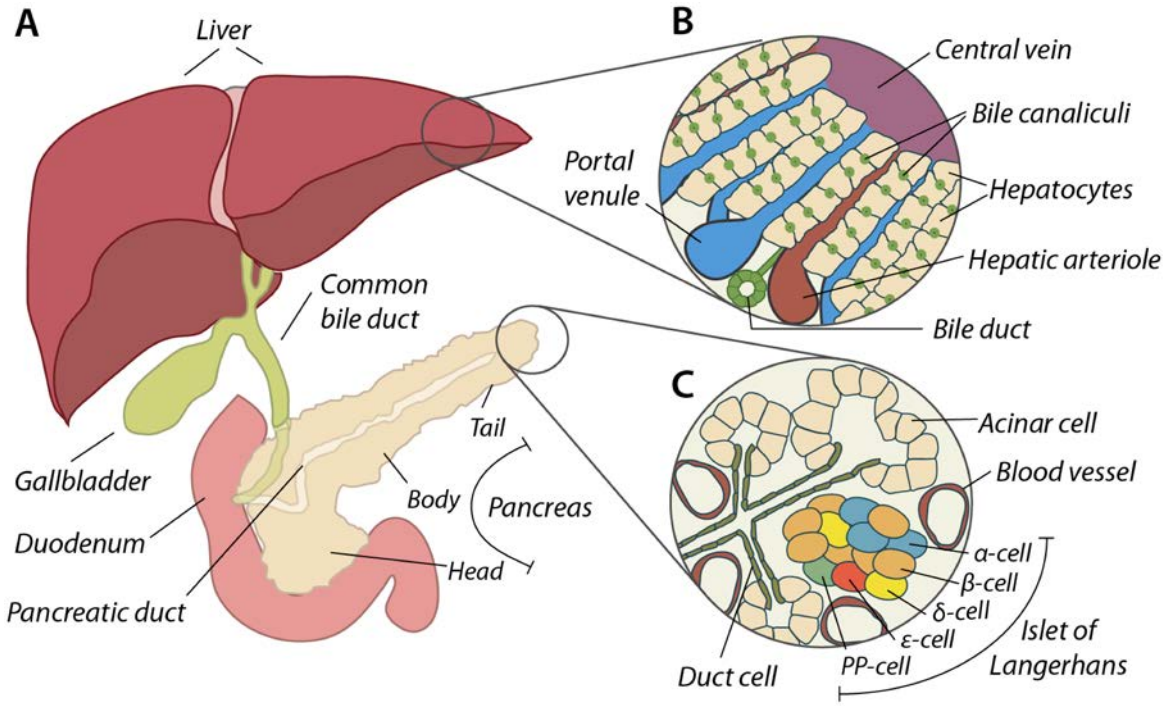

Fig. 1: Morphology of the adult liver and pancreas. (A) Representation of the adult human liver and pancreas. The liver is connected via the biliary ducts to the gallbladder and via the common bile duct to the duodenum. The human pancreas is morphologically divided into head, body and tail, and connected to the duodenum via the pancreatic duct. **(B)** Schematic representation of the liver histology. The functional cells of the liver are the hepatocytes located in a network of arteries (hepatic arterioles), veins (central vein and portal venules), bile ducts, and bile canaliculi. **(C)** Schematic representation of the pancreas histology. The exocrine pancreas is divided into the functional exocrine cells (acinar cells), which produce and secrete digestive enzymes, and the ductal cells, which form a tubular network for the transport of secreted digestive enzymes to the duodenum. The endocrine pancreatic cells are organized into the well-vascularized islets of Langerhans, which consist of cells of multiple endocrine lineages including α-cells, β-cells, δ-cells, ε-cells, and pancreatic-polypeptide (PP) cells. (partially adapted from Edlund, 2002[1])

The adult human liver is a well vascularized organ that receives blood via the hepatic portal vein and hepatic arteries[11,15–17]. Hepatocytes, the main functional cell type of the liver, lie in between these blood vessels (Figs. 1A, 1B, 2A, 2B)[11,15,18]. Hepatocytes contribute to a wide

range of essential metabolic functions, such as nutrient processing, maintenance of blood metabolite and protein concentrations, as well as life-saving detoxification processes[19]. During embryonic development the liver is also the primary site of hematopoiesis[19–21]. Hepatocytes are intermingled with a dense network of bile ducts that transport hepatocyte-produced bile acid to the gallbladder for storage[18,22,23]. Bile acid is needed for lipid digestion and discharged from the gallbladder into the duodenum via the common bile duct (Figs. 1A, 1B, 2B)[18,23].

The adult pancreas is a gland composed of exocrine and endocrine tissues with divergent metabolic functions[1,12]. The exocrine pancreas is organized as a branched ductal system with clusters of exocrine cells, also called acini, at the ducts' ends (Fig. 1C)[24]. The functional exocrine cells, termed acinar cells (Fig. 2A, C, D), produce and secrete digestive enzymes, such as trypsin and chymotrypsin[25]. These digestive enzymes are stored in granules and released as zymogens into the pancreatic ducts for transport to the duodenum[25]. The endocrine pancreas is organized in functional cell clusters called islets of Langerhans that are intermingled with the exocrine-ductal system (Figs. 1C, 2C, 2D)[13,24]. Islets are well vascularized to allow efficient distribution of pancreatic hormones into the bloodstream[26]. Each islet contains multiple endocrine cell types[1,13,26], mainly the glucagon-expressing α-cells[27,28], the insulin-producing β-cells[27,28], the somatostatin-producing δ-cells[27,28], and the pancreatic polypeptide-producing PP-cells[29] (Fig. 2A, C, D). Minor islet cell types include the ghrelin-producing ε-cells[30]. The pancreatic hormones produced by islet cells can be generalized as essential regulators of metabolism and homeostasis[26]. The most abundant and disease-relevant pancreatic hormones are glucagon and insulin that control blood glucose levels[13]. Glucagon increases blood glucose levels, for example by promoting hepatic glycogenolysis and gluconeogenesis[31]. By contrast, insulin decreases blood glucose levels by promoting hepatic glycogenesis and glucose uptake in muscle and adipose tissue[26,32].

Among the most common diseases affecting the hepato-pancreatic system are chronic liver disease and diabetes mellitus[4]. Chronic liver disease is a condition characterized by the continuous deterioration of liver function[33], accounting for more than 40,000 deaths in 2016 in the US alone[34]. Chronic liver disease can be the result of excessive alcohol consumption[33,35] or infections with hepatitis B or hepatitis C viruses[36]. Diabetes mellitus (DM) is the clinical

term for a group of metabolic disorders with different etiology that feature pathologically elevated glucose levels due to the inability of the body to regulate blood-glucose homeostasis[37,38]. As of 2017, diabetes affects more than 400 million people worldwide and accounts for approximately 4 million deaths in 2017[39]. The most frequent forms of DM are type I (10% of cases) and type II DM (90% of cases)[2,37]. Type I DM is caused by an autoimmune

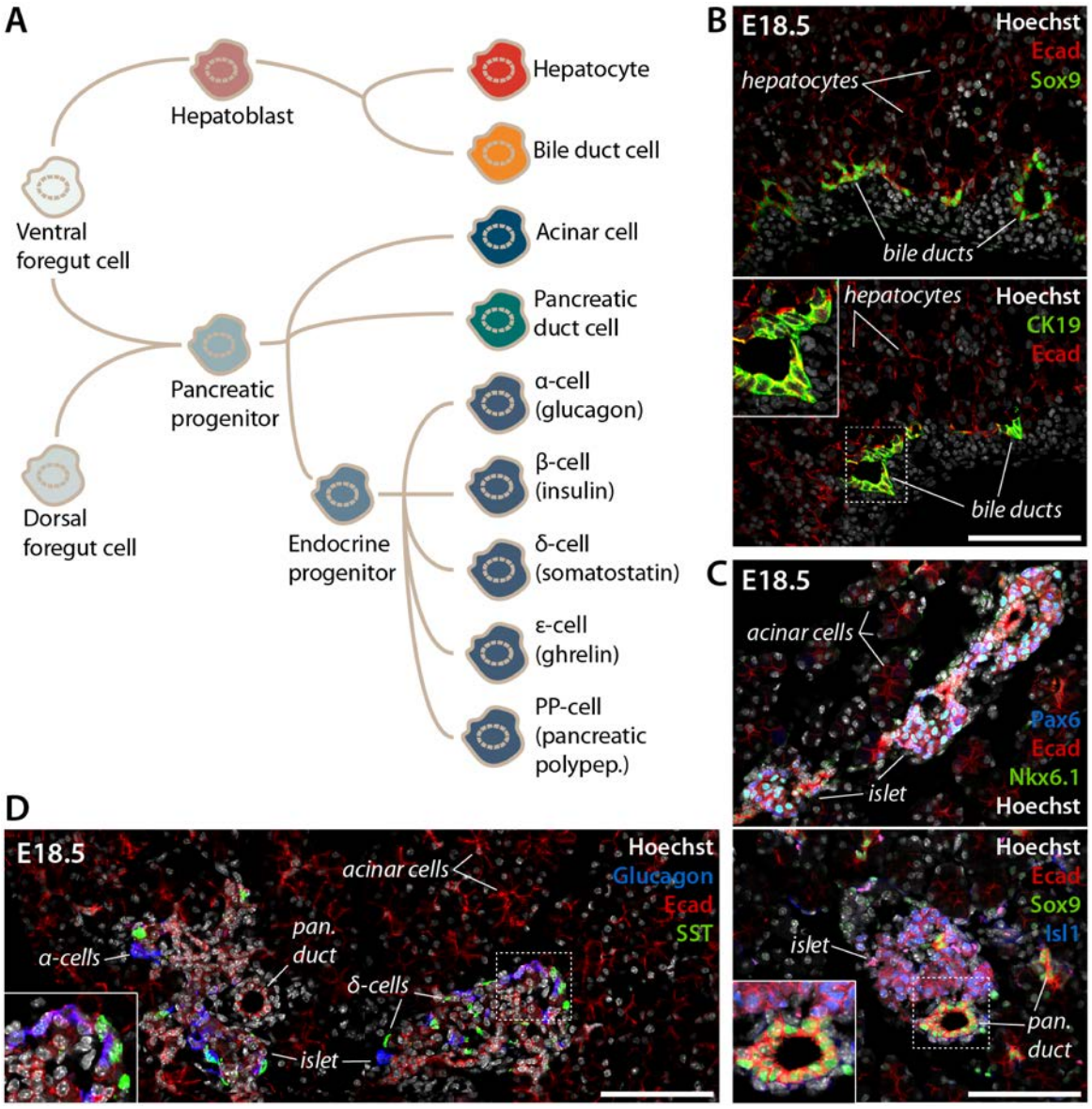

Fig. 2: Hepato-pancreatic cell lineages. (A) Schematic representation of the hepato-pancreatic cell lineages during differentiation. **(B-D)** Representative IF stainings of cryosections of E18.5 embryos. Immunostaining for Ecad (red) marks all hepatic (B) and pancreatic cells (C, D). Immunostaining for Sox9 (green) marks bile duct cells (upper panel in B) and pancreatic duct cells (lower panel in C). Bile duct cells are also marked by immunostaining for cytokeratin 19 (CK19). (C) Immunostaining for Pax6 (blue, upper panel), islet-1 (Isl1) (blue, lower panel), and Nkx6.1 (green, upper panel) marks endocrine cells organized in islets of Langerhans. (D) Immunostaining for glucagon (blue) and somatostatin (SST, green) marks α-cells and δ-cells within islets of Langerhans. Insets shows higher magnifications of the boxed area (dotted line) in the respective overview image. Tissues are counterstained with Hoechst dye (grayscale). (scale bars: 100μm)

destruction of pancreatic β-cells, leading to an inability to produce insulin[40]. Type II DM primarily affects people suffering from obesity and involves a combination of insulin resistance and relative insulin deficiency[41]. Apart from these two main types of diabetes, there also exist rare cases of monogenetic diabetes[42]. This form of DM is usually caused by familial or spontaneous mutations in genes essential for the development of the pancreas in general or for pancreatic β-cells in particular[43,44].

Despite their close embryonic origin, liver and pancreas differ profoundly in their regenerative capacities. The liver can offset massive cell loss through regeneration both in the embryo and in the adult[4,11,35,45,46]. By contrast, the pancreas mass is determined by the size of the embryonic progenitor cell pool[47,48]. Consequently, loss of pancreatic progenitors during development leads to substantial organ size reduction in adults[47,48]. The lack of regenerative abilities in pancreatic progenitors persists after birth, as the pancreas shows limited tissue regeneration following injury or disease[1,4,49,50]. Therefore, the demand for cell-based regenerative therapies is especially high for degenerative diseases of the pancreas. Conceptually, such regenerative therapies aim at the *in vitro* generation of destroyed or dysfunctional cell types or tissues, and their subsequent transplantation into patients[1,3,4,51]. Obviously, this procedure requires a profound knowledge of the cellular differentiation processes underlying normal embryonic development of the cells or tissues in question. Considerable progress has been achieved in the *in vitro* generation of β-cells, with promising approaches involving either differentiation of human embryonic stem cells (hESCs)[52,53] or patient-derived induced pluripotent stem cells (iPSCs)[54]. An elegant alternative to the use of pluripotent stem cells is the use of patient-derived liver cells and their subsequent transdifferentiation into the pancreatic lineage[10,55]. However, no safe and reliable protocols for the either approach have been established so far. The lack of such a protocol calls for more detailed investigation of the developmental biology of liver and pancreas. Of special interest would be the dissection of the cellular and molecular mechanisms of hepato-pancreatic lineage segregation, as it would provide us with the knowledge of how to reverse such lineage decisions *in vitro*.

1.2 Embryonic development of liver and pancreas

Liver and pancreas are derivatives of the endoderm, one of the three primary germ layers (ectoderm, endoderm, mesoderm) formed during development that give rise to all tissues of the mammalian organism[56–58]. During early development the endoderm becomes patterned along the anterior-posterior axis (A-P-axis) into fore-, mid-, and hindgut, each of which harbors distinct organ domains (Fig. 3)[59]. The vertebrate foregut gives rise to a multitude of organs and tissues, including thyroid, esophagus, lung, stomach, liver, pancreas, and the biliary system[56]. The midgut will differentiate into the small intestine, while the hindgut forms the colon[56]. The following chapter details the formation of the endoderm and the subsequent specification and organogenesis of pancreas and liver in the mouse embryo.

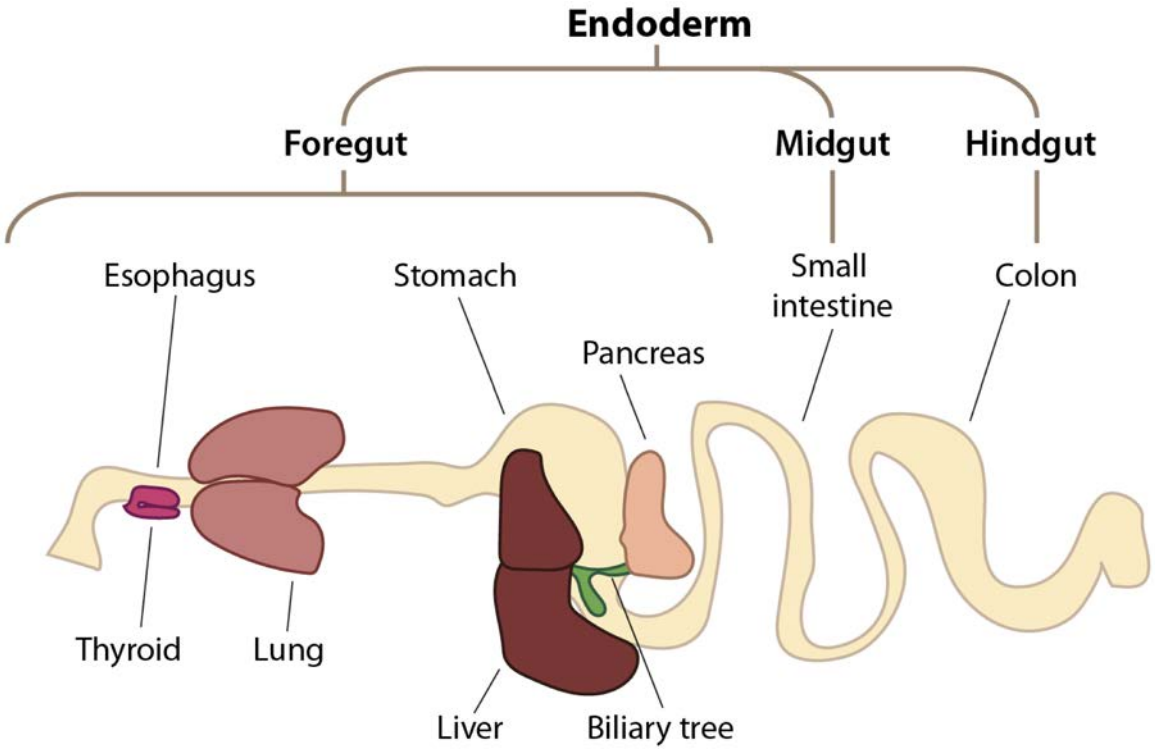

Fig. 3: The endoderm and its derivatives. Representation of vertebrate organs of endodermal origin. During development the emerging endodermal germ layer gets patterned into fore-, mid-, and hindgut. The foregut gives rise to esophagus, thyroid, lung, stomach, liver, biliary system, and pancreas. The small intestine is a derivative of the midgut, while the colon originates from hindgut cells. (adapted from Zorn and Wells, 2009[56])

1.2.1 Gastrulation and endoderm patterning

Following fertilization, the mouse zygote undergoes cleavage, i.e. a series of rapid cell divisions that ends with the formation of the blastocyst[57,60]. The blastocyst consists of a spherical sheet of trophoblast cells, which give rise to extra-embryonic structures, and the inner cell mass (ICM), a population of pluripotent cells forming all tissues of the developing organism[61–63]. Eventually, the ICM differentiates into two distinct cell layers, the epiblast (upper layer) and the hypoblast (lower layer)[60]. The hypoblast contributes to the formation of extra-embryonic endoderm, also termed visceral endoderm, while the epiblast gives rise to all embryonic tissues as well as extra-embryonic ecto- and mesoderm[60].

The next step in ontogeny is the conversion of the epiblast, in essence a single-layered epithelium, into the three primary germ layers, namely the ectoderm, the endoderm, and the mesoderm[57,58]. This process is called gastrulation and occurs between embryonic day (E) 6.5 and E7.75 in the mouse[64]. Gastrulation begins with the formation of the primitive streak (PS) at the posterior end of the epiblast[58]. While the PS progresses anteriorly, some epiblast cells ingress and migrate through the PS, forming the prospective mesoderm and the definitive endoderm (DE) (Fig. 4A-C)[58]. In contrast, epiblast cells not passing through the PS form the embryonic ectoderm (Fig. 4A, B). Cells destined to become endoderm ingress together with mesodermal progenitors through the anterior region of the PS (Fig. 4B, D)[58]. A gradient of Nodal, a signaling factor of the Transforming Growth Factor β (TGFβ) superfamily, is responsible for differential lineage commitment to mesodermal or endodermal cell fate (Fig. 4B)[65–68]. High Nodal signaling promotes expression of genes required for establishing and maintaining endodermal fate[65,69]. Among these factors are the transcription factors (TFs) Eomesodermin (Eomes)[70,71], Forkhead box protein A2 (Foxa2)[72], Sex-determining region Y-box 17 (Sox17)[69,73–76], and members of the GATA[77] and Mix-like homeodomain proteins[78–80] (Fig. 4B-D). Contrary to high Nodal activity, low Nodal signaling cues lead to the expression of Fibroblast Growth Factors (FGFs) and the TF Brachyury (Brachy) that promote mesodermal fate[81–83]. Endodermal progenitors insert into the visceral endodermal epithelium, creating a layer of embryonic endoderm, termed the definitive endoderm (DE)[60,84]. The mesodermal

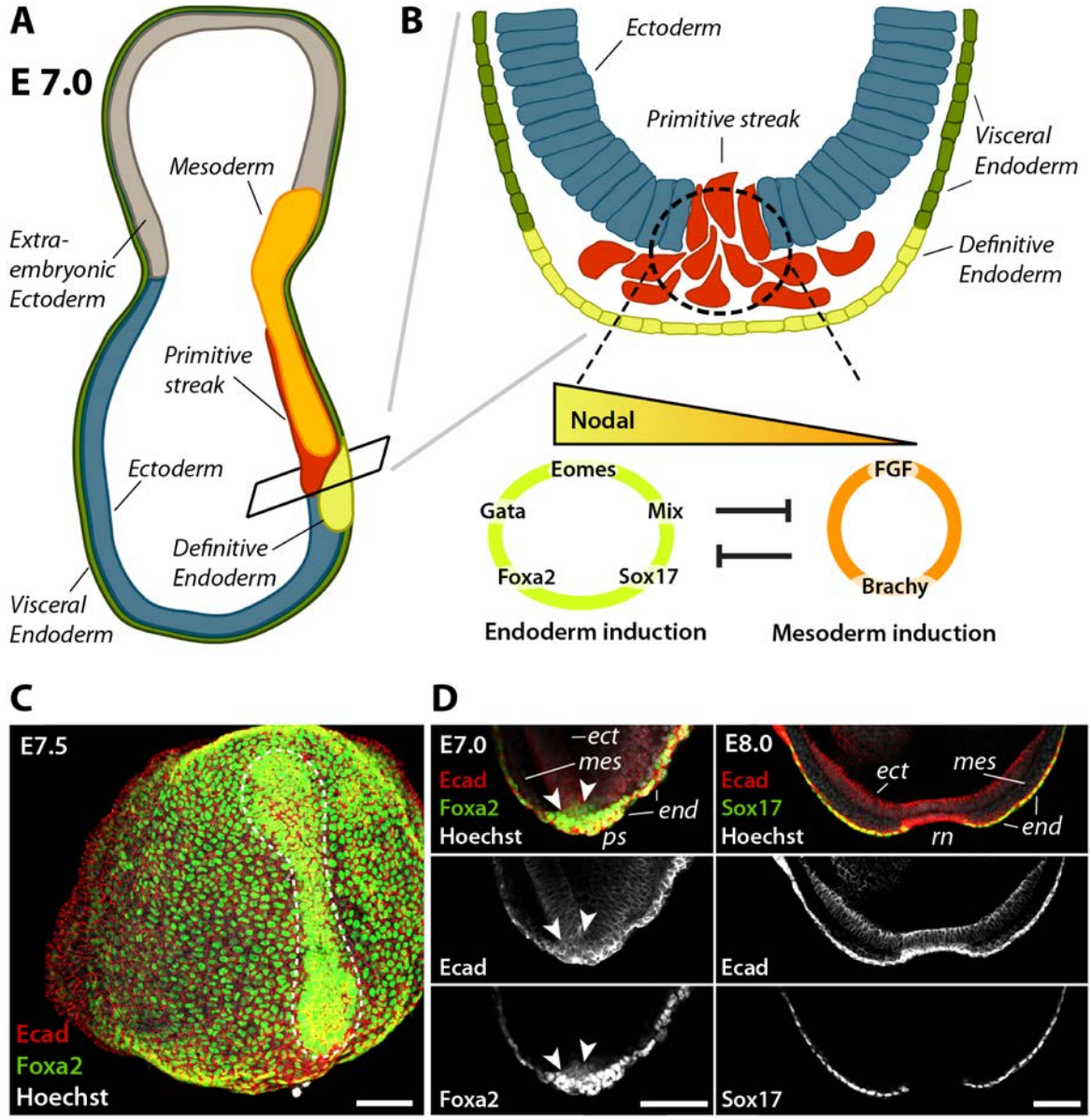

Fig. 4: Gastrulation and endoderm formation. (A) Sagittal view of a mouse embryo during gastrulation (around embryonic day (E) 7.0). The embryonic tissue is surrounded by extra-embryonic ectoderm and visceral endoderm. Through action of the primitive streak, the embryonic tissue separates into the three germ layers ectoderm, endoderm, and mesoderm. **(B)** Cross section through the mid-gastrulation mouse embryo (plane of view indicated in panel A). Certain epiblast cells (red) undergo epithelial-to-mesenchymal transition and migrate though the primitive streak. Depending on the Nodal concentration, they are exposed to, endodermal (high Nodal) or mesodermal (low Nodal) differentiation is induced. Transcription factors and growth factors important for mesoderm or endoderm induction are indicated. (partially adapted from Zorn and Wells, 2009[56]) **(C)** Representative wholemount immunofluorescence staining (WMIF) of an E7.5 embryo during gastrulation. Immunostaining for Ecad (red) marks epithelial cells while immunostaining for Foxa2 (green) marks the endoderm and the primitive streak, including the node (dotted line). Tissues are counterstained with Hoechst dye (grayscale). **(D)** Optical sections of representative WMIF of an embryo during (left panels) and after (right panels) gastrulation. Immunostaining for Ecad (red) marks epithelial cells. Immunostaining for Foxa2 or Sox17 (green) marks the endoderm. Tissues are counterstained with Hoechst dye (grayscale). The left panel shows cells migrating through the primitive streak (*ps*) (see arrowheads). The right panel shows a post-gastrulation embryo consisting of the three germ layers ectoderm (*ect*), mesoderm (*mes*), and endoderm (*end*). The $Sox17^{-}$ region within the endoderm represents the remnant of the node (*rn*). Images are given as merged color or as single channel grayscale configuration. (scale bars 100μm)

progenitors establish a mesenchymal cell layer between embryonic ectoderm and definitive endoderm (Fig. 4A, B, D)[58].

Within 48 hours following the establishment of the three primary germ layers, the endoderm forms the primitive gut tube[7,56,59,85,86]. Starting at around E8.0, the definitive endoderm in the anterior region of the embryo folds over and creates the foregut pocket (Fig. 5). Shortly after, an analogous structure will form at the posterior end of the embryo, the so-called hindgut pocket. The openings of foregut and hindgut pockets are termed anterior intestinal portal (AIP) and posterior intestinal portal (PIP), respectively[85]. While the endoderm continues to fold into the primitive gut tube, the AIP moves posteriorly and the PIP moves anteriorly, eventually fusing upon completion of the gut tube structure (around E9.5)[56].

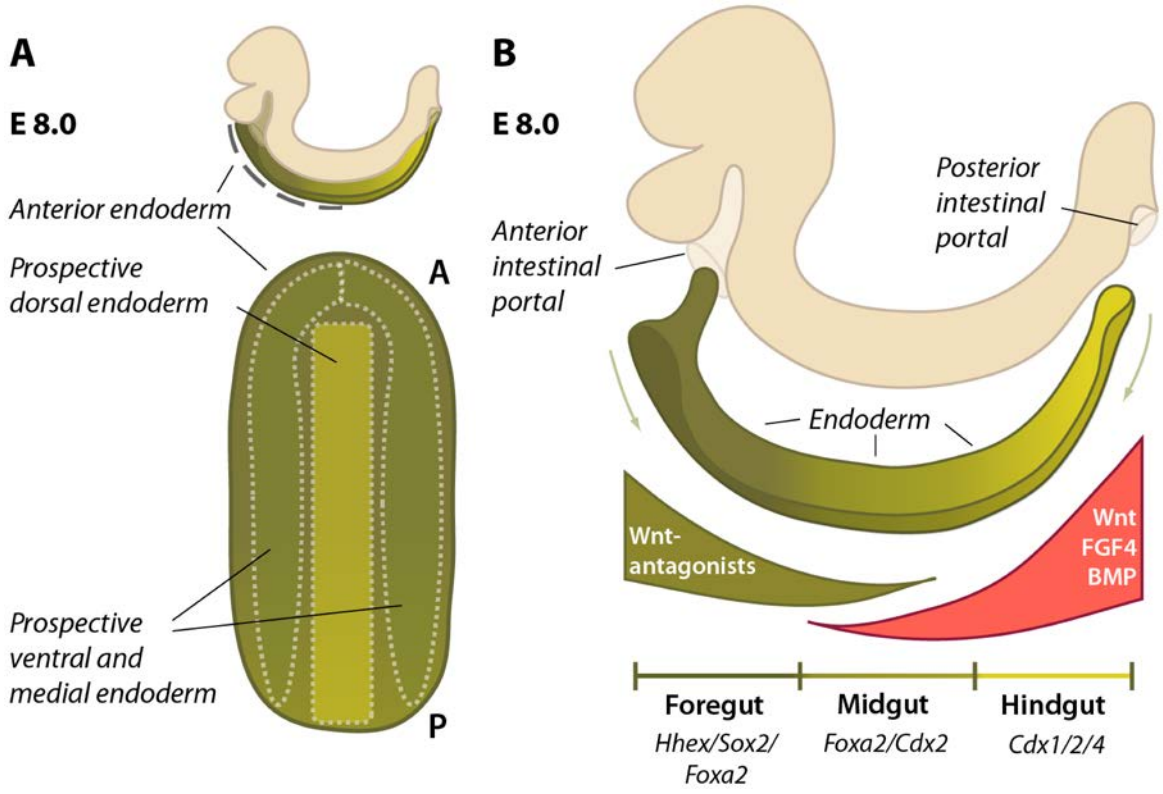

Fig. 5: Endoderm patterning. (A) Schematic representation of dorso-ventral patterning of the endoderm during early gut tube formation (around E8.0). During gut tube formation, an epithelial sheet of endodermal cells folds to form the primitive gut tube. Cells in the midline of the sheet will contribute to the dorsal gut tube while anterior-most and lateral cells will contribute jointly to the ventral and medial gut tube. **(B)** Schematic representation of anterior-posterior patterning of the endoderm during early gut tube formation (around E8.0). Endodermal cells are broadly patterned into foregut, midgut, and hindgut by factors secreted by the mesoderm (Wnt, FGF4, BMP) and anterior endoderm (Wnt antagonists). Consequently, they start to express the indicated foregut, midgut, or hindgut specific markers.

Throughout the process of gut tube morphogenesis, the endoderm is being patterned (or regionalized) in an anterior-posterior (A-P) and dorso-ventral (D-V) direction[87]. The D-V patterning of the endoderm is predetermined by morphological changes that lead to gut tube formation[7,59,86]. As the flat sheet of cells constituting the endoderm after gastrulation folds over, the midline endodermal cells remain in place and become the dorsal cells of the gut tube (Fig. 5A). However, anterior-most and lateral endodermal cells ultimately contribute to the ventral and medial endoderm of the gut tube (Fig. 5A)[7]. Concurrently, the forming gut tube is patterned along its A-P axis into fore-, mid-, and hindgut by signals originating from adjacent mesodermal tissues and the endoderm itself (Fig. 5B)[56,59,72,88–91]. Mesoderm-derived factors, such as retinoic acid (RA)[92–95], FGF4[96,97], ligands of the Wingless-related integration site family (Wnt)[98,99], and Bone Morphogenetic Proteins[100,101] (BMPs) provide signals to induce mid- and hindgut identity in the gut tube. The posteriorizing effect of Wnt ligands is limited to the prospective hindgut by the expression of soluble Wnt antagonists in the anterior endoderm[102]. Through the inhibition of Wnt signaling in the anterior endoderm, the expression of the foregut markers Hematopoietically expressed homeobox[103–105] (Hhex), Sox2, and Foxa2[72,74,79] is induced. The foregut will give rise to gastrointestinal structures, like the esophagus and stomach as well as to many endoderm-derived organs such as lung, liver, pancreas, and thyroid[56].

1.2.2 Organ fate specification

As a result of instructive signaling cues from endo- and mesodermal tissues, endodermal cells acquired positional information[56,59,106]. Upon conclusion of the broad regionalization of the endoderm, specific populations of endodermal cells gained competence to respond to diverse specification signals[87,107,108]. In development, the term ‘competence’ refers to the ability of cells or tissues to appropriately respond to specific inductive cues to which they are exposed. However, definitive commitment to specific endodermal lineages is not yet achieved at E8.0 and endodermal cells retain a certain degree of fate plasticity[108–110]. Additional inductive signaling cues from the surrounding mesoderm during the early somite stages (around E8.25-8.5) are required for further lineage commitment of endodermal regions, thus specifying the future organ domains.

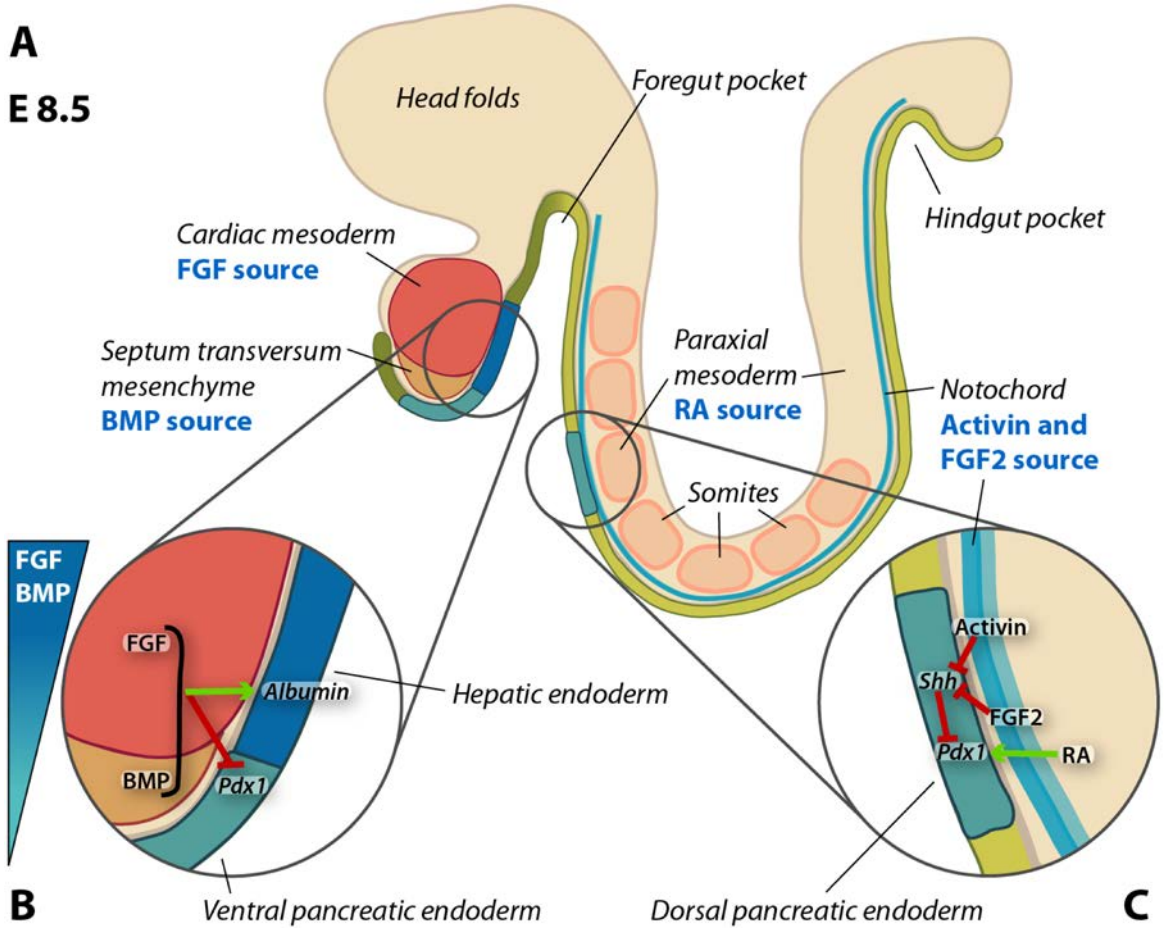

Fig. 6: Specification of hepatic and pancreatic organ domains. (A) Sagittal view of a mouse embryo at E8.5. The ventral (dark green) and dorsal endoderm (light green) receive inductive signals from neighboring mesodermal tissues (septum transversum mesenchyme (STM), cardiac mesoderm, paraxial mesoderm, notochord). The factors secreted by the respective tissues are indicated. As a result, future organ domains are specified within the endoderm (e.g., liver, ventral, and dorsal pancreas). **(B)** Schematic overview of the specification of hepatic and ventral pancreatic endoderm. A concentration gradient of fibroblast growth factors (FGFs) secreted from the cardiac mesoderm and bone morphogenetic proteins (BMPs) produced by the STM specify hepatic and ventral pancreatic endoderm by promoting hepatic and inhibiting pancreatic fate. Consequently, specified organ domains express hepatic (*albumin*) or pancreatic markers (*Pdx1*). **(C)** Schematic overview of the specification of the dorsal pancreatic endoderm. Activin and FGF2 secreted by the notochord repress expression of sonic hedgehog (*Shh*) in the presumptive dorsal pancreatic endoderm allowing for expression of *Pdx1*. *Pdx1* expression is further promoted by retinoic acid (RA) from the paraxial mesoderm. (partially adapted from Zaret and Grompe, 2008[4])

Fig. 6A shows an overview of the mouse embryo at E8.5, the time point of organ fate specification. The AIP and PIP have formed and start to move towards the midgut region. At this stage, the prospective hepatic endoderm lies in close proximity to the cardiac mesoderm and the septum transversum mesenchyme (STM)[7,56,111]. In contrast to the liver, the future pancreas will develop from two distinct domains, one situated in the dorsal foregut endoderm and the other posterior to the hepatic organ domain in the ventral foregut endoderm (Fig. 6A)[8,24,27,112,113]. While the hepatic endoderm forms a single bud giving rise to the liver, the

future pancreas is formed by a fusion of the dorsal and ventral pancreatic buds at late developmental stages[24,27]. At E8.5, the ventral pancreas is positioned next to the STM and cardiac mesoderm[7,8,113]. The dorsal pancreatic endoderm is in direct contact with the notochord and close to the paraxial mesoderm, which includes somitic and pre-somitic mesoderm[27,90,93].

Due to their separate positions in the dorsal and ventral foregut, the two pancreatic organ rudiments are exposed to quite distinct tissue and signaling contexts during development[1,13,27]. This is a remarkable feature, as organ induction and early organogenesis usually require a highly specific combination of factors to proceed. However, the two emerging pancreatic rudiments are subject to dissimilar instructive signals by different tissues that still instruct the same genetic program for pancreatic development[13,27]. Although dorsal and ventral buds contribute to distinct parts of the adult pancreas to a certain extent, adult tissue composition reveals only minor differences distinguishing pancreatic tissues originating from the ventral or dorsal organ rudiment[13]. For instance, in humans, pancreatic polypeptide (PP) expressing endocrine cells can only be found in tissues derived from the dorsal pancreas[114].

The dorsal pancreatic organ domain becomes specified upon exposure to Activin, a member of the TGFβ superfamily, and FGF2 signals originating from the notochord[115–117] as well as by RA from the paraxial mesoderm[92–94,118–120] (Fig. 6C). At the site of the prospective dorsal pancreatic endoderm, the notochord is in direct contact with the endodermal epithelium. Thus, the notochord-derived signaling factors Activin and FGF2 both signal to the endoderm and repress expression of Sonic hedgehog (*Shh*)[115–117]. Consequently, autocrine SHH signaling is inhibited in this part of the endoderm. Together with RA signaling from the paraxial mesoderm, absence of SHH activity leads to the induction of Pancreatic duodenal homeobox 1 (*Pdx1*) expression, specifying the dorsal pancreatic organ domain.

The ventral foregut endoderm, that includes the prospective hepatic and ventral pancreatic organ domains, receives two major signaling cues from neighboring mesodermal tissues, namely FGFs from the cardiac mesoderm[5,111,121,122] and BMPs from the STM[6,9,123] (Fig. 6B). Experiments with endodermal explants showed that the default program for the ventral foregut is pancreatic fate specification[5]. FGFs and BMPs prevent this fate by acting as activators of the hepatic program and by repressing pancreatic specification[5,6,111,124]. However, it is still not completely understood how exactly FGF and BMP signaling is controlled *in vivo*. Most likely, the proximity to the mesodermal sources of these signaling factors as well as the duration of their actions are major determinants in the acquisition of either hepatic or pancreatic fate[13,56,125]. In response to high or low FGF and BMP signals, the ventral foregut endoderm starts to express hepatic (*albumin*) or pancreatic (*Pdx1*) markers, respectively[5,6,122]. One of the earliest common markers of the hepatic and pancreatic endoderm is the

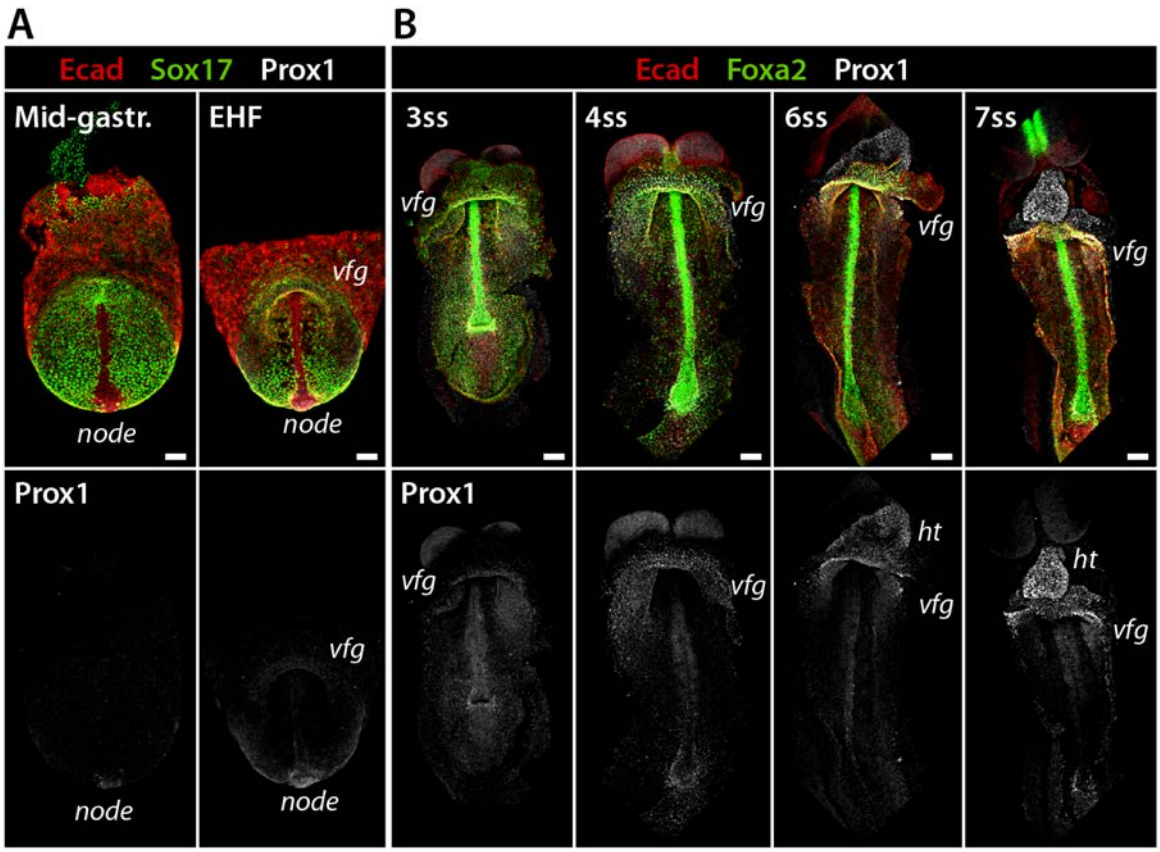

Fig. 7: Prox1 marks hepato-pancreatic progenitors in the ventral foregut during early development. (A, B) Representative WMIF stainings of E7.5-8.5 embryos (mid-gastrulation-7ss). Immunostaining for Ecad (red) marks the endodermal and ectodermal epithelium, whereas immunostaining for Sox17 (green, A) or for Foxa2 (green, B) marks endodermal cells. Immunostaining for Prox1 (grayscale) marks the ventral foregut (*vfg*), a region harbouring hepato-pancreatic progenitors. From 6ss onwards, Prox1 is also expressed in the heart (*ht*). EHF, early head fold stage (scale bars: 100μm)

homeodomain transcription factor Prospero homeobox 1 (Prox1)[126]. Prox1 is specifically expressed in endodermal tissues destined to become hepatic and pancreatic endoderm from E8.0 onwards (Fig. 7). Its expression continues in hepatic and pancreatic cells until late developmental stages (Figs. 8-11). Its role during early specification and differentiation of liver and pancreatic progenitors (E8.0-9.0) is incompletely understood. To date, Prox1 has ascribed roles during hepatic morphogenesis[127] and in pancreatic cell differentiation, especially in the emergence of pancreatic endocrine cells around E13.5[128].

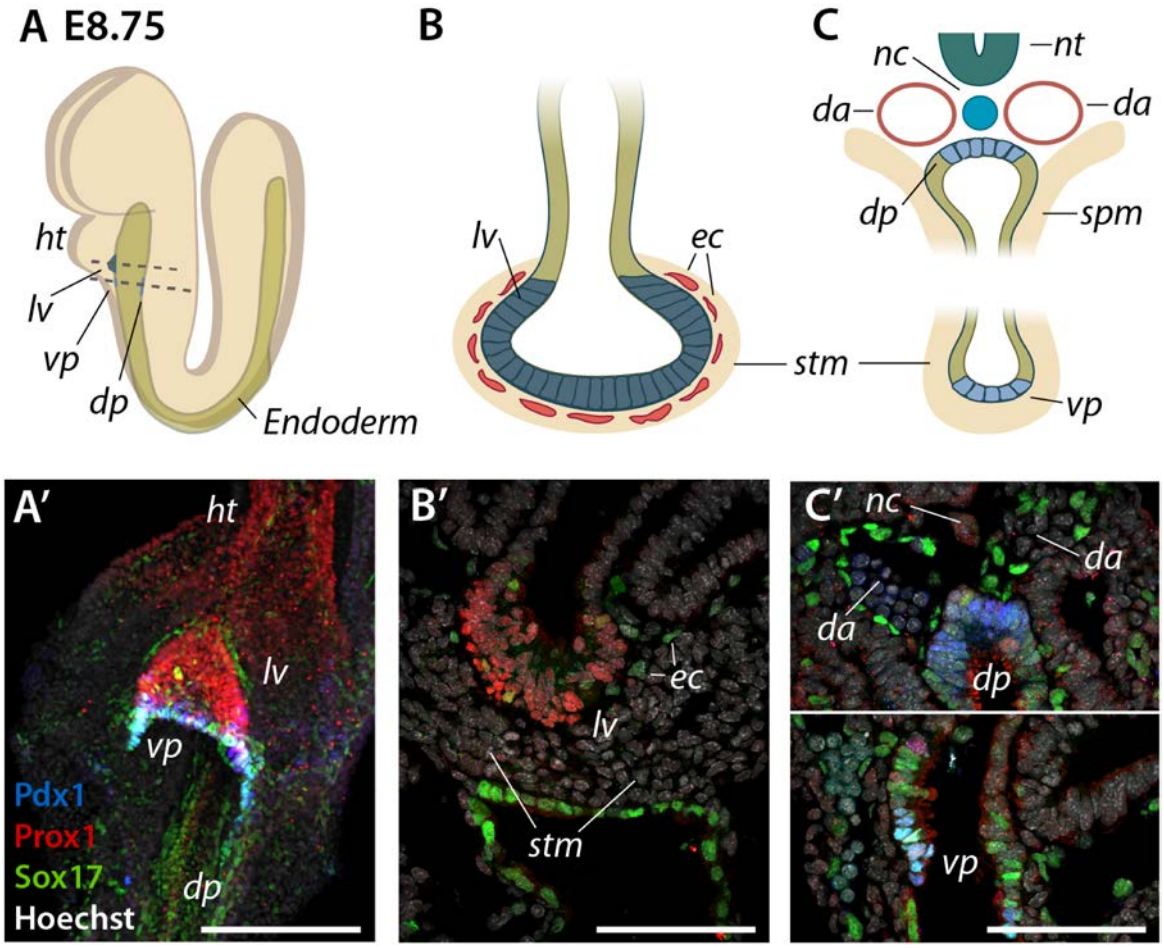

Fig. 8: Organogenesis of liver and pancreas at E8.75. (A) Representation of a mouse embryo at E8.75. The positions of the endoderm (green) and the developing hepatic (dark blue) and pancreatic buds (light blue) are indicated. **(B)** Transverse section through the developing liver at E8.75 (plane of view indicated by dotted line in panel A). **(C)** Transverse section through the developing pancreas at E8.75 (plane of view indicated by dotted line in panel A). **(A', B', C')** Representative immunofluorescence (IF) staining of an E8.75 embryo either in wholemount (A') or on cryosections (B', C'). Staining for Prox1 (red) marks all hepato-pancreatic tissues, staining for Pdx1 (blue) marks ventral and dorsal pancreatic buds, and staining for Sox17 (green) marks ventral pancreas and endothelial cells. Tissues are counterstained with Hoechst dye (grayscale). *ht*, heart; *lv*, liver; *dp*, dorsal pancreas; *vp*, ventral pancreas; *da*, dorsal aorta; *ec*, endothelial cells; *stm*, septum transversum mesenchyme; *nt*, neural tube; *nc*, notochord; *spm*, splanchnic mesoderm (scale bars: 100μm)

1.2.3 Early organogenesis of liver and pancreas

Following the specification of future organ domains, the organ rudiments mature during a process termed organogenesis[12,19,112]. During organogenesis, primary organ buds are established and grow through cell proliferation[129,130]. Progenitor cells acquire lineage-specific transcriptional programs enabling cellular differentiation and morphological changes to achieve adult tissue architecture.

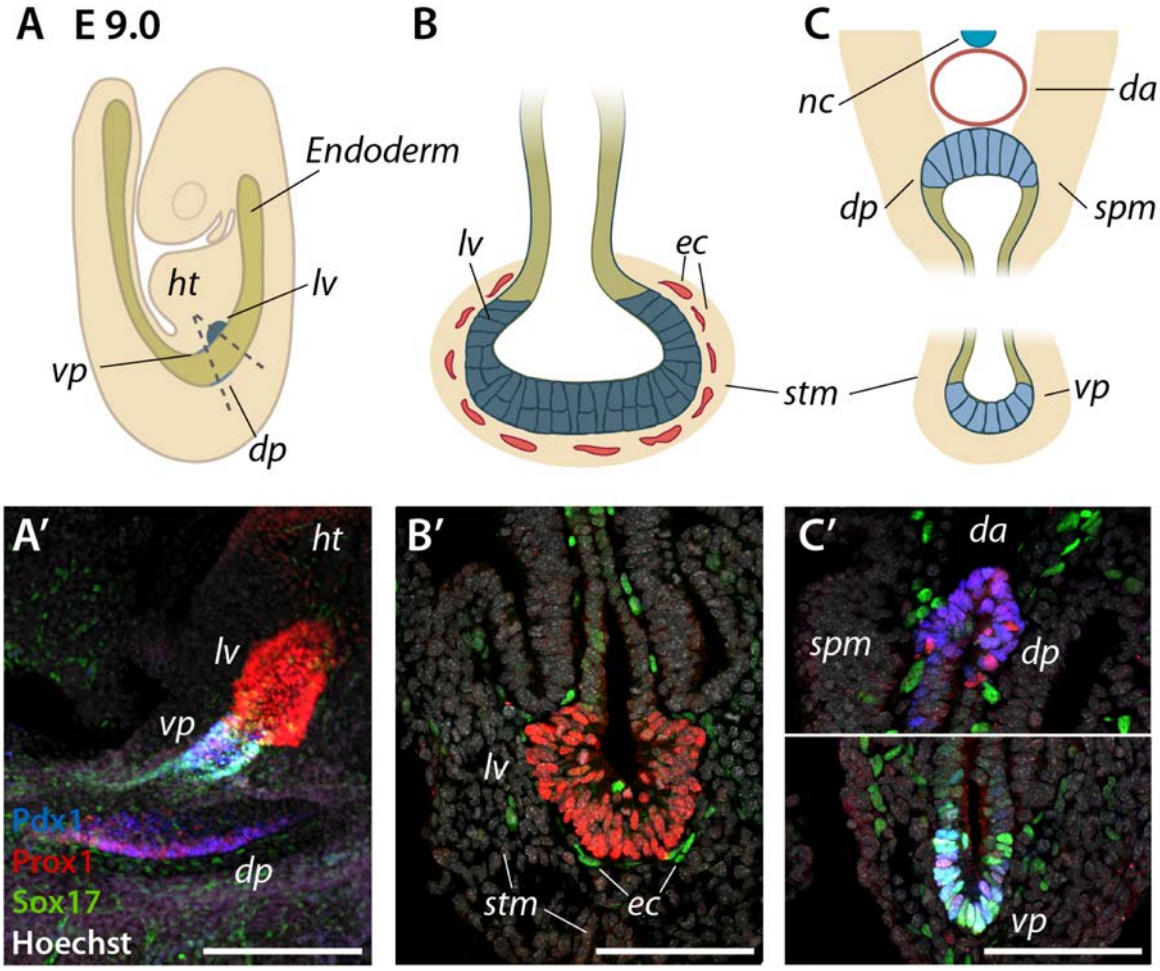

Fig. 9: Organogenesis of liver and pancreas at E9.0. (A) Representation of a mouse embryo at E9.0. The positions of the endoderm (green) and the developing hepatic (dark blue) and pancreatic buds (light blue) are indicated. **(B)** Transverse section through the developing liver at E9.0 (plane of view indicated by dotted line in panel A). **(C)** Transverse section through the developing pancreas at E9.0 (plane of view indicated by dotted line in panel A). **(A', B', C')** Representative IF staining of an E9.0 embryo either in wholemount (A') or on cryosections (B', C'). Staining for Prox1 (red) marks all hepato-pancreatic tissues, staining for Pdx1 (blue) marks ventral and dorsal pancreatic buds, and staining for Sox17 (green) marks ventral pancreas and endothelial cells. Tissues are counterstained with Hoechst dye (grayscale). *ht*, heart; *lv*, liver; *dp*, dorsal pancreas; *vp*, ventral pancreas; *da*, dorsal aorta; *ec*, endothelial cells; *stm*, septum transversum mesenchyme; *nc*, notochord; *spm*, splanchnic mesoderm (scale bars: 100μm)

After specification around E8.5, epithelial cells of the hepatic endoderm change their shape from a cuboidal to a pseudostratified columnar epithelium (also called liver diverticulum) and start protruding into the surrounding STM (Fig. 8A, A', B, B')[15,45,123]. Starting from E 9.0, the hepatic endoderm proliferates and becomes a multilayered epithelium (Fig. 9A, A', B, B'). The neighboring mesenchyme and endothelial cells induce the expression of matrix metalloproteinases (MMPs) in the hepatic endoderm[131,132], leading to a steady disintegration of the basal lamina surrounding the nascent liver bud. Consequently, the hepatic precursor cells (hepatoblasts) delaminate from the epithelium and invade the neighboring mesodermal tissues forming characteristic hepatic chords (Fig. 10A, A', B, B')[19,127,130,133,134].

Early organogenesis of the dorsal pancreas is marked by subsequent signaling events from a series of mesodermal tissues[27,135]. First, specification of the dorsal pancreatic endoderm is dependent on the close proximity of the notochord and the signaling molecules Activin and FGF2, which are released from it (Figs. 6C, 8A, A', C, C')[27,115–117]. As described above, robust expression of pancreatic marker *Pdx1* is established by signaling from the notochord and the somites[12,24,27]. Between E8.75 and E9.0, the notochord gets displaced from the pancreatic endoderm by the paired dorsal aortas, fusing at the embryonic midline (Fig. 9A, A', C, C')[136]. Subsequently, as yet unidentified signals from the endothelial cells of the dorsal aorta induce expression of Pancreas-specific transcription factor 1a (*Ptf1a*) in the dorsal pancreatic domain[137]. Pdx1[138–141] and Ptf1a[142,143] are arguably the two earliest and most important pancreas-specific transcription factors. However, from E10.0 onwards Pdx1 is also expressed in the posterior stomach, the duodenum, and the bile duct (Fig. 11B)[56,112]. At E9.5, the mesodermal environment around the dorsal pancreatic bud changes as the dorsal aorta is displaced from the endoderm by splanchnic mesoderm accumulating around the dorsal pancreas (Fig. 10A, A', C, C')[27,144]. Among the factors secreted by cells of the splanchnic mesoderm is FGF10[145,146]. It upregulates proliferation of pancreatic precursors, while delaying their differentiation, thereby allowing for expansion of the pancreatic progenitor cell pool.

In contrast to the dorsal pancreas, little information is available about external factors guiding organogenesis of the ventral pancreas[24,27]. Exclusion of cardiac FGF[5,111] and STM-derived BMP[6] signals, which would otherwise promote liver development, seems to be crucial for ventral pancreas specification. Work from the laboratory of Francesca Spagnoli identified a

non-canonical Wnt signature specifically in the ventral pancreas but not in the liver bud that is likely underlying a pro-pancreatic lineage decision[147]. In addition, very recent work of the Spagnoli laboratory, included in this thesis, identified the Robo-Slit signaling pathway as an essential pro-pancreatic signaling cue in the ventral foregut, allowing maintenance of pancreatic and suppression of hepatic identity in ventral pancreatic cells during organogenesis[148]. Still, whether other mesoderm-derived factors promote the proliferation and differentiation of ventral pancreatic precursors is not known.

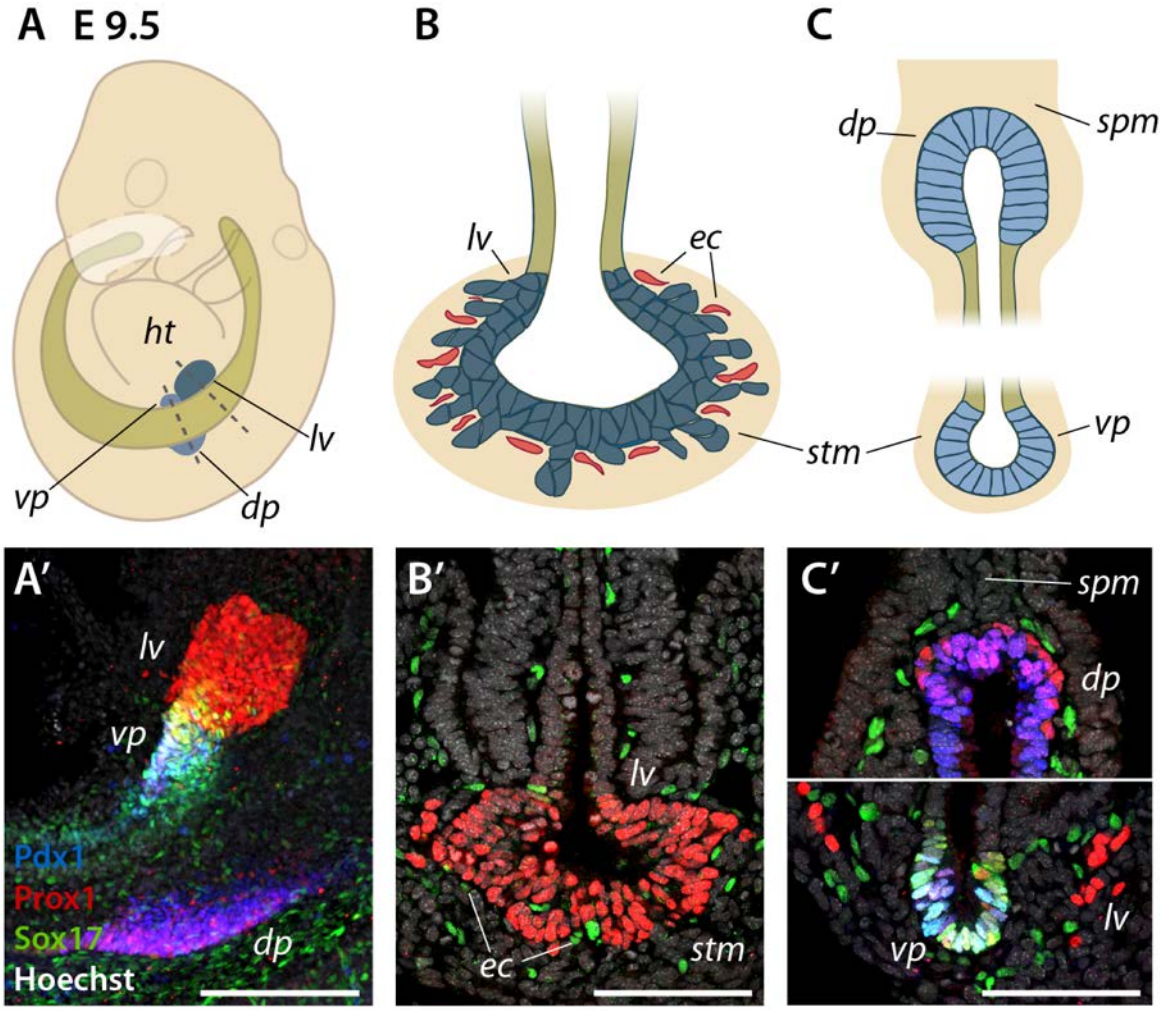

Fig. 10: Organogenesis of liver and pancreas at E9.5. (A) Representation of a mouse embryo at E9.5. The positions of the endoderm (green) and the developing hepatic (dark blue) and pancreatic buds (light blue) are indicated. **(B)** Transverse section through the developing liver at E9.5 (plane of view indicated by dotted line in panel A). **(C)** Transverse section through the developing pancreas at E9.5 (plane of view indicated by dotted line in panel A). **(A', B', C')** Representative IF staining of an E9.5 embryo either in wholemount (A') or on cryosections (B', C'). Staining for Prox1 (red) marks all hepato-pancreatic tissues, staining for Pdx1 (blue) marks ventral and dorsal pancreatic buds, and staining for Sox17 (green) marks ventral pancreas and endothelial cells. Tissues are counterstained with Hoechst dye (grayscale). *ht*, heart; *lv*, liver; *dp*, dorsal pancreas; *vp*, ventral pancreas; *ec*, endothelial cells; *stm*, septum transversum mesenchyme; *spm*, splanchnic mesoderm (scale bars: 100μm)

During early organogenesis, cells of the ventral pancreas still differ in a number of ways from their dorsal counterparts. While dorsal pancreatic cells at this stage give rise only to pancreatic tissues[24,27,56], the ventral pancreatic domain contains cells of the future pancreas, the gallbladder, and the common duct[22,23,123,149]. One feature specific to the ventral pancreas is the expression of the transcription factor Sox17, which is downregulated in dorsal pancreatic cells at E9.0 (Fig. 9C') but co-expressed with Pdx1 in ventral pancreatic cells until about E10.0 (Figs. 8C', 9C', 10C')[56,150,151]. Apart from the acquisition of a pancreas-specific transcriptional profile[24,27], the pancreatic endoderm undergoes distinct morphological changes in the time period between E8.5 and E9.5[13,112]. From E8.75 to E9.5, the small cuboidal cells of the pancreatic endoderm in both buds acquire a columnar elongated shape (Figs. 8C, C', 9C, C', 10C, C') and form a distinct bud separated from the gut tube[112]. Additionally, at around E10.0, the ventral pancreas separates into two distinct buds marked by the exclusive expression of either Pdx1 or Sox17[150,151]. The $Pdx1^{+}$ domain is thought to consist entirely of pancreatic progenitors, while the $Sox17^{+}$ domain harbors potential progenitors of the gallbladder[150,151].

1.2.4 Late organogenesis of liver and pancreas

At E10.5, the growing liver bud has separated into distinct lobes[15,19,123] and has been colonized by hematopoietic stem cells, as the liver is the major organ for fetal hematopoiesis[20,21]. In contrast to other endoderm-derived organs, the liver does not develop as a branching epithelium but rather as a mesenchymal condensate of endodermal hepatoblasts and mesodermal stellate cells (i.e., the hepatic mesenchyme)[15,19,123,149]. The growth of the liver bud is actually sustained by growth factors released from the STM and stellate cells[99,152–156]. During further development, the liver undergoes accelerated growth and vascularization while acquiring adult organ tissue architecture (Fig. 11A)[15,19,123]. Concurrently, the hepatoblasts undergo differentiation into two distinct lineages[15,19,123]. Hepatoblasts situated around the portal vein become biliary epithelial cells (a.k.a. cholangiocytes)[22,23,157], while those cells not in contact with the portal vein become hepatocytes (Fig. 2A, B)[152,158–160].

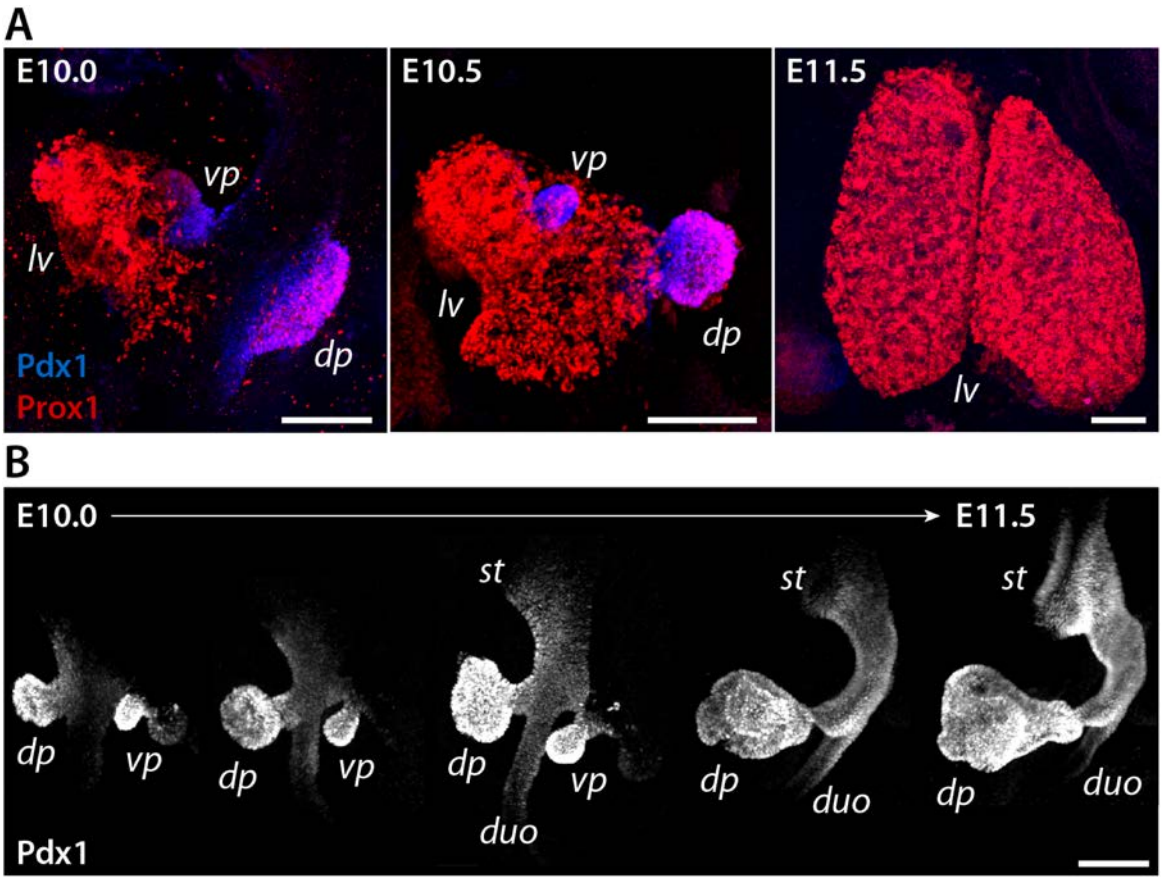

Fig. 11: Late stage of organogenesis of liver and pancreas. (A) Representative WMIF of E10.0-11.5 embryos. Immunostaining for Prox1 (red) marks all hepato-pancreatic tissues, while immunostaining for Pdx1 (blue) marks ventral (*vp*) and dorsal pancreas (*dp*). As is evident, the liver (*lv*) undergoes a dramatic growth phase during this developmental time window. **(B)** Representative WMIF of E10.0-11.5 embryos. Immunostaining for Pdx1 (grayscale) marks ventral and dorsal pancreatic buds, as well as the posterior stomach (*st*) and the duodenum (*duo*). While the ventral and dorsal pancreatic buds grow, the gut tube rotates, leading to the repositioning of the ventral pancreatic bud alongside the dorsal pancreas (in the images shown at later stages the ventral pancreas is positioned behind the dorsal pancreas). (scale bars: 100μm)

At E10.5, both the dorsal and ventral pancreatic bud consist of multipotent pancreatic progenitor cells[27,112]. Independently of their position in the ventral or the dorsal bud, these cells are characterized by the co-expression of a distinct set of transcription factors, namely Pdx1[138–141], Ptf1a[137,142,143], Sox9[47,161–164], and the members of the NK family of homeodomain proteins Nkx2.2[165,166], Nkx6.1[167–169], Nkx6.2[170,171]. While retaining a luminal connection to the gut tube via a stalk, the pancreatic buds begin to grow into the surrounding spleno-pancreatic mesenchyme[12,112]. From E10.5 onwards, the dorsal pancreatic epithelium undergoes branching morphogenesis while growing markedly in size (Fig. 11B)[14,172–174]. Branching processes likely depend on the interaction between the epithelium and the pancreatic mesenchyme that is condensing around the dorsal pancreatic bud[175–177]. Concurrently, the

rotation of the gut tube brings the ventral pancreatic bud into close proximity to its dorsal counterpart, ultimately allowing the fusion of the two organ rudiments (Fig. 11B).[1,14,112,172] As development progresses, extensive growth and branching morphogenesis occur in ventral and dorsal pancreata resulting in the formation of a highly structured tissue architecture (Fig. 12A)[14,112,172–174]. Concurrently, pancreatic progenitors commit to distinct pancreatic cell lineages (exocrine, endocrine, ductal) and form specialized cell types, such as insulin- or glucagon-expressing endocrine cells (Fig. 12B)[1,12,14,24,27,112].

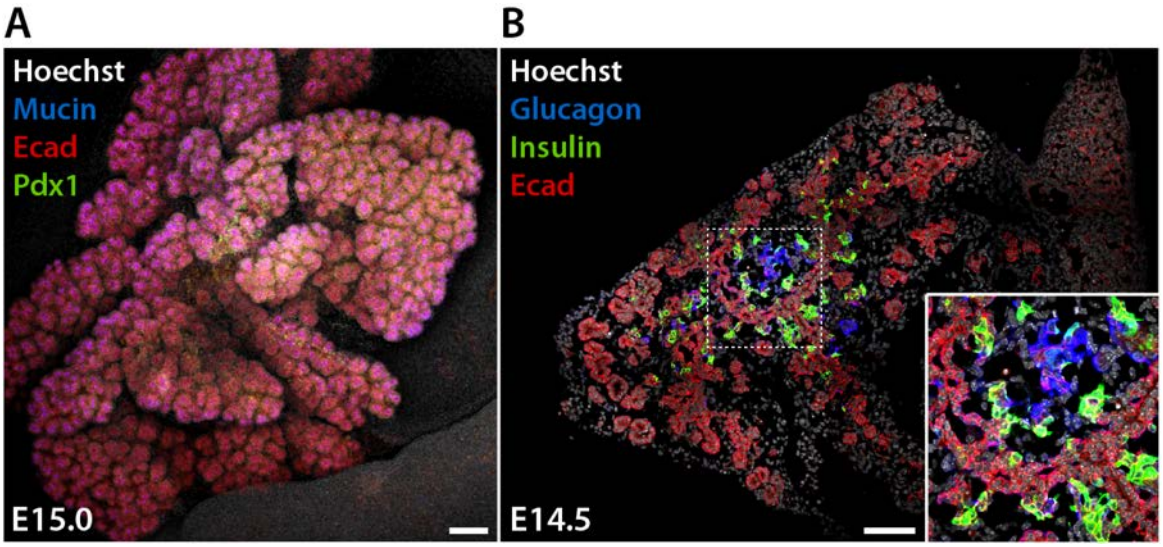

Fig. 12: Branching morphogenesis and endocrine cell differentiation. (A) Representative WMIF of the E15.0 dorsal pancreas. Immunostaining for Ecad (red) marks the pancreatic epithelium, immunostaining for mucin (blue) marks the ductal network, whereas immunostaining for Pdx1 (green) marks pancreatic cells. During late developmental stages the pancreas undergoes branching morphogenesis and pancreatic cells differentiate into acinar, endocrine, and duct cells. Tissues are counterstained with Hoechst dye (grayscale). **(B)** Representative IF staining of a cryosection of dorsal pancreatic tissue at E14.5. Immunostaining for Ecad (red) marks the pancreatic epithelium. Immunostaining for insulin (green) and glucagon (blue) marks progenitors of β- and α-cells, respectively. Inset shows higher magnification of the boxed area (dotted line) in the overview image. Tissues are counterstained with Hoechst dye (grayscale). (scale bars: 100μm)

1.3 Deciphering bipotentiality in the ventral foregut

An exciting debate in hepato-pancreatic development concerns the presumed existence of bipotent progenitor cells in the early endoderm that can contribute to both liver and pancreas. In 2001, two publications provided evidence for the existence of such a cell population[5,6]. Using explant cultures of E8.0-8.5 mouse endoderm, the authors showed that culturing ventral foregut endoderm, which harbors the presumptive hepatic and pancreatic progenitors, without mesodermal tissue results in the expression of the pancreatic marker Pdx1[5,6]. Furthermore, they showed that this apparent default pancreatic program could be diverted by adding FGF and BMP to the explant cultures, thereby promoting hepatic fate acquisition[5]. Interestingly, dorsal foregut endoderm cultured without the notochord failed to activate pancreas-specific gene expression. Again, these results highlight the differences in specification of dorsal and ventral pancreas. They also hint at the existence of a homogeneous cell population in the ventral foregut that relies on external stimuli for hepato-pancreatic lineage segregation. The hypothesis, that liver and ventral pancreas arise from a common progenitor domain was corroborated by lineage tracing in fish[9] and fate mapping experiments in the mouse[7,8,178]. Taken together, these different studies concluded that the ventral foregut contains both hepatic and ventral pancreatic progenitors, while dorsal pancreatic progenitors reside in a separate progenitor domain in the dorsal foregut. The identified ventral embryonic region in the mouse was later shown to be marked by the expression of Prox1 (Fig. 7)[126].

Despite some progress in deciphering the early stages of liver and pancreas lineage segregation, important questions remain unanswered. For example, definitive genetic proof for the existence of a bipotent progenitor population in the mammalian hepato-pancreatic system is lacking. Furthermore, our knowledge about the timing of the hepato-pancreatic lineage segregation as well as of the spatial relationship between bipotent ventral foregut cells and their descended liver and ventral pancreatic cells remains limited. Conceptually, a powerful experimental approach to explore hepato-pancreatic lineage segregation is the use of genetic lineage tracing[179–181]. The term lineage tracing describes experimental procedures to label individual cells or cell populations with a traceable marker and to analyze the cells' progeny by tracing the genetic label through ontogeny (Fig. 13A, B).

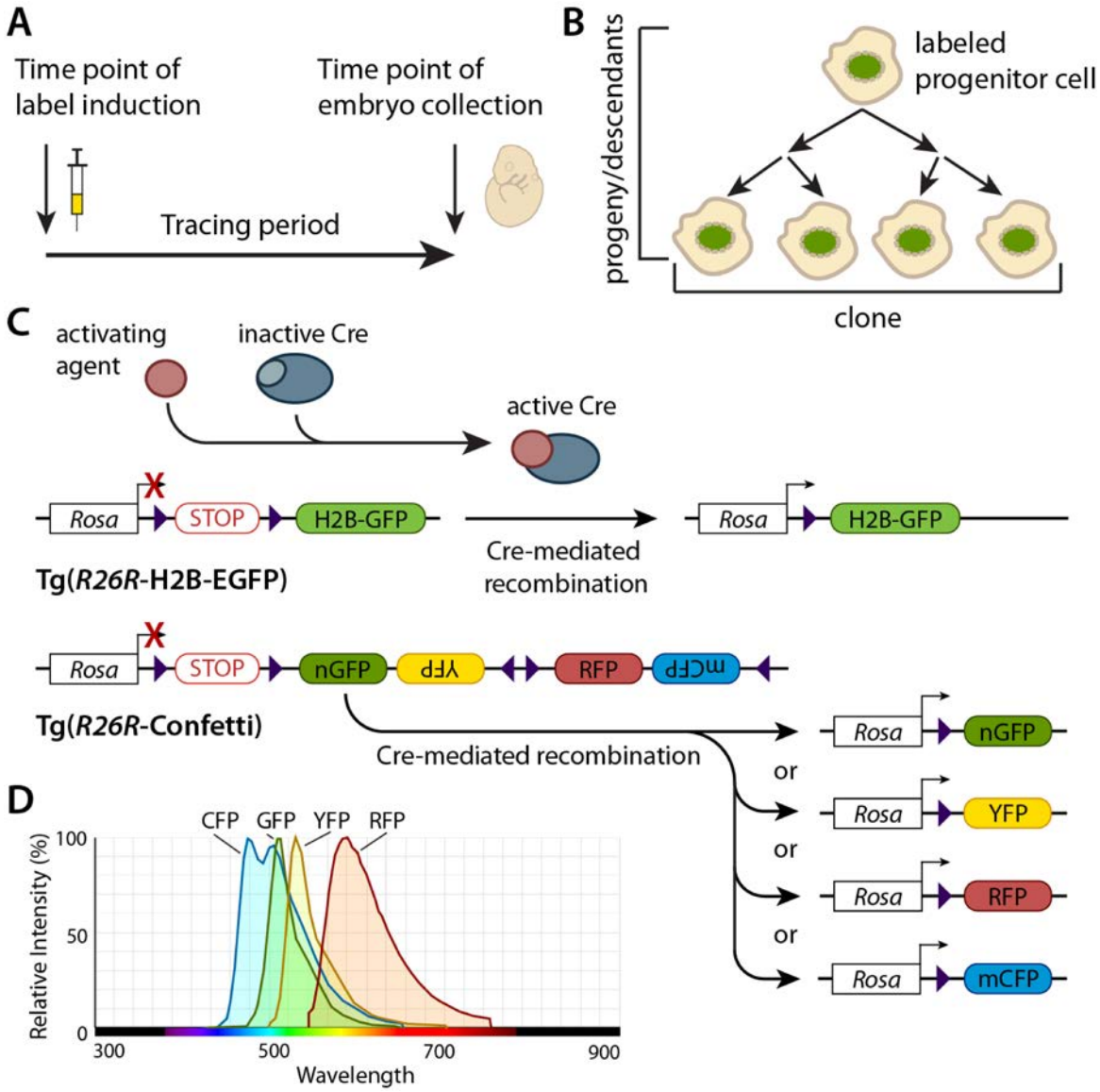

Fig. 13: Genetic lineage tracing. (A) Schematic representation of a lineage tracing experiment. **(B)** Schematic representation of a labeled cell clone. A labeled progenitor cell undergoes several rounds of cell division creating labeled descendants. The entirety of the progeny of the initially labeled progenitor are called a clone. **(C)** Schematic representation of genetic labeling. Genetic labeling relies on the stable and inheritable expression of a transgene, often encoding for a fluorescent reporter protein. Unicolor reporter transgenes such as Tg(*R26R*-H2B-EGFP) encode for a single fluorescent reporter while multicolor reporter transgenes such as Tg(*R26R*-Confetti) (Confetti) encode for several reporter proteins. Most reporter transgenes carry a transcriptional stop site flanked by loxP sites (purple triangles) that prevents transcription of the downstream transgene. Cre recombinase-mediated recombination at the reporter gene locus excises the stop site and enables transgene expression. Often, tissue-specific and inducible Cre recombinases are used for lineage tracing studies as they allow time- and tissue-specific lineage tracing experiments. In the case of the Confetti reporter, recombination at the transgenic locus allows for expression of only one of the four genes encoding for fluorescent reporter proteins. **(D)** Emission spectra of fluorescent reporter proteins encoded by the Confetti transgene. Different emission and excitation spectra for GFP, YFP, RFP, and CFP enable separate detection of their native fluorescence.

A popular experimental system for genetic lineage tracing in the mouse uses the Cre-lox system, which enables inducible and tissue-specific activation of a traceable marker gene locus (Fig. 13C)[179–181]. To achieve Cre recombinase-dependent control of marker gene expression, the marker gene is preceded by a *loxP-STOP-loxP* ("floxed" *STOP*) sequence that needs to be excised to allow transcription to proceed through the transgene. Unicolor reporter constructs (e.g. Tg(*R26R*-YFP)[182], Tg(*R26R*-H2B-EGFP)[183]) encode for one specific fluorescent reporter protein and enable analysis of labeled cells by either native fluorescence or by immunodetection. Multicolor reporters (e.g. Tg(*R26R*-Confetti)[184]) encode for different fluorescent reporters facilitating clonal analysis of the labeled cell populations. As multicolor lineage tracing strategies depend on the expression of variants of the same protein (e.g., green fluorescent proteins, GFP), detection of native reporter fluorescence is required to analyze these lineage tracing experiments[179–181]. Although the fluorescent proteins are immunologically indistinguishable, they elicit distinct emission spectra which can be used to identify differently labeled cells (Fig. 13D). Genetic lineage tracing studies led to the discovery of stem cell populations in intestine[184] and lung[185], and of bipotent stem cells in the mammary gland[186], just to name a few examples. Conceptually, genetic lineage tracing approaches should also aid in elucidating the existence of a bipotent hepato-pancreatic progenitor cell population and the dynamics of their segregation into hepatic and ventral pancreatic cell lineages.

1.4 Aim of the study

In recent years, the study of liver and pancreas development has gained significant attention concerning the development of cell-based therapies for degenerative diseases, such as diabetes and chronic liver disease. In this respect, the early lineage relationship between liver and ventral pancreas is of crucial importance. These two organ rudiments arise from a putative common progenitor domain and develop in close proximity to one another throughout early development[4–9,112,126,149]. Still, the cellular and tissue dynamics defining hepatic and pancreatic lineage segregation from a common progenitor tissue remain incompletely understood. Further elucidation of these biological concepts will advance our understanding of hepato-pancreatic tissue development and help in devising novel strategies for regenerative therapies for diseases targeting these vital organs.

The overall aim of my Ph.D. study was to explore the cellular dynamics underlying lineage segregation during specification of the hepato-pancreatic organ domains. Specifically, I wished to elucidate the location and cellular composition of a putative hepato-pancreatic progenitor domain in the ventral foregut and to establish the developmental time window during which it retains its bipotent nature to form liver and ventral pancreas. To address this question, I developed advanced lineage tracing strategies in transgenic mouse models to trace endodermal, hepato-pancreatic, and ventral pancreatic cells and to define their respective contributions to hepato-pancreatic organ rudiments. I quantitatively assessed the growth dynamics of hepato-pancreatic organs and determined the cellular differentiation dynamics of hepato-pancreatic progenitor populations during liver and pancreas organogenesis.

2. Material and Methods

2.1 Mouse strains

Mice used in this study were on a C57BL/6 genetic background and kept under standard housing conditions. The following mouse lines were used for genetic lineage tracing experiments in this study:

Tab. 1: Transgenic mouse strains for lineage tracing.

Strain	*Genetic modification*	*Source*
Tg(*Foxa2*-CreERT)	Foxa2$^{tm2.1(cre/Ers1*)Moon}$	*Park et al., 2008* [199]
Tg(*Pdx1*-Cre)	Tg(Pdx1-cre)6Tuv	*Hingorani et al., 2003* [212]
Tg(*TetO*-Cre)	Tg(tetO-cre)1Jaw	*Perl et al., 2002* [205]

The Tg(*Prox1*-rtTA) transgenic mouse line was generated by Igor Pongrac in the Spagnoli laboratory by modifying a mouse bacterial artificial chromosome (BAC) clone (RP23-360I16) spanning the Prox1 gene and its up- and downstream regulatory sequences[187,188]. In brief, a transgenic expression cassette encoding for a reverse tetracycline-controlled transactivator (rtTA) fused to mCherry via a 2A protease cleavage sequence was inserted at the ATG of the Prox1 open reading frame using a shuttle-vector system[189]. This transgene-modified BAC was subsequently introduced into the germline of C57BL/6 mice using pro-nuclear injection (Igor Pongrac, PhD thesis: "Spatiotemporal analysis of BMP signaling in pancreas versus liver fate decision"; Pongrac and Spagnoli, unpublished results). In addition, the following reporter mouse lines were used in this study:

Tab. 2: Transgenic reporter mouse strains.

Strain	*Genetic modification*	*Source*
Tg(*R26R*-Confetti)	Gt(ROSA)26Sor$^{tm1(CAG-Brainbow2.1)Cle}$	*Snippert et al., 2010* [184]
Tg(*R26R*-H2B-EGFP)	Gt(ROSA)26Sor$^{tm2(HIST1H2BB/EGFP)Sia}$	*Abe et al., 2011* [183]
Tg(*R26R*-YFP)	Gt(ROSA)26Sor$^{tm1(EYFP)Cos}$	*Srinivas et al., 2001* [182]
Tg(*Prox1*-EGFP)	Tg(Prox1-EGFP)KY221Gsat	*GENSAT project* [187]

To investigate the role of roundabout receptors (Robo) 1 and 2 during hepato-pancreatic development, mice carrying targeted knockout alleles for Robo1 (allele synonym: Robo1^{tm1Matl})[190] and Robo2 (allele synonym: Robo2^{tm1Mrt})[191] were used. These mice were produced by intercrossing animals carrying the Robo1 or Robo2 knockout alleles to obtain animals double heterozygous for both gene defects (Robo1/2 het). Embryos homozygous for both gene defects (Robo1/2 KO) and their control littermates were derived by timed matings of Robo1/2 het animals.

2.2 Animal experimentation

All animal experimentation was performed after approval of protocols and according to the regulations of local authorities (Landesamt für Gesundheit und Soziales, Berlin).

Timed matings were conducted by placing male and female mice into a breeding cage overnight and by performing daily plug checks. The presence of a vaginal plug in the morning was noted as embryonic day (E) 0.5. Embryos were collected between E7.5 and E18.5 and dissected under a stereomicroscope. Embryonic tissues were fixed in 4% paraformaldehyde (PFA) in phosphate buffered saline (PBS) for 2h at room temperature (E7.5-9.5 embryos) or overnight at 4°C (E10.5-18.5 embryos).

To assess the accurate age of each embryo, images of the individual embryos were taken under a stereomicroscope and used to stage the embryos according to Theiler staging criteria (E7.5)[192,193] or by counting somites (E8.0-E11.5)[192–194].

To induce genetic labeling in mouse embryos, pregnant females were injected with doxycycline (Dox) or tamoxifen (TAM). Doxycycline powder was dissolved in sterile PBS at a concentration of 20μg/μl and aliquots were stored at -20°C. Tamoxifen powder was dissolved in corn oil solution (in 10% vol/vol ethanol) at a concentration of 25μg/μl and aliquots were stored at -20°C. Dox and TAM solutions were warmed up to 37°C before injection. Dox was administered by tail vein injection at 75μg, 100μg, or 150μg Dox/g body weight (bw). TAM was administered by intraperitoneal injection at 12μg, 25μg, or 75μg TAM/g bw.

2.3 Genotyping

To extract genomic DNA for genotyping of adult mice, ear punch biopsies were obtained and lysed in 250µl tail lysis buffer (50mM Tris pH 8, 100mM EDTA pH 8, 100mM NaCl, 1% SDS, 1.5µl Proteinase K (20mg/ml)) for at least 2h at 55°C under continuous shaking. Next, the samples were cleared by centrifugation. The supernatant was transferred into a new reaction tube. DNA was precipitated by adding 250µl isopropanol. The samples were again

Tab. 3: Protocols for genotyping PCRs.

Genotyping Tg(TetO*-Cre*), Tg(Pdx1*-Cre*)		
Temperature	*Time*	
94°C	2 min	
94°C	30 sec	*35 cycles*
56°C	30 sec	
72°C	30 sec	
72°C	2 min	

Genotyping Tg(Prox1*-rtTA*)		
Temperature	*Time*	
94°C	2 min	
94°C	45 sec	*30 cycles*
56°C	45 sec	
72°C	45 sec	
72°C	7 min	

Genotyping Tg(R26R*-Confetti*)		
Temperature	*Time*	
94°C	2 min	
94°C	30 sec	*35 cycles*
58°C	30 sec	
72°C	30 sec	
72°C	2 min	

Genotyping Tg(R26R*-H2B-EGFP*)		
Temperature	*Time*	
94°C	2 min	
94°C	30 sec	*35 cycles*
65°C	30 sec	
72°C	30 sec	
72°C	5 min	

Genotyping Tg(Prox1*-EGFP*)		
Temperature	*Time*	
94°C	2 min	
94°C	45 sec	*30 cycles*
58°C	45 sec	
72°C	45 sec	
72°C	7 min	

Genotyping Tg(R26R*-YFP*)		
Temperature	*Time*	
94°C	2 min	
94°C	30 sec	*35 cycles*
58°C	1 min	
72°C	1 min	
72°C	2 min	

Genotyping Tg(Foxa2*-CreERT*)		
Temperature	*Time*	
94°C	3 min	
94°C	30 sec	*35 cycles*
55°C	30 sec	
72°C	30 sec	
72°C	2 min	

Genotyping Robo1/2 KO		
Temperature	*Time*	
94°C	2 min	
94°C	30 sec	*35 cycles*
58°C	30 sec	
72°C	30 sec	
72°C	7 min	

centrifuged, the supernatant discarded, and the DNA pellet air-dried for 10min. After resuspension of the pellet in TE buffer (10mM Tris, 1mM EDTA), the DNA was used as template for genotyping PCRs (for protocols see Tab. 3, for PCR primers see Tab. 4).

Tab. 4: Primers used for genotyping PCRs.

Allele	*Primer sequence*	*Band size*
Cre internal control	5' CTA GGC CAC AGA ATT GAA AGA TCT 3' 5' GTA GGT GGA AAT TCT AGC ATC ATC C 3'	324bp
Cre transgene	5' GCG GTC TGG CAG TAA AAA CTA TC 3' 5' GTG AAA CAG CAT TGC TGT CAC TT 3'	100bp
Prox1-rtTA internal control	5' CTA GGC CAC AGA ATT GAA AGA TCT 3' 5' GTA GGT GGA AAT TCT AGC ATC ATC C 3'	324bp
Prox1-rtTA transgene	5’ GAA CAG GAG CAT CAA GTA GC 3' 5' CAA GGA GTT CAT GCG CTT CAA G 3'	447bp
Confetti wildtype	5’ CCA GAT GAC TAC CTA TCC TC 3’ 5' AAA GTC GCT CTG AGT TGT TAT 3'	386bp
Confetti transgene	5’ CCA GAT GAC TAC CTA TCC TC 3’ 5’ GAA TTA ATT CCG GTA TAA CTT CG 3'	300bp
H2B-EGFP wildtype	5' AAC CCC AGA TGA CTA CCT ATC CTC C 3' 5’ TCC CTC GTG ATC TGC AAC TCC AGT C 3'	217bp
H2B-EGFP transgene	5' AAC CCC AGA TGA CTA CCT ATC CTC C 3' 5’ GGG GGA GGA TTG GGA AGA CAA TAG C 3'	297bp
Prox1-EGFP internal control	5' CTA GGC CAC AGA ATT GAA AGA TCT 3' 5' GTA GGT GGA AAT TCT AGC ATC ATC C 3'	324bp
Prox1-EGFP transgene	5’ ATC CTG GTC GAG CTG GAC GGC GAC G 3' 5' TCA GGT AGT GGT TGT CGG GCA GCA G 3'	580bp
YFP wildtype	5' AAA GTC GCT CTG AGT TGT TAT 3' 5’ GGA GCG GGA GAA ATG GAT ATG 3’	600bp
YFP transgene	5' AAA GTC GCT CTG AGT TGT TAT 3' 5’ AAG ACC GCG AAG AGT TTG TC 3'	320bp
Foxa2-CreERT wildtype	5' GAC TTT TCT GCA ACA ACA GCA 3' 5’ CTC AAG GGA GCA GTC TCA CC 3'	215bp
Foxa2-CreERT transgene	5' GAC TTT TCT GCA ACA ACA GCA 3' 5' ATA CTA TCT AGA GAA TAG GAA CTT CG 3'	166bp
Robo1 wildtype	5’ TGG CAC GAA GGT ATA ATG GC3' 5' GAA GGA CTG GTG GTT TTG AG 3'	400bp
Robo1 mutant	5’ TGG CAC GAA GGT ATA ATG GC3' 5’ CCT CCG CAA ACT CCT ATT TC 3’	320bp
Robo2 wildtype	5’ AAG TGC AAC GTC TCT GAA GTC CC 3' 5’ TTC TTT AGA AGG CAC AAC AAT CTC AGA G 3’	342bp
Robo2 mutant	5’ AAG TGC AAC GTC TCT GAA GTC CC 3' 5' GGC GGA ATT CTT AAT TAA GGC GCG 3'	250bp

To extract genomic DNA for genotyping of mouse embryos, tissue biopsies were lysed in 75µl embryo lysis buffer (100mM Tris pH 8, 50mM KCl, 2mM $MgCl_2$, 0.1mg/ml gelatin, 0.45% NP40, 0.45% Tween, 1.8µl Proteinase K (20mg/ml)) for at least 2h at 55°C while shaking the samples. Following heat inactivation of Proteinase K by boiling samples for 10min at 95°C, the DNA was

used as template for genotyping PCRs. Genotyping PCRs for adult or embryonic tissues were analyzed by standard agarose gel electrophoresis and genotypes assigned according to band size of the PCR products (Tab. 4).

2.4 Immunohistochemical analyses

2.4.1 Histology

For histological analysis, fixed embryonic tissues were equilibrated overnight in 20% sucrose solution (in PBS) for cryoprotection. Next, tissues were embedded in O.C.T. compound (Tissue-Tek®, Sakura®, Finetek) and subsequently frozen and stored at -80°C. Cryosections were cut at a thickness of 10µm using a CM3050 S Leica cryostat and collected on standard glass slides (Thermo Scientific). Tissue sections were stored at -80°C.

2.4.2 Immunofluorescence staining on cryosections

Slides containing tissue sections were transferred to room temperature and air dried for 1-3h. The tissue sections were circled with a PAP pen, providing a hydrophobic barrier for application of solutions. Next, sections were blocked for at least 1h at room temperature with TSA buffer (10% horse serum (HS), 0.5% TSA blocking powder (TSA Fluorescein System, Perkin Elmer), and 0.1% Triton X100 in PBS). Primary antibodies were diluted according to table 5 in HS/BSA buffer (3% HS, 0.3% bovine serum albumin (BSA), and 0.1% Triton X100 in PBS), and sections incubated overnight at 4°C in 400µl primary antibody solution. The following day, slides were washed three times for 5min each with PBT (PBS, 0.1% Triton X100). Secondary antibodies as well as fluorescent dyes (Hoechst, phalloidin) were diluted 1:750 in HS/BSA buffer and sections incubated for at least 1h at room temperature in 200µl secondary antibody solution. Thereafter, the slides were washed again three times for 5min each with PBT (PBS, 0.1% Triton X100) and one time for 10min with PBS. Next, the slides were air dried for 10min and subsequently mounted with Dako fluorescent mounting medium. After the mounting medium was allowed to solidify overnight at room temperature, the slides were stored at 4°C. Images were acquired on a Zeiss LSM 700 confocal microscope using a 40x or 63x oil immersion objective.

Tab. 5: Antibodies, dyes, and fluorescent probes used for immunofluorescence stainings.

Antibody/Dye/Fluorescent probe	*Company, Catalogue number*	*Host species*	*Dilution*
anti-Albumin	DakoCytomation, A0001	rabbit	1:600
anti-BrdU	Biozol, CL2700AP	rat	1:100
anti-Cytokeratin 19	Abcam, ab133496	rabbit	1:200
anti-E-cadherin	Sigma, U3254	rat	1:500
anti-α-fetoprotein	DAKO, A000829-2	rabbit	1:600
anti-Foxa2	Abcam, ab108422	rabbit	1:300
anti-GFP	Aves, GFP-1020	chicken	1:400
anti-Glucagon	Immunostar Inc., 20076	rabbit	1:500
anti-Hes1	gift from Birchmeier Lab	rabbit	1:500
anti-Insulin	Invitogen, PAI-26938	guinea-pig	1:250
anti-Islet-1	Hybridoma Bank, 39.4D5	mouse	1:100
anti-Laminin	Sigma, L9393	rabbit	1:1000
anti-Mucin	Thermo Scientific, HM-1630-P1	arm. hamster	1:500
anti-Nkx6.1	Hybridoma Bank, F55A10	mouse	1:500
anti-Neurogenin 3	BCBC, AB2774	goat	1:1500
anti-Pax6	Covance, PRB-278P	rabbit	1:200
anti-Pbx1	Cell Signaling, 4342	rabbit	1:400
anti-Pdx1	Abcam, ab47308	guinea-pig	1:500
anti-pH3	Millipore, 06-570	rabbit	1:200
anti-Prox1	RELIATech GmbH, 102-PA32S	rabbit	1:200
anti-Prox1	R&D Systems, AF2727	goat	1:100
anti-RFP	Chromotek, ABIN334653	rat	1:400
anti-Somatostatin	Santa Cruz, sc-7819	goat	1:100
anti-Sox2	Santa Cruz, sc-17320	goat	1:1000
anti-Sox9	Millipore, AB5535	rabbit	1:500
anti-Sox17	R&D Systems, AF1924	goat	1:200
Hoechst 33342	Invitrogen, H1399	/	1:500/750
Phalloidin-555	Invitrogen, A34055	/	1:200
anti-arm. hamster IgG 649	Dianova (Jackson), 127-495-099	goat	1:500/750
anti-chicken IgG 488	Invitrogen, A11039	goat	1:500/750
anti-goat IgG 488	Invitrogen, A11055	donkey	1:500/750
anti-goat IgG 594	Invitrogen, A11058	donkey	1:500/750
anti-guinea-pig IgG 488	Dianova (Jackson), 706-545-148	donkey	1:500/750
anti-guinea-pig IgG 647	Invitrogen, A21450	goat	1:500/750
anti-guinea-pig IgG 647	Dianova (Jackson), 706-605-148	donkey	1:500/750
anti-mouse IgG 488	Invitrogen, A21202	donkey	1:500/750
anti-rabbit IgG 488	Invitrogen, A21206	donkey	1:500/750
anti-rabbit IgG 594	Invitrogen, A21207	donkey	1:500/750
anti-rabbit IgG 647	Invitrogen, A31573	donkey	1:500/750
anti-rat IgG 594	Invitrogen, A-21209	donkey	1:500/750
anti-rat IgG 647	Dianova (Jackson), 712-605-153	donkey	1:500/750

Abbreviations: BrdU, bromodeoxyuridine; Foxa2, Forkhead box A2; GFP, Green fluorescent protein; Hes1, Hairy and enhancer of split 1; Nkx6.1, Nkx6 homeobox 1; Pax6, Paired box protein 6; Pbx1, Pre-B-cell leukemia transcription factor 1; Pdx1, Pancreatic duodenal homeobox 1; pH, Phospho-histone; Prox1, Prospero homeobox 1; RFP, Red fluorescent protein; Sox, Sex-determining region on Y box protein; arm., Armenian; IgG, Immunoglobulin G

2.4.3 Whole mount immunofluorescence staining

Fixed embryos or embryonic tissue for wholemount analyses were blocked for at least 1h in PBSMT (2% milk powder, 0.5% Triton X100, in PBS). The primary antibodies were diluted according to table 5 in PBSMT and the embryos incubated overnight at 4°C in 300µl primary antibody solution. The following day, the embryos were washed several times in PBST (PBS, 0.5% Triton X100) for at least 5h in total. Secondary antibodies and Hoechst dye were diluted 1:500 in PBSMT and the embryos incubated overnight at 4°C in 500µl secondary antibody solution. The following day, the embryos were again washed several times in PBST for at least 5h in total. Next, the embryos were dehydrated in a methanol dilution series and stored at 4°C. Prior to imaging, the embryos were clarified with methyl salicylate. Clarified embryos were imaged on a paraffin-sealed glass depression slide with a Zeiss LSM 700 confocal microscope using a 10x water immersion objective.

2.5 BrdU incorporation assay

To label embryonic cells in S-phase with bromodeoxyuridine (BrdU), BrdU powder was dissolved in H_2O (containing 0.9% NaCl and 7mM NaOH) at a concentration of 16µg BrdU/µl. Next, BrdU was administered by intraperitoneal injection to pregnant females at a concentration of 75µg BrdU/g bw. Embryos were collected at the indicated time points after BrdU administration, dissected, and fixed in 4% PFA (as described in chapter 2.2). Then, the embryos were embedded in O.C.T. compound and cryosections prepared as described in chapter 2.4.1.

For immunostaining of BrdU in combination with immunostainings for proteins (e.g. Prox1, Pdx1), immunostaining for the proteins was performed first according to the protocol described in section 2.4.2. Following application of primary and secondary antibodies and after the last 10min washing step in PBS, the sections were post-fixed with 4% PFA solution for 15min at 4°C. Afterwards, the slides were washed two times for 5min with PBS. Next, the slides were treated with prewarmed 2.4M HCl for 30min at 37°C to denature the genomic DNA, allowing anti-BrdU antibodies to bind their antigen. After HCl treatment, the slides were

washed twice with PBS for 5min and once with PBT (PBS, 0.1% Triton X100) for 10min. Subsequently, the slides were again immunostained following the protocol described in chapter 2.4.2 using an anti-BrdU antibody as well as the previously used antibodies (primary and secondary) directed against proteins expressed in the embryonic tissue.

2.6 Imaging native reporter fluorescence

To image native fluorescence of reporter proteins in wholemount preparations, the fixed embryonic tissues were clarified in Sca*l*eA2[195] (4M urea, 0.1% Triton X-100, 10% glycerol, in H_2O) for at least 2 weeks and up to 3 months at 4°C. The clarified tissues were mounted in paraffin-sealed CoverWell™ imaging chambers and imaged using a Zeiss LSM 700 confocal microscope (for unicolor reporter imaging) or a LaVision BioTec TriM Scope II 2-photon microscope (for multicolor reporter imaging). Anca Margineanu (Advanced Light Microscopy Facility, MDC) provided guidance for image acquisition and analyses.

2.7 Live imaging of mouse embryos

Tg(*Prox1*-EGFP)[187] embryos were collected at E8.5 and placed in dissection medium (75% DMEM/F12, 25% fetal bovine serum (FBS)) at 37°C. The decidua around the embryo was carefully removed to keep the embryonic membranes (chorion, amnion) intact. The embryos were somite-staged prior to imaging. For *ex vivo* time-lapse imaging by confocal microscopy, the embryos were placed in a CoverWell™ imaging chamber inside a glass-bottom MaTek dish. To immobilize the growing embryo, an eyelash was pierced through the ectoplacental cone of the embryo. In this fashion, the embryo was suspended through the holes of the CoverWell™ imaging chamber. During the imaging process, the embryos were cultured in growth medium (75% rat serum (produced in house), 25% DMEM/F12). Growth conditions in the confocal imaging chamber were kept at 37°C and 5% CO_2. Confocal Z-stacks of the developing embryo were acquired every 5min for up to 16h with a Zeiss LSM 700 confocal microscope using a 10x objective.

2.8 Image analysis

Images were analyzed using ImageJ, Imaris, Adobe Photoshop, as well as Adobe Illustrator.

In detail, H2B-GFP labeled cells and $pH3^+$ cells were counted manually using Adobe Photoshop and Adobe Illustrator in combination. ImageJ was used for measurement of tissue area and organ bud volume. Total cell counts as well as counts of cells positive for BrdU or cleaved caspase 3 (cCas3) were obtained using ImageJ. Liver cell counts of embryos older than E10.0 were obtained by using the automatic spot detection function of Imaris with manual editing. The region-of-interest (ROI) tool of ImageJ was applied to quantify fluorescence intensities. Coordinates of cells for analysis of Pdx1-Cre lineage tracings were obtained by using the spot detection function of Imaris with manual editing. Channel intensities of images were modified using Adobe Photoshop and ImageJ.

Analysis of Confetti lineage tracing experiments required tile stitching[196] of acquired images and spectral unmixing of individual channels using ImageJ. Coordinates of labeled cells were obtained by using the automatic spot detection function of Imaris with manual editing. The cluster analysis was performed by Anca Margineanu using "Hierarchical Clustering on Principle Components"[197,198].

2.9 Statistical analysis

Statistical analyses were performed using GraphPad Prism. Unless stated otherwise, data are shown as mean $\pm$ standard deviation and statistical significance ($p<0.05$) was determined using Mann-Whitney or Kruskal-Wallis test with Dunn's multiple comparisons test. Regression lines were plotted using GraphPad Prism with regression line type and R^2 value indicated at the respective figure legends.

3. Results

3.1 Analysis of tissue dynamics during hepato-pancreatic development

To elucidate the principles of hepato-pancreatic lineage segregation, I set out to examine the underlying mechanisms of cell fate acquisition, proliferation, and growth in the foregut of the mouse embryo. Towards this aim, I followed two distinct experimental approaches. In the first approach, I focused on lineage tracing of endodermal cells from gastrulation to the establishment of hepato-pancreatic organ domains. Thereby, I wished to gain insight into the dynamics of how multipotent endodermal cells contribute to these distinct organ primordia. My second approach focused on assessing tissue dynamics in the developing hepato-pancreatic system by investigating organ growth and proliferation throughout early organogenesis.

3.1.1 Establishing an unbiased tool for lineage tracing of endodermal cells during hepato-pancreatic fate acquisition

For analysis of fate acquisition of endodermal cells (approach 1), an inducible genetic system for lineage tracing in the entire endoderm was required, without biased expression of the tracer in early hepatic or pancreatic progenitors. These requirements were met by a transgenic (Tg) mouse Cre line (Tg(*Foxa2*-Cre-ERT); hereafter abbreviated Foxa2-Cre) co-expressing a tamoxifen-inducible Cre recombinase transgene (Cre-ERT) together with the Foxa2 coding sequence from the *Foxa2* locus by virtue of an engineered internal ribosomal entry site (Fig. 14A)[199]. The Cre-ERT transgene consisted of a Cre recombinase sequence flanked by sequences coding for the murine estrogen receptor (mER). As described in the introduction (Figs. 4, 7), Foxa2 is one of the earliest pan-endodermal genes and starts to be expressed in definitive endodermal cells as they progress through the primitive streak during gastrulation[56,69].

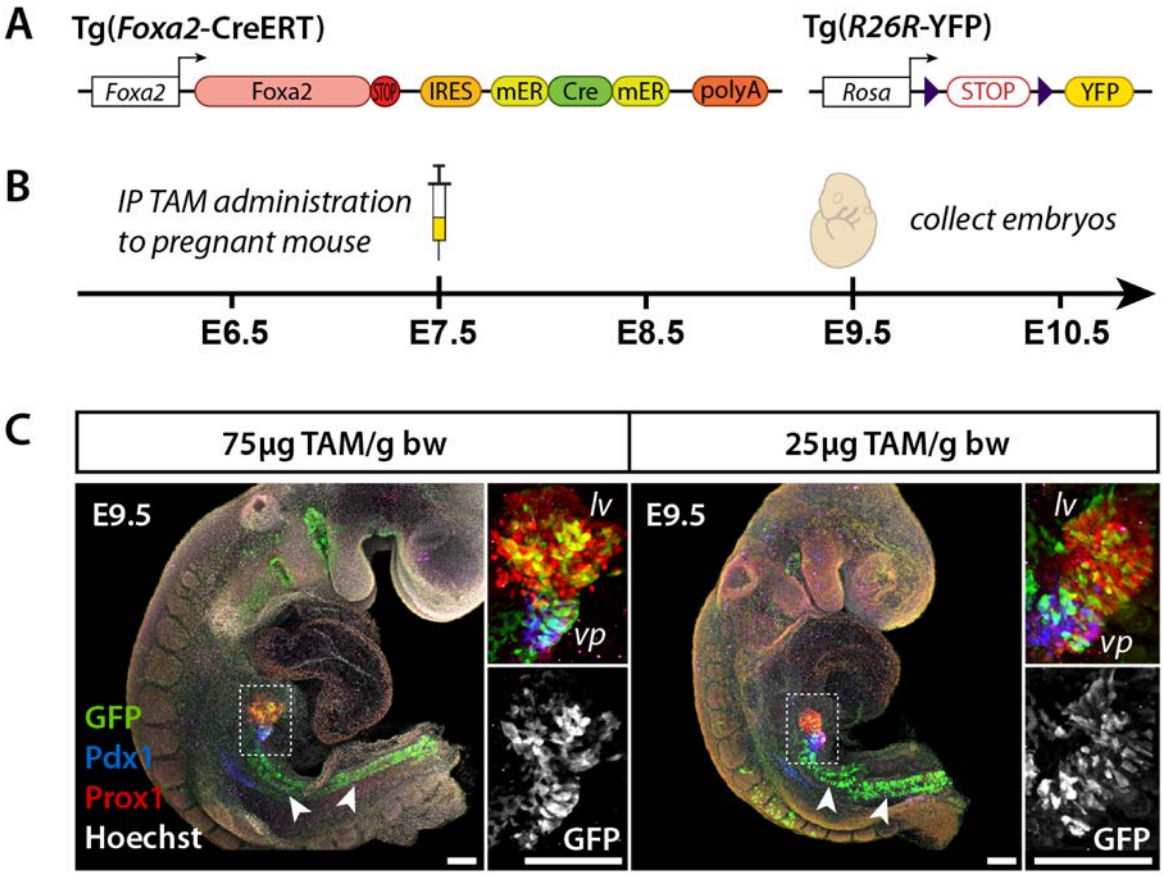

Fig. 14: Establishing the Foxa2-Cre-ERT mouse line as a tool for lineage tracing of hepato-pancreatic progenitors. (A) Schematic representation of transgenes used in this experimental approach. (IRES, internal ribosome entry site; mER, murine estrogen receptor; loxP sites shown as purple triangles) **(B)** Schematic representation of the experimental setup. Pregnant females were injected with a single dose of tamoxifen (75 or 25µg/g body weight) at E7.5 by intraperitoneal (IP TAM) injection. Embryos were subsequently collected at E9.5. **(C)** Representative wholemount immunofluorescence (WMIF) of E9.5 Tg(*Foxa2*-Cre-ERT; *R26R*-YFP) embryos that received the indicated doses of tamoxifen. Immunostaining of YFP using an anti-GFP antibody documents YFP^+ (labeled) cells throughout the gut tube (arrowheads) including liver (*lv*) and ventral pancreas (*vp*). Insets show higher magnifications of the areas marked by white dotted box as merged color images and single GFP channel in grayscale. Immunostaining of Prox1 (red) marks hepatic, co-immunostaining of Prox1 and Pdx1 (blue) pancreatic buds. Tissues are counterstained with Hoechst dye (grayscale). (scale bars: 100µm)

Initially, I determined the suitability of this mouse line for lineage tracing studies. I set up timed matings between Foxa2-Cre males and Tg(*R26R*-YFP) transgenic females (hereafter abbreviated YFP), in which the YFP reporter construct is introduced into the *Rosa26* gene locus (Fig. 14A)[182]. Cre-mediated recombination at the YFP transgene locus removes a transcriptional stop sequence flanked by loxP sites to drive stable expression of cytoplasmic YFP in genetically labeled cells and their progeny. Based on a protocol described by Park et al.[199], pregnant females were injected intraperitoneal (IP) with 25µg or 75µg tamoxifen/g body weight (bw) at E7.5. Subsequently, embryos were collected at E9.5 (Fig. 14B) and

subjected to wholemount immunofluorescence staining (WMIF). The presence of YFP-expressing cells in the endoderm was documented using an anti-GFP-antibody (Fig. 14C). Under both experimental conditions (25µg or 75µg tamoxifen/g bw) I observed dense labeling of the gut tube, including the hepatic and ventral pancreatic buds (Fig. 14C, insets).

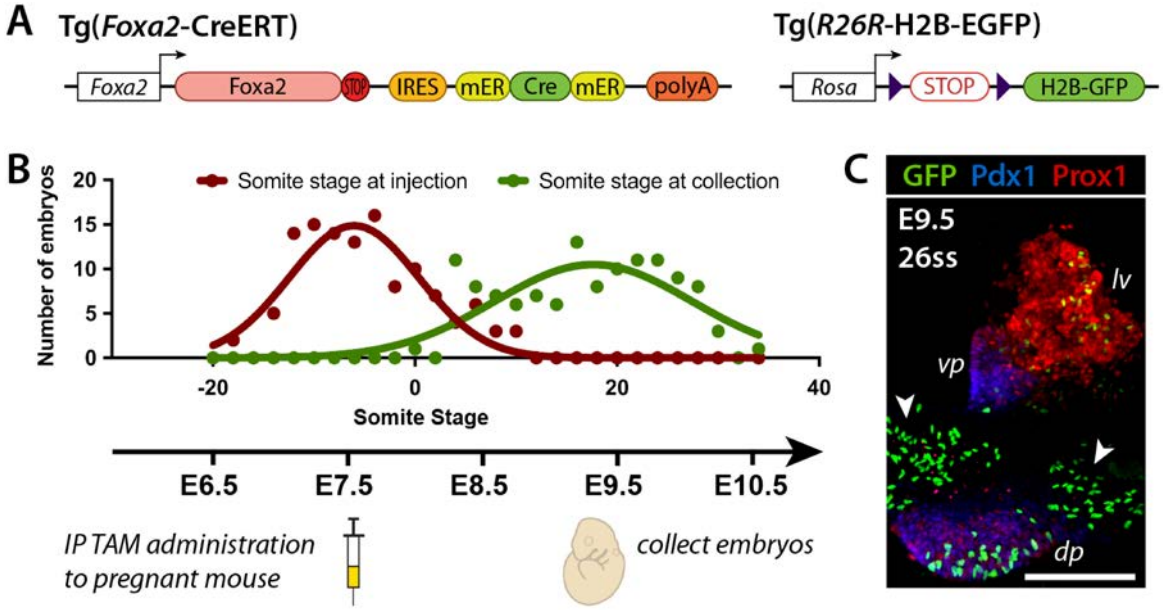

Fig. 15: Experimental setup for lineage tracing of hepato-pancreatic progenitors. (A) Schematic representation of transgenes used in this experimental approach. (IRES, internal ribosome entry site; mER, murine estrogen receptor; loxP sites shown as purple triangles) **(B)** Schematic representation of the experimental setup. Pregnant females were injected with a single dose of tamoxifen (12µg/g body weight) around E7.5 by intraperitoneal (IP TAM) injection. Embryos were subsequently collected at about E9.5. The upper diagram shows a graphical representation of the spread of embryonic stages at the time points of injection or embryo collection in the dataset (n=120). **(C)** Representative WMIF of E9.5 Tg(*Foxa2*-Cre-ERT; *R26R*-H2B-GFP) embryo. Immunostaining of GFP documents GFP^+ (labeled) cells throughout the gut tube (arrowheads) including liver (*lv*), ventral (*vp*), and dorsal pancreas (*dp*). Immunostaining of Prox1 (red) marks hepatic, co-immunostaining of Prox1 and Pdx1 (blue) pancreatic buds. (scale bar: 100µm)

As my initial experiments documented a high density of labeled cells in the hepato-pancreatic organ buds, I reduced the tamoxifen dosage for further lineage tracing experiments to 12µg/g bw. Also, Foxa2-Cre Tg animals were intercrossed with the mouse Tg reporter line Tg(*R26R*-H2B-EGFP)[183] (hereafter abbreviated H2B-GFP) (Fig. 15A). Cre-mediated recombination at the H2B-GFP transgene introduced into the *Rosa26* locus causes stable expression of a histone 2B-GFP fusion protein in genetically labeled cells and their progeny[183]. I chose the H2B-GFP reporter instead of the previously used YFP line, because its nuclear localization facilitates quantification of labeled cell counts. Indeed, compared to the cytoplasmic YFP signal (Fig. 14C), the strong nuclear H2B-GFP signal enabled easier identification of labeled cells,

especially when in close proximity to one another (Fig. 15C). Accordingly, pregnant females were IP injected with tamoxifen at E7.5 and embryos subsequently collected at different time points between E8.5 and E10.5 (Fig. 15B). The aim of this broad sampling strategy was to investigate the contribution of labeled endodermal cells to the hepato-pancreatic organ rudiments at different developmental stages. A total of 120 embryos were analyzed. The spread of their respective somite stages at the time points of tamoxifen injection and subsequent collection is illustrated in Fig. 15B.

At these early stages of mouse development, the embryonic stage can be more accurately defined by somite stage (ss) than by embryonic day (E)[194]. Somites are transient mesodermal structures formed in the vertebrate embryo during a process called somitogenesis[200,201]. Somites are formed in the mouse between E8.0 and E11.5. Commonly, a 2h time period corresponds to the formation of a somite in the mouse[201,202], allowing for a precise calculation of the embryonic stage at the time of label induction and the time of embryo collection. The precise identification of embryonic stages is important because the mouse embryo undergoes dramatic changes between E8.0 and E11.5. By using somite stages to stage embryos, I was able to more accurately describe the time course of hepato-pancreatic development. Of note, in Fig. 15B I included “negative somite stages” on the X-axis of the chart. I chose this is strategy to standardize the measurement of embryonic stages throughout my experiments, even at time points preceding somite formation. Specifically, I recalculated all time periods, which preceded 0ss, for example by assigning 40h prior to the formation of the first somite as -20ss. Subsequent to staging, the presence of GFP-labeled cells in hepato-pancreatic organ domains was documented by WMIF analysis for GFP (Fig. 15C).

Of the 120 embryos analyzed, a subset of embryos (Fig. 16; n=30) did not show discriminable hepatic and ventral pancreatic organ domains, but a common ventral foregut tissue expressing Prox1 (0-9ss, examples shown in Fig. 16A, B). Apparently, these embryos received tamoxifen around E7.0 (-10ss) and were collected around E8.0-8.5 (0-9ss) (compare Fig. 15B and Fig. 16C). These embryos were therefore used to assess the dynamics of progenitor labeling prior to hepato-pancreatic lineage segregation. The contribution of labeled cells to the ventral foregut, which harbors hepato-pancreatic progenitors, was documented by co-immunostaining for GFP and Prox1 (Fig. 16B). Quantification of the labeled cells in the entire

endoderm (Fig. 16D) and the Prox1^{+} ventral foregut (Fig. 16E) showed a broad spread in the number of labeled cells in both tissues. Interestingly, the fraction of labeled endodermal cells found in the ventral foregut followed a distinct trend if plotted against the time point of label induction (Fig. 16F). Following the progression from early gastrulation (-15ss) to late gastrulation (-5ss), I noted a distinct drop in the fraction of labeled cells in the ventral foregut from 25% to about 5% of the entire population of labeled endodermal cells. This observation

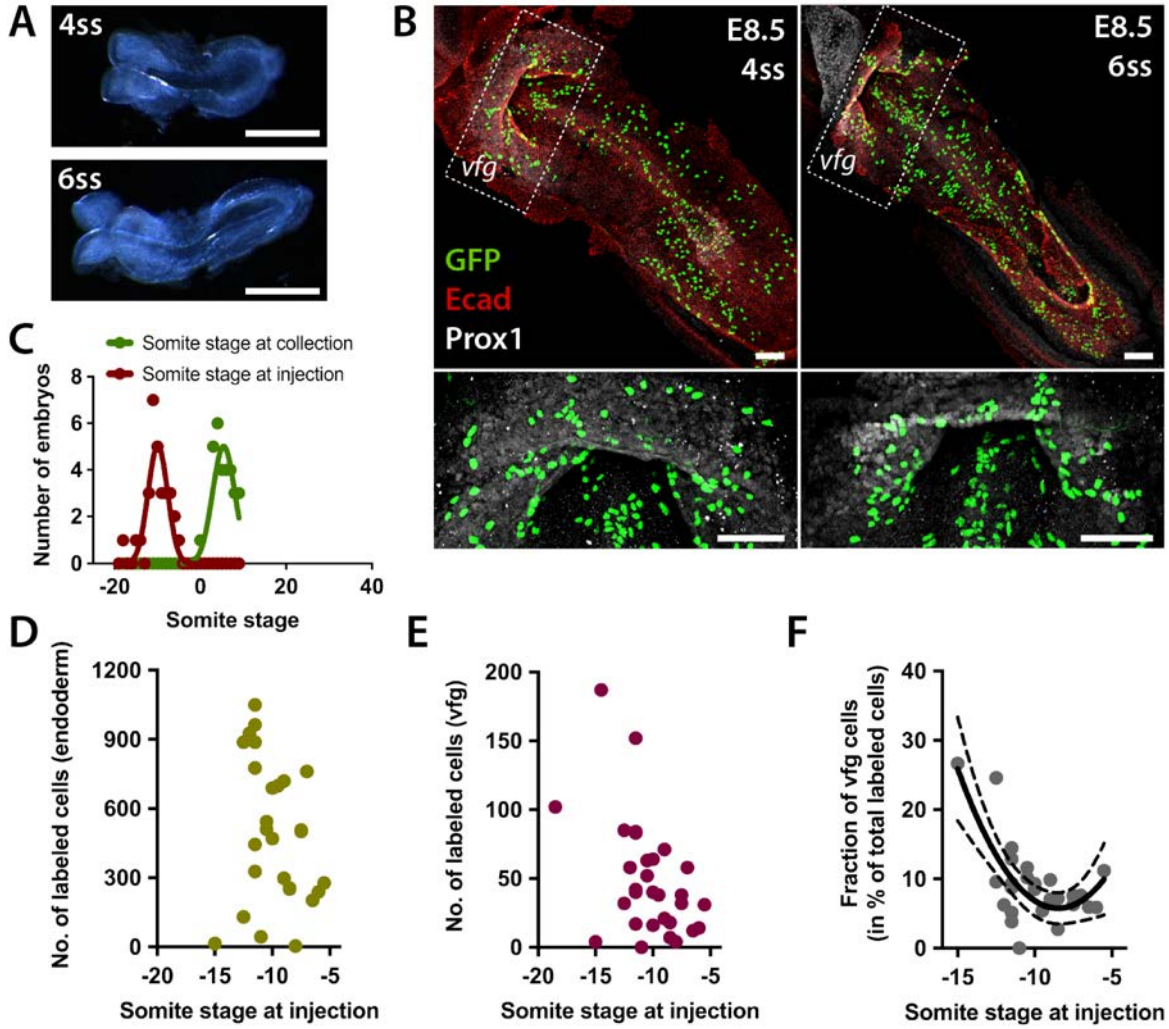

Fig. 16: Lineage tracing of ventral foregut progenitor cells. (A) Representative images of embryos of the indicated somite stage (ss) taken on a stereomicroscope. **(B)** Representative WMIF of E8.5 Tg(*Foxa2*-Cre-ERT; *R26R*-H2B-GFP) embryos. Immunostaining for GFP documents GFP^{+} (labeled) cells throughout the endoderm (marked by Ecad in red) including the ventral foregut (*vfg*, marked by Prox1 in grayscale). Lower panels show higher magnifications of the areas marked by white dotted boxes without the Ecad staining. **(C)** Graphical representation of the spread of embryonic stages at the time points of injection and embryo collection in the dataset (n=30). **(D, E)** The number of labeled cells in the total endoderm (D) or ventral foregut (E) are plotted against the somite stage at the time of injection. **(F)** Negative correlation of the fraction of ventral foregut cells (% of all GFP^{+} cells) in the endoderm with the somite stage at injection. (regression curve: 2nd order polynomial with 95% confidence interval; adjusted R^2: 0.46) (scale bars: (A) 1mm; (B) 100µm)

highlighted the fact that prospective foregut cells are amongst the first Foxa2^{+} definitive endodermal cells arising during gastrulation. Thus, label induction events during early gastrulation are more likely to result in a high percentage of labeled ventral foregut cells. By contrast, label induction at later gastrulation stages allows for labeling of cells already allocated to the fore-, mid-, and hindgut, lowering the % contribution of ventral foregut cells to the total population of GFP^{+} cells.

In conclusion, I successfully established the Foxa2-Cre line as a useful tool for unbiased lineage tracing of endodermal cells acquiring hepato-pancreatic fate. I established an experimental system and tamoxifen treatment protocol that enabled labeling of hepato-pancreatic organ rudiments. By analyzing time-dependent changes in the labeling efficiency of the ventral foregut as compared to the rest of the endoderm, I further demonstrated that developmental features of Foxa2 expression during gastrulation are faithfully recapitulated by the Foxa2-Cre transgene.

3.1.2 Lineage tracing uncovers time-dependent plasticity in the relationship of labeled cells in ventral foregut derivatives

A second subset of traced H2B-GFP embryos (Fig. 15B) encompassed 90 embryos that showed discriminable hepatic and pancreatic organ domains. These embryos received tamoxifen around E7.5, were collected between E8.5 and E10.5 (compare Fig. 15B and Fig. 17A) and used for analysis of hepato-pancreatic lineage segregation events. Towards this aim, the embryos were subjected to WMIF analysis and the number of GFP-labeled cells in liver, ventral, and dorsal pancreatic buds were quantified. Immunostaining for Prox1 was used to mark all hepato-pancreatic tissues, while Pdx1 immunostaining specifically marked ventral and dorsal pancreatic buds. First, I assessed whether ventral and dorsal hepato-pancreatic tissues showed comparable labeling behavior. To answer this question, the number of labeled cells in liver and ventral pancreas (Fig. 17B) or in dorsal pancreas (Fig. 17C) of each embryo were plotted against the respective somite stage at the time of tamoxifen injection. Indeed, a similar maximum in labeling intensity, as indicated by the peak of the respective regression

curves (compare Fig. 17 panel B and C), in these embryonic tissues was noted in the 20h time window preceding the formation of the first somite (-10-0ss).

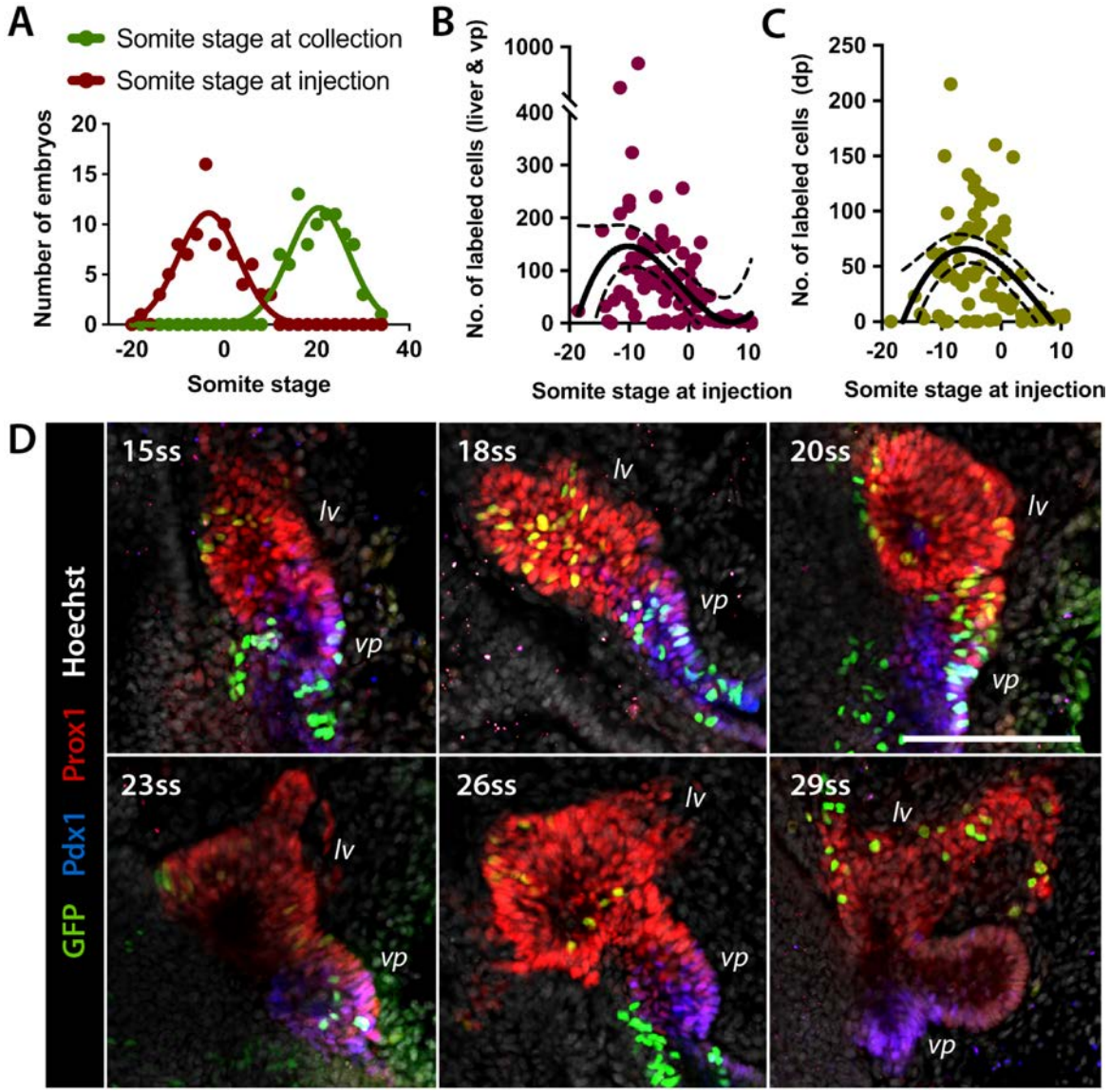

Fig. 17: Tracing of hepato-pancreatic cells. (A) Graphical representation of the spread of embryonic stage at the time points of injection and embryo collection in the dataset (n=90). **(B, C)** The number of GFP^+ (labeled) cells in the liver and ventral pancreas (B) or dorsal pancreas (C) are plotted against the somite stage at the time point of injection. A maximum in the labeling intensity is observable in the 20h time window prior to establishing the first somite (-10 to 0 somite stage) in both ventral and dorsal hepato-pancreatic tissues. (regression curves: 3rd order polynomial with 95% confidence interval; adjusted R^2: 0.15 (B), 0.19 (C)) **(D)** Representative WMIF of Tg(*Foxa2*-Cre-ERT; *R26R*-H2B-GFP) embryos at 15-29ss. Immunostaining of Prox1 (red) marks liver (*lv*), co-immunostaining of Prox1 and Pdx1 (blue) ventral pancreas (*vp*). Cells are counterstained with Hoechst dye (grayscale). Immunostaining of GFP documents labeled cells in liver and ventral pancreas. A reduction in the density of labeled cells in the ventral pancreas is observable with increasing somite stage. (scale bar: 100μm)

Interestingly, I observed distinct time-dependent changes in the number of labeled ventral pancreatic cells at the time of embryo collection. As documented in Fig. 17D, labeled cells were readily found in ventral pancreatic and hepatic tissue of younger embryos (E9.0-9.5; 15-20ss). However, as development progressed (E9.5-10.0; 23-29ss), I saw a distinct reduction in the density of GFP^+ cells in the ventral pancreatic ($Prox1^+$, $Pdx1^+$) but not in the hepatic domain ($Prox1^+$). To confirm that this reduction was ventral pancreas specific, I plotted the number of GFP-labeled cells in liver, ventral, and dorsal pancreas (Fig. 18A, B, and C,

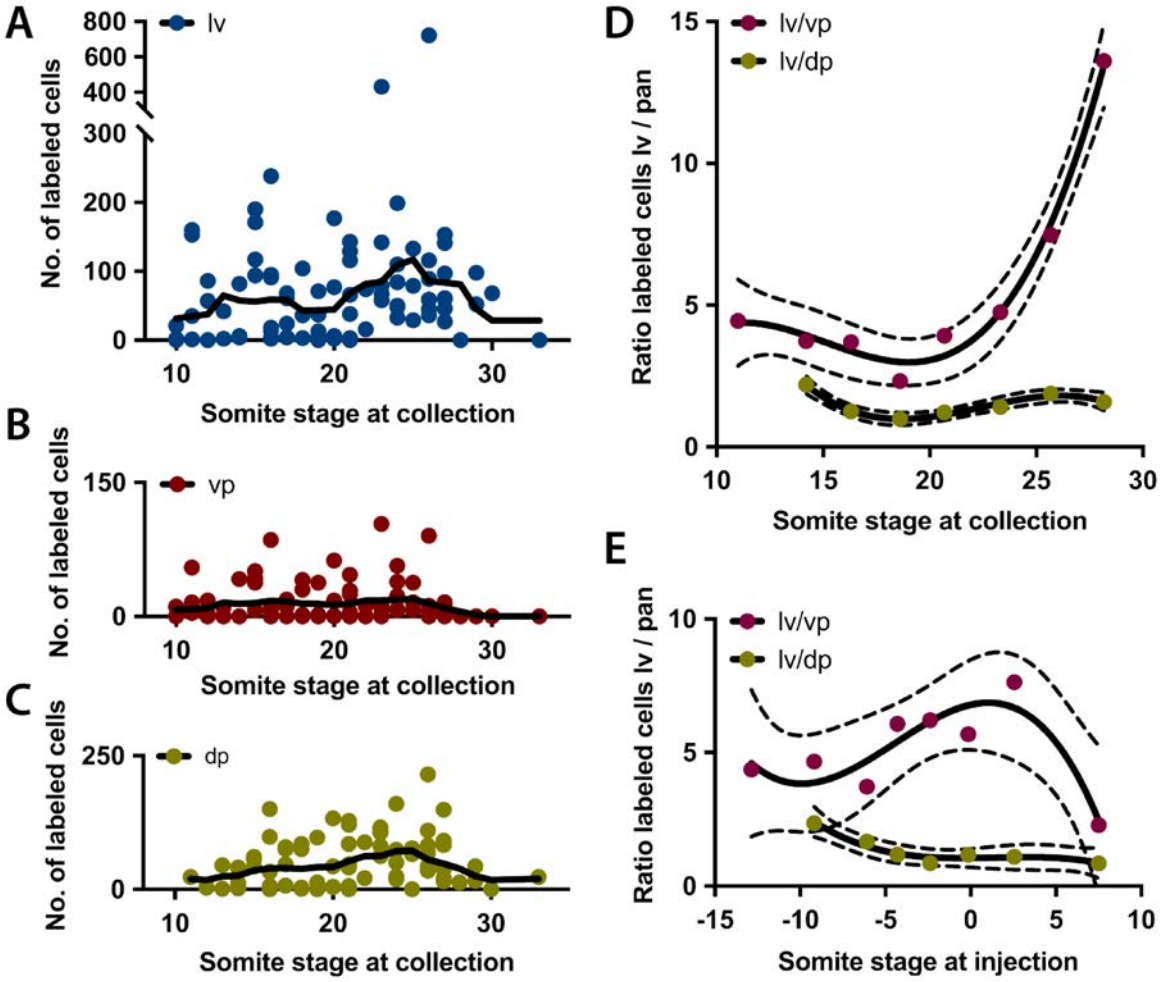

Fig. 18: The ratio of labeled cells in liver and ventral pancreas shifts with increasing somite stage. (A-C) The number of GFP^+ (labeled) cells in the liver (lv) (A), ventral (vp) (B), or dorsal pancreas (dp) (C) are plotted against the somite stage at the time of collection (n=90; line shows 2-neighbor running average). No labeled cells are found in the ventral pancreas of embryos older than 27 somites. **(D, E)** The ratio of labeled cells in liver to either ventral pancreas (lv/vp) or dorsal pancreas (lv/dp) is plotted against the somite stage at the time of collection (D) or injection (E). For this purpose, embryos of similar somite stage (collection or injection) were grouped and the sum of all labeled cells in lv, vp, and dp were used for calculation of the depicted ratios. A positive correlation between the somite stage at collection and the ratio of labeled lv cells to vp cells is observable (D). (regression curves: 3rd order polynomial with 95% confidence interval; adjusted R^2 for lv/vp: 0.98 (D), 0.63 (E); adjusted R^2 for lv/dp: 0.94 (D), 0.88 (E))

respectively) against the somite stages at the time of embryo collection. The graphs in Fig. 18A-C represent 2-neighbor-running average and document only a slight drop in the number of labeled cells in liver and dorsal pancreas after 27ss. However, for the ventral pancreas I did not observe any labeled cells in embryos older than 27ss.

To further elucidate why the labeling density in the ventral pancreas dropped in later stage embryos, I examined the relationship between the ventral foregut derivatives liver and ventral pancreas systematically. Towards this aim, embryos of similar somite stages at the time of collection in this dataset were grouped and the sum of labeled liver and labeled ventral pancreatic cells, as well as their ratio was calculated. Next, the calculated liver to ventral pancreas ratios were plotted against the average somite stage at the time of collection of the respective group of embryos (Fig. 18D). Evaluating the regression line through the data points, it was apparent that the liver to ventral pancreas ratio (lv/vp) remained fairly constant until around 20ss. Thereafter, a strong positive correlation of the labeled cell ratio (lv/vp) with the somite stage at the time of embryo collection became visible. This observation suggested that after the initial separation of ventral hepato-pancreatic progenitors towards hepatic or pancreatic fate, a second developmental mechanism must be in place resulting in a constant shift in the ratio of labeled liver to labeled ventral pancreatic cells. To control that this phenomenon was specific to the ventral foregut derivatives I performed an analogous analysis using the same groups of embryos to calculate the ratio between labeled liver and labeled dorsal pancreatic cells (lv/dp). Fig. 18D shows that the liver to dorsal pancreas ratio remained fairly constant over the entire sampling period.

To exclude that the time-dependent changes in the ratio of labeled liver to labeled ventral pancreatic cells were an artefact of differential labeling of hepatic versus ventral pancreatic progenitors, I went on to examine the influence of the time point of label induction on the liver to ventral pancreas cell ratio. Towards this aim, the previously analyzed dataset was differently grouped: embryos of similar somite stages at the time of label induction were grouped and the sum of labeled liver, ventral, and dorsal pancreatic cells within each group calculated. The respective ratios of liver to ventral (lv/vp) or liver to dorsal pancreas (lv/dp) were derived and plotted against the average somite stage at the time of label induction within each group (Fig. 18E). No correlation between the ratio of either labeled liver to labeled

ventral pancreas or labeled liver to labeled dorsal pancreas with the somite stage at the time of label induction was observed. Thus, in contrast to the somite stage at the time of embryo collection, the embryonic stage at the time of label induction had no influence on the ratio of labeled liver to labeled ventral pancreatic cells (compare Fig. 18D and Fig. 18E).

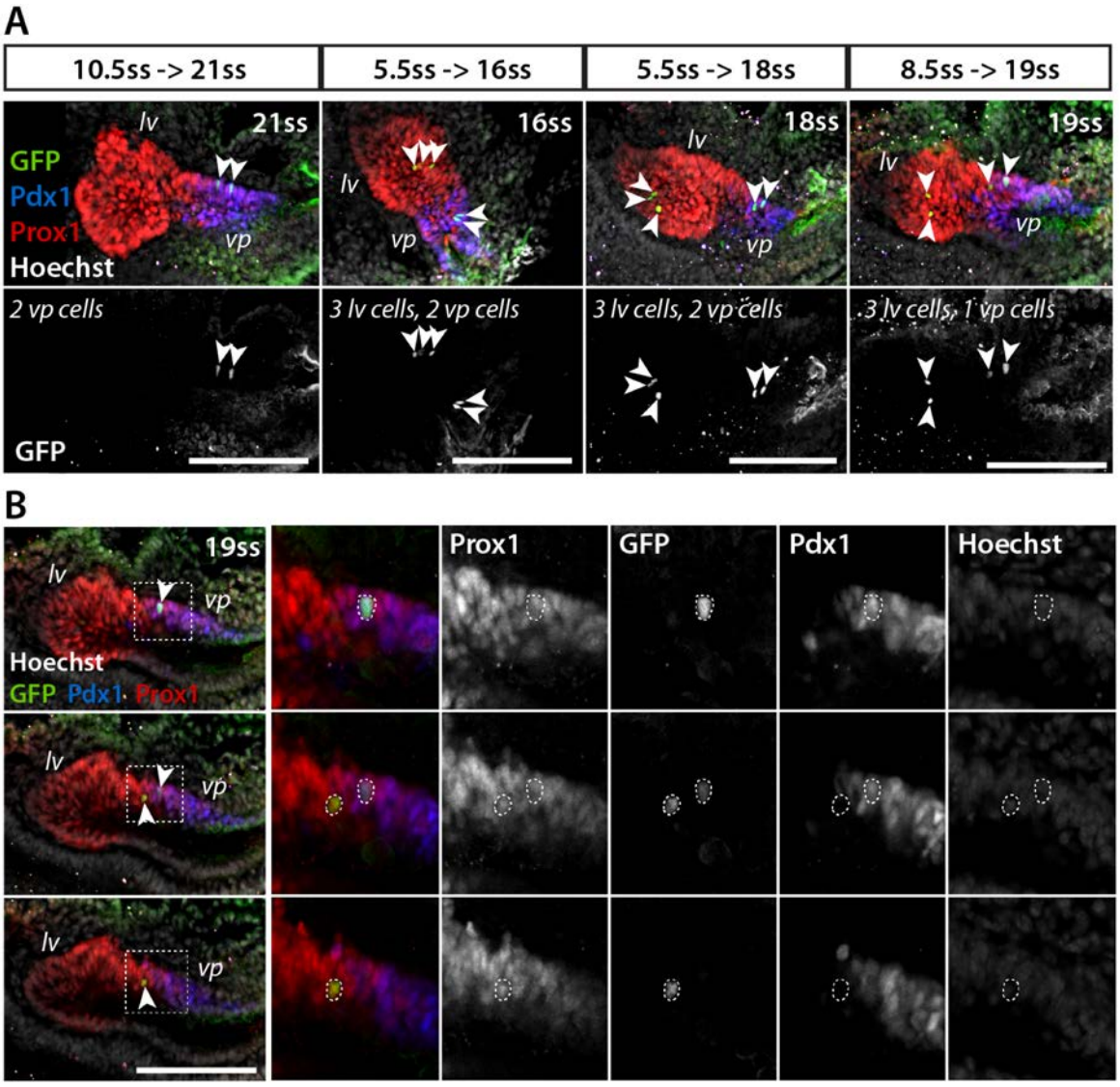

Fig. 19: Label induction at E8.5 allows clonal labeling of hepato-pancreatic progenitors. (A) WMIF of E9.5 Tg(*Foxa2*-Cre-ERT; *R26R*-H2B-GFP) embryos (16-21ss) labeled by tamoxifen injection at E8.5 (5.5-10.5ss). Immunostaining of Prox1 (red) marks liver (*lv*), co-immunostaining of Prox1 and Pdx1 (blue) ventral pancreas (*vp*). Cells are counterstained with Hoechst dye (grayscale). Immunostaining of GFP documents low numbers of labeled cells in liver and ventral pancreas (arrowheads). Commonly, 2-3 labeled cells are in close proximity to one another and likely represent descendants of a common labeled progenitor cell. The lower row shows the GFP channel in grayscale. The number of labeled cells found in liver and ventral pancreas are stated in the upper left corner. **(B)** Optical sections of the WMIF of the 19ss embryo shown in panel A. Left panels show entire hepatic and ventral pancreatic domain, while right panels show magnifications and single fluorophore channels of the boxed region of interest. The indicated cells (arrowheads or dotted line) represent descendants of a single bipotent progenitor cell. One cell has adopted a hepatic fate (absence of Pdx1; see right panels) while the other adopted a pancreatic fate (expression of Pdx1; see right panels). (scale bars: 100μm)

During my Foxa2-Cre-ERT lineage tracing experiments, I also achieved clonal labeling in a small subset of embryos. Clonal labeling refers to a labeling event in a single progenitor in a tissue of interest. Subsequent analysis of the fate of its progeny might reveal the developmental potential(s) of the originally labeled cell. Fig. 17B shows that the number of labeled cells in embryos that received tamoxifen at time points later than 5ss drops dramatically. WMIF images of a subset of these embryos are presented in Fig. 19. All depicted embryos show less than 6 labeled cells in liver and ventral pancreas. Commonly, 2-3 labeled cells are in close proximity to one another and likely represent descendants of a common labeled progenitor cell. An interesting observation was made in the 19ss embryo shown in Fig. 19A (maximum intensity projection) and highlighted in Fig. 19B (optical sections). The indicated GFP^+ cells are likely descendants of a common progenitor due to their close proximity in the tissue. However, while one cell has adopted a pancreatic identity, as shown by Pdx1 expression, the other one acquired a hepatic fate, as documented by the absence of Pdx1. This observation argued for the existence of a common bipotent progenitor cell with the developmental potential for hepatic or ventral pancreatic fate.

3.1.3 Analysis of tissue dynamics shows difference in organ growth of liver and ventral pancreas despite similar proliferative properties

Employing the Foxa2-Cre mouse line for lineage tracing, my studies thus far showed that dorsal pancreatic and ventral hepato-pancreatic domains present similar labeling dynamics. However, my studies also uncovered the surprising finding that the ratio of labeled liver to labeled ventral pancreatic cells is dependent on the somite stage at the time of embryo collection (Fig. 18D). One possible explanation for the increase in the ratio of labeled liver to labeled ventral pancreatic cells at later somite stages might be differences in proliferation dynamics in liver versus ventral pancreatic buds. Specifically, higher levels of proliferative activity in the liver as compared to the ventral pancreas may lead to a more pronounced increase in the number of labeled liver cells over time. To test this hypothesis, I set out to explore hepato-pancreatic tissue dynamics during early development in more detail.

First, I collected embryos with somite stages ranging from E8.5 (10ss) to E10.0 (30ss) and analyzed the expression of the hepato-pancreatic marker Prox1 and pancreatic marker Pdx1 by WMIF. A selection of these WMIF images is shown in Fig. 20. They illustrate the immense morphological changes undergone by the ventral foregut endoderm during its early development. Next, I quantified the organ volume of liver (n=90) as well as ventral (n=93) and dorsal pancreata (n=86) throughout the analyzed developmental time period (Fig. 21). Organ volume was determined from WMIF confocal z-scans by measuring organ area on individual optical sections. The average area was then multiplied by tissue depth to obtain the total organ volume. Fig. 21A shows continuous growth of the liver throughout the analyzed period, while little change in ventral pancreas volume was detectable.

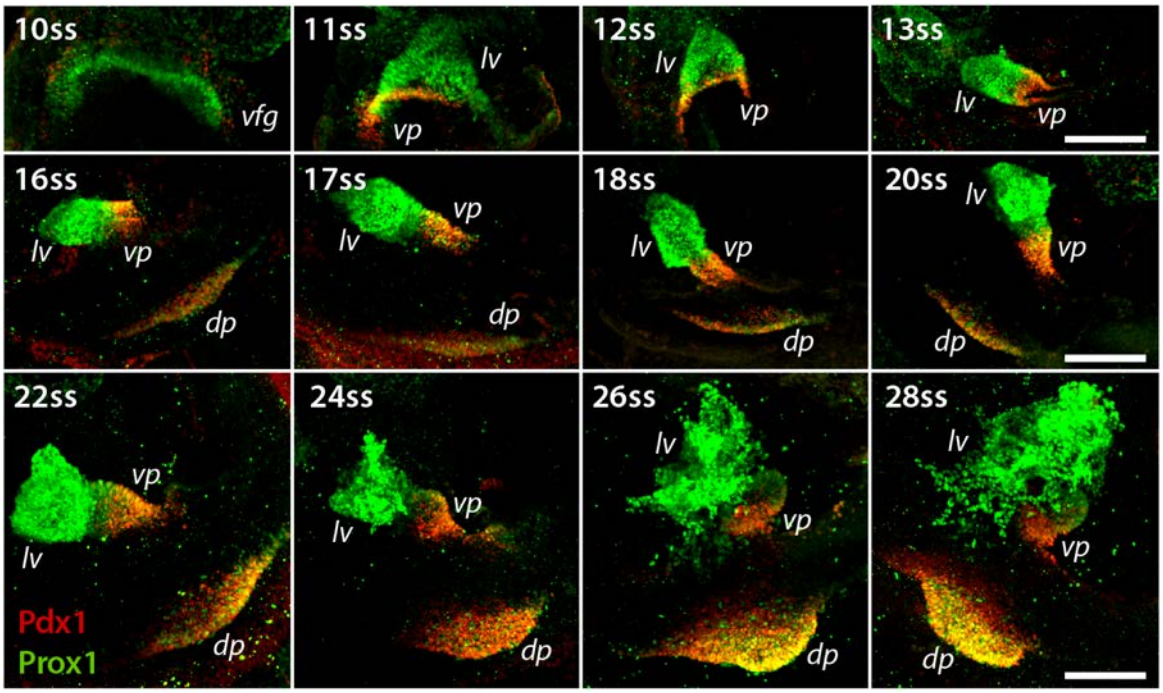

Fig. 20: Ventral foregut morphogenesis. Representative WMIF of embryos from E8.5 to E9.75 (10-28ss). Immunostainings of Prox1 (green) and Pdx1 (red) mark the ventral foregut region (*vfg*) as well as liver (*lv*), ventral (*vp*) and dorsal pancreatic buds (*dp*). Substantial time-dependent changes in morphology of these developing organs are observable. (scale bars: 100μm)

This observation was corroborated by plotting the ratio of liver to ventral pancreas volumes of individual embryos against the somite stage of the respective embryo (Fig. 21C). A strong positive correlation between the ratio of liver to ventral pancreas volume and the somite stage was evident. In contrast to the ventral pancreas, the dorsal pancreas showed a more pronounced volume growth (Fig. 21B). To discern the relationship between ventral and dorsal

hepato-pancreatic organ growth, the ratio of the volume of ventral foregut derivates (sum of liver and ventral pancreas volume) to dorsal pancreas volume was calculated for each embryo. Plotting this ratio against the somite stage of the respective embryo, a slight increase in the ratio of ventral foregut to dorsal pancreas volume at later somite stages was seen (Fig 21D). Notably, this increase was considerably less dramatic (Fig. 21D, slope: 0.13/ss) as compared to the liver to ventral pancreas ratio over somite stage (Fig. 21C, slope: 0.43/ss).

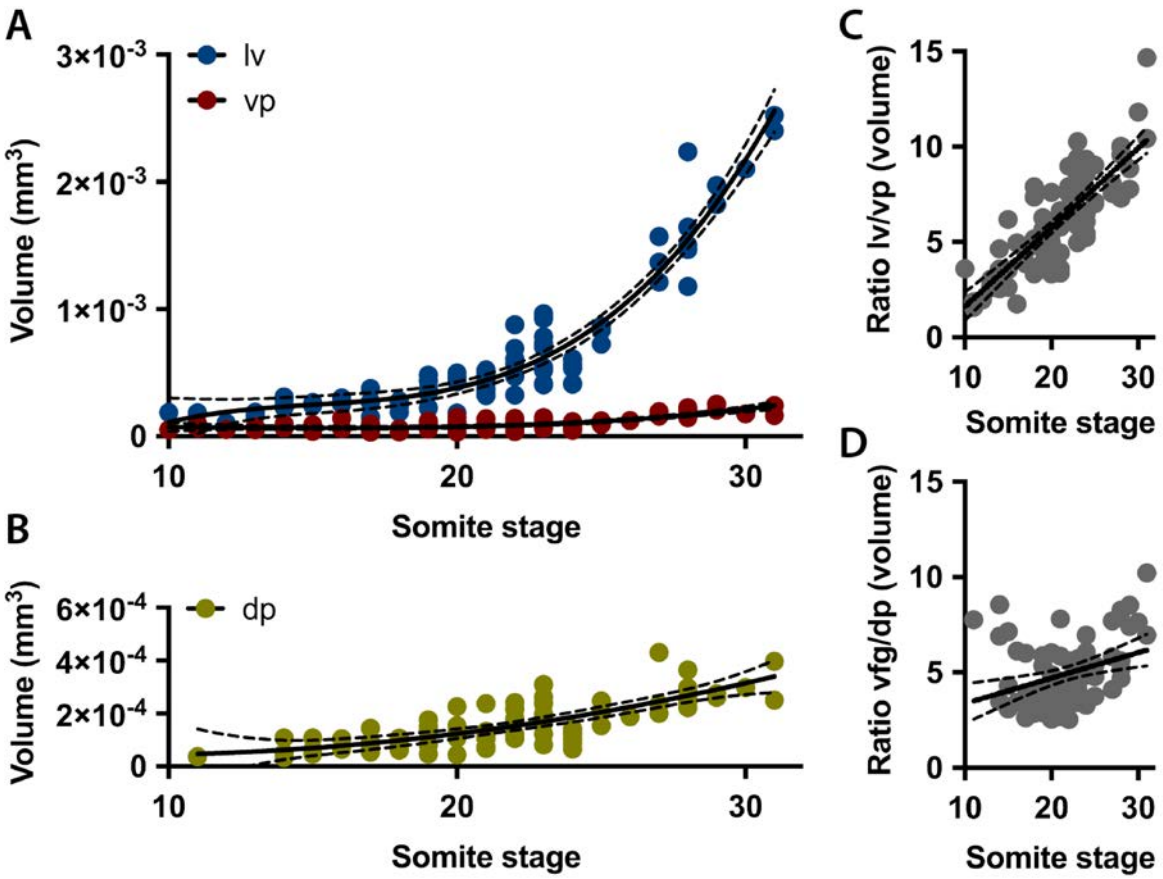

Fig. 21: Organ volume changes during hepato-pancreatic development. (A, B) Measurement of organ bud volume of liver (lv; n=90) and ventral (vp; n=93) (A), as well as dorsal pancreas (dp, n=86) (B) at the indicated somite stages shows a stronger increase in liver volume as compared to dorsal and ventral pancreas. (regression curves: 3rd order polynomial with 95% confidence interval; adjusted R^2: 0.91 (lv), 0.62 (vp), 0.56 (dp)) **(C, D)** The ratios of volume of liver versus ventral pancreas (C) or of liver and ventral pancreas (vfg) versus dorsal pancreas (D) increase with somite stages. The increase in ratio over time is more pronounced in (C) (slope: 0.42) as compared to (D) (slope: 0.13). (regression lines: linear with 95% confidence interval; adjusted R^2: 0.67 (C), 0.10 (D))

The results of the organ volume analyses argued for a stronger increase in organ bud growth in the liver as compared to the ventral pancreas. Yet, bud volume per se might not be the most informative parameter for comparing organ growth in liver and ventral pancreas. Indeed, the morphology of the liver undergoes dramatic changes during the investigated time

period (Fig. 20)[15,19]. Hepatoblasts begin as a multilayered epithelium but soon form hepatic chords and invade the surrounding mesenchyme. In contrast, the ventral pancreas remains an epithelial bud throughout the analyzed time period[13,112]. As organ volume is also influenced by cell and tissue morphology, I chose to refine the tissue growth analysis by

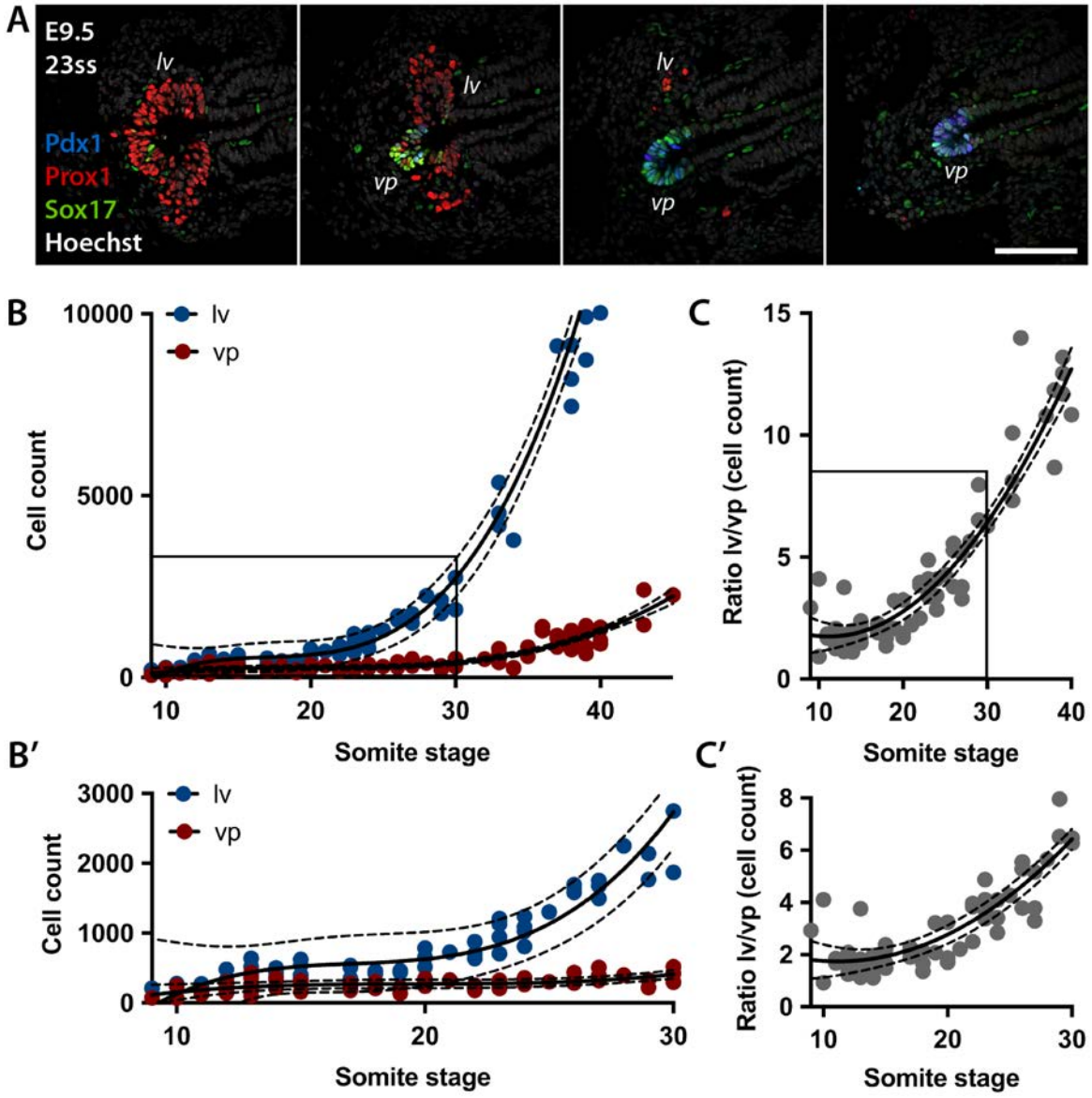

Fig. 22: Quantitative histological analysis reveals differences in growth of liver and ventral pancreas. (A) Representative IF staining of consecutive cryosections of the developing liver (*lv*) and ventral pancreatic bud (*vp*) of an E9.5 (23ss) embryo. Immunostaining of Prox1 (red) marks liver, while co-immunostaining of Prox1, Pdx1 (blue), and Sox17 (green) marks ventral pancreas. Cells are counterstained with Hoechst dye (grayscale). **(B, B')** Measurements of organ bud cell count at the indicated somite stages show a stronger increase in the liver (n=72) as compared to the ventral pancreas (n=95). Panel B' shows magnification of the boxed region in panel B. (regression curves: 3rd order polynomial with 95% confidence interval; adjusted R^2: 0.90 (lv), 0.85 (vp)) **(C, C')** The ratio of liver versus ventral pancreas cell count increases dramatically with later somite stages. Panel C' shows magnification of the boxed region in panel C. (regression curve: 3rd order polynomial with 95% confidence interval; adjusted R^2: 0.89) (scale bar: 100μm)

examining changes in liver and ventral pancreas cell counts, thereby eliminating any bias from differences in average cell size in the two organs.

Accordingly, I collected embryos from E8.5 to E11.5 (9-45ss) and prepared two series of 10μm cryosections per embryo. One series per embryo was subjected to immunofluorescence (IF) staining for the hepato-pancreatic marker Prox1 and the ventral pancreatic markers Pdx1 and Sox17. Sections of the entire liver and ventral pancreatic bud were imaged, as exemplified in Fig. 22A. Cell counts for liver ($Prox1^+$) and ventral pancreas ($Prox1^+$, $Pdx1^+$, $Sox17^+$) were manually quantified and plotted against the somite stage of the respective embryo (Fig. 22B and B'). In accordance with the volume analysis (Fig. 21A), I observed a strong and continuous increase in cell counts in the liver bud. By contrast, the ventral pancreatic cell count remained almost constant until about 30ss when it started to increase moderately. The discrepancy between the increase of liver and ventral pancreatic cell counts was again illustrated by plotting the ratio of liver to ventral pancreas cell counts for each embryo against its respective somite stage (Fig. 22C and C').

The most likely explanation for the differential increase in cell counts between liver and ventral pancreas might be that the two tissues exhibit different proliferation dynamics. Specifically, hepatic cells may show a higher proliferative activity or a shorter cell cycle length and thus increase more dramatically in numbers over time as compared to ventral pancreatic cells. To test this hypothesis, I collected embryos from E8.5 to E10.0 (10-29ss) and subjected them to WMIF analysis (Fig. 23A and B). The embryos were stained for the mitotic marker phospho-histone 3 (pH3) as well as for proteins marking the developing gut tube (Ecad), the liver (Prox1 and Ecad), and the ventral pancreatic bud (Ecad, Prox1, and Pdx1). Embryos of similar somite stages were grouped and the number of $pH3^+$ cells per organ rudiment quantified and normalized to the respective organ bud volume (Fig. 23C). I noticed that with increasing somite stage the rate of $pH3^+$ cells per volume decreased in liver as well as ventral pancreas with no statistically significant difference between the two organ buds at any time point (Kruskal-Wallis test, Dunn's multiple comparisons test) (Fig. 23C).

The fact that no difference in numbers of $pH3^+$ cells existed comparing liver and ventral pancreatic bud argued that the two tissues show similar proliferative activity between E8.5

and E10.0. To corroborate this finding, I performed a bromodeoxyuridine (BrdU) incorporation assay in developing embryos. This assay is based on the fact that cells in S-phase incorporate the thymidine-analog BrdU into the replicating DNA strands. Subsequently, BrdU

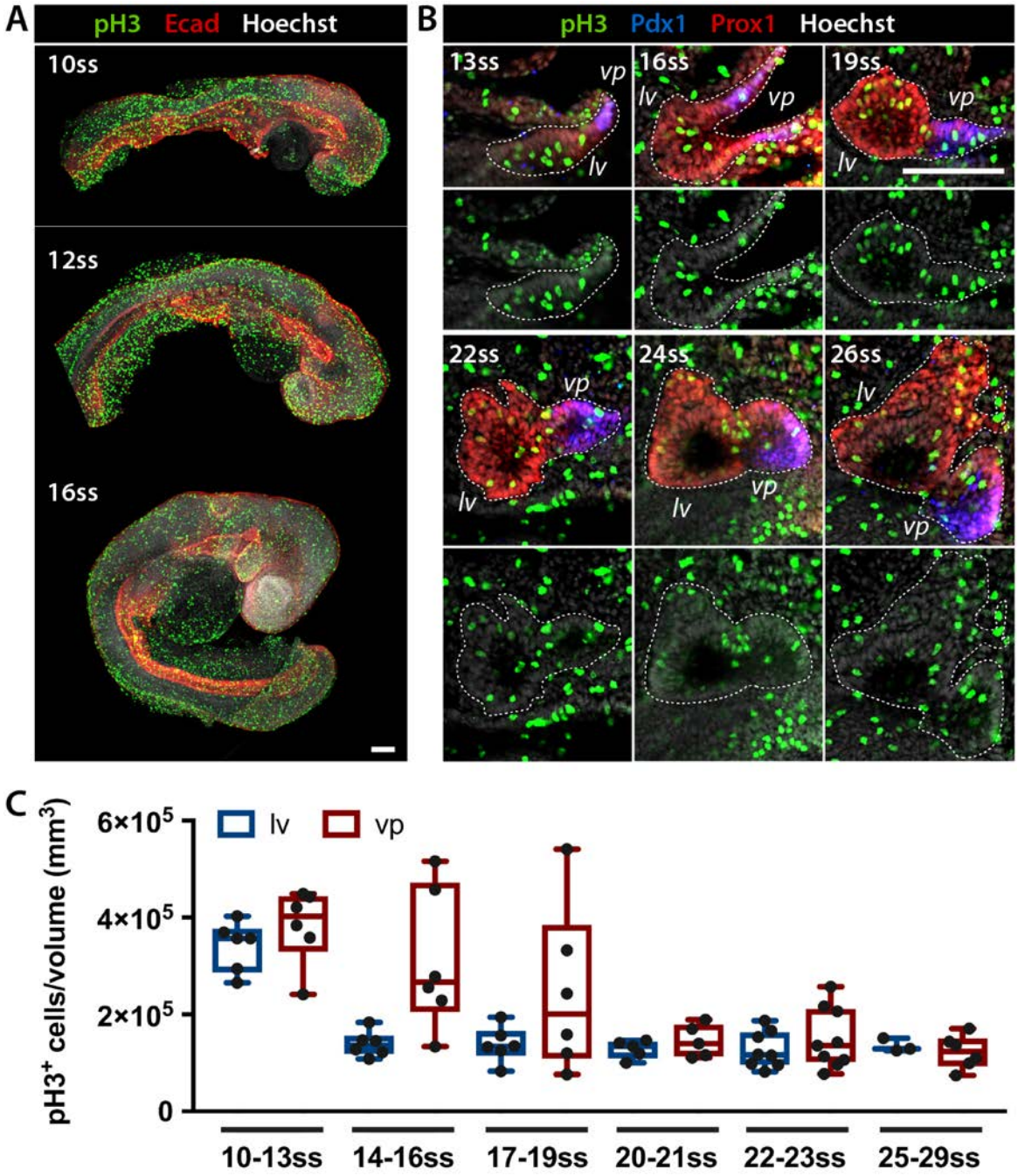

Fig. 23: Similar phospho-histone 3 dynamics in liver and ventral pancreas. (A) Representative WMIF of E8.5-E9.0 (10-16ss) embryos for the mitotic marker phospho-histone 3 (pH3, green). Immunostaining of Ecad (red) serves to visualize the developing gut tube. **(B)** Representative WMIF of E8.75-E9.5 (13-26ss) embryos for pH3 marking mitotic cells. Immunostaining of Prox1 (red) marks liver (*lv*), co-immunostaining of Prox1 and Pdx1 (blue) the ventral pancreas (*vp*). Tissues are counterstained with Hoechst dye (grayscale). **(C)** Measurements of $pH3^+$ cells normalized to organ volume at the indicated somite stages show a reduction in the mitotic rate with increasing somite stage in liver (n=34) and ventral pancreas (n=38). No statistically significant difference between the two tissues is seen. (scale bars: 100μm)

can be detected by IF staining providing a measure of the cell fraction that was in S-phase during the labeling period. To examine the cell fraction in S-phase in the developing hepatic and ventral pancreatic organ rudiments, I injected pregnant females with BrdU (75μg/g bw) at E8.5 or E9.5 and used tracing periods of 1h, 2h or 4h. Subsequently, the embryos were collected and cryosections prepared for IF analysis for BrdU, Prox1, as marker of liver and ventral pancreas, and Pdx1 as marker of the ventral pancreas (Fig. 24A). Fig. 24 panels B and C show the quantification of the $BrdU^+$ cell fractions in liver and ventral pancreas for different tracing periods at E8.5 (Fig. 24B) or E9.5 (Fig. 24C). At no developmental time point or tracing period did I observe statistically significant differences in the size of the $BrdU^+$ cell fractions in liver and ventral pancreas (Kruskal-Wallis test, Dunn's multiple comparisons test).

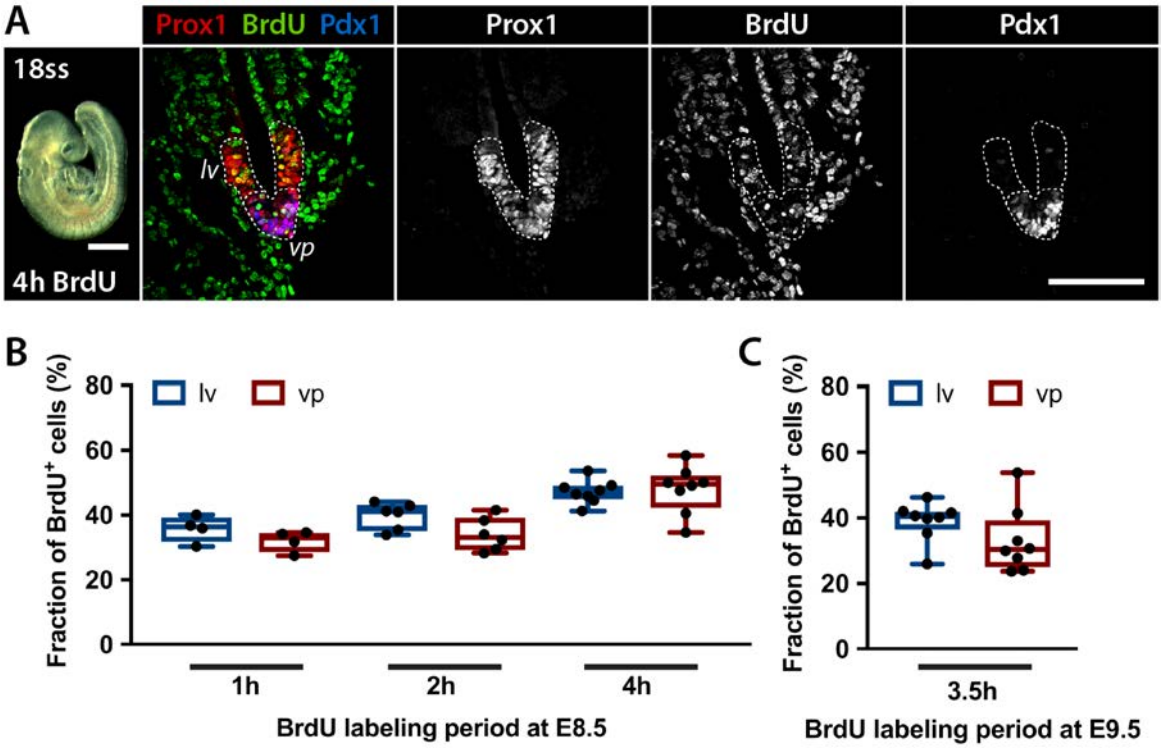

Fig. 24: Bromodeoxyuridine incorporation assay reveals similar proliferation dynamics in liver and ventral pancreas. (A) Panel on the left shows the image of a 18ss embryo taken on a stereomicroscope. Panels on the right show IF staining of cryosections from an E9.0 (18ss) embryo for incorporation of bromodeoxyuridine (BrdU) during 4h BrdU labeling period. Immunostaining of Prox1 (red) marks liver (*lv*), co-immunostaining of Prox1 and Pdx1 (blue) the ventral pancreas (*vp*). Images are given as merged color or as single channel gray scale configuration. **(B, C)** Measurements of $BrdU^+$ cell fractions in liver and ventral pancreas at E8.5 (B) or E9.5 (C) show no statistically significant difference between the two organ buds for the indicated BrdU labeling periods. ((B) 1h: n=4; 2h: n=6; 4h: n=8; (C) n=8 (shows combined data for 2h: n=2 and 4h: n=6)) (scale bars: 1mm (A, left panel), 100μm (A, right panels))

In line with the results obtained by analyzing $pH3^+$ levels in liver and ventral pancreas (Fig. 23), the BrdU incorporation assay also suggested that cells in liver and ventral pancreas show similar proliferative activities. To ascertain that the difference in cell count increase between liver and ventral pancreas was not due to an accelerated cell cycle time in liver cells, I performed an additional analysis using the data from the BrdU incorporation assay. Sanders et al.[203] as well as van den Berg et al.[204] reported a method to estimate the average cell cycle length in a tissue of interest on the basis of multiple BrdU incorporation assays using different tracing times. In accordance with their methods[203,204], I plotted the data of the $BrdU^+$ cell fractions in liver (Fig. 25A) and ventral pancreas (Fig. 25B) for E8.5 embryos against the respective tracing period. Next, I plotted linear regression lines through the data points and determined the slope of the regression lines for liver and ventral pancreas data. The resulting overlap of the two regression lines and their 95% confidence intervals (CI) are shown in Fig. 25C, substantiating the apparent similarity in BrdU incorporation dynamics in liver and ventral pancreas. To corroborate this similarity, I performed a two-way-ANOVA analysis to test for an influence of the tracing period or tissue type on the $BrdU^+$ cell fraction. While the length of the tracing period showed a significant influence ($p\text{-value}<0.0002$) on the $BrdU^+$ cell fraction, no significant influence of the tissue type, i.e. liver or ventral pancreas, could be documented.

To estimate the average cell cycle length in cells of liver and pancreas I calculated the reciprocal for the slope of the regression line (equation shown in Fig. 25D). According to this calculation, the average cell cycle length for hepatic cells at E8.5 was 26.6h, while ventral pancreatic cells exhibited an average cell cycle length of 17.3h. If the slopes of the upper and lower confidence interval limits were considered, the average cell cycle length was 19 to 44.7h for hepatic and 12.2 to 29.6h for ventral pancreatic cells (Fig. 25D). Statistical analyses of the hepatic and ventral pancreatic cell cycle length by Mann-Whitney test did not document a significant difference between the two tissues. Thus, the estimation of the average cell cycle length in liver and ventral pancreas ruled out the possibility of an accelerated cell cycling time in hepatic cells underlying the increase in cell count and organ volume in liver over ventral pancreas.

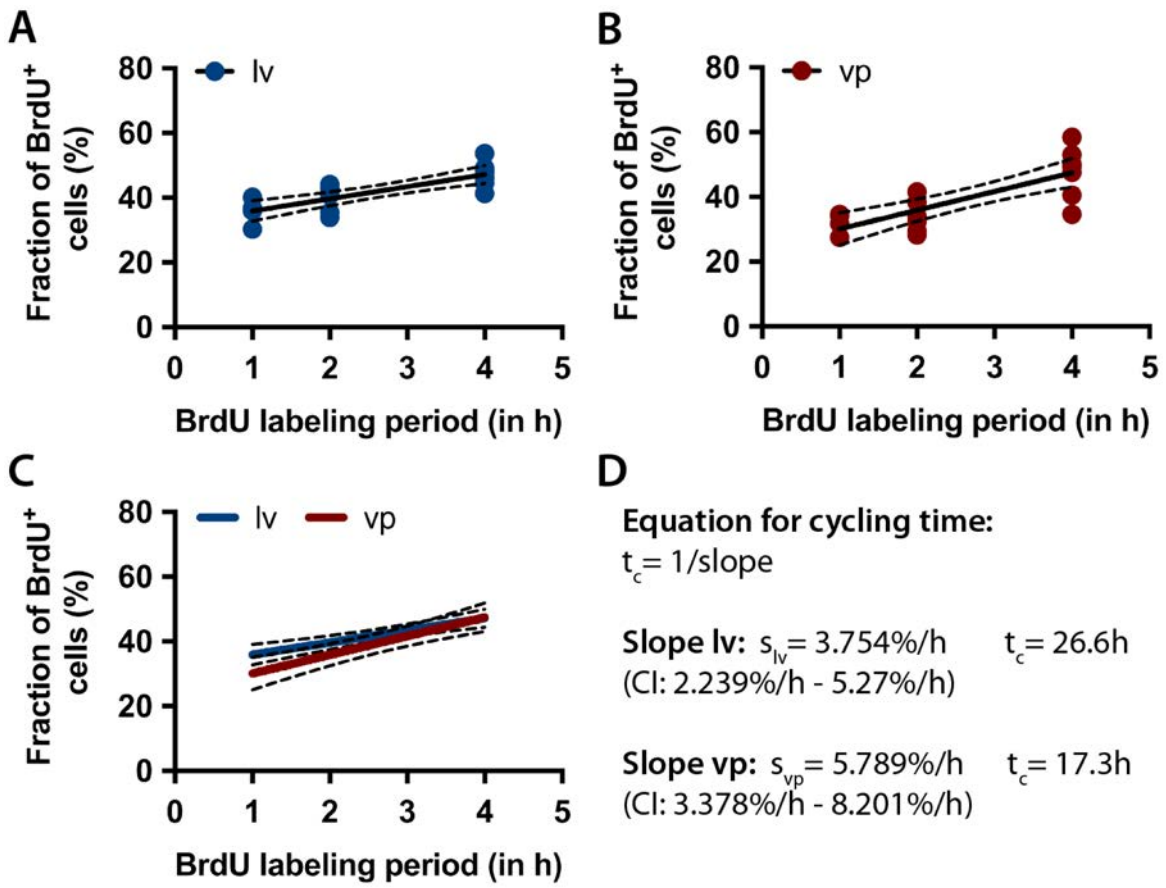

Fig. 25: Estimated cell cycle times of hepato-pancreatic progenitors. (A, B) Measurements of the increase in $BrdU^+$ cell fractions in hepatic (lv) (A) and ventral pancreatic (vp) domains (B) at E8.5. (regression lines: linear with 95% confidence interval (CI); adjusted R^2: 0.61 (A), 0.59 (B)) **(C)** Overlap of regression lines for liver and ventral pancreatic progenitors demonstrates similar proliferation dynamics. **(D)** Approximation of the cell cycle length on the basis of BrdU incorporation (Sanders et al., 1993[203]; van den Berg et al., 2009[204]) argues for an increased cell cycling time in hepatic as compared to ventral pancreatic progenitors. (lv: 26.6h (range 95% CI: 44.7h-19h); vp: 17.3h (range 95% CI: 29.6h-12.2h))

3.2 Lineage tracing analysis reveals plasticity between ventral pancreas and liver at late developmental time points

In chapter 3.1, I documented profound differences in the growth of liver and ventral pancreas. Liver bud volume and cell number increased dramatically over the time period of E8.5 to E11.5, whereas the ventral pancreas remained relatively consistent in terms of organ size and cell count between E8.5 to E10.0 and noticeable growth occurred only after about 30ss. My results also suggested that the difference in organ growth is not due to different proliferation dynamics in liver and ventral pancreas (Figs. 23-25).

In the light of these results, I considered another hypothesis for testing. The change in the ratio of labeled liver to labeled ventral pancreatic cells and the concurrent difference in organ growth (albeit at similar proliferation dynamics) may be explained by a constant flux of ventral pancreatic cells contributing to the growing liver bud. To test this hypothesis, I performed additional lineage tracing studies in hepato-pancreatic and ventral pancreatic progenitors to follow up on my findings from the Foxa2-Cre lineage tracing in endodermal cells (Figs. 14-19).

3.2.1 Dorsal and ventral hepato-pancreatic progenitors arise from distinct embryonic regions but are both characterized by expression of Prox1

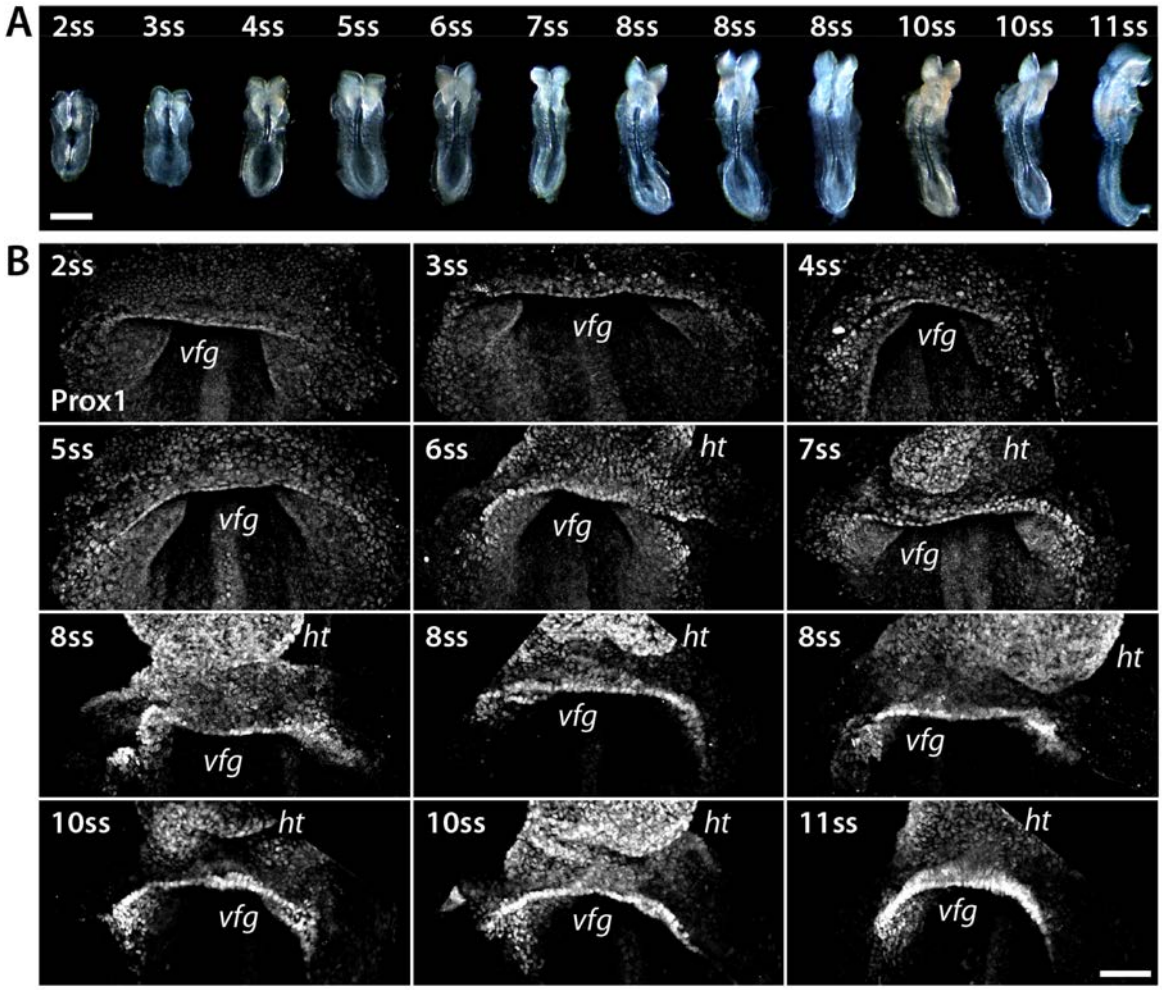

Fig. 26: Prox1 expression in the ventral foregut at E8.5. (A) Representative images of embryos of the indicated somite stage taken on a stereomicroscope. **(B)** Representative WMIF of embryos from E8.0 to E8.75 (2-11ss). Immunostaining of Prox1 marks the ventral foregut region (*vfg*) throughout the indicated somite stages as well as the developing heart (*ht*) from 6ss onwards. (scale bars: (A) 1mm; (B) 100μm)

To perform lineage tracing studies in hepato-pancreatic progenitors, I required a suitable marker gene specifically expressed in this cell type. As introduced in chapter 1.2.2, the homeobox transcription factor Prox1 is the earliest marker specific for all three hepato-pancreatic organ domains, namely liver, ventral, and dorsal pancreas. Fig. 26 documents Prox1 expression by WMIF in the ventral foregut region from early somite stages (>2ss) onwards. While Prox1 at early somite stages (Fig. 26B, 2-6ss) is detected at low levels, its expression level increases as development progresses (Fig. 26B, 6-11ss). Still, I was only able

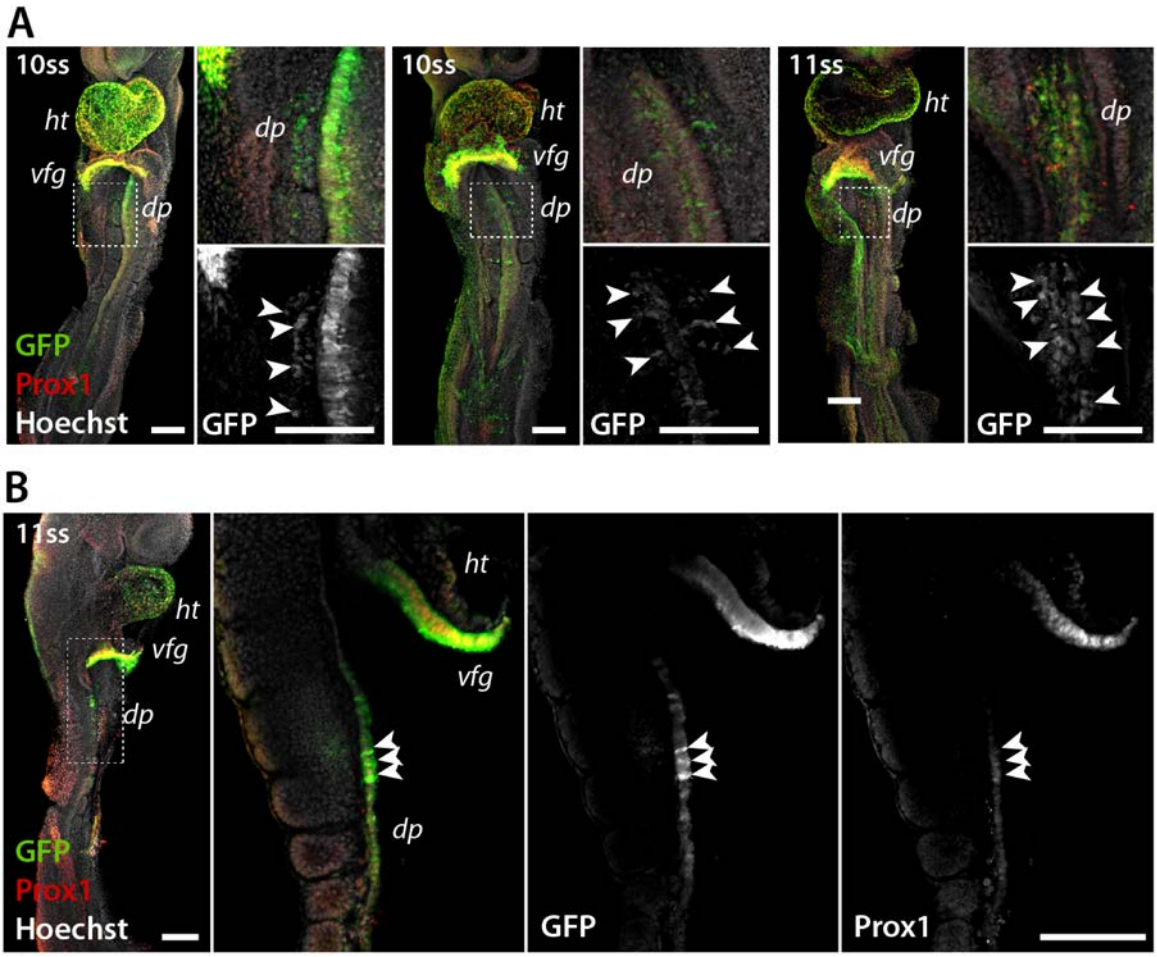

Fig. 27: Early induction of Prox1 expression in dorsal pancreatic progenitors as revealed by use of the Tg(*Prox1*-EGFP) mouse strain. (A) Representative WMIF of E8.5 (10-11ss) Tg(*Prox1*-EGFP) embryos. Induction of EGFP expression in dorsal pancreatic progenitors (*dp*) in the lateral dorsal foregut endoderm is documented by anti-GFP antibody staining (green, see arrowheads). At this embryonic stage, expression of Prox1 (red) is too low to be detected in the majority of dorsal pancreatic cells. In heart (*ht*) and ventral foregut (*vfg*), co-expression of Prox1 and EGFP is clearly visible. Tissues are counterstained with Hoechst dye (grayscale). Panels to the right show higher magnification of boxed area indicated in the respective panel on the left (merged and as single GFP channel). **(B)** WMIF of a 11ss Tg(*Prox1*-EGFP) embryo showing co-expression of Prox1 and EGFP in a subset of dorsal pancreatic progenitor cells (arrowheads). Panels to the right show higher magnification of an optical section (merged or as single channels) of the boxed area in the overview image to the left. (scale bars: 100μm)

to detect endogenous Prox1 expression in the ventral (Fig. 26) but not in the dorsal foregut at early somite stages.

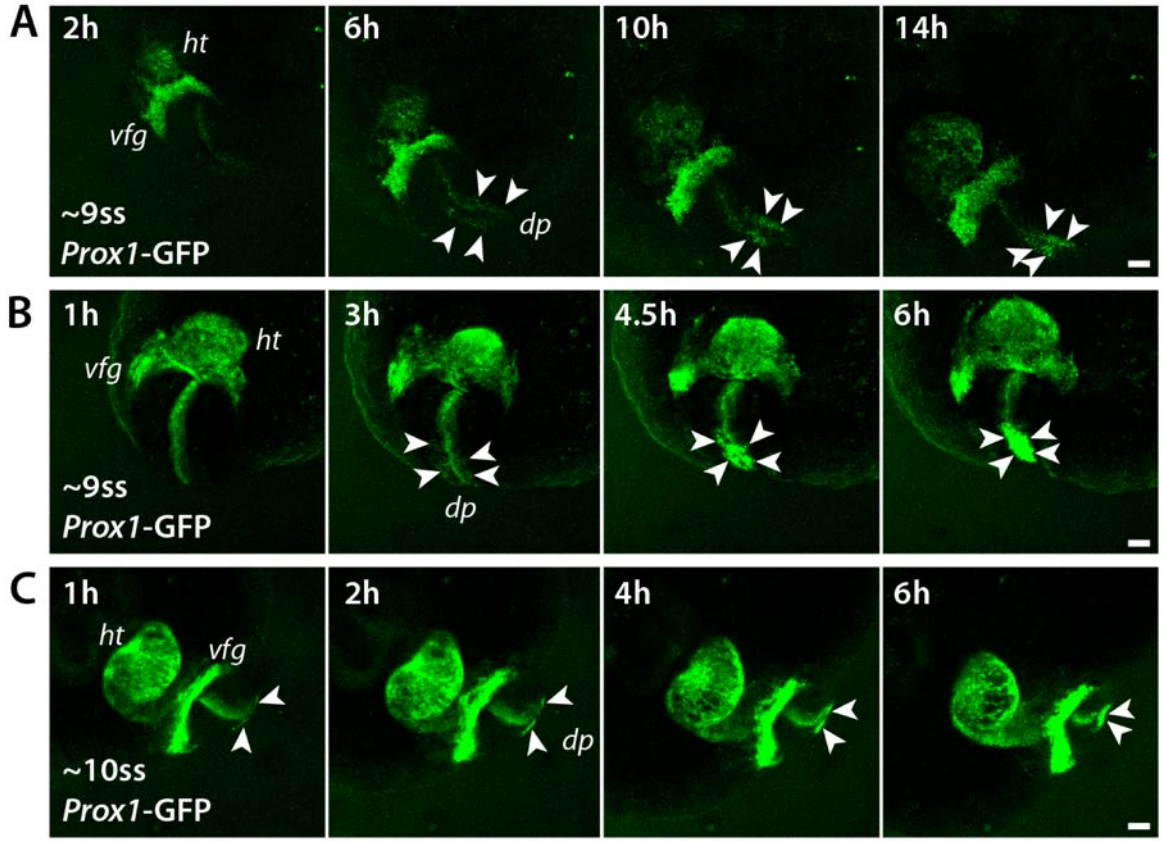

Fig. 28: Time-lapse imaging of *ex vivo* cultured Tg(*Prox1*-EGFP) mouse embryos illustrates dynamics of dorsal pancreatic specification. (A-C) Confocal images of 3 different time-lapse imaging experiments. Tg(*Prox1*-EGFP) embryos were cultured *ex vivo* under controlled conditions under a confocal microscope for up to 16h and imaged for native EGFP fluorescence every 5min. Time given in the upper left corner of each image indicates the time point since start of time-lapse imaging (in hours). Approximate somite stage (ss) of the respective embryo at the beginning of the experiment is given in the lower left corner of the first image of each time series. Arrowheads pinpoint the emergence of EGFP expression in dorsal pancreatic progenitors in the lateral dorsal foregut endoderm and their subsequent conjunction at the embryonic midline. (scale bars: 100μm)

To directly visualize the emergence of Prox1^{+} dorsal pancreatic progenitors as well as ventral hepato-pancreatic progenitors in the foregut, I employed the Tg(*Prox1*-EGFP) mouse line (hereafter abbreviated Prox1-GFP)[187]. This mouse strain carries a transgene expressing EGFP under the control of the Prox1 gene regulatory elements. I collected E8.5 embryos transgenic for Prox1-GFP and subjected them to WMIF for endogenous Prox1 and GFP. As shown in Fig. 27, I documented the presence of GFP^{+} cells, a subset of which also expressed endogenous Prox1 (Fig. 27B), in the lateral dorsal foregut endoderm of 10-11ss embryos. These cells

demarcated the first dorsal pancreatic progenitors distinguishable from the surrounding non-pancreatic dorsal foregut endoderm.

Of note, the dorsal pancreatic progenitors shown in Fig. 27 (E8.5), presented only as interspersed cells in the lateral dorsal foregut endoderm, while the dorsal pancreas at E9.0-E9.5 (Fig. 20; >16ss) consisted of a uniform bud in the gut midline. To better appreciate the transition between these two states, I performed time-lapse imaging of *ex vivo* cultured Prox1-GFP embryos. To this end, I collected Tg(*Prox1*-EGFP) embryos around 8-11ss, the time point when GFP^+ cells emerged in the dorsal foregut. The collected embryos were cultured *ex vivo* under a confocal microscope under controlled conditions for up to 16h and imaged for native EGFP fluorescence every 5min. Fig. 28 shows images from 3 independent experiments taken at the indicated time points during the *ex vivo* culture. In all cases, I detected the emergence of EGFP expression in dorsal pancreatic progenitors in the lateral dorsal foregut as well as in the ventral foregut endoderm (Fig. 28). In addition, video recording documented how the dorsal pancreatic progenitors subsequently converge onto the embryonic midline while concurrently upregulating Prox1 expression, as documented by the increased EGFP fluorescence intensity at later imaging time points (Fig. 28).

3.2.2 Establishing Prox1-rtTA as a tool for lineage tracing of hepato-pancreatic progenitors

In chapter 3.2.1 I established that Prox1 is a suitable marker for early hepato-pancreatic progenitors in the ventral and dorsal foregut. To label these progenitor populations, I used a mouse strain transgenic for a reverse-tetracycline controlled transactivator (rtTA) expressed under the gene regulatory elements of Prox1 (referred to as Tg(*Prox1*-rtTA)). This line was generated by Igor Pongrac, a former PhD student in the Spagnoli laboratory (Pongrac, Spagnoli, unpublished data). This Tet-ON BAC transgenic system also contains a sequence encoding for mCherry to facilitate identification of cells and tissues expressing rtTA. The coding sequences for rtTA and mCherry are separated by a 2A protease cleavage site allowing separation of the co-expressed rtTA and mCherry polypeptides (Fig. 29A). Initially, I confirmed the expression pattern of the transgene in the hepato-pancreatic system and its co-

expression with endogenous Prox1. Fig. 29B shows a 16ss embryo analyzed by WMIF for the pancreatic marker Pdx1 and for mCherry (detected with an anti-RFP antibody). The expression of mCherry was documented in the hepatic, ventral, and dorsal pancreatic organ domains. WMIF analysis for Prox1 and RFP at later embryonic stages (E9.5 and E10.25) showed a perfect overlap in expression of endogenous Prox1 and mCherry (Fig. 29C).

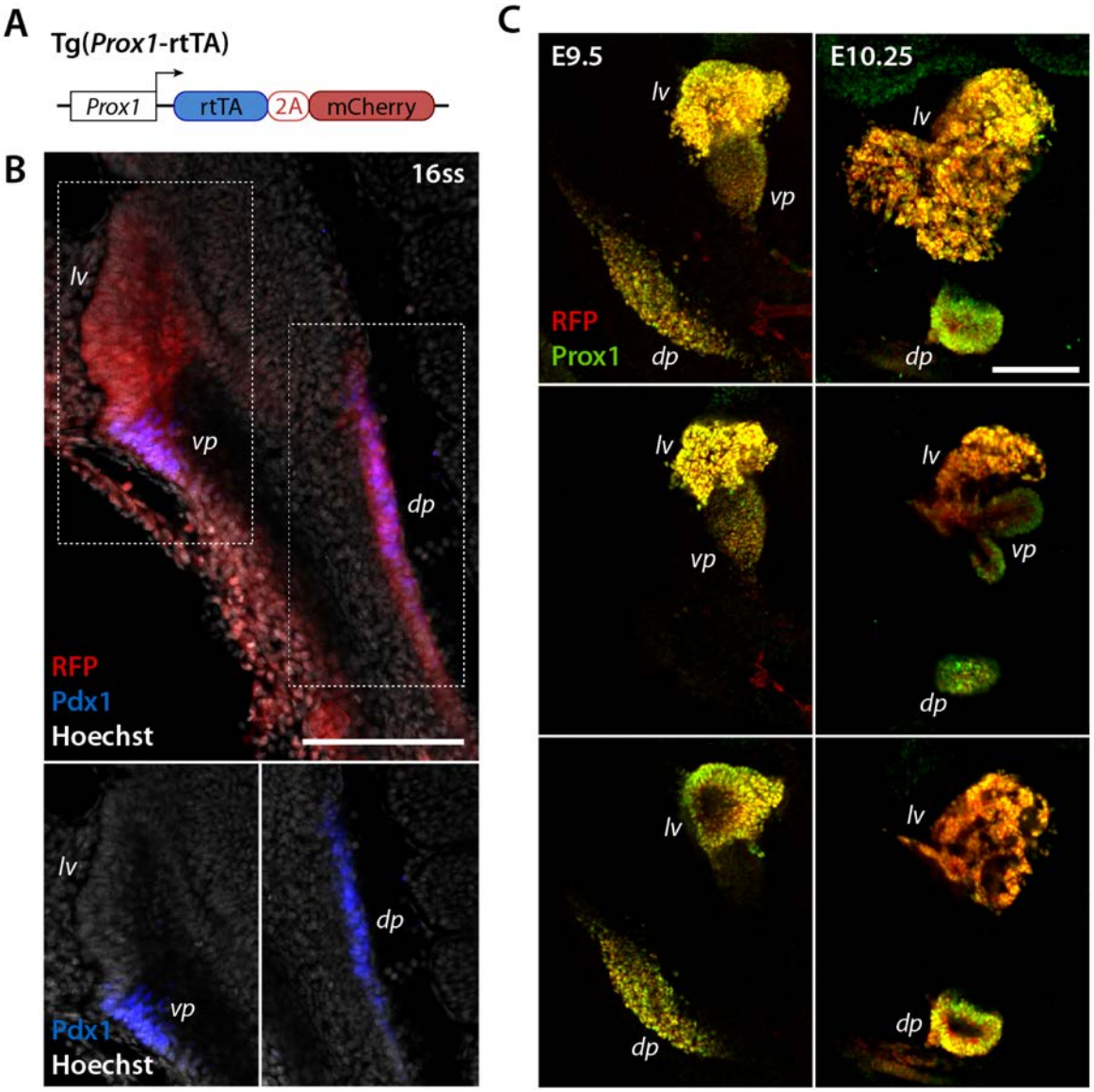

Fig. 29: Tg(*Prox1*-rtTA) is co-expressed with Prox1 during hepato-pancreatic development. A) Schematic representation of the Tg(*Prox1*-rtTA) transgene. (rtTA, reverse tetracycline-controlled transactivator; 2A, proteolytic cleavage site) **(B)** Optical section of a WMIF of an E9.0 (16ss) Tg(*Prox1*-rtTA) embryo. Staining for mCherry with an anti-RFP antibody (red) shows expression of the transgene in liver (*lv*) and ventral (*vp*) and dorsal pancreatic buds (*dp*). Immunostaining for Pdx1 (blue) marks pancreatic organ buds. Cells are counterstained with Hoechst dye (grayscale). Lower panels show boxed areas in upper panel without RFP staining. **(C)** WMIF staining of E9.5 and E10.25 Tg(*Prox1*-rtTA) embryos. Co-immunostaining for Prox1 (green) and RFP (red) documents co-expression of Prox1 and the Tg(*Prox1*-rtTA) transgene. (scale bars: 100µm)

Having established that the expression of the Tg(*Prox1*-rtTA) faithfully recapitulated endogenous Prox1 expression, I next analyzed this mouse line for its suitability as a lineage tracing tool. To this end, males double-transgenic for Tg(*Prox1*-rtTA) and Tg(*TetO*-Cre)[205] (hereafter abbreviated Prox1-rtTA) and H2B-GFP Tg females were used for timed matings (Fig. 30A). Upon exposure of the resulting Tg(*Prox1*-rtTA; *TetO*-Cre; *R26R*-H2B-EGFP) embryos to doxycycline, doxycycline binds to the rtTA and induces its translocation into the nucleus, where it binds to the TetO sequence to induce expression of Cre recombinase, which, in turn, activates the H2B-GFP reporter gene locus and allows stable H2B-GFP expression (Fig. 30A). At E8.5, pregnant H2B-GFP females were intravenously (IV) injected with doxycycline at increasing concentrations of 75μg, 100μg, or 150μg/g bw. The embryos were collected at E9.5, subjected to WMIF analysis, and the numbers of labeled (GFP^+) cells in each organ domain were determined. The experimental setup and the spread of embryonic stages at time of label induction and embryo collection for the 150μg/g bw condition are shown in Fig. 30B. WMIF analysis documented labeled cells in all hepato-pancreatic tissues, with labeling events in the ventral pancreas being less frequent as compared to dorsal pancreas or liver (Fig. 30E).

To gain insight into the labeling characteristics of the Prox1-rtTA mouse line, I plotted the total number of labeled cells in each embryo for each experimental condition (75μg, 100μg, or 150μg/g bw) against the somite stage of the respective embryo at the time of label induction (Fig. 30C). Two distinct labeling characteristics were concluded from this representation of the dataset. First, the number of labeled cells increased with the somite stage of the embryo at the time of label induction. Second, embryos that received a higher dose of doxycycline showed higher numbers of labeled cells, arguing that a higher doxycycline dose increased the chance of labeling events. This second observation was corroborated by quantifying the fraction of labeled embryos in different experimental conditions (Fig. 30D). While the percent (%) of labeled embryos was only 36% at 75μg/g bw doxycycline (n=22) or 41% at 100μg/g bw doxycycline (n=29), almost 90% of transgenic embryos showed labeled cells after exposure to 150μg/g bw doxycycline (n=116). Since my aim was to analyze the dynamics of hepato-pancreatic tissue labeling, I chose the most effective labeling dose of 150μg/g bw doxycycline for further experiments.

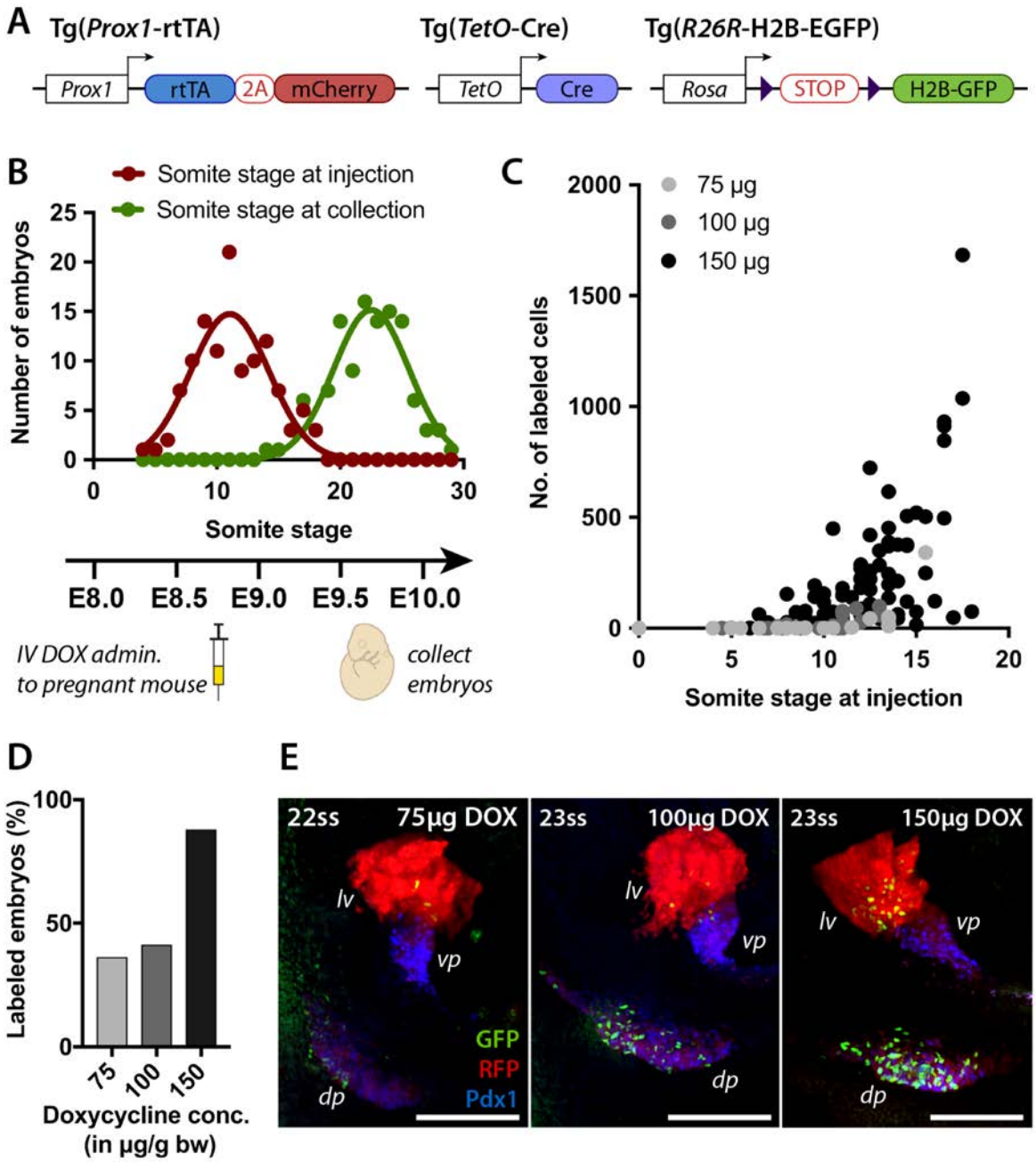

Fig. 30: Establishing lineage tracing using the Tg(*Prox1*-rtTA) mouse line. (A) Schematic representation of transgenes used in this experimental approach. **(B)** Schematic representation of the experimental setup. Pregnant females were intravenously injected with a single dose of doxycycline (75µg, 100µg, or 150µg/g body weight) around E8.5 (IV DOX). Embryos were subsequently collected at E9.5. The upper diagram shows a graphical representation of the spread of embryonic stages at the time points of injection or embryo collection in the dataset (for 150µg/g bw doxycycline, n=116) **(C)** The number of GFP^+ (labeled) cells in each embryo is determined and plotted against the somite stage of the respective embryo at the time of label induction, showing a positive correlation between labeled cell number and somite stage. Data shown include experiments with different doxycycline doses used (75µg/g bw, n=22; 100µg/g bw, n=29; 150µg/g bw, n=116). Visibly, cell label induction is higher with increasing doxycycline doses. **(D)** Measuring the frequency of embryos with an induced label shows that the chance of labeling increases with the doxycycline dose. **(E)** Representative WMIF of E9.5 Tg(*Prox1*-rtTA; *R26R*-H2B-GFP) embryos that received the indicated doses of doxycycline. Immunostaining of GFP (green) documents labeled cells in liver (*lv*) and dorsal pancreas (*dp*). The density of labeled cells increases with doxycycline concentrations used for label induction. Immunostaining of RFP (red) marks liver, co-immunostaining of RFP and Pdx1 (blue) pancreatic buds. (scale bars: 100µm)

The analyses of the Prox1-rtTA lineage tracing experiments were designed to assess the labeling dynamics of each hepato-pancreatic organ rudiment individually as well as their relationship to each other. In my analysis, I included 116 embryos that were treated with 150μg/g bw doxycycline. As a first step, I plotted the number of labeled cells found in the liver (Fig. 31B), in ventral (Fig. 31C), and in dorsal pancreatic bud (Fig. 31D) for each embryo against the respective somite stage at the time of label induction. In line with the analysis of the total number of labeled cells (Fig. 30C), I observed a positive correlation between the number of labeled cells in all hepato-pancreatic organ rudiments (Fig. 31B-D) and the somite stage at the time of label induction. This fact is visible in WMIF images of representative embryos in Fig. 31A, documenting labeled cells by immunostaining for GFP. As expected, immunostaining for RFP marked the liver and pancreatic buds, while immunostaining for Pdx1 specifically marked dorsal and ventral pancreas (Fig. 31A). In general, I observed robust labeling efficiencies in dorsal pancreas and liver from 8/9ss (as time point of label induction) onwards. Labeling events in the ventral pancreas were more sporadic and labeling efficiency lower as compared to that in dorsal pancreas and liver.

After the analysis of the labeling dynamics in each individual hepato-pancreatic tissue, I investigated their labeling dynamics with respect to each other. Towards this aim, I plotted the number of labeled cells in the liver of each embryo against the number of labeled cells in either the dorsal or ventral pancreas of the respective embryo (Fig. 31E). Thereafter, I plotted regression curves through the two datasets. The regression curves through the liver versus dorsal pancreas and the liver versus ventral pancreas dataset followed quite distinct patterns (Fig. 31E). While the relationship between labeled liver and ventral pancreatic cells showed an almost linear relationship, that of labeled liver and dorsal pancreatic cells resembled a logarithmic curve approaching a plateau. The divergence in the relationship between liver versus ventral and liver versus dorsal pancreas was indicative of the different embryonic origin of the two pancreatic domains. Conceivably, a higher number of labeled cells induced in the common progenitor region in the ventral foregut[5,6,8,9] will result in higher numbers of labeled cells in both liver and ventral pancreas. The dorsal pancreas, however, originates from a separate organ domain in the dorsal foregut (Figs. 27, 28)[8]. The distinctly non-linear relationship between labeled liver and labeled dorsal pancreatic cells underscored this fact

and illustrated differences in the Prox1-rtTA labeling dynamics comparing ventral and dorsal hepato-pancreatic tissues.

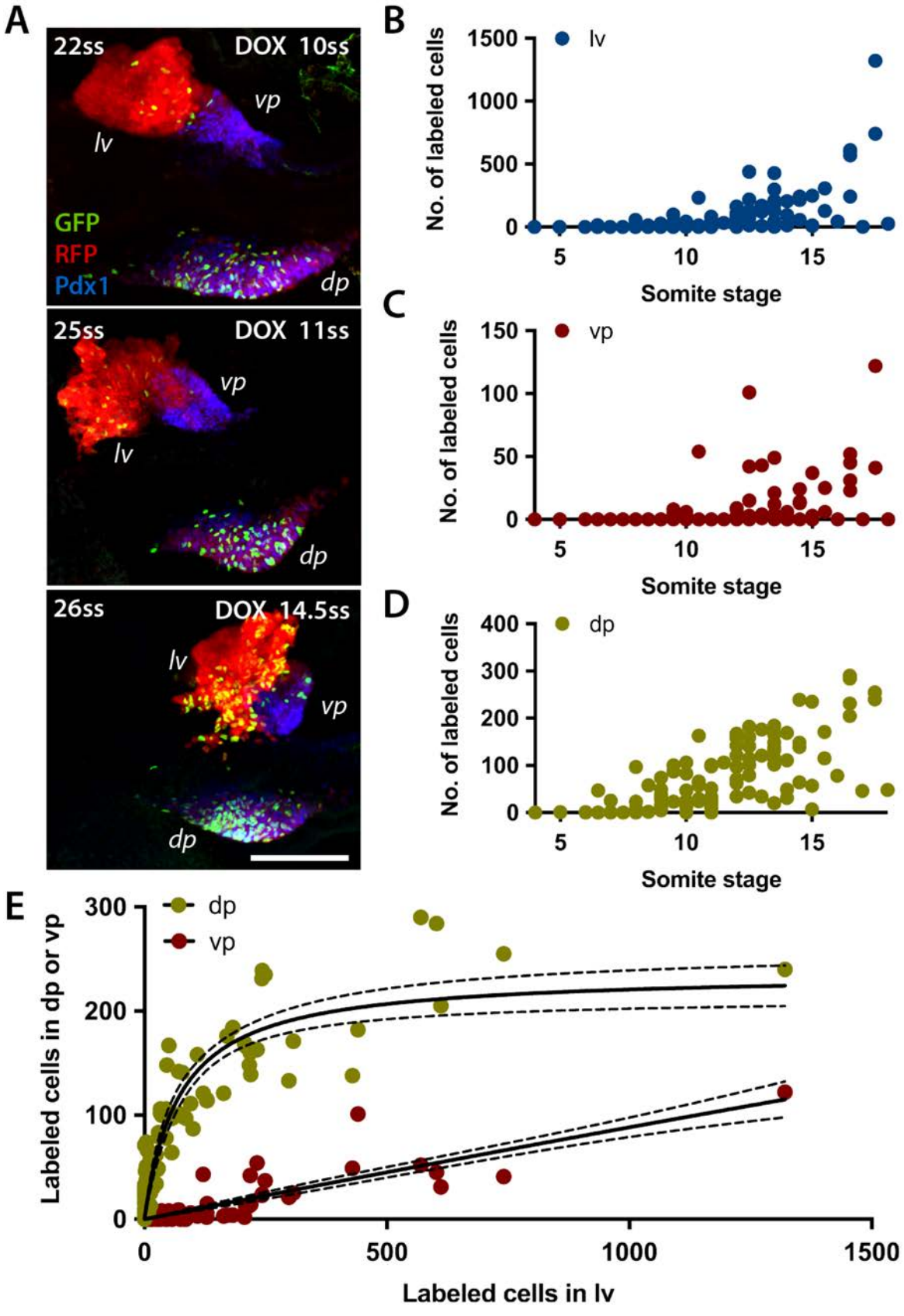

Fig. 31: Lineage tracing shows different dynamics of labeling of dorsal versus ventral hepato-pancreatic progenitors. (A) Representative WMIF of E9.5 Tg(*Prox1*-rtTA; *R26R*-H2B-GFP) embryos with time point of label induction indicated in upper right corner (DOX). Immunostaining of GFP documents labeled cells in liver (*lv*), ventral (*vp*), and dorsal pancreas (*dp*). Labeling density increases with label induction at later embryonic stages. Immunostaining of RFP (red) marks liver, co-immunostaining of RFP and Pdx1 (blue) pancreatic buds. **(B-D)** Numbers of labeled cells in liver (B) as well as ventral (C) and dorsal pancreatic buds (D) are plotted against the somite stages of the respective embryo at time point of label induction. All hepato-pancreatic tissues show a positive correlation between labeled cell numbers and somite stages at label induction. **(E)** The number of labeled cells in dorsal or ventral pancreas is plotted against the number of labeled cells in the liver of the respective embryo. While the relationship between labeled liver and ventral pancreatic cells is linear, that between labeled liver and dorsal pancreatic cells resembles a logarithmic curve approaching a maximum. This observation argues for distinctly different labeling dynamics in the dorsal pancreas as compared to the ventral foregut derivatives liver and ventral pancreas. (regression curves: hyperbola with 95% confidence interval; adjusted R^2: 0.85 (dp), 0.76 (vp)) (scale bar: 100μm)

3.2.3 Prox1-rtTA lineage tracing documents contribution of dorsal Prox1$^+$ progenitors to cell population in the stomach

To examine whether Prox1$^+$ foregut cells only constitute progenitors of the hepato-pancreatic organ system or can also contribute to other endodermal derivatives, I carried out Prox1-rtTA lineage tracing experiments in a later developmental time window. Specifically, I injected pregnant YFP or H2B-GFP females from timed mating with Prox1-rtTA males with doxycycline (150μg/g bw) at E9.5 and collected the embryos at E11.5 (Fig. 32A and B). The embryos were analyzed by WMIF and YFP or H2B-GFP expression documented by immunostaining with an anti-GFP antibody (Fig. 32C and D). Immunostaining for RFP detected the mCherry protein expressed from the Prox1-rtTA transgene in liver and pancreatic buds, while immunostaining for Pdx1 marked pancreatic buds, duodenum, and the posterior stomach region (Fig. 32C and D). Label induction at E9.5 resulted in almost complete labeling of the entire hepato-pancreatic cell population at E11.5.

Interestingly, apart from liver, dorsal, and ventral pancreatic buds, I also detected labeled cells in a distinct region of the dorsal posterior stomach (Fig. 32C and D). This observation was remarkable, because in previous experiments I did not detect endogenous Prox1 expression in gastric tissues. Also, labeled E11.5 embryos did not express mCherry from the Prox1-rtTA transgene in the labeled stomach region, as documented by the absence of an RFP immunosignal (Fig. 32). The lack of expression of Prox1 or Prox1-rtTA in gastric progenitors

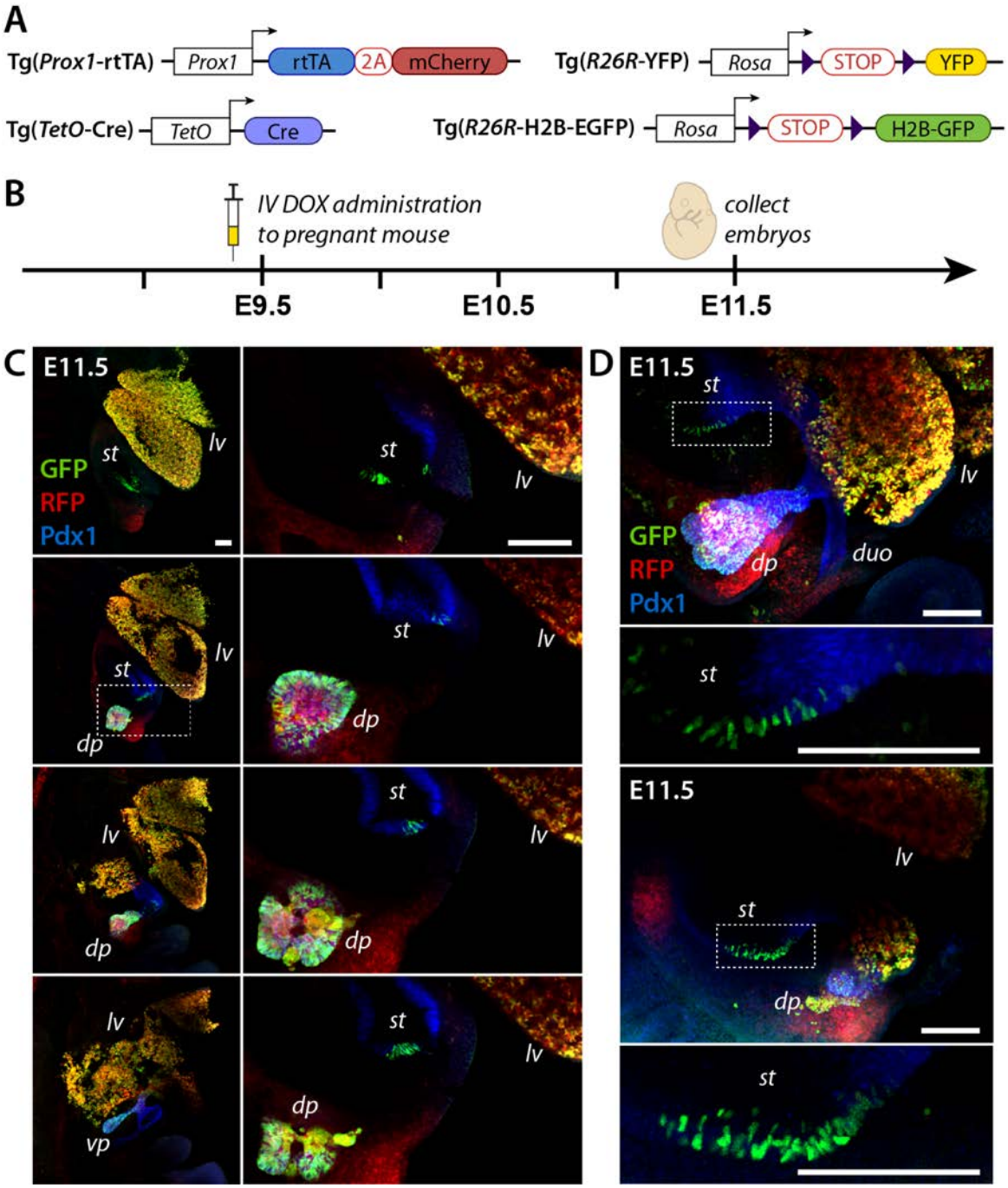

Fig. 32: Lineage tracing using Tg(*Prox1*-rtTA) at late time points reveals contribution of descendants of Prox1$^+$ cells to distinct dorsal proximal stomach region. (A) Schematic representation of transgenes used in this experimental setup. **(B)** Schematic representation of the experimental setup. Pregnant females were injected with a single dose of 150µg/g bw doxycycline around E9.5 by intravenous injection (IV DOX). Embryos were subsequently collected at about E11.5. **(C, D)** WMIF of Tg(*Prox1*-rtTA; *R26R*-YFP) (C) and two Tg(*Prox1*-rtTA; *R26R*-H2B-GFP) (D) embryos labeled according to the experimental setup described in (B). Immunostaining of RFP (red) and Pdx1 (blue) marks liver (RFP), vp (RFP, Pdx1), dp (RFP, Pdx1), duodenum (Pdx1), and posterior stomach (Pdx1). (C) Panels on the left are partial maximum intensity projections showing dense YFP labeling, as documented by staining with an anti-GFP antibody, in liver (*lv*), ventral (*vp*) and dorsal pancreatic buds (*dp*) as well as in a distinct region in the dorsal posterior part of the stomach (*st*). Panels on the right show magnifications of different optical sections of boxed area of the partial maximum intensity projection. (D) GFP staining documents labeled cells in liver (*lv*), dorsal pancreas (*dp*) and the dorsal posterior part of the stomach (*st*). Lower panels show magnification of boxed area in the respective upper panel. (C, D) (scale bars: 100µm)

suggested the intriguing possibility that labeled gastric cells may be descended from an earlier genetically labeled Prox1^{+} population, possibly of dorsal pancreatic origin. This hypothesis was supported by the localization of these labeled gastric cells in the dorsal part of the posterior stomach, which is adjacent to the dorsal pancreatic organ domain.

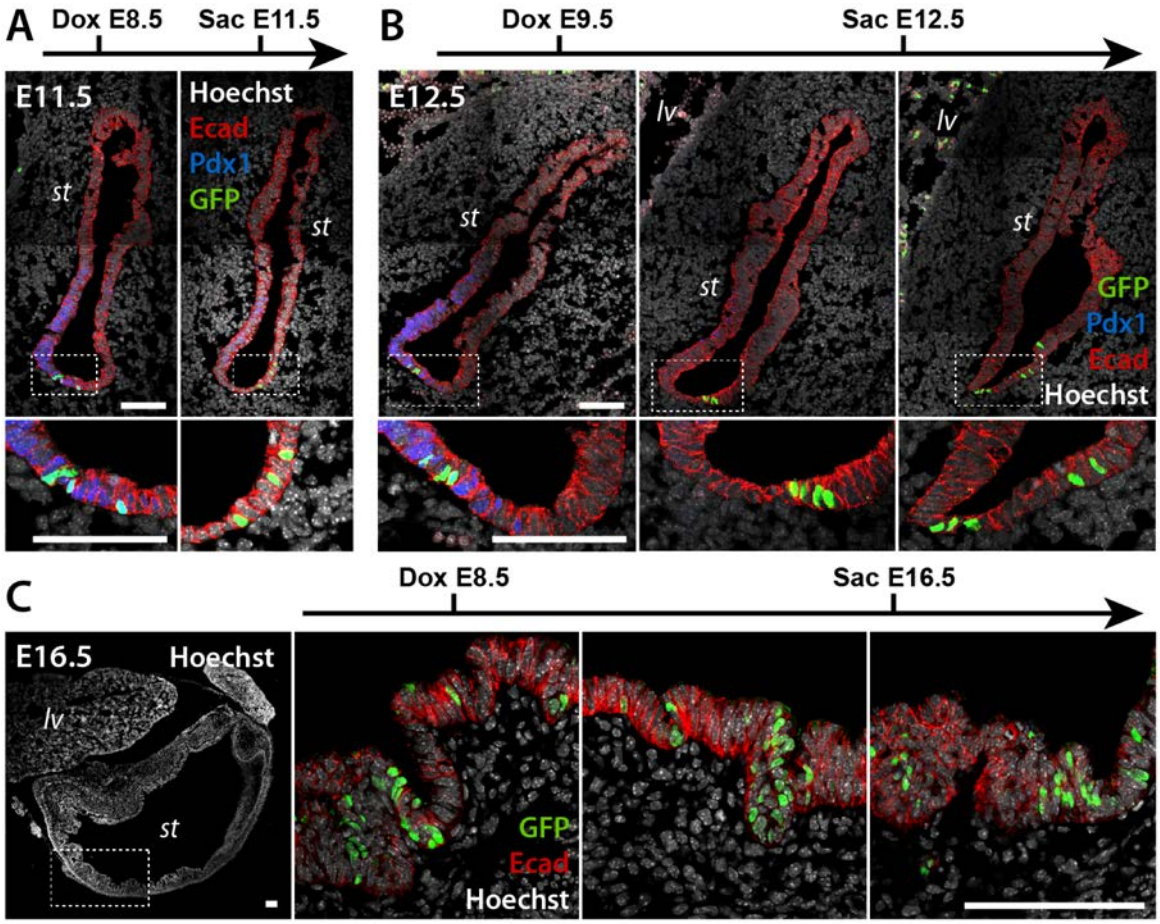

Fig. 33: Long-term lineage tracing experiments using Tg(*Prox1*-rtTA) show persistence of labeled cells in the stomach. (A-C) IF staining of cryosections of stomach tissue from long-term lineage tracing experiments. Pregnant females were intravenously injected with a single dose of 150μg/g bw doxycycline (Dox) at E8.5 (A, C) or E9.5 (B). Tg(*Prox1*-rtTA; *R26R*-H2B-GFP) embryos were subsequently collected at E11.5 (A), E12.5 (B), or E16.5 (C) (Sac). Time course of the respective experiment is given above each image. Immunostaining for GFP documents labeled cells descended from Prox1^{+} progenitors in the dorsal posterior part of the stomach in a majority of analyzed embryos ((A) 2/2, (B) 4/7, (C) 2/2). Immunostaining for Ecad (red) marks the epithelium of the developing stomach. Immunostaining for Pdx1 (blue) specifically marks the posteriormost stomach region. Tissues are counterstained with Hoechst dye (grayscale). (scale bars: 100μm)

To query the specificity of the observed labeling events in the stomach, I performed additional lineage tracing experiments (Fig. 33). First, I determined whether these putative gastro-pancreatic progenitors were a specific cell population arising at E9.5, or if this cell population was already present at E8.5 when labeling in dorsal pancreatic progenitors was typically

induced. Towards this aim, pregnant H2B-GFP females were IV injected with doxycycline (150μg/g bw) at E8.5 (Fig. 33A) and embryos collected at E11.5. Cryosections of transgenic embryos were IF stained for GFP to document labeled cells. Immunostaining for E-cadherin (Ecad) marked the entire stomach epithelium, while immunostaining for Pdx1 specifically marked the posteriormost (antral) stomach region. In line with my previous experiments (Fig. 32), I detected labeled (GFP^+) cells in the dorsal posterior region of the stomach (Fig. 33A), documenting that $Prox1^+$ progenitors of gastric cells already existed at E8.5. In a second experiment, I asked whether the labeled gastric cells remained in the same region in the stomach at a later developmental stage. To this aim, I prolonged the tracing period and collected embryos at E12.5 (instead of E11.5) (Fig. 33B). Cryosections of transgenic embryos were IF stained for GFP to document labeled cells. Again, I detected labeled GFP^+ cells in the same dorsal posterior region of the stomach as in previous experiments with shorter tracing periods (Fig. 33B).

Finally, I performed lineage tracing experiments with an even further extended tracing period of 8 days to confirm the long-term contribution of the labeled cell population to the growing stomach epithelium. In these experiments, pregnant H2B-GFP females were injected with doxycycline (150μg/g bw) at E8.5 and embryos collected at E16.5 (Fig. 33C). GFP-labeled cells were still present in the dorsal posterior part of the stomach, providing evidence for the long-term contribution of descendants of $Prox1^+$ progenitors to the stomach. Often, the labeled cells were found in groups of more than 10 cells along the entire length of the gastric crypts (Fig. 33C), suggesting that they represented descendants of one labeled gastro-pancreatic progenitor.

The gastrointestinal tract contains enteroendocrine cell types, which exert endocrine functions similar to those of endocrine cells of the pancreas[206–208]. To explore the hypothesis of a putative embryonic relationship between the two cell types, I collected stomach tissue from E16.5 and E18.5 embryos as well as from 4-day old mice (post-natal day 4, P4). Cryosections of the tissues were IF stained for E-cadherin (stomach epithelium) and for either the pancreatic marker Sox9 (Fig. 34A) or the endocrine markers Pax6, Ngn3, somatostatin (SST), or glucagon (Fig. 34B). Sox9 showed strong expression throughout the stomach at E16.5 but became restricted to the base of the stomach crypts at E18.5 (Fig. 34A). As Sox9 showed

a broad expression pattern in the stomach and was not restricted to the dorsal posterior stomach, I did not consider it further as a possible marker specific to the descendants of Prox1^{+} progenitors.

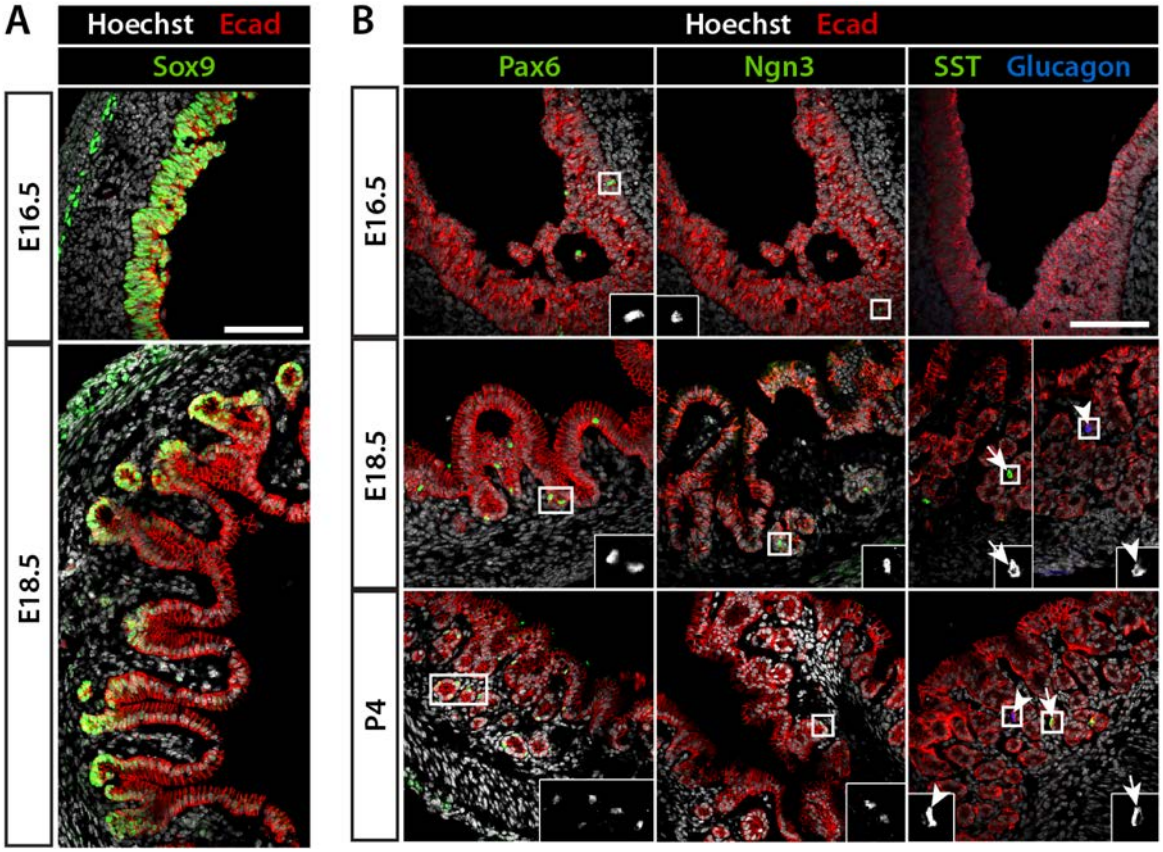

Fig. 34: Characterization of endocrine cell populations in the stomach. (A) IF staining of cryosections of stomach tissue. The pancreatic marker Sox9 (green) is highly expressed in the stomach at E16.5 and becomes more restricted to the base of stomach crypts at E18.5. **(B)** Pancreatic endocrine markers Pax6, Ngn3, Somatostatin (SST), and Glucagon are expressed in few stomach cells between E16.5 and postnatal day 4 (P4) marking a rare population of gastroendocrine cells. Insets show higher magnification of cells in boxed area expressing these endocrine markers. Arrows mark SST positive cells while arrowheads indicate Glucagon positive cells. Ecad (red) staining in panels A and B marks the stomach epithelium. All tissues are counterstained with Hoechst dye (grayscale). (scale bars: 100μm)

Thus, I went on to evaluate the expression patterns of the endocrine progenitor markers Pax6 and Ngn3. Both markers were seen in cells of the antral stomach from E16.5 onwards and increased in density at E18.5 and P4 as the stomach epithelium matured (Fig. 34B). Of note, Pax6^{+} cells were more commonly found than Ngn3^{+} cells. I also evaluated the expression of the hormones somatostatin and glucagon in the stomach (Fig. 34B). Although both are better known as pancreatic hormones, somatostatin and glucagon are also expressed in gastro- and entero-endocrine cells[208]. Their expression was detected in rare cells at E18.5 but slightly

more frequent at P4 in the antral stomach. In summary, cells positive for the endocrine markers Pax6, Ngn3, SST, and glucagon were found in the dorsal part of the posterior stomach, where they overlapped with the gastric domain harboring GFP^+ cells from the Prox1-rtTA lineage tracing experiments. However, cells expressing these endocrine markers were also found in the ventral posterior stomach, arguing that these gastric endocrine cell fates are not specific to the stomach region harboring descendants of $Prox1^+$ progenitors. This observation suggested that descendants of putative gastro-pancreatic progenitors do not acquire a unique cell fate but rather contribute to the normal spectrum of gastric cell types found in the antral stomach.

Finally, I characterized the labeled cell population in further detail to explore how these cells may contribute to the stomach. For instance, these labeled dorsal pancreatic progenitors may reach the stomach by a gradual shift towards the gastric organ domain at early developmental stages or alternatively by collective cell migration at later developmental time points. To distinguish between these two possibilities, I focused on earlier time points of development. Specifically, I analyzed E9.5 embryos collected from Prox1-rtTA lineage tracing experiments for evidence of labeled cells at the border between dorsal pancreas and stomach (Fig. 35A). The analyzed embryos had been treated with doxycycline at E8.5 and collected at E9.5. WMIF staining for RFP and Pdx1 marked the dorsal pancreas, while immunostaining for GFP marked the labeled cells. I identified GFP^+ cells in the stomach organ domain and at the border between dorsal pancreas and stomach in embryos of different somite stages (20-29ss) (Fig. 35A).

These findings suggested that the labeled cells found in the stomach from E11.5 onwards persisted within the gastric domain since their label induction and did not migrate there from the dorsal pancreas at later stages. Thus, the labeled cells in the stomach likely originated from anterior dorsal pancreatic progenitors that upregulated Prox1 expression (Fig. 27, Fig. 28) but failed to converge posteriorly to contribute to the dorsal pancreatic organ rudiment. This observation also entails that early dorsal pancreatic progenitors retain plasticity towards a gastric fate. Following early induction of Prox1, dorsal pancreatic progenitors, which failed to contribute to the dorsal pancreatic bud, might revert/convert to a gastric fate in the absence of additional pro-pancreatic cues.

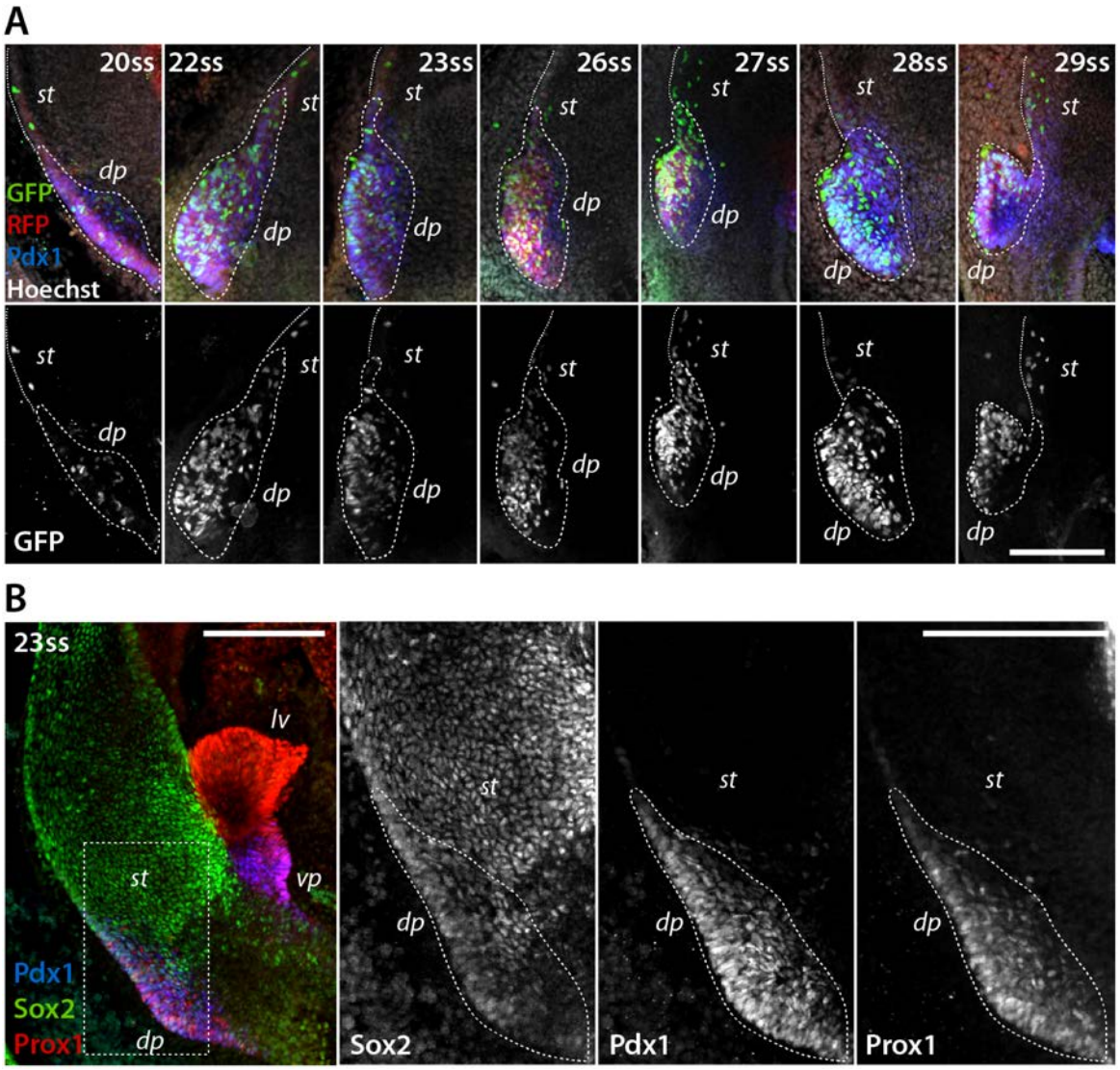

Fig. 35: Cells labeled by Tg(*Prox1*-rtTA) overlap with a cell population expressing stomach and pancreatic marker genes. (A) Optical sections of WMIF of Tg(*Prox1*-rtTA; *R26R*-H2B-GFP) E9.5 embryos. H2B-GFP label was induced at E8.5. Dotted lines demarcate dorsal pancreatic (*dp*) from stomach regions (*st*). Staining for GFP (green) documents cells throughout the dorsal pancreas and within the stomach at E9.5-E10.0 (20ss-29ss). Co-immunostaining for RFP (red) and Pdx1 (blue) marks the dorsal pancreas. Tissues are counterstained with Hoechst dye (gray scale). The upper row shows merged color images while the lower row gives the corresponding GFP channel in grayscale. **(B)** WMIF of a 23ss embryo for the indicated pancreatic and stomach marker genes. Immunostaining for Prox1 (red) marks the liver (*lv*), co-immunostaining for Prox1 and Pdx1 (blue) marks ventral (*vp*) and dorsal pancreatic buds (*dp*). Immunostaining for the stomach marker Sox2 (green) shows overlap in the gastric Sox2 expression domain (*st*) with markers of the dorsal pancreas but not with markers of liver and ventral pancreas. The left panel shows a merged overview picture while right panels show magnifications of the boxed area in single grayscale channels. (Scale bars: 100μm)

To ultimately test this hypothesis, I assessed the expression patterns of gastric and hepato-pancreatic markers at E9.5 to determine if a lineage relationship existed between early gastric and dorsal pancreatic progenitors. Accordingly, E9.5 embryos were stained for Prox1 to mark all hepato-pancreatic tissues, for Pdx1 to specifically mark the pancreatic buds, and for Sox2

to mark the early stomach organ domain. As shown in Fig. 35B, the Sox2 expression domain at E9.5 (23ss) overlapped with the anterior half of the dorsal pancreatic bud, documenting shared expression of this marker between gastric and dorsal pancreatic organ domains. Interestingly, Sox2 expression was excluded from liver and ventral pancreas, creating a sharp boundary between gastric and ventral hepato-pancreatic tissues. Expression domains for Prox1, Pdx1, and Sox2 in the foregut at E8.5 (Fig. 36) showed a similar situation with Sox2 expression being excluded from the Prox1^{+} ventral foregut region, while being abundant in the dorsal foregut (Fig. 36B).

In conclusion, lineage tracing experiments using the Prox1-rtTA mouse line documented labeling events in the dorsal posterior stomach from E9.5 to E16.5. Analysis of gastric and hepato-pancreatic marker genes showed overlapping expression of Sox2 in the stomach and in the dorsal pancreatic organ domain at E8.5 and E9.5. Together, these results hinted at a hitherto under-appreciated lineage relationship between gastric and dorsal pancreatic progenitors.

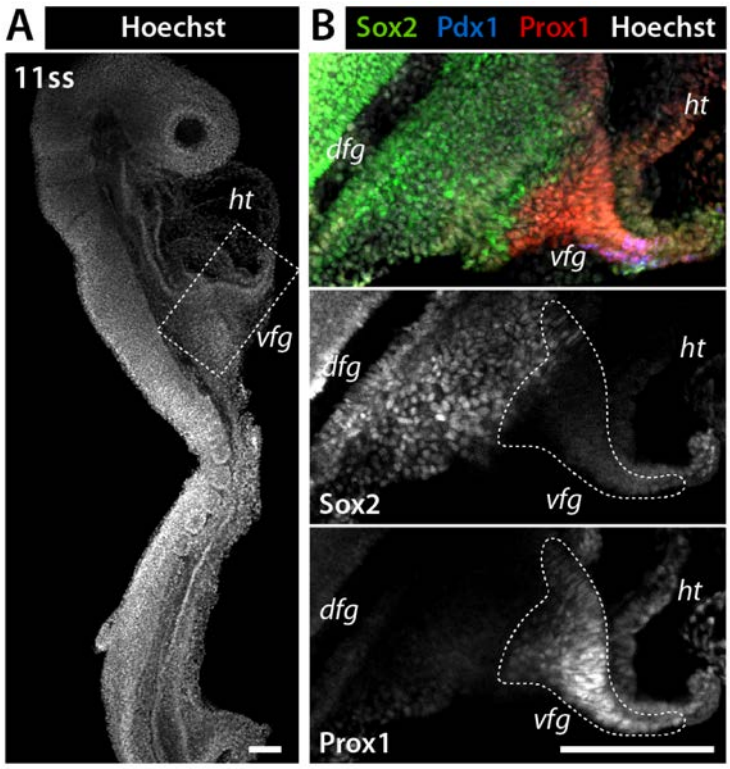

Fig. 36: Exclusion of Sox2 expression from the ventral foregut region is already detectable at E8.5. (A, B) WMIF analysis of an E8.5 (11ss) embryo. (A) Image of the entire embryo stained with Hoechst dye (grayscale). (B) WMIF of the foregut region indicated by boxed area in panel A. Immunostaining for Prox1 (red) marks the ventral foregut (*vfg*) harboring hepatic and ventral pancreatic progenitors (co-immunostained with Pdx1 (blue)). Immunostaining for Sox2 (green) shows exclusion of Sox2 from the ventral foregut (demarcated by dotted line), but high expression in the dorsal foregut (*dfg*), harboring dorsal pancreatic and stomach progenitors. The upper panel shows the merged color image, while lower panels give Sox2 and Prox1 channels in grayscale. (*ht*, heart) (scale bars: 100μm)

3.2.4 Prox1-rtTA lineage tracing argues for cell fate plasticity between ventral pancreas and liver

My initial Prox1-rtTA lineage tracing experiments (see chapter 3.2.2), documented different labeling dynamics in dorsal versus ventral hepato-pancreatic organ buds. This fact is illustrated in Fig. 31E by plotting the number of labeled cells in the liver against the number of labeled cells in either dorsal or ventral pancreas. While the liver versus dorsal pancreas dataset showed a distinctly non-linear trend, I found that the liver versus ventral pancreas dataset followed a linear correlation, suggesting a common origin of the ventral hepato-pancreatic tissues. Here, I further investigated the labeling dynamics during cell fate divergence within the ventral hepato-pancreatic compartment.

First, I determined whether the ratio of labeled liver versus ventral pancreatic cells exhibited time-dependent changes comparable to the Foxa2-Cre lineage tracing results (Fig. 18). For this analysis, I used 116 embryos that were treated with 150μg/g bw doxycycline (Fig. 30B, Fig. 31). Pregnant H2B-GFP females had received doxycycline by IV injection at E8.5 and embryos had been collected at E9.5. Subsequently, the embryos were analyzed by WMIF for RFP to mark all hepato-pancreatic tissues, for Pdx1 to specifically mark the pancreatic buds, and for GFP to document H2B-GFP-labeled cells (Fig. 37A, B). Comparing the ratio of labeled liver to ventral pancreatic cells in individual embryos, two variables emerged as the primary factors influencing this ratio. Late somite stages and longer tracing periods both correlated with an increase in the ratio of labeled liver versus labeled ventral pancreatic cells (Fig. 37A, B). Next, embryos of similar somite stages at the time of collection (Fig. 37C) or similar tracing period (Fig. 37D) in this dataset were grouped and the sum of labeled liver and labeled ventral pancreatic cells as well as their ratio calculated. The liver to ventral pancreas ratio was then plotted against the average somite stage at the time of collection (Fig. 37C) or the length of the tracing period (Fig. 37D) of the respective group of embryos. By plotting regression curves through the datasets, I confirmed that the liver to ventral pancreas ratio positively correlated with both the somite stage at the time of embryo collection (Fig. 37C) and with the length of the tracing period (Fig. 37D).

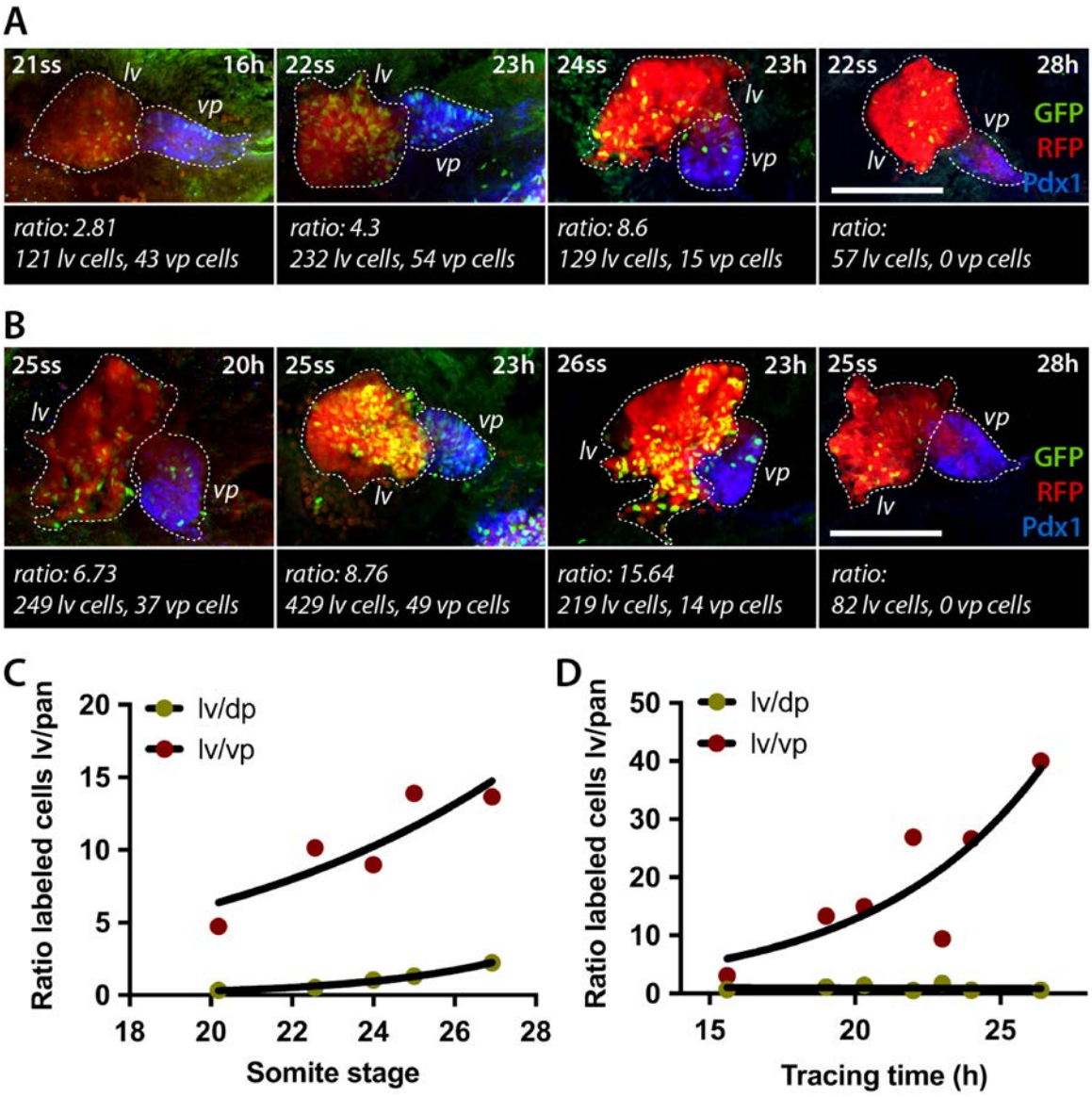

Fig. 37: Ratio between Tg(*Prox1*-rtTA) labeled ventral pancreatic and liver cells shifts with increasing somite stage and tracing period. (A, B) Representative WMIF of E9.5 Tg(*Prox1*-rtTA; *R26R*-H2B-GFP) embryos of similar somite stages (A, 21-24ss; B, 25-26ss). The tracing period is indicated in the upper right corner (in hours). Immunostaining of GFP (green) documents labeled cells in liver (*lv*) and ventral pancreas (*vp*). Immunostaining of RFP (red) marks liver while co-immunostaining of RFP and Pdx1 (blue) marks ventral pancreas. Hepatic and ventral pancreatic bud are encircled by dotted lines. The numbers of labeled liver and ventral pancreatic cells as well as their ratio are given below each image. The ratio between labeled liver and ventral pancreatic cells is increasing with the tracing period. In addition, comparison between the ratios in (A) and (B) shows an increase in the ratio in embryos of later somite stages. **(C, D)** The ratio of labeled cells in liver to either ventral pancreas (lv/vp) (as exemplified in panel A and B) or dorsal pancreas (lv/dp) is plotted against the somite stage at time of embryo collection (C) or against the tracing period (D) (n=116). For this purpose, embryos of similar somite stages at time of collection or similar tracing period were grouped and the sum of all labeled cells in lv, vp and dp used for calculation of the depicted ratios. In panel C, a positive correlation between the somite stage at the time of embryo collection and the ratio of liver to pancreatic (pan) cells is seen for both regression lines. However, this positive correlation is more pronounced for the lv/vp ratio than the lv/dp ratio. In panel D, the lv/vp ratio shows a strong positive correlation with the length of the tracing period. Such a positive correlation is not seen with the lv/dp ratio. (regression curves: exponential growth equation; R^2 for lv/vp: 0.77 (C), 0.74 (D); adjusted R^2 for lv/dp: 0.99 (C), 0.01 (D)) (scale bar: 100μm)

To assess whether this finding was specific to the ventral pancreas, I repeated the analysis using the same groups of embryos and calculated the ratio between labeled liver and labeled dorsal pancreatic cells. Here, I observed a positive correlation between the liver to dorsal pancreas ratio and the somite stage at the time of collection. However, the time-dependent increase in liver to dorsal pancreas ratio was much less pronounced in the analyzed developmental time window as compared to changes in the liver to ventral pancreas ratio (Fig. 37C). By contrast, the tracing period length had no influence on the ratio of labeled liver to labeled dorsal pancreatic cells (Fig. 37D).

In summary, Prox1-rtTA lineage tracing showed that the ratio of labeled liver to labeled ventral pancreatic cells depends on the somite stage at the time of embryo collection (Fig. 37C), corroborating the results obtained with the Foxa2-Cre mouse line (Fig. 18) in a different experimental system. In addition, I identified the length of the tracing period as a major factor influencing the ratio of labeled liver versus labeled ventral pancreatic cells in the Prox1-rtTA lineage tracing experiments (Fig. 37D). Both results showed that over time (embryonic time or experimental tracing time) a relative increase in liver labeling at the expense of labeling events in the ventral pancreas was observable. As such, these findings support my hypothesis that a constant flux of ventral pancreatic cells contributes to the growing liver bud from E8.5 to E9.5.

3.2.5 Clonal analyses of lineage tracing experiments support a novel concept of cell fate plasticity in the ventral foregut derivatives

Next, I employed the Prox1-rtTA mouse line for long-term lineage tracing experiments with a 3-day tracing period. My aim was to analyze individual clones of labeled cells to gain insight into the cellular dynamics of individual hepato-pancreatic progenitors and their contribution to liver and pancreas. Towards this aim, I changed from the unicolor H2B-GFP reporter system to the multicolor Tg(*R26R*-Confetti) transgene (hereafter abbreviated Confetti). The rationale behind my choice was that a multicolor reporter system facilitates clonal analysis by allowing differential labeling of cells and their progeny through the stochastic activation of different reporter genes. The Confetti transgene encodes four different fluorescent proteins with

different cellular localization (cytoplasmic RFP, cytoplasmic YFP, nuclear GFP (nGFP), membrane-associated CFP (mCFP)) (Fig. 38A, B). Cre-mediated recombination of the Confetti locus results in the exclusive expression of either one of the four reporter proteins.

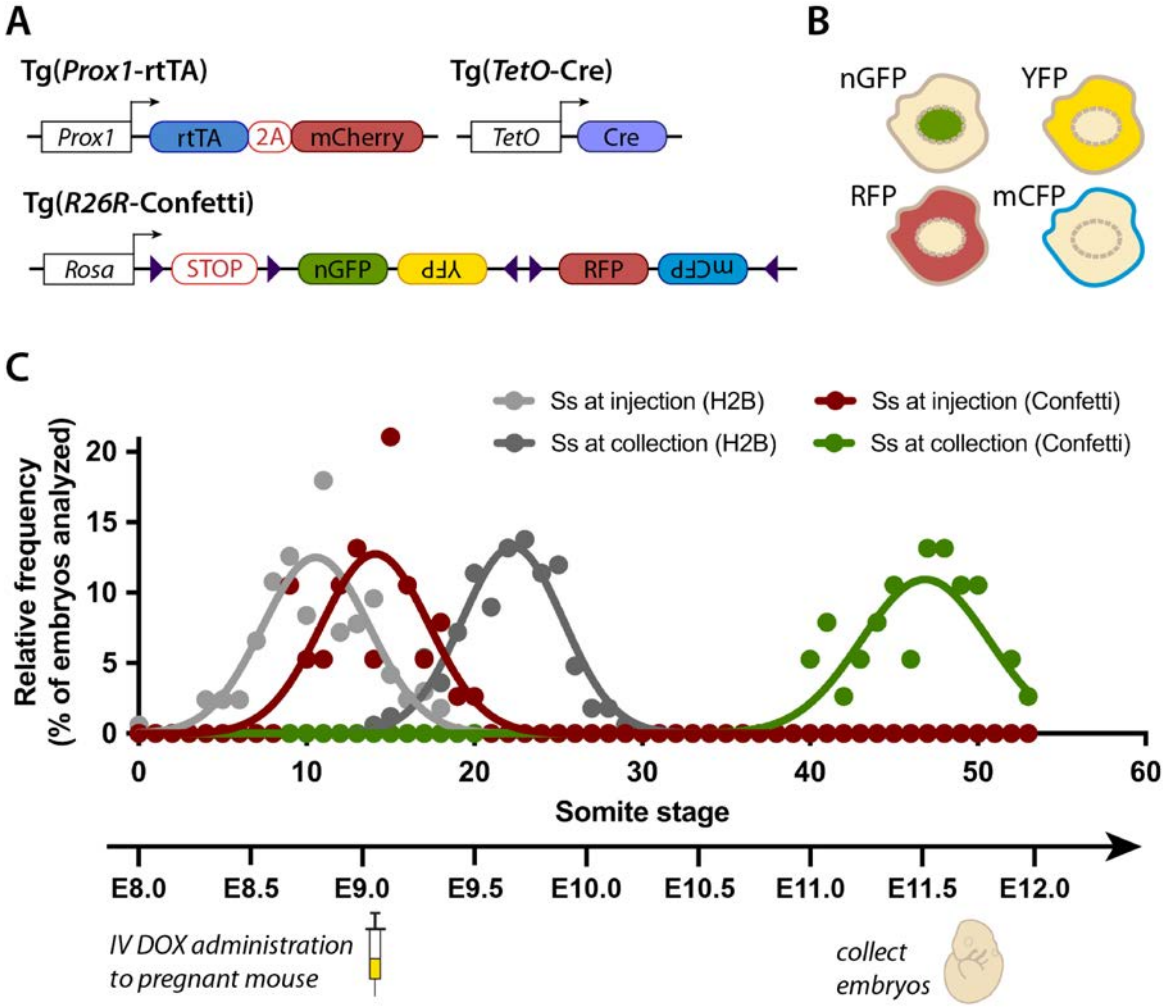

Fig. 38: Experimental setup for Tg(*R26R*-Confetti) lineage tracing. (A) Schematic representation of transgenes used in this experimental approach. **(B)** Schematic representation of cells labeled by the different fluorophores that can be expressed from the *Confetti*-locus. Labeled cells can either express nuclear GFP (nGFP), cytoplasmic RFP or YFP, or membrane-associated CFP (mCFP). **(C)** Schematic representation of the experimental setup. Pregnant females were injected with a single dose of doxycycline (150µg/g body weight) around E9.0 by intravenous injection (IV DOX). Embryos were subsequently collected at E11.5. The upper diagram shows a graphical representation of the spread of embryonic stages at the time points of injection (red graph) and embryo collection (green graph) in the analyzed dataset (n=38). For comparison, the spread in embryonic stages at the time points of injection (light gray graph) and embryo collection (dark grey graph) in the H2B-GFP lineage tracing analysis is shown.

For my experiments, Prox1-rtTA and Confetti Tg mice were intercrossed. Pregnant females were IV injected with doxycycline (150µg/g bw) at E9.0 and embryos were collected at E11.5. The experimental setup and the spread of embryonic stages at the time of label induction and

embryo collection for the Confetti experiments are shown in Fig. 38C. As a reference, the spread of embryonic stages at the time of label induction and embryo collection for the H2B-GFP lineage tracing experiments is shown as well (Fig. 38C). By comparing the two different experimental setups, it can be noted that I collected Confetti embryos at distinctly later developmental time points than H2B-GFP labeled embryos. Also, I decided to induce genetic labeling at a slightly later time point in the Confetti setup as compared to the H2B-GFP experiments (E8.5 versus E9.0). My reasoning for this was that later time points of label induction correlated with a higher chance of genetic labeling events in the ventral pancreas (Fig. 31C).

Initially, I performed Confetti lineage tracing experiments (not included in Fig. 38C), to confirm that label induction in all hepato-pancreatic tissues was achievable with this reporter line. Pregnant females were IV injected with doxycycline at E8.5 and embryos collected at E11.5. Embryos were subjected to WMIF for RFP to mark all hepato-pancreatic tissues expressing the Prox1-rtTA transgene and for Pdx1 to specifically mark the pancreatic buds. Immunostaining for GFP documented labeled cells in all hepato-pancreatic tissues (Fig. 39). In line with my short-term Prox1-rtTA lineage tracing using the H2B-GFP reporter line, I detected labeled cells in liver and dorsal pancreas at a higher density than in the ventral pancreas (Fig. 39B).

However, the initial analysis of the Confetti lineage tracing experiments also highlighted a technical problem arising from the analysis by WMIF. As several of the fluorescent proteins used in this lineage tracing approach shared structural similarities they were recognized by the same antibodies. Namely, anti-GFP antibodies recognized GFP, YFP, and CFP, while anti-RFP antibodies recognized both RFP and mCherry. Although differential sub-cellular localization of the reporter proteins (nuclear GFP, membrane-associated CFP) may be used to distinguish their immunosignals, I considered these distinctions too problematic for reliable lineage tracing. Thus, to fully exploit the advantages of the Confetti reporter system, I established a protocol for wholemount imaging of native reporter fluorescence in the hepato-pancreatic system.

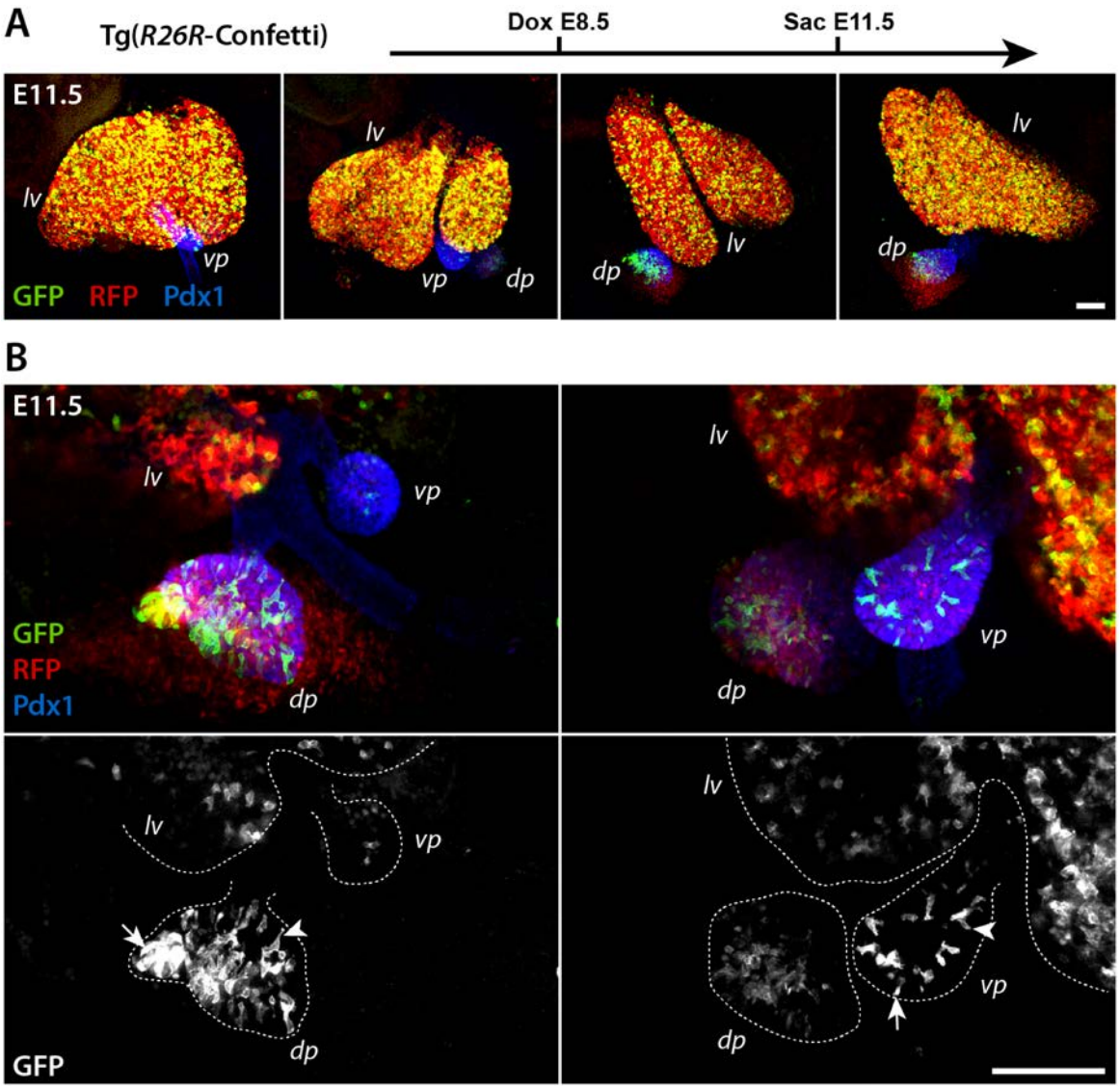

Fig. 39: Confetti labeling experiments highlight the need for imaging of native fluorescence. (A, B) WMIF of E11.5 Confetti Tg embryos. Pregnant females were injected with a single dose of 150μg/g bw doxycycline around E8.5 by intravenous injection (Dox) and Tg(*Prox1*-rtTA; *R26R*-Confetti) embryos were collected at about E11.5 (Sac). Immunostaining for GFP (green) documents cells positive for YFP ((B) arrows) and CFP ((B) arrowheads) expressed by Tg(*R26R*-Confetti). Immunostaining for RFP (red) detects mCherry expression driven by Tg(*Prox1*-rtTA) in liver (*lv*) and pancreatic buds (*vp*, *dp*), as well as cells expressing RFP driven by Tg(*R26R*-Confetti). Immunostaining for Pdx1 (blue) serves to mark pancreatic buds. Panel A demonstrates dense labeling for YFP and CFP (as detected by anti-GFP antibody) in liver and dorsal pancreas, whereas panel B documents more discrete labeling events in the ventral pancreas. Upper row in panel B shows merged color images while the lower row gives the corresponding GFP channel in gray scale. Dotted lines encircle liver, as well as ventral and dorsal pancreatic tissues. Notably, the information gained from the Confetti multicolor reporter is limited when analyzed by WMIF due to antibody cross-reactivity between YFP and CFP as well as RFP and mCherry. (scale bars: 100μm)

Imaging tissues in wholemount is technically challenging as the multitude of refractive indexes found in biological specimen typically results in considerable light scatter and, consequently, reduced tissue penetration during imaging by confocal microscopy[209].

Therefore, a process called clarification is needed before biological specimen can be analyzed by light microscopy. Clarification aims at matching the refractive indexes in a tissue to reduce light scatter and improve tissue penetration depth as well as image quality[209]. While many clarification techniques for immunostained tissues exist, they typically involve dehydration steps in methanol or ethanol which results in inactivation of fluorescent proteins. Therefore, I tested newly published solutions offering tissue clarification without compromising native reporter fluorescence and found Sca*l*eA2[195] to best suit my purposes.

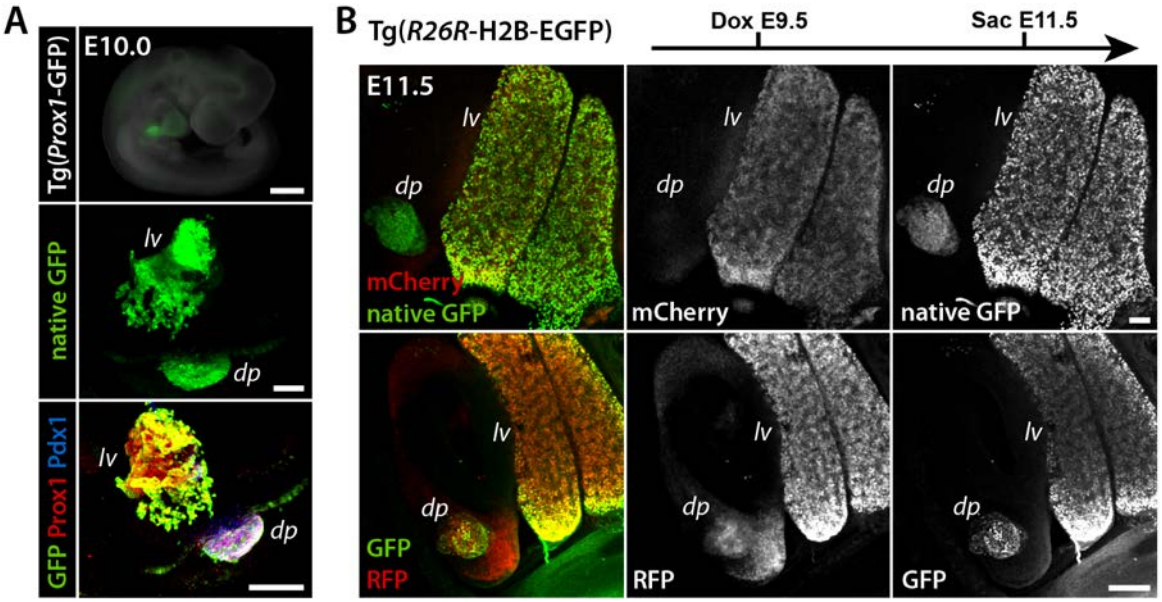

Fig. 40: Clarification solution Sca*l*eA2 preserves native fluorescence and allows for wholemount microscopy analysis. (A) Panels show an E10.0 Tg(*Prox1*-EGFP) embryo imaged on a fluorescent stereomicroscope (top) or confocal microscope (middle) following 6-day clarification in Sca*l*eA2 solution. Native fluorescence from EGFP is seen in the hepato-pancreatic organ system. The lower panel shows subsequent WMIF staining of the same embryo for GFP (green), corroborating EGFP transgene expression. Immunostaining for Prox1 (red) marks hepatic (*lv*), co-immunostaining for Prox1 and Pdx1 (blue) dorsal pancreatic bud (*dp*). **(B)** Confocal scan of native reporter fluorescence (upper panel) followed by subsequent WMIF (lower panel) in an E11.5 Tg(*Prox1*-rtTA; *R26R*-H2B-EGFP) embryo with label induction at E9.5. The experimental timeline of label induction (Dox) and embryo collection (Sac) is given above the images. Native fluorescence was imaged following 6-day clarification of the embryo in Sca*l*eA2 solution. Expression of mCherry and GFP is detected under both imaging conditions in liver, ventral (not shown) and dorsal pancreatic buds. For both native fluorescence and WMIF, the left panel shows the merged color image, while panels to the right show the indicated single channels in grayscale. (scale bars: 100μm (confocal), 1mm (stereomicroscope))

To test Sca*l*eA2 (see methods section for details), I used two different tissues expressing different fluorescent proteins, namely an E10.0 Prox1-GFP embryo and an E11.5 Tg(*Prox1*-rtTA; *TetO*-Cre; *R26R*-H2B-GFP) embryo that received doxycycline (150μg/g bw) at E9.5. Both embryos were clarified for 6 days in Sca*l*eA2 and subsequently imaged by confocal

microscopy. Native GFP fluorescence was detected in the E10.0 and the E11.5 embryo, as was mCherry fluorescence in the E11.5 embryo (Fig. 40). Subsequently, both tissues were subjected to WMIF and reimaged to confirm the expression of the fluorescent proteins by immunodetection. The E10.0 Prox1-GFP embryo was immunostained for Prox1 marking all hepato-pancreatic tissues and Pdx1 to specifically mark the pancreatic buds. Immunostaining for GFP confirmed the expression of the Prox1-GFP transgene in all hepato-pancreatic tissues (Fig. 40A). The E11.5 Tg(*Prox1*-rtTA; *TetO*-Cre; *R26R*-H2B-GFP) embryo was immunostained for RFP and GFP, confirming expression of H2B-GFP and mCherry in liver and dorsal pancreas (Fig. 40B).

Having established the proper clarification method for imaging native Confetti reporter fluorescence in the hepato-pancreatic organ system, I then required a suitable imaging platform. I chose a 2-photon laser microscopy setup, developed by Dr. Anca Margineanu (Advanced Light Microscopy Facility, MDC) for its precision in fluorophore excitation and detection[210] (personal communication). The E11.5 Confetti embryos were manually dissected to isolate the hepato-pancreatic organ system. The hepato-pancreatic tissues were clarified in Sca*l*eA2 for up to 3 months and subsequently imaged. Native reporter fluorescence for YFP, RFP, and CFP, but not GFP was detected in liver, dorsal, and ventral pancreatic buds (Fig. 41). To eliminate crosstalk between emission spectra of the different fluorophores, spectral unmixing was applied to separate the acquired images into individual channels for RFP, YFP, and CFP, as shown for the dorsal (grayscale images in Fig 41B) and ventral pancreatic buds (grayscale images in Fig 41C). Of note, detection of labeled hepatic cells was hampered by the high levels of autofluorescence of blood cells in the liver bud (Fig. 41A).

Following image acquisition and spectral unmixing, I characterized the labeling dynamics in my Confetti lineage tracing dataset and compared it to previous H2B-GFP lineage tracing experiments. Accordingly, I quantified the total number of labeled cells for each individual fluorophore in dorsal and ventral pancreata using the spot detection function of the Imaris imaging software. Due to the high autofluorescence and large tissue size of the hepatic bud at E11.5, it was not feasible to measure the total number of labeled cells in the liver in this way. Instead, I quantified the density of labeled cells in the hepatic organ domain by assessing

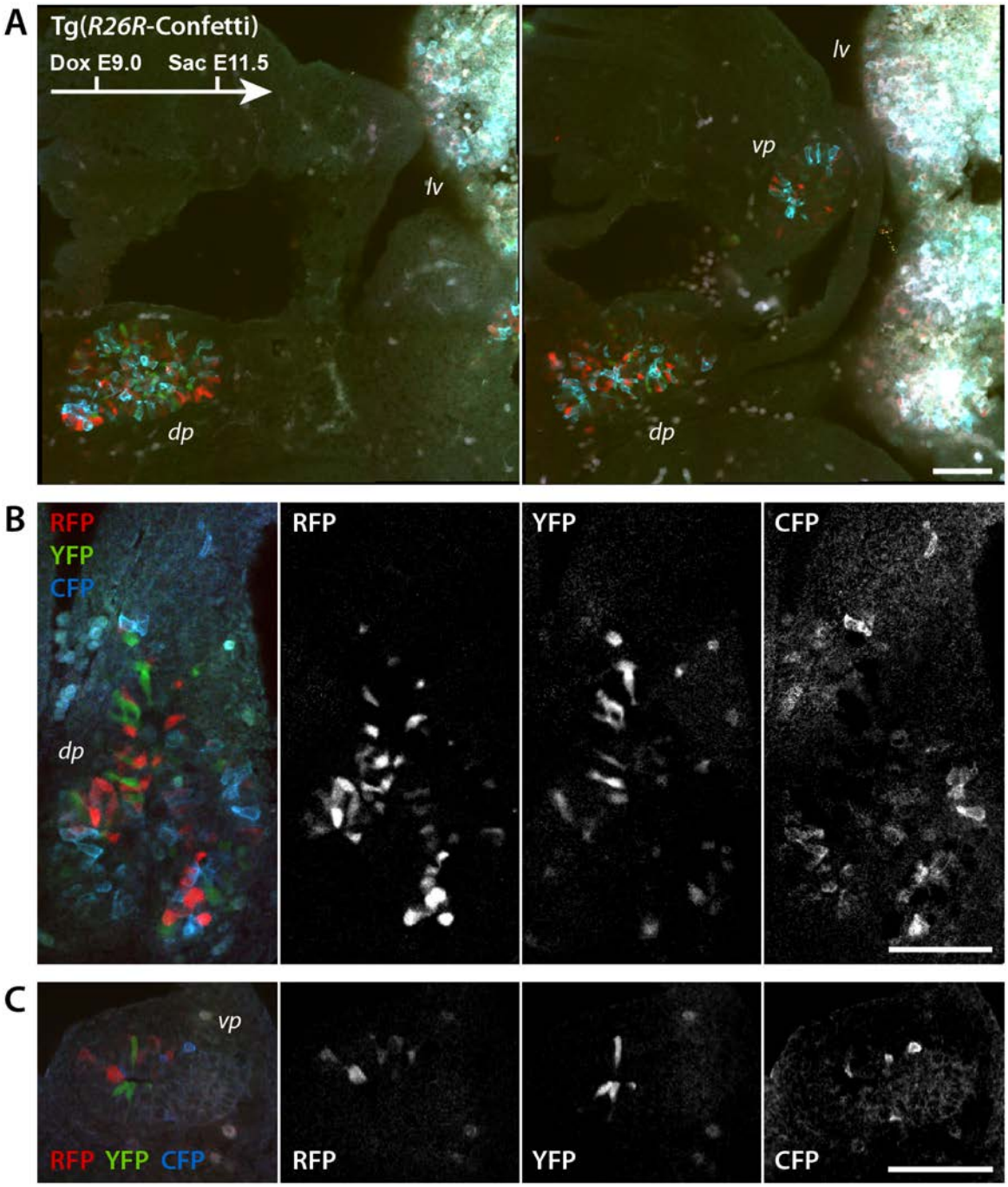

Fig. 41: Sca*l*eA2 clarification followed by 2-photon microscopy enables imaging of native fluorescence of labeled cells in wholemounts. (A-C) Native reporter fluorescence imaged by 2-photon microscopy in E11.5 Confetti Tg embryos. Pregnant females were injected with a single dose of 150µg/g bw doxycycline around E9.0 (Dox). Tg(*Prox1*-rtTA; *R26R*-Confetti) embryos were subsequently collected at E11.5 (Sac). The hepato-pancreatic organ system was dissected from the embryos in its entirety and clarified for up to 3 months in Sca*l*eA2 solution. Panel A shows optical sections giving an overview of labeled liver (*lv*), ventral (*vp*), and dorsal pancreatic tissues (*dp*) as well as unlabeled tissue surrounding the developing hepato-pancreatic organ system. Panels B and C show higher magnification images as merged color (left) or single channels in grayscale configuration (right). Labeled cells expressing YFP (green), RFP (red), or CFP (blue) can be detected in liver (A), ventral (A and C) and dorsal pancreatic buds (A and B). Detection of labeled cells in the liver is compromised by the high autofluorescence of blood cells in the liver bud (A). (scale bars: 100µm)

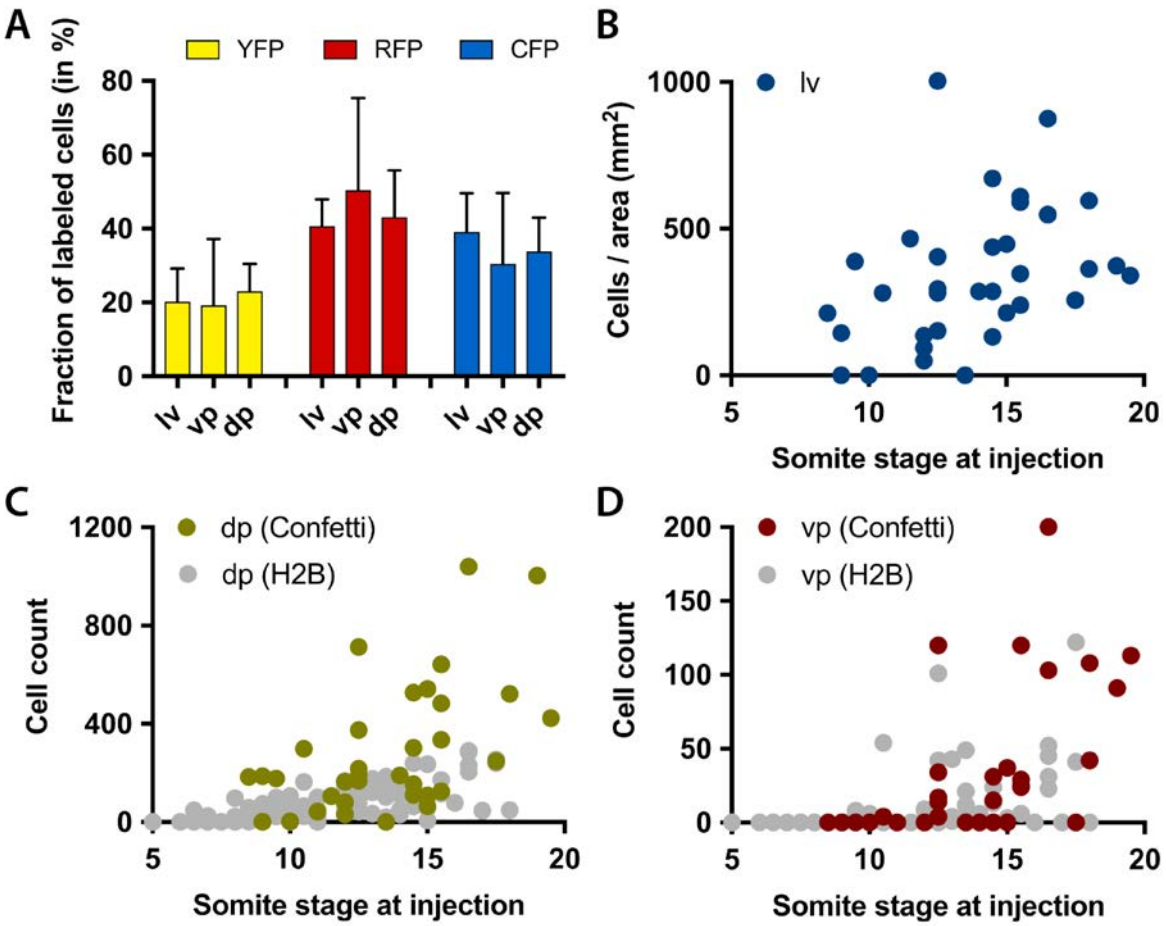

Fig. 42: Confetti lineage tracing results are in line with labeling experiments using H2B-GFP. (A) Quantification of the contribution of the indicated fluorophores to the total number of labeled cells in individual tissues and embryos shows a discrete induction efficiency for each fluorophore. **(B)** The number of labeled cells per surface area in the liver (lv) is plotted against the somite stages of the respective embryo at the time of label induction. Labeled cells in the liver show a positive correlation between labeled cell number and somite stage at label induction recapitulating results obtained for H2B-GFP lineage tracing (Fig. 31B). **(C, D)** Numbers of labeled cells in dorsal (dp, (C)), and ventral pancreatic buds (vp, (D)) are plotted against the somite stages of the respective embryo at the time of label induction. In both tissue buds, a positive correlation between the number of labeled cells and the somite stage at label induction can be observed. Similar results are obtained by H2B-GFP lineage tracing (plotted in gray). For data in (C), the distinct difference in the cell counts in the dorsal pancreas comparing Confetti (green) and H2B (gray) datasets is a result of increased cell proliferation during the prolonged tracing period in the Confetti experiment. This divergence in the Confetti and H2B datasets is not seen in the ventral pancreatic cell counts in panel D.

the number of labeled cells for each fluorophore on three representative optical sections and by calculating the average cell number per area. Next, I determined the contribution of each fluorophore to the total number of labeled cells in each tissue to exclude any labeling bias for a specific fluorophore in liver, ventral, or dorsal pancreas (Fig. 42A). As previously reported[184], recombination at the Confetti locus resulting in nGFP expression was rare and no GFP^+ cells were observed in my dataset. In contrast, YFP^+, RFP^+, and CFP^+ cells were found in all hepato-

pancreatic tissues at similar frequencies (YFP: 21%; RFP: 44%; CFP: 35%). Statistical analysis (Kruskal-Wallis test, Dunn's multiple comparisons test) showed no significant difference between hepato-pancreatic tissues, excluding any labeling bias for specific fluorophores in the analyzed tissues.

Next, I plotted the number of labeled cells in the liver (Fig. 42B), dorsal (Fig. 42C), or ventral pancreas (Fig. 42D) against the somite stage at the time of label induction. Similar to the results obtained in the H2B-GFP lineage tracing (Fig. 31B-D), a positive correlation between the number of labeled cells and the somite stage at the time of label induction was seen in all hepato-pancreatic tissues. To illustrate this similarity in labeling dynamics in Confetti and H2B-GFP lineage tracing experiments, the numbers of labeled cells observed in dorsal and ventral pancreatic buds of H2B-GFP embryos are shown together with the Confetti data in Fig. 42C, D (gray data points). Due to the extended tracing period in the Confetti experiments, dorsal pancreata of Confetti embryos showed higher labeled cell counts as compared to those in H2B-GFP embryos (Fig. 42C). However, this was not the case for the ventral pancreas, which showed similar numbers of labeled cells in Confetti and H2B-GFP embryos (Fig. 42D).

Having established the characteristics of labeling dynamics in the Confetti system, I further advanced the clonal analyses. To start defining clonal cell clusters, I first acquired data on the spatial relationship of labeled cells within the hepatic and pancreatic organ rudiments. I performed this analysis only on the pancreatic buds as quantification of all labeled cells in the liver was not possible for technical reasons detailed above. Specifically, I quantified the number of labeled cells per each fluorophore in dorsal and ventral pancreatic buds using the spot detection function in the Imaris software. I not only obtained data on the number of labeled cells but also on the XYZ-coordinates within the imaged Z-stack for each identified cell in the respective organ bud. Consequently, I was able to recreate the imaged tissue *in silico* by plotting all labeled cells according to their XYZ-coordinates, as shown in Fig. 43.

By repeating this analysis for all imaged dorsal and ventral pancreatic buds, I observed that ventral pancreata featured spatially restricted cell clusters comprising only a few labeled cells (Fig. 44). Spatially restricted cell clusters are likely descendants of a single labeled progenitor and represent a clone. The cell clusters highlighted in Fig. 44 were distinctly smaller as

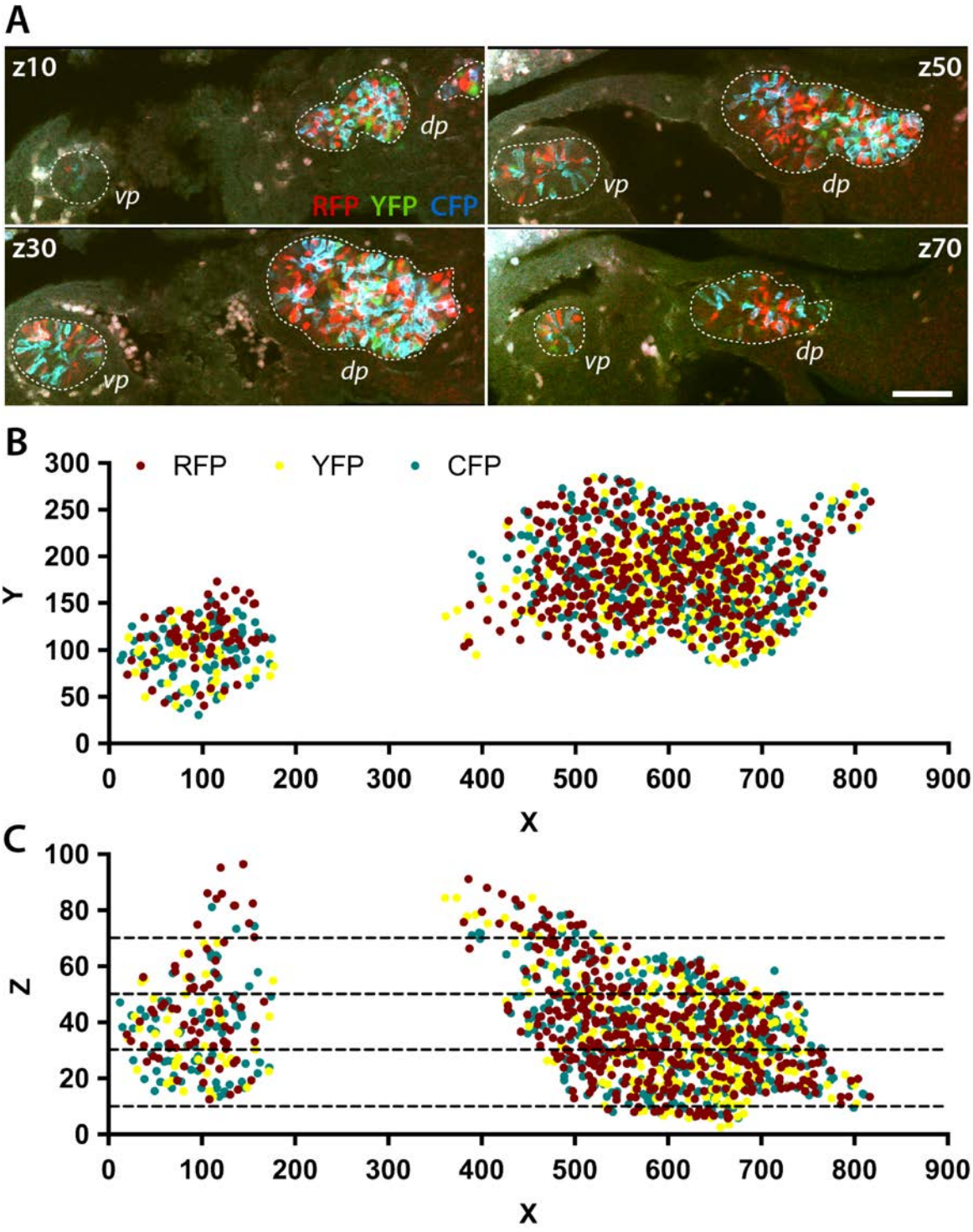

Fig. 43: Quantitative analysis of Confetti-labeled pancreata allows *in silico* reconstruction of pancreatic buds for cluster analysis. (A) Optical sections from a 2-photon microscopy scan of an E11.5 Tg(*Prox1*-rtTA; *R26R*-Confetti) embryo. Labeled cells expressing YFP (green), RFP (red), or CFP (blue) are detected in ventral (*vp*) and dorsal pancreatic buds (*dp*). The Z-position of the optical section is indicated in each image and corresponds to Z-positions indicated in (C). Dorsal and ventral pancreatic buds are encircled by dotted line. **(B, C)** Spot detection analysis using Imaris software enables identification of individual labeled cells and their XYZ-coordinates. As a result, the labeled tissue can be recreated *in silico* (see (B) for XY-plot and (C) for XZ-plot) as shown by overlap with the data in (A). Information on XYZ-coordinates of labeled cells within the labeled tissue can subsequently be used for the analysis of clonal clusters. (scale bar: 100μm)

compared to other cell clusters found in the same tissue or in other ventral or dorsal pancreatic organ buds. There are two reasons why a smaller cell cluster may be observed. The labeled progenitor cell may have proliferated less during the tracing period as compared to other labeled cells, or part of the clone is no longer present in the organ domain but contributed to a different tissue.

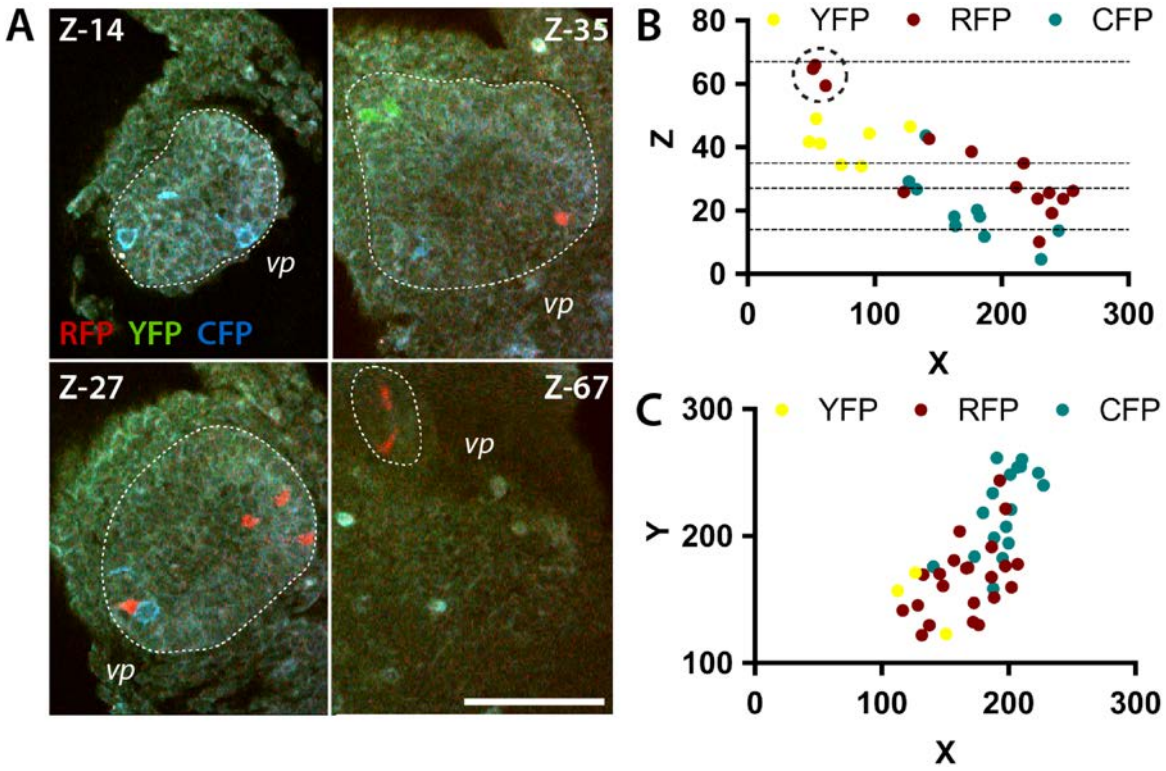

Fig. 44: Confetti-labeled ventral pancreata show distinct clusters comprising few cells. (A) Optical sections from a 2-photon microscopy scan of an E11.5 Tg(*Prox1*-rtTA; *R26R*-Confetti) embryo. Labeled cells expressing YFP (green), RFP (red), or CFP (blue) are detected in the ventral pancreas (*vp*, marked by dotted line). The Z-position of the optical sections are indicated in the upper left or right corner of each image and correspond to the Z-positions indicated in (B). **(B)** *In silico* XZ-plot of the labeled ventral pancreatic cells shown in (A). The RFP^+ cells shown in Z-67 in panel A are part of a small cluster of only three RFP^+ cells (marked by dotted circle in (B)). **(C)** *In silico* XY-plot of a ventral pancreas showing a cluster of only three YFP^+ cells. (scale bar: 100μm)

I followed up on this observation by quantifying the cell cluster size of putative labeled clones in dorsal and ventral pancreatic buds in Confetti embryos. This clustering analysis was performed in collaboration with Dr. Anca Margineanu (Advanced Light Microscopy facility, MDC) using the "Hierarchical Clustering on Principle Components" algorithm[197,198] in the R software package. This algorithm uses the geometric distances of labeled cells towards each other to divide the datasets into clusters based on their distance similarities. A prerequisite

for this analysis was the specification of the minimum and maximum number of clusters that could be identified in each sample. We performed this clustering analysis using four different sets of parameters to explore if similar patterns in cluster size distributions emerged in dorsal and ventral pancreatic buds independent of the individual parameter set. These parameter sets were based an assumption of how many cell divisions occurred during the tracing period. Basically, clones of different sizes can be generated according to the number of cell divisions during the tracing period: 2-cell clone for one cell division; 4-cell clone for two cell divisions; 8-cell clone for three cell divisions. In all models, the maximum number of clusters was set to half the number of labeled cells in the sample, as this would be the number of clones if each labeled cell divided once. The minimum number of clusters was calculated in a similar way by dividing the number of labeled cells in the sample by 4, 6, 8, or 12, depending on the underlying assumption of the average cell division of labeled cells in that particular sample (either 2, 2.5, 3, or 3.5 cell divisions).

Having established the parameter sets for our cluster analysis, Dr. Margineanu applied the clustering algorithm for each fluorophore separately in all dorsal and ventral pancreatic buds. As a result, we obtained data on the number of identified clusters in dorsal and ventral pancreata for each parameter set as well as on the individual cell count within each cluster. The cluster size distributions for ventral and dorsal pancreas for each parameter set are shown in Fig. 45. Considering an equally distributed proliferative potential in a tissue, the expected clone size distribution in a lineage tracing experiment follows a Gaussian-like distribution. Intriguingly, I observed a Gaussian-like distribution for the cluster size in the dorsal but not in the ventral pancreatic bud independently of the used parameter set (Fig. 45A-D). In fact, the cell cluster size distribution in the ventral pancreas showed a bimodal distribution in Fig. 45B-D. In all plots, ventral pancreatic cell clusters showed higher levels of clusters with low cell numbers as compared to the dorsal pancreas (Fig. 45A: 1 cell/cluster; Fig. 45B: 1-2 cells/cluster; Fig. 45C: 1-3 cells/cluster; Fig. 45D: 1-6 cells/cluster). In addition, I observed in the ventral pancreas a reduced number of clusters with high cell numbers as compared to the dorsal pancreas, as shown in Fig. 45C (>6 cells/cluster) and Fig. 45D (>7 cells/cluster).

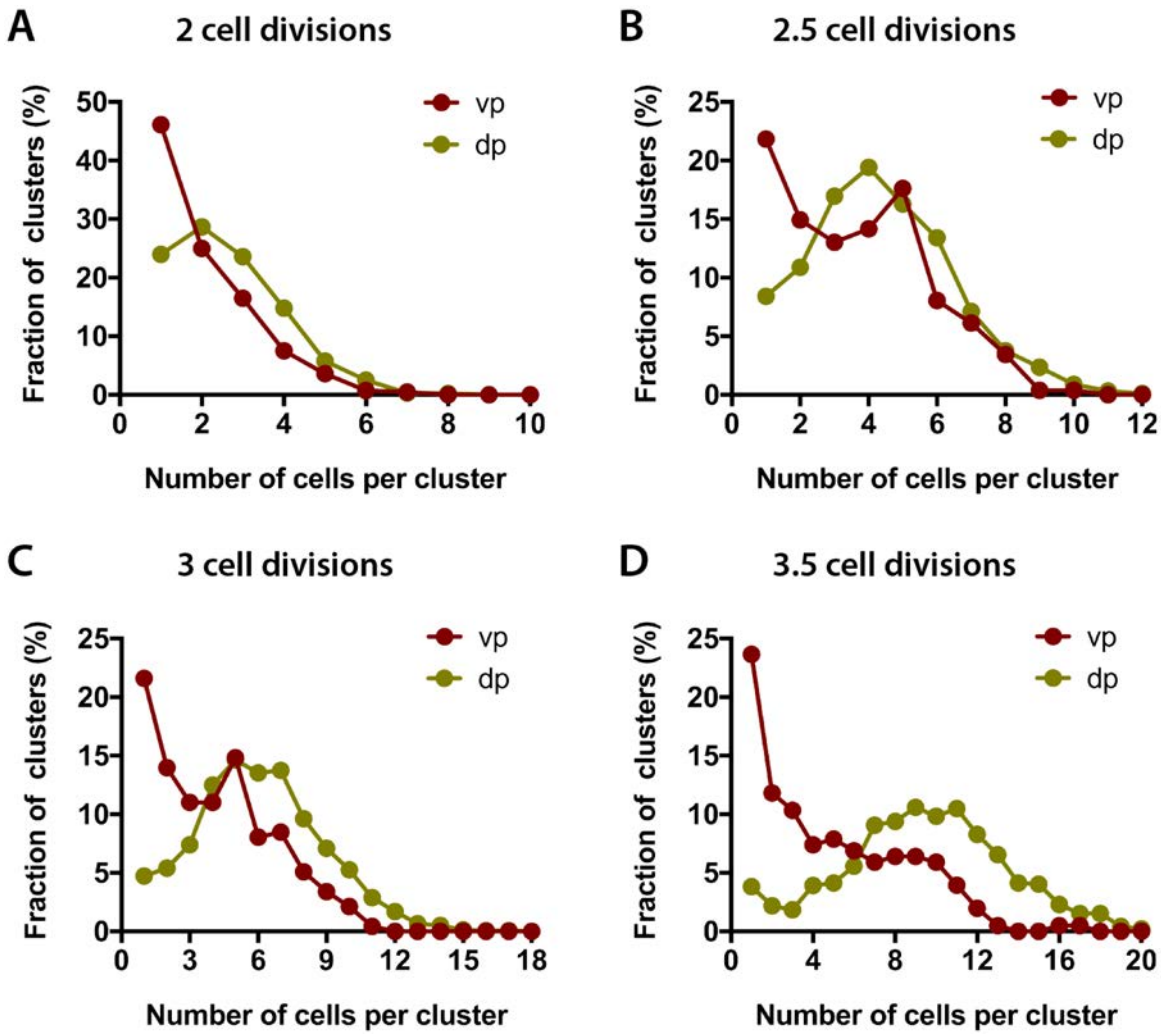

Fig. 45: Cluster analysis reveals differences in clone size distribution between dorsal and ventral pancreatic buds. (A-D) Results of four distinct clustering experiments for establishing clone size distribution in dorsal (dp) and ventral pancreatic buds (vp) from Confetti lineage tracing experiments. The clustering algorithm used for this analysis was "Hierarchical Clustering on Principal Components" (Husson et al., 2010[197]) and was applied by Anca Margineanu (Advanced Light Microscopy facility, MDC Berlin). The XYZ-coordinates of labeled cells in ventral and dorsal pancreatic buds were used for clustering individual cells into clonal clusters as a function of their geometric distance from one another. Different estimations of average cell division in labeled cells during the tracing period were used for individual clustering at 2 cell divisions (A), 2.5 cell divisions (B), 3 cell divisions (C), or 3.5 cell divisions (D). The distribution between ventral pancreatic and dorsal pancreatic clone sizes differs considerably, independent of the clustering conditions used. While the dorsal pancreatic clone size distribution resembles a Gaussian distribution, the ventral pancreas often shows a bimodal distribution (as in B, C, D). In addition, the ventral pancreas typically shows a higher percentage of small cluster sizes (1-4 cells per cluster) as compared to the dorsal pancreas.

The differences in data distribution between dorsal and ventral pancreas argued that distinct mechanisms might drive differential clonal expansion of labeled cells in the two organ rudiments. Considering the identified clusters as bona fide labeled cell clones, the clone size distribution in the dorsal pancreas may be explained by variation in the proliferation rate of individual labeled cells compared to the average proliferation rate in this tissue. This

assumption was supported by a Gaussian-like distribution of the observed clone sizes. Smaller cell clones in the ventral as compared to the dorsal pancreas could be explained by a lower average proliferation rate if the spread of data in the ventral pancreas had followed a Gaussian-like distribution. However, the ventral pancreatic clone size followed a non-Gaussian (Fig. 45A) or even bimodal distribution (Fig. 45B-D). It is therefore likely that a mechanism other than a lower proliferation rate underlies the average clone size in the ventral pancreas. Actually, the observed small ventral pancreatic clusters may be the result of progeny of cells becoming separated soon after specification and contributing to distinct organ domains as previously reported in heart development[211].

3.2.6 Lineage tracing of ventral pancreatic cells reveals contribution to the growing hepatic bud

Comparative analysis of labeling dynamics in hepato-pancreatic organ rudiments by Prox1-rtTA lineage tracing experiments documented a time-dependent increase in the ratio of labeled liver to labeled ventral pancreatic cells (Fig. 37), thereby corroborating findings obtained from an independent Foxa2-Cre lineage tracing approach (Fig. 18). By analyzing hepato-pancreatic tissue dynamics (Figs. 21-25) I documented that liver and ventral pancreas exhibit profound differences in their organ growth during organogenesis despite similar proliferation dynamics. Consequently, both lineage tracing approaches and my analyses of tissue dynamics supported the concept of plasticity between hepatic and ventral pancreatic organ rudiments during organogenesis. Finally, I used the multicolor Confetti reporter system to perform long-term Prox1-rtTA lineage tracing experiments. Cluster analysis of labeled cells in the ventral pancreas showed higher numbers of small clusters as compared to the dorsal pancreas as well as a non-Gaussian distribution of cluster sizes (Fig. 45).

Taken together, these results suggest the hypothesis that ventral pancreatic cells retain a certain cell-fate plasticity throughout organogenesis. Thus, instead of solely contributing to the growth of the ventral pancreas during this developmental time window, ventral pancreatic cells may also contribute to the rapid expansion of the liver bud. Consistent with this assumption, non-Gaussian cluster size distribution in the ventral pancreatic buds of

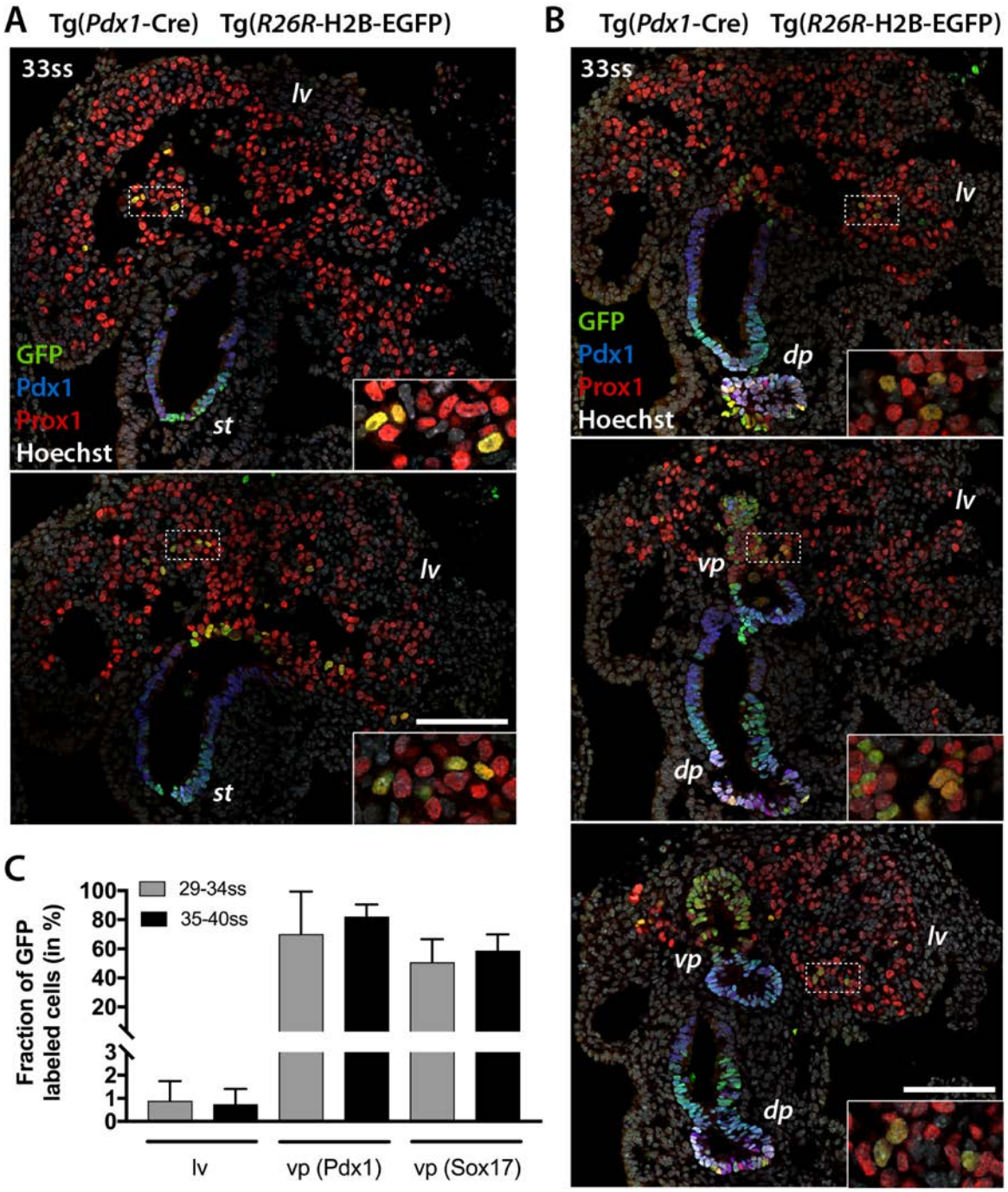

Fig. 46: Tracing of ventral pancreatic progenitors argues for a contribution of ventral pancreatic cells to the growing liver bud. (A, B) IF staining of consecutive cryosections of an E10.5 Tg(*Pdx1*-Cre; *R26R*-H2B-GFP) embryo from a Pdx1-Cre lineage tracing experiment. Immunostaining of Prox1 (red) marks hepatic and co-immunostaining of Prox1 and Pdx1 (blue) pancreatic organ buds. Immunostaining for GFP (green) documents labeled cells descended from Pdx1$^+$ progenitors in Pdx1$^+$ tissues, including the posterior stomach (*st*, (A)), dorsal (*dp*, (B)), and ventral pancreatic buds (*vp*, (B)). In addition, GFP$^+$ cells are found scattered throughout the liver bud (*lv*, (A, B)). **(C)** Measurements of the GFP$^+$ cell fractions in liver and ventral pancreas at E10.25 (29-34ss) and E10.5 (35-40ss) shows 70-80% of cells in the Pdx1$^+$ ventral pancreatic bud and 50-60% of cells in the Sox17$^+$ ventral pancreatic bud to be labeled (E10.25: n=6; E10.5: n=11). Labeling density in the liver bud averages at 0.74-0.89% (E10.25: n=7; E10.5: n=7). (scale bars: 100μm)

Confetti lineage tracing experiments (Fig. 45) might result from unequal contribution of individual labeled ventral pancreatic clones to liver growth.

For testing this intriguing hypothesis and documenting a direct contribution of ventral pancreatic cells to the hepatic organ domain, I performed additional lineage tracing experiments. For this, I used the Tg(*Pdx1*-Cre)[212] (hereafter abbreviated Pdx1-Cre) mouse line allowing expression of the Cre recombinase and subsequent genetic labeling in $Pdx1^+$ tissues, including the ventral pancreas. I set up timed matings between Pdx1-Cre males and H2B-GFP females and collected embryos at E10.25-10.5. Cryosections of embryos were prepared and IF stained for Prox1 to mark all hepato-pancreatic tissues and for Pdx1 to mark tissues expressing the Cre recombinase. As expected, immunostaining for GFP detected labeled (GFP^+) cells in all $Pdx1^+$ tissues, namely dorsal and ventral pancreas, duodenum and posterior stomach, in all analyzed embryos (19/19) (Fig. 46A, B). Interestingly, labeled cells were also detected in the liver of almost all analyzed embryos (18/19) (Fig. 46A, B). Of note, all labeled cells found in the liver were $Pdx1^-$, arguing that they were descendants of $Pdx1^+$ progenitor cells, but had shut down expression of this transcription factor.

I continued by quantifying the GFP^+ cell fraction in liver and ventral pancreas at E10.25 (29-34ss) and E10.5 (35-40ss) (Fig. 46C). As mentioned in the introduction (chapters 1.2.3 and 1.2.4), at E10.5 the ventral pancreas has divided into primarily $Sox17^+$ or $Pdx1^+$ subpopulations[150]. Therefore, I analyzed the labeled cell population in the ventral pancreas separately in these two subpopulations. Quantification of the labeled cell fraction in the $Pdx1^+$ ventral pancreas served as an estimate of the labeling efficiency of the Pdx1-Cre transgene. At E10.25 and E10.5 about 70-80% of cells in the $Pdx1^+$ ventral pancreatic bud and about 50-60% of cells in the $Sox17^+$ ventral pancreatic bud were GFP^+. At the same stages, a significant labeling density was evident in the liver bud (0.74-0.89%), confirming that the liver harbors descendants of $Pdx1^+$ progenitor cells. In all likelihood, these $Pdx1^+$ progenitors originated from the ventral pancreatic bud.

Next, I recreated the analyzed hepatic and ventral pancreatic buds *in silico* to determine whether GFP^+ hepatic cells were restricted to a specific region in the hepatic bud (Fig. 47A, B). To this aim, I used the spot detection function in Imaris to obtain XY-coordinates (in μm)

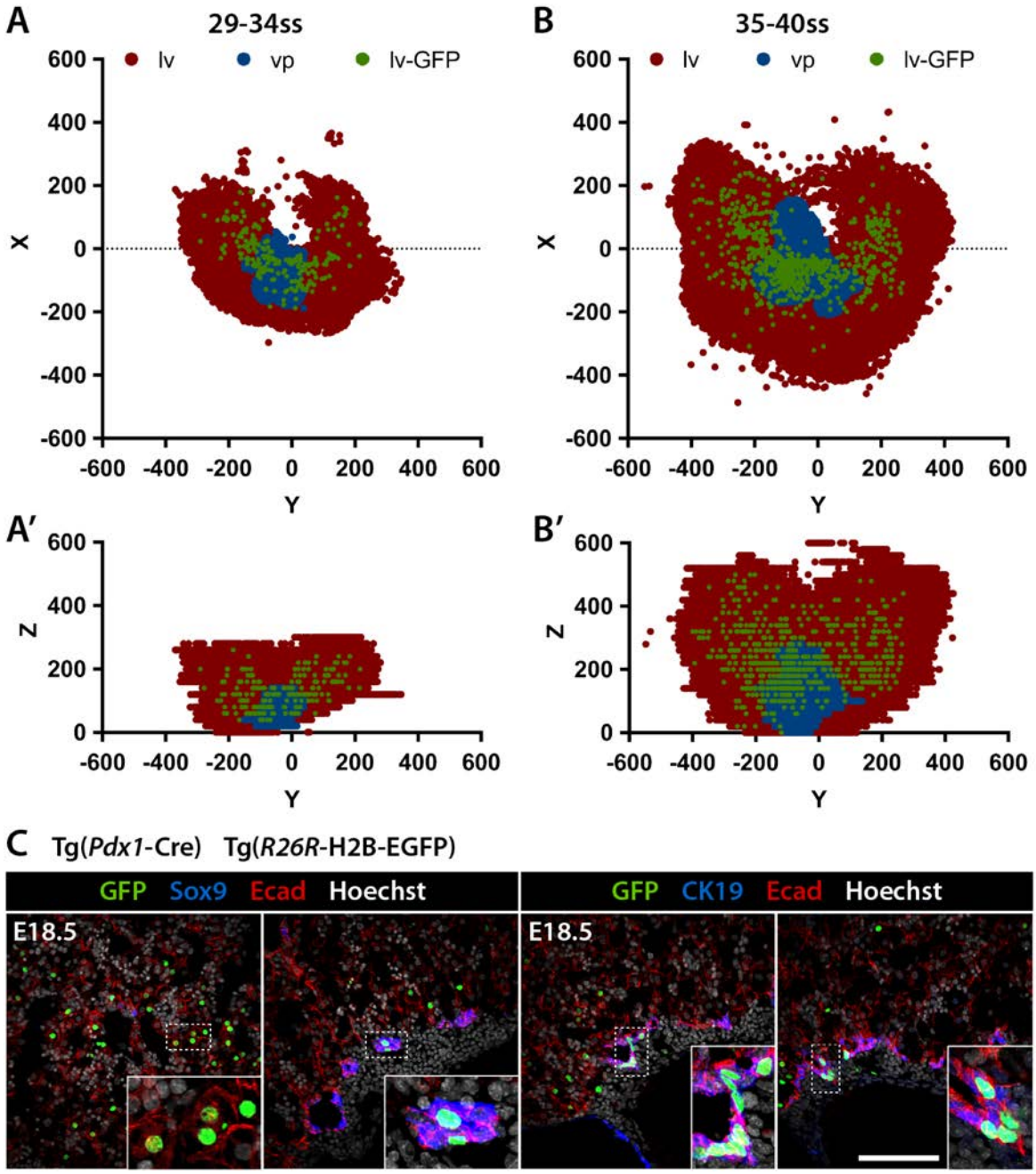

Fig. 47: Quantitative analysis of Pdx1-Cre lineage tracing documents the presence of ventral pancreas descended cells throughout the liver bud. (A, A', B, B') Quantitative representation of *Pdx1*-Cre lineage tracing experiments. IF analyses of cryosections from E10.25-E10.5 Tg(*Pdx1*-Cre; *R26R*-H2B-GFP) embryos stained for Prox1, Pdx1, and GFP (as exemplified in Fig. 46, panels A and B) were digitalized and XYZ-coordinates for individual GFP^--liver cells (lv), GFP^+-liver cells (lv-GFP), and ventral pancreatic cells (vp) obtained. Data from E10.25 ((A, A') 29-34ss, n=8) and E10.5 ((B, B') 35-40ss, n=11) embryos were combined. 18 out of 19 analyzed embryos showed labeled cells in the liver bud. The quantification demonstrates that descendants of $Pdx1^+$ ventral pancreatic cells are spread throughout the growing liver bud. Notably, GFP^+-liver cells are found at a higher density in close proximity to the ventral pancreas. **(C)** IF staining of cryosections from E18.5 Tg(*Pdx1*-Cre; *R26R*-H2B-GFP) embryos for the indicated markers. Long term *Pdx1*-Cre lineage tracing experiments document that GFP^+ cells persist in the liver until E18.5 as visualized by GFP immunostaining (green). Co-immunostaining of Ecad (red) marks hepatocytes, while Sox9 (blue) and CK19 (blue) mark bile duct cells. Insets represent high magnification images of the boxed areas in the corresponding overview images. (scale bar: 100μm)

for hepatic GFP^+ and GFP^- cells as well as for ventral pancreatic cells of each cryosection of the analyzed Pdx1-Cre embryos. The Z-position of each cell was assigned according to the anterior to posterior position of the respective cryosection. Then, I grouped the embryos into somite stages 29-34ss (E10.25; Fig. 47A, A') and 35-40ss (E10.5; Fig. 47B, B') and plotted the identified ventral pancreatic as well as GFP^+ and GFP^- liver cells according to their XY- (Fig. 47A, B) or YZ-coordinates (Fig. 47A', B'). Although GFP-labeled cells were found throughout the hepatic tissue, they clearly clustered at higher density in the hepatic region in close proximity to the ventral pancreatic bud, suggesting that this region is the source of the labeled liver cells.

To query the long-term contribution of this labeled cell population to the maturing liver, I performed Pdx1-Cre experiments with an extended tracing period. In detail, I collected E18.5 Tg(Pdx1-Cre; R26R-H2B-GFP) embryos and prepared cryosections of liver tissue. IF staining for E-cadherin (Ecad) marked all hepatic cells, while staining for Sox9 or cytokeratin 19 (CK19) marked bile duct cells. Immunostaining for GFP confirmed the continued presence of GFP-labeled cells in the E18.5 liver (Fig. 47C). GFP staining was detected in hepatocytes ($Ecad^+$, $Sox9^-$, $CK19^-$) as well as in bile duct cells ($Ecad^+$, $Sox9^+$, $CK19^+$), documenting that descendants of $Pdx1^+$ ventral pancreatic cells contributed to different hepatic cell populations.

Together, these results strongly support a remarkable cell fate plasticity in the ventral foregut and its derivatives. While previous studies argued that the early ventral foregut endoderm is bipotent[5,6,8,9] and can differentiate into either hepatic or pancreatic endoderm[5,6,8,9], my results argued that this bipotency is retained in ventral pancreatic cells. In fact, my studies indicated that the potential to acquire hepatic or pancreatic fate is maintained in ventral pancreatic cells for much longer during development than previously expected. However, the mechanism by which pancreatic identity and cell fate plasticity, i.e. the potential for hepatic or pancreatic fate acquisition, are maintained in the ventral pancreas remains unknown.

3.3 The Robo signaling pathway acts as a gatekeeper of pancreatic identity during the hepato-pancreatic lineage divergence

Overall, the mechanisms and distinct signaling pathways involved in the establishment and maintenance of pancreatic identity in the ventral foregut endoderm are still poorly understood. While signaling cues promoting hepatic (FGF, BMP)[5,6,9] or pancreatic fate in the dorsal foregut (FGF2, Activin)[115,116] are well characterized, the same is not true for the ventral pancreatic domain. In an effort to address this still open question, the Spagnoli laboratory used RNA-sequencing approaches to define distinct hepatic, dorsal, and ventral pancreatic signaling signatures during early fate acquisition (E8.5-10.5)[147].

Among the genes specifically upregulated in ventral pancreatic progenitors were *Robo1* and *Robo2*, which encode for the Roundabout guidance receptor (Robo) 1 and 2, respectively. Robo proteins are transmembrane receptors that signal primarily through the binding of Slit ligands[213]. Although the Robo signaling pathway is primarily known for its function in axon guidance[190,214], an increasing body of work has recently identified its role during the development of a multitude of organs, including kidney[191], heart[215–218], and mammary gland[219,220]. Recent work in the Spagnoli laboratory discovered the importance of the Robo-Slit signaling pathway also during pancreatic development[148]. I contributed to this recently published study[148] by investigating the specific functions of Robo1 and Robo2 during early hepato-pancreatic lineage segregation. Specifically, I focused on the question whether Robo-Slit signaling regulates cell plasticity in the ventral pancreas while preserving pancreatic identity.

To investigate the relevance of Robo-Slit signaling in early ventral pancreatic development, I collected E9.5 embryos either wild-type (control) or genetically deficient for Robo1[190] and Robo2[191] (Robo1/2 KO). The embryos were subjected to WMIF for Prox1 marking all hepato-pancreatic tissues and for Pdx1 marking the pancreatic buds (Fig. 48A). Robo1/2 KO embryos featured distinctly smaller ventral pancreatic buds, often coinciding with a disorganized morphology of this tissue (Fig. 48A, right panel). Next, I quantified the volume of hepato-pancreatic buds in control and Robo1/2 KO embryos. Organ bud volume was determined from

WMIF confocal Z-scans by measuring organ area on individual optical sections. Then, the average organ area was multiplied by tissue depth to calculate the organ volume. Robo1/2 KO embryos showed significantly smaller ventral pancreatic buds as compared to control littermates, while no difference in volume of liver or dorsal pancreas was observed (Fig. 48B).

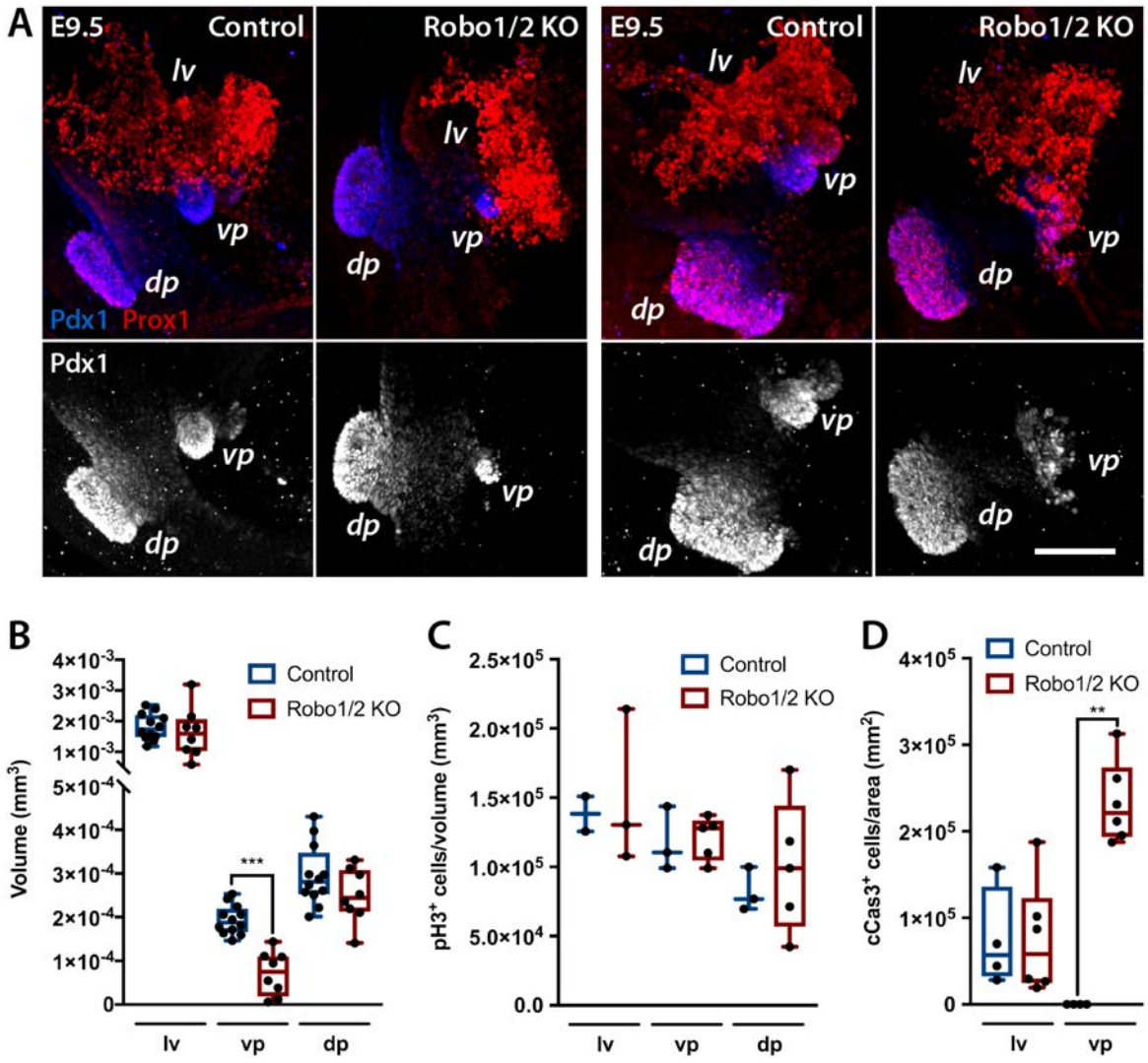

Fig. 48: Combined loss of Robo1 and 2 leads to specific reduction in size of the ventral pancreas. (A) Representative WMIF of E9.5 embryos either wild-type (control) or genetically deficient for Robo1 and Robo2 (Robo1/2 KO). Immunostaining of Prox1 (red) marks liver (*lv*), co-immunostaining of Prox1 and Pdx1 (blue) marks ventral (*vp*) and dorsal pancreatic buds (*dp*). A clear reduction in the ventral pancreas size in mutants as compared to control littermates can be observed. Lower panels show Pdx1 staining in grayscale. **(B)** Measurements of hepato-pancreatic organ volume at E9.5 in Robo1/2 KO embryos (n=8) and control littermates (n=12) show a statistically significant reduction in ventral pancreatic organ volume whereas liver and dorsal pancreas volumes are unaffected. **(C)** Quantification of cells stained for mitotic marker phospho-histone 3 (pH3) by IF in E9.5 in Robo1/2 KO embryos (lv: n=3; vp: n=5; dp: n=5) and control littermates (lv: n=2; vp: n=3; dp: n=3) fails to detect a difference in cell numbers comparing the indicated hepato-pancreatic organ buds. **(D)** Apoptotic cells in liver and ventral pancreas were identified by IF detection of cleaved Caspase 3 (cCas3). Quantification of $cCas3^+$ cells documents elevated levels of apoptosis in the ventral pancreas but not in the liver of Robo1/2 KO embryos (n=6) as compared to control littermates (n=4). (Mann-Whitney test; $p<0.01$: **; $p<0.001$: ***) (scale bar: 100µm)

To determine the reason behind this difference in organ rudiment size, I assessed proliferation rates and levels of apoptosis in Robo1/2 KO and control embryos. To evaluate proliferation rates, E9.5 control and KO embryos were subjected to WMIF for Prox1 to mark hepato-pancreatic organ buds, for Pdx1 to mark pancreatic buds, and for pH3 to mark proliferating cells. Analysis of $pH3^{+}$ cell numbers at E9.5 in liver as well as dorsal and ventral pancreatic buds showed no significant difference between control and Robo1/2 KO embryos (Fig. 48C). Next, I analyzed levels of apoptosis in liver and ventral pancreas by quantifying cleaved Caspase 3^{+} (cCas3) cell numbers. In detail, I collected E9.5 control and Robo1/2 KO embryos, prepared cryosections, and performed IF staining for Prox1 to mark liver and ventral

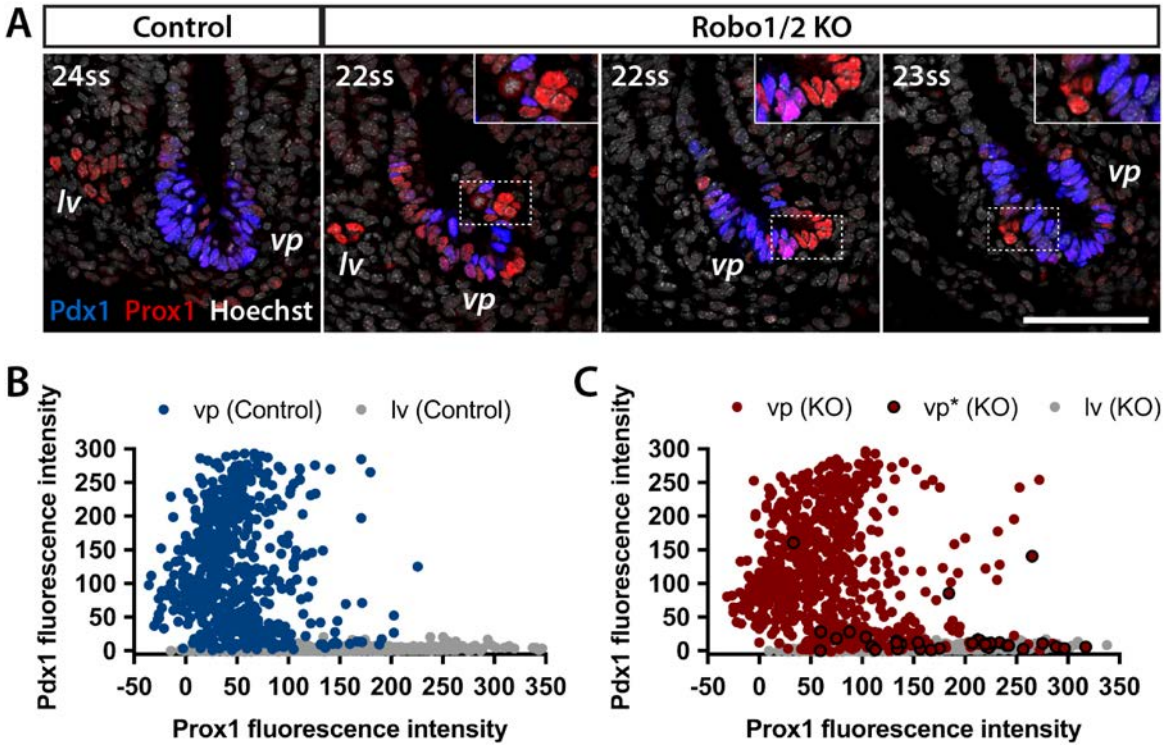

Fig. 49: Qualitative differences in pancreatic marker gene expression are observable at E9.5 by comparing Robo1/2 KO and control embryos. (A) Representative IF staining of cryosections from E9.5 (22-24ss) Robo1/2 KO embryos and a control littermate. Immunostaining of Prox1 (red) marks liver (*lv*) while co-immunostaining of Prox1 and Pdx1 (blue) marks ventral pancreas (*vp*). Tissues were counterstained with Hoechst dye (grayscale). Insets show higher magnification images of boxed area in the overview images. Robo1/2 KO ventral pancreata show distinct cells that downregulated the pancreatic marker Pdx1 but express Prox1 at higher levels as compared to neighboring $Pdx1^{+}$ cells (see insets), thus resembling hepatic cells (*lv*). **(B, C)** Quantification of IF stained cryosections from E9.5 control (B; n=3) and Robo1/2 KO littermates (C; n=3). Prox1 and Pdx1 fluorescence intensity were measured for ventral pancreatic cells (564 cells in B; 713 cells in C) and hepatic cells (1261 cells in B; 1036 cells in C) of the respective embryo. Robo1/2 KO embryos show a considerable number of ventral pancreatic cells overlaying with liver cells (C). This feature is particularly pronounced in the cell population vp*, which denominates cells that appear segregated from the surrounding ventral pancreatic epithelium as highlighted in the insets in panel A. (scale bar: 100μm)

pancreas, for Pdx1 to specifically mark the ventral pancreas, and for cCas3 to stain apoptotic cells. Quantification of $cCas3^{+}$ cell numbers showed a specific increase in apoptosis in the ventral pancreas of KO embryos, but not in the liver as compared to control littermates (Fig. 48D).

Although Robo1/2 KO ventral pancreata showed increased levels of apoptosis as compared to control tissues, the numbers of observed apoptotic cells were still low. Therefore, I reasoned that increased apoptosis may not be the main mechanism responsible for the massive decrease in ventral pancreatic organ volume observed in Robo1/2 KO embryos (Fig. 48A, B). To analyze the Robo1/2 KO phenotype in more detail, I further examined Prox1 and Pdx1 expression in ventral pancreatic cells at the single-cell level. Specifically, I performed IF stainings for Prox1 and Pdx1 on cryosections of E9.5 control and KO embryos. Ventral pancreatic cells in control embryos showed co-expression of Prox1 and Pdx1 (Fig. 49A). In contrast, Robo1/2 KO ventral pancreata featured cells within the ventral pancreatic bud that showed no Pdx1 expression but elevated expression of Prox1, similar to hepatoblasts (Fig. 49A). These cells often formed clusters that appeared to be segregated from the surrounding ventral pancreatic epithelium (see insets in Fig. 49A).

To follow up on this observation, I quantified Prox1 and Pdx1 fluorescence intensities in all ventral pancreatic cells of control and Robo1/2 KO embryos individually using ImageJ. To allow for comparison between ventral pancreatic cells and hepatoblasts, fluorescence intensities in liver cells of the respective embryos were quantified as well. I plotted Pdx1 fluorescence intensity against Prox1 fluorescence intensity and observed a clear separation of ventral pancreatic and hepatic cells in control embryos, with minimal overlap of the two cell populations (Fig. 49B). By performing the same analysis for Robo1/2 KO embryos (Fig. 49C), I instead observed a considerably increased overlap of ventral pancreatic and hepatic cells. Especially, ventral pancreatic cells, which appeared segregated from the surrounding ventral pancreatic epithelium (see insets in Fig. 49A) and marked as vp* in Fig. 49C, overlapped with liver cells in Fig. 49C. Taken together, these analyses documented qualitative differences in the expression patterns of Prox1 and Pdx1 in ventral pancreatic cells of Robo1/2 KO and control embryos, suggesting similarity of the $Pdx1^{-}$ $Prox1^{high}$ ventral pancreatic cells in Robo1/2 KO embryos to hepatoblasts.

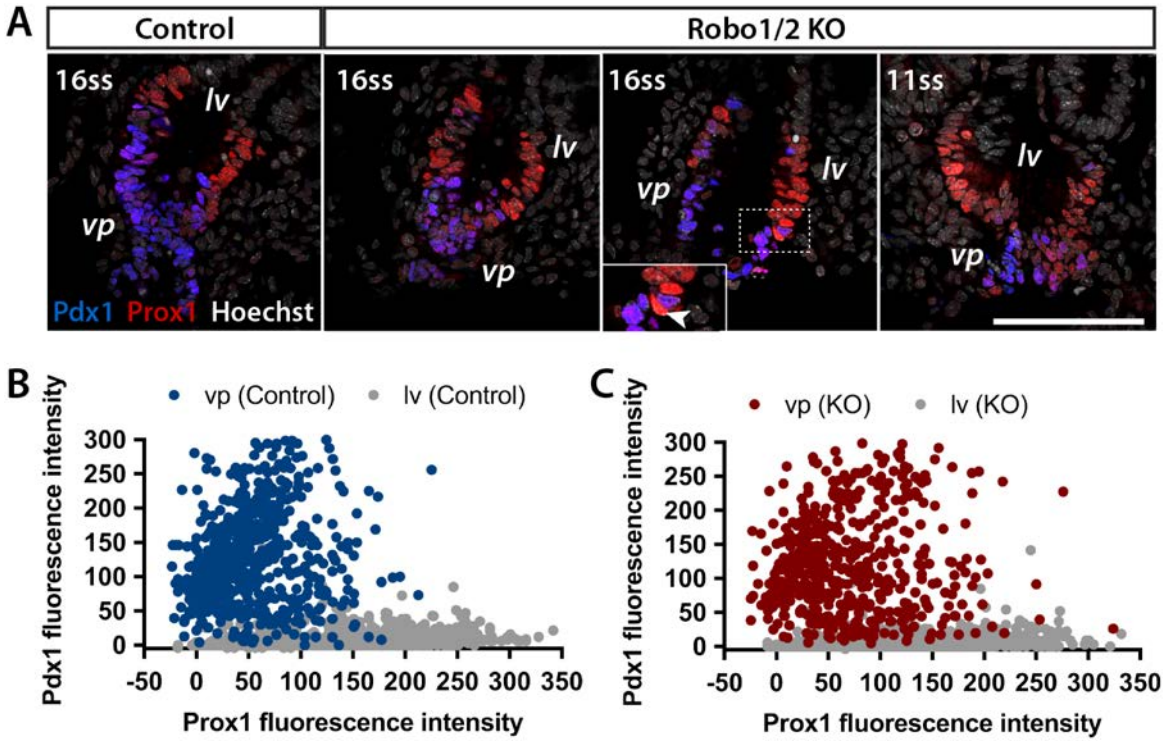

Fig. 50: Expression of pancreatic marker genes is comparable in Robo1/2 KO and control embryos until E9.0. (A) Representative IF staining of cryosections from E8.5-9.0 (11-16ss) Robo1/2 KO embryos and a control littermate. Immunostaining of Prox1 (red) marks liver (*lv*), while co-immunostaining of Prox1 and Pdx1 (blue) marks ventral pancreas (*vp*). Tissues are counterstained with Hoechst dye (grayscale). The inset shows a higher magnification image of the boxed area in overview image. Robo1/2 KO ventral pancreata rarely show cells that downregulated the pancreatic marker Pdx1 and express Prox1 at higher levels compared to control ventral pancreatic cells (see arrowhead in inset and compare to Fig. 49A). **(B, C)** Quantification of IF stained cryosections of E8.5-9.0 control (B; n=6) and Robo1/2 KO (C; n=6) embryos. Prox1 and Pdx1 fluorescence intensity were measured for ventral pancreatic cells (658 cells in B; 516 cells in C) and hepatic cells (1484 cells in B; 1288 cells in C) of the respective embryo. No discernible difference in the signal distribution in ventral pancreatic cells is seen comparing Robo1/2 KO and control embryos. (scale bar: 100μm)

Next, I investigated whether Pdx1^{-} Prox1^{high} cells were present in the Robo1/2 KO ventral pancreas from the time of ventral pancreatic specification (E8.5-9.0) or only at later time points. Towards this aim, I assessed the expression of Prox1 and Pdx1 in ventral pancreatic and hepatic cells in E8.5-9.0 control and KO embryos (Fig. 50A), like the analysis performed at E9.5 (Fig. 49). In contrast to the situation at E9.5, Pdx1^{-} Prox1^{high} cells were rarely found at earlier stages (see inset in Fig. 50A). Moreover, the quantification of Prox1 and Pdx1 fluorescence intensities showed ventral pancreatic and hepatic cells clustering in two populations independently of the genotype, as shown by comparing control (Fig. 50B) and Robo1/2 KO (Fig. 50C) tissues. Although I detected Robo1/2 KO ventral pancreatic cells with higher Prox1 levels than observed in the control ventral pancreas dataset, the difference

between the genotypes was less pronounced at E8.5-9.0 as compared to E9.5 (compare Fig. 49B, C to Fig. 50B, C). Taken together, my analysis of the Robo1/2 KO phenotype at E8.5-9.0 showed that the expression of the pancreatic marker genes Prox1 and Pdx1 in early ventral pancreatic cells is comparable between control and KO embryos. Distinct differences in Prox1 and Pdx1 expression, accompanied by the emergence of cells resembling hepatoblasts, appeared in Robo1/2 KO embryos only after E9.0.

I then asked the question whether Pdx1^{-} Prox1^{high} cells in the Robo1/2 KO ventral pancreata actually adopted hepatic features. In detail, cryosections from E9.5 Robo1/2 KO and control embryos were immunostained for Prox1 to mark liver and ventral pancreas, for Pdx1 to mark the ventral pancreas, and for the hepatic genes, such as albumin (Fig. 51A) or α-fetoprotein (Fig. 51B). Ventral pancreatic cells in control embryos did not express albumin and only rarely α-fetoprotein, whereas a large proportion of Pdx1^{-} Prox1^{high} cells in the ventral pancreas of Robo1/2 KO embryos not only downregulated the pancreatic marker Pdx1 but also expressed hepatic markers instead (Fig. 51A and B). To determine whether these hepatoblast-like cells also lost pancreatic markers other than Pdx1, I performed IF stainings for Sox9. As shown in Fig. 51E, Sox9 was highly expressed in control ventral pancreata but downregulated in ventral pancreatic cells of Robo1/2 KO embryos, especially in hepatoblast-like cells.

Around E9.5, liver cells start to leave the stratified epithelium of the hepatic bud and invade the surrounding septum transversum mesenchyme[123,127,133,134]. For this, hepatoblasts degrade and cross the basal lamina surrounding them[123,131,132]. This process is accompanied by profound changes in their actin cytoskeleton, as they change their cell morphology from that of an epithelial cell with typical apical-basal polarity to a migratory mesenchymal-like cell[123,127]. To investigate whether of Robo1/2 KO hepatoblast-like cells acquired similar features, cryosections from E9.5 Robo1/2 KO and control embryos were immunostained for Prox1 to mark liver and ventral pancreas as well as for Pdx1 to mark the ventral pancreas together with laminin or F-actin. Co-immunostaining for laminin demonstrated that hepatoblast-like cells, grouped in large clusters within the ventral pancreatic epithelium, had a thinner basal lamina and looked like invading the mesenchyme surrounding the ventral pancreatic bud (Fig. 51C). Additionally, phalloidin staining for F-actin documented changes in the actin-cytoskeleton of such hepatoblast-like cells as compared to the rest of the ventral

pancreatic epithelium (Fig. 51D). While ventral pancreatic cells in control embryos showed strong apical-basal polarity and apical accumulation of F-actin, hepatoblast-like cells in Robo1/2 KO embryos often presented reduced apical, but distinct basal or lateral accumulation of F-actin (Fig. 51D).

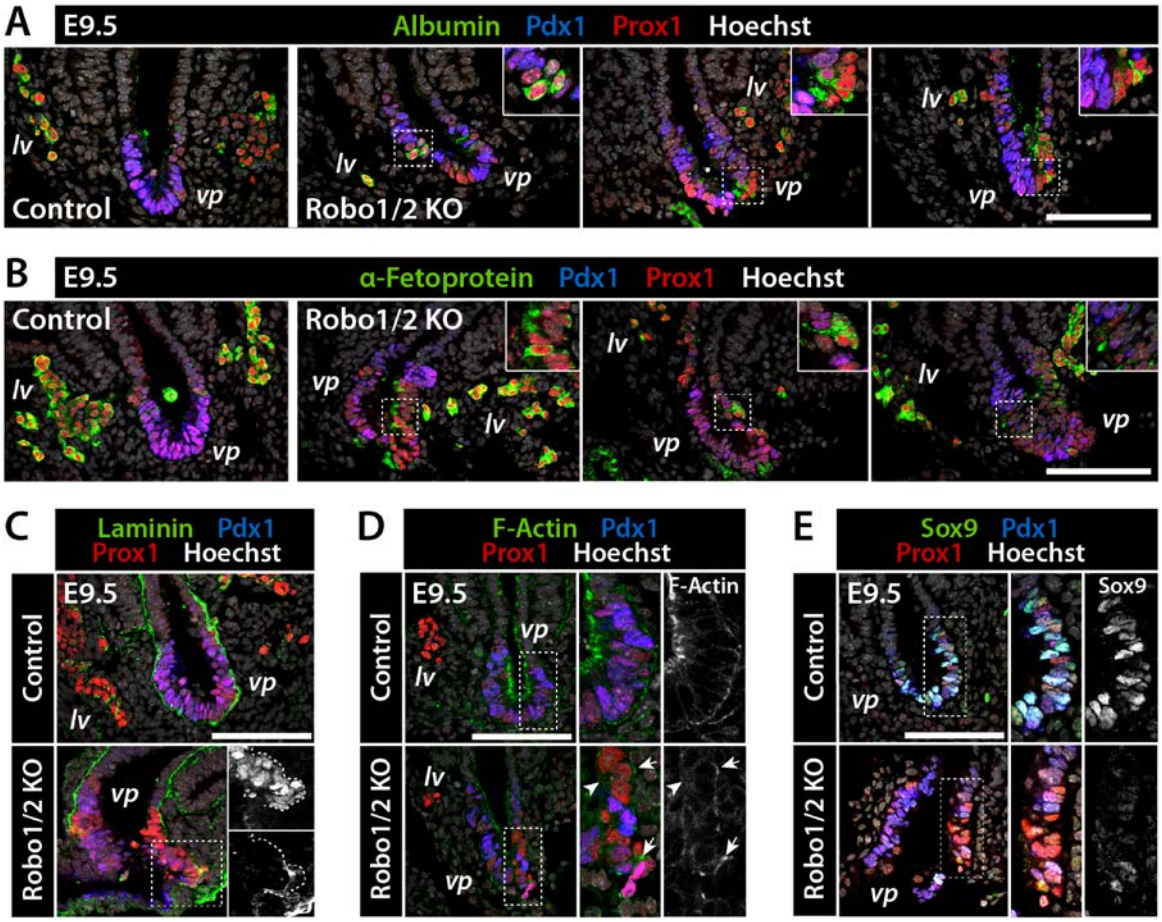

Fig. 51: Ventral pancreatic cells in Robo1/2 KO embryos lose pancreatic identity and acquire hepatoblast features. Representative IF staining of cryosections of E9.5 Robo1/2 KO embryos and control littermates for the indicated markers (green). Immunostaining of Prox1 (red) marks liver (*lv*), while co-immunostaining of Prox1 and Pdx1 (blue) marks ventral pancreas (*vp*). Tissues are counterstained with Hoechst dye (grayscale). **(A, B)** Ventral pancreatic cells in Robo1/2 KO embryos, that downregulate Pdx1, start to express hepatic markers, such as albumin (A) and α-fetoprotein (B) and appear hepatoblast-like. Insets depict higher magnification of the marked area in the overview. **(C)** Hepatoblast-like cells in the Robo1/2 KO tissue leave the ventral pancreatic epithelium and cross the basal membrane marked by IF staining for laminin (green). The insets in the mutant micrograph show grayscale images of single channels of Prox1 (upper) and laminin (lower). The dotted line demarcates the domain of Prox1 expressing cells, of which some already crossed the basal membrane. **(D)** Control ventral pancreatic cells show an apical accumulation of f-actin (green). In contrast, hepatoblast-like cells in the mutants show an altered organization of f-actin, often with low apical (arrowhead in the high magnification image) but distinct basal or lateral accumulation (arrows in the high magnification image). **(E)** Hepatoblast-like cells in the Robo1/2 KO ventral pancreata show lower levels of the ventral pancreatic marker Sox9 (green) as compared to control tissue. This difference is seen in the merged color overview image (to the left) and accentuated in the higher magnification images (right) depicting the merged color image and the single Sox9 channel in grayscale. (scale bars: 100μm)

Having established that hepatoblast-like cells in Robo1/2 KO embryos recapitulate many features of liver cells, I investigated whether they also contribute to the growing liver bud by performing lineage tracing experiments using the Pdx1-Cre line in combination with the H2B-GFP reporter line. An initial analysis of the contribution of ventral pancreatic cells to the liver bud of Robo1/2 KO and control embryos was performed by Sophie Escot. She collected lineage-traced embryos at E10.5 and subjected them to WMIF analysis. Immunostaining for Prox1 marked all hepato-pancreatic organ rudiments whereas Pdx1 marked pancreatic buds. Immunostaining for GFP documented labeled cells in dorsal and ventral pancreas as well as in the liver.

Quantification of GFP^+ cells in the liver showed significantly increased levels of labeled cells in the liver of Robo1/2 KO embryos as compared to control littermates (Student's T-test) (Fig. 52A). Subsequently, I performed additional lineage tracing experiments by collecting Robo1/2 KO and control embryos at E14.5 (Fig. 52B) and E18.5 (Fig. 52C). Cryosections of liver tissues at both stages were analyzed by IF staining for GFP to mark labeled cells. Immunostaining for either albumin or E-cadherin marked hepatocytes and for CK19 bile duct cells. At both embryonic stages I observed a higher density of labeled cells in the liver of Robo1/2 KO embryos as compared to control littermates. This finding may be explained by the fact that hepatoblast-like cells, which are descendants of $Pdx1^+$ ventral pancreatic cells, contributed to the growing liver bud, thereby leading to the increase in labeled cell density observed in the liver of Robo1/2 KO embryos.

In summary, I found that the Robo signaling pathway plays an essential role during early ventral pancreatic development. Active Robo signaling appeared to sustain pancreatic identity in ventral pancreatic progenitor cells, while its absence resulted in loss of pancreatic and an aberrant gain of hepatic identity in cells within the ventral pancreatic organ domain. Consequently, Robo1/2 KO embryos present with a severely reduced ventral pancreatic bud. In this model, the reduced size of the ventral pancreata is due to a combination of increased apoptosis and enhanced acquisition of hepatic identity by ventral pancreatic cells. These findings supported the hypothesis that the Robo signaling pathway preserves pancreatic identity while allowing for maintenance of cell fate plasticity in ventral pancreatic cells.

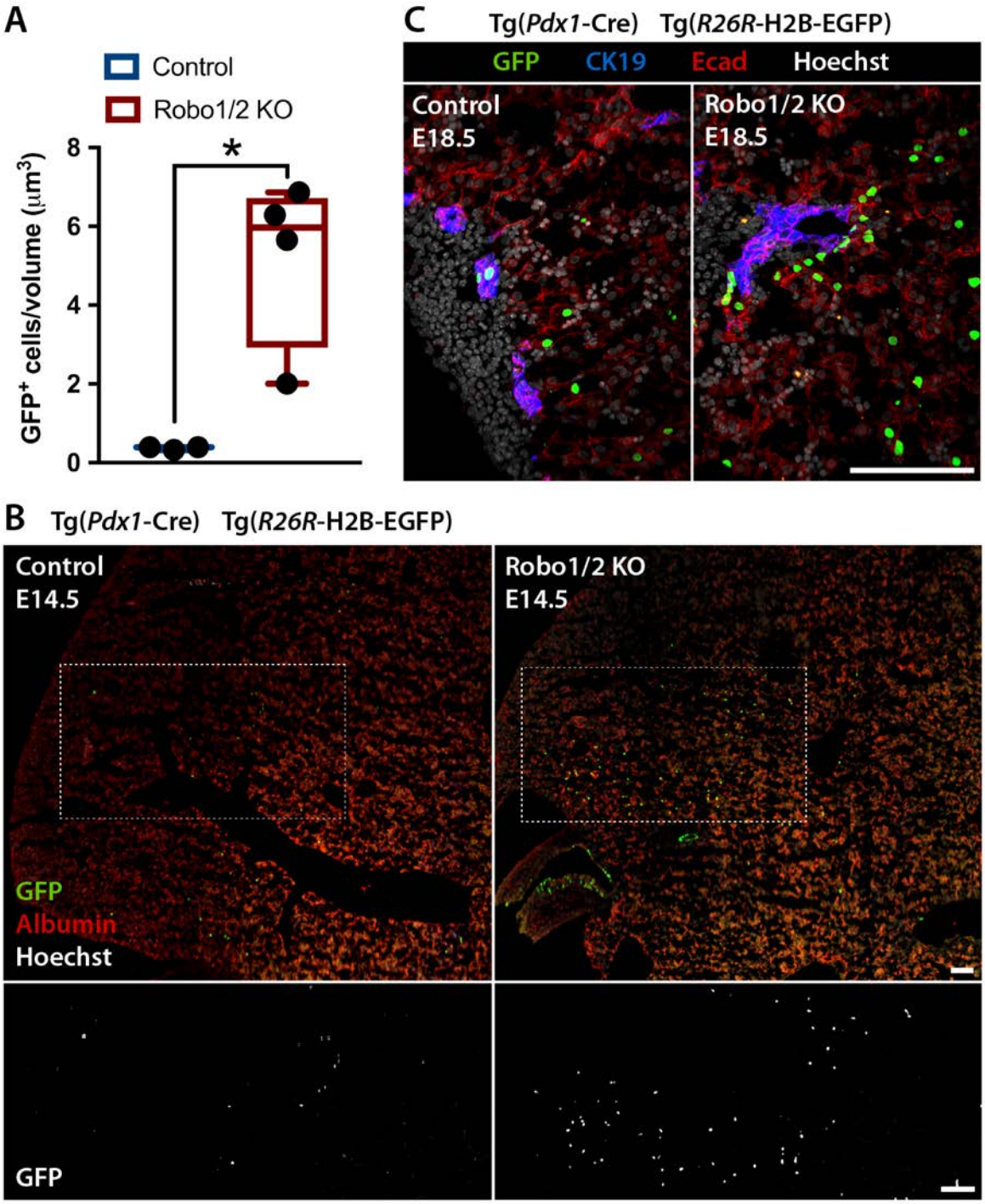

Fig. 52: Ventral pancreatic cells contribute stronger to the liver in Robo1/2 KO as compared to control embryos. Results of Pdx1-Cre lineage tracing experiments using the H2B-GFP reporter system in Robo1/2 KO and control embryos are shown. **(A)** Measurement of GFP^+ cells in liver buds at E10.5 documents significantly higher levels of labeled cells in Robo1/2 KO embryos as compared to control littermates. Experiments and analysis of data presented in (A) were performed by Sophie Escot. (Student's t-test, $p<0.05$). **(B, C)** Representative IF stainings of cryosections from E14.5 (B) and E18.5 (C) lineage-traced Robo1/2 KO and control embryos. Immunostainings for albumin (red, B) or Ecad (red, C) marks hepatocytes, while CK19 (blue, C) marks bile duct cells. Immunostaining for GFP (green) documents a higher density of labeled cells in the liver of Robo1/2 KO as compared to control embryos. Tissues are counterstained with Hoechst dye (grayscale). Lower panels in (B) show higher magnification images of the GFP channel of the boxed areas in the overview images above. (scale bars: 100µm)

3.4 Time-dependent changes in Pdx1 and Sox17 expression mark the formation of distinct subpopulations in the ventral pancreas

During my studies, I obtained evidence for a remarkable cell fate plasticity in the ventral hepato-pancreatic organ system not appreciated before. Particularly, my results indicated that ventral pancreatic cells retained the capacity to acquire either a pancreatic or hepatic fate until at least E10.0. To address whether this plasticity was common to all ventral pancreatic cells or only to a distinct subpopulation, I explored if distinct subsets of ventral pancreatic cells were identifiable during the developmental time window of E8.5-11.5. Towards this aim, I characterized the expression of different marker genes for ventral pancreatic progenitors to determine if they became restricted to distinct domains within the ventral pancreatic epithelium during development. I collected embryos of different somite stages (12-23ss; E8.75-9.5) and subjected them to WMIF for Prox1 to mark all hepato-pancreatic cells and for Pdx1 to specifically mark ventral pancreatic cells in combination with additional genes expressed in the early ventral foregut endoderm[27], including Hes1[150,221–223], Pax6[224,225], Pbx1[226,227], Sox9[47,161–164], and Sox17[150,151].

Immunostaining analyses for Hes1 (Fig. 53A), Pax6 (Fig. 53B), or Pbx1 (Fig. 53C) documented reduced expression of the respective marker in the ventral pancreas as development progressed from E8.75 to E9.5. By contrast, immunostaining for Sox9 (Fig. 53D) showed increased expression in ventral pancreatic cells at later somite stages, while Sox17 (Fig. 53E) was highly expressed in the ventral pancreas at all time points. Of all analyzed markers, only Sox17 showed a time-dependent change in its expression pattern towards a distinct ventral pancreatic subdomain (see arrowheads in Fig. 53E).

Accordingly, I selected Sox17 as a promising candidate to assess the existence of ventral pancreatic subdomains in closer detail. I collected embryos of different somite stages ranging from E8.5-10.0 (10-28ss) and subjected them to WMIF. Immunostaining for Prox1 marked all hepato-pancreatic cells, while immunostaining for Pdx1 and Sox17 specifically marked ventral pancreatic cells (Fig. 54). Pdx1 and Sox17 were co-expressed in the majority of ventral pancreatic cells until about 24ss. However, I detected exclusive expression of Sox17 in a small

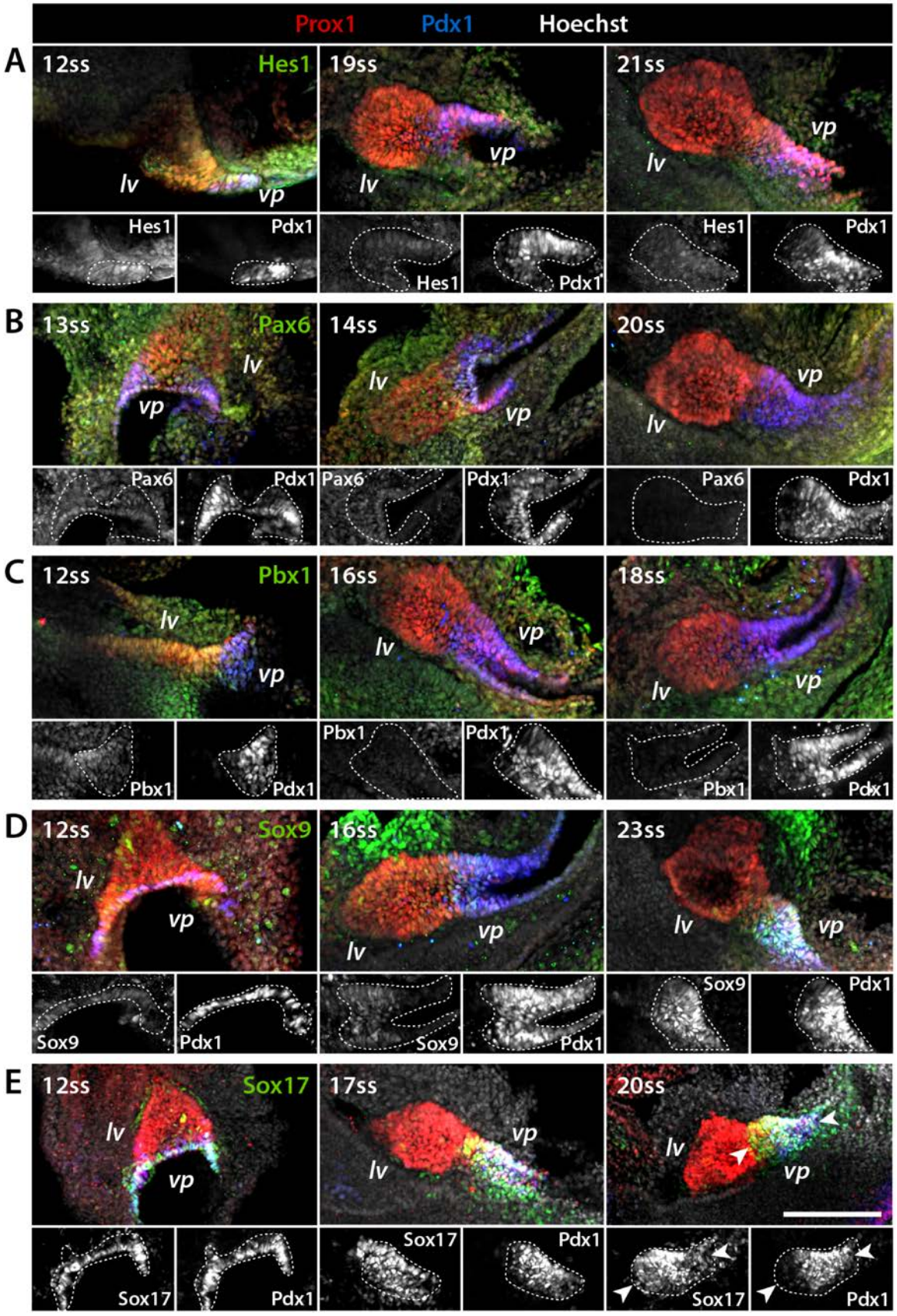
Prox1
Pdx1
Hoechst
A
12ss
Hes1
lv
vp
19ss
21ss
Hes1
Pdx1
B
13ss
Pax6
14ss
20ss
C
12ss
Pbx1
16ss
18ss
D
12ss
Sox9
16ss
23ss
E
12ss
Sox17
17ss
20ss

Fig. 53: Analysis of ventral pancreatic marker expression during early ventral pancreas morphogenesis. Representative WMIF of embryos from E8.75 to E9.5 (12-23ss). Immunostaining of Prox1 (red) marks liver (*lv*) and co-immunostaining for Prox1 and Pdx1 (blue) marks ventral pancreas (*vp*). Tissues are counterstained with Hoechst dye (gray scale). The expression dynamics of several ventral pancreatic progenitor cell markers (green) are assessed at different embryonic stages. Hes1 **(A)**, Pax6 **(B)**, and Pbx1 **(C)** show a reduction in expression as development progresses. In contrast, Sox9 **(D)** shows an increased expression at later somite stages. Sox17 **(E)** is highly expressed in the ventral pancreas at all analyzed somite stages. However, at 20ss, Sox17 and Pdx1 expression patterns do not overlap entirely (see arrowheads) but mark distinct subpopulations within the ventral pancreatic bud. Upper panels show merged color images of liver and ventral pancreas. Lower panels give single channels in grayscale for the indicated ventral pancreatic markers. Dotted lines demarcate the ventral pancreatic domain. (scale bar: 100μm)

domain of the anterior ventral pancreatic bud and exclusive expression of Pdx1 in the posteriormost domain of the ventral pancreas. After 24ss, these two organ domains underwent expansion and the expression of Sox17 and Pdx1 became increasingly restricted to distinct subdomains within the ventral pancreatic bud (see arrowheads in Fig. 54).

To analyze the separation of the two ventral pancreatic subpopulations in closer detail, I assessed Pdx1 and Sox17 expression levels in individual cells from E8.5 to E11.5 (9-43ss). In detail, I collected embryos of different somite stages and prepared cryosections thereof. Subsequent IF staining for Pdx1 and Sox17 marked ventral pancreatic cells (Fig. 55A, Fig. 56A). Then, I measured fluorescence intensities for Pdx1 and Sox17 in all ventral pancreatic cells individually using ImageJ. The data obtained from embryos of similar somite stage were combined and the fluorescence intensity values for Sox17 plotted against those for Pdx1 (Fig. 55B). Fluorescence intensity data of ventral pancreatic cells between 9ss and 24ss documented co-expression of Pdx1 and Sox17 in a majority of cells, albeit with considerable heterogeneity in expression levels.

As development progressed, I observed an increase in fluorescence intensity for both markers in ventral pancreatic cells of 25-43ss embryos. However, the increase in fluorescence intensity coincided with an increasingly restricted expression of Pdx1 or Sox17 within ventral pancreatic cells. Beginning at 25-30ss, this trend ultimately resulted in the separation of the ventral pancreas into two mutually exclusive cell populations marked by either Pdx1 or Sox17 (Fig. 55B). Of note, even though the majority of ventral pancreatic cells acquired either a $Pdx1^+$ or $Sox17^+$ fate at later somite stages, a small population of ventral pancreatic cells

continued to co-express Pdx1 and Sox17 until the end of the analyzed time period (43ss, Fig. 55B).

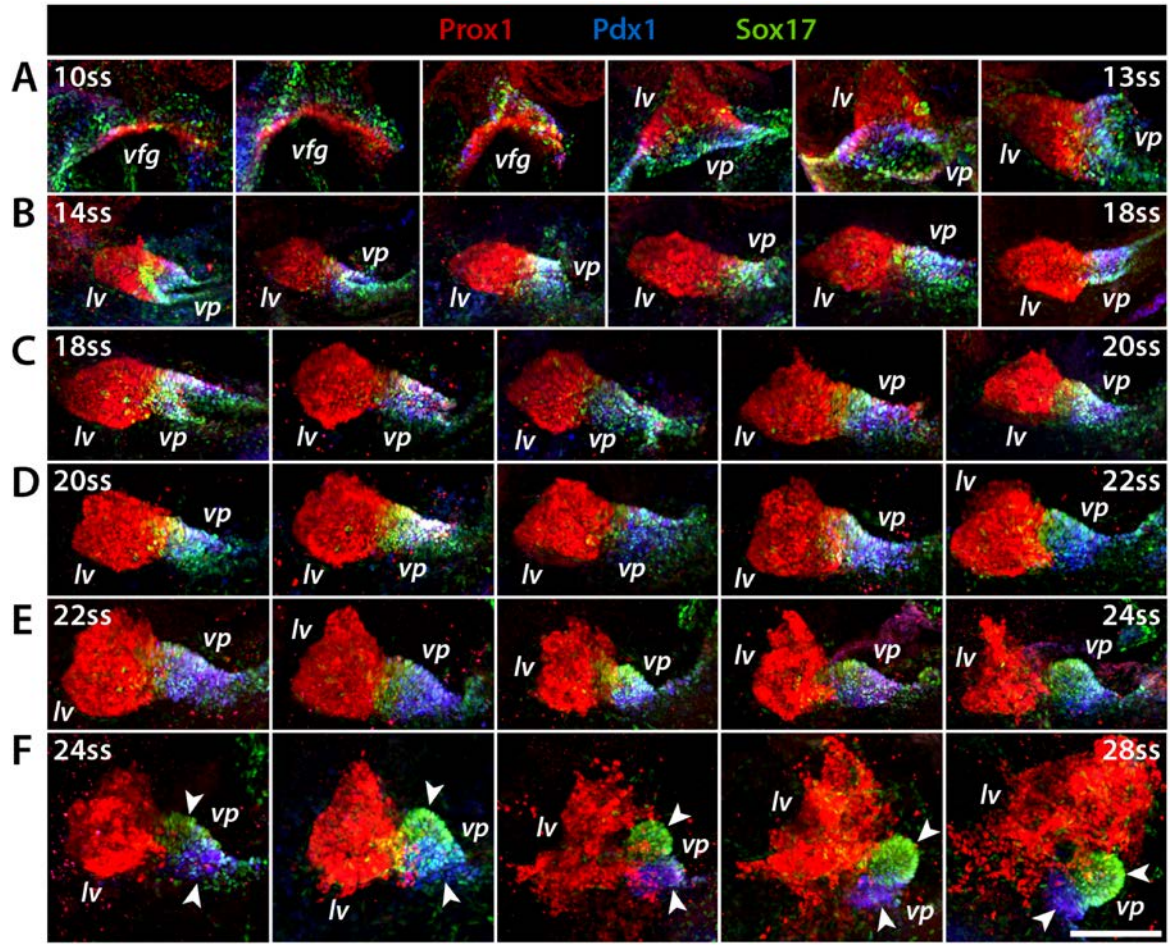

Fig. 54: Sox17 and Pdx1 expression become restricted to distinct domains within the ventral pancreas at late E9.5 stages. Representative WMIF of embryos from E8.5 to E10.0 (**(A)** 10-13ss, **(B)** 14-18ss, **(C)** 18-20ss, **(D)** 20-22ss, **(E)** 22-24ss, **(F)** 24-28ss) are depicted. Immunostaining of Prox1 (red) marks liver (*lv*), co-immunostaining for Prox1, Sox17 (green), and Pdx1 (blue) marks ventral pancreas (*vp*). Considerable overlap between Sox17 and Pdx1 expression domains is documented throughout ventral pancreas morphogenesis. However, at later somite stages (>24ss) Sox17 and Pdx1 expression becomes restricted to distinct domains within the ventral pancreas, marking distinct subpopulations of ventral pancreatic cells (see arrowheads in F). (scale bar: 100μm)

To facilitate the analysis of time-dependent changes in the cellular composition of the ventral pancreas, I gated all individual cells plotted in Fig. 55B into four subgroups according to their fluorescence intensity (FI) of Sox17 and Pdx1. Specifically, the cells were categorized into either Pdx1^{high}-Sox17^{high} (Pdx1-FI>50, Sox17-FI >50), Pdx1^{low}-Sox17^{low} (Pdx1-FI<50, Sox17-FI<50), Pdx1^{high}-Sox17^{low} (Pdx1-FI>50, Sox17-FI<50), or Pdx1^{low}-Sox17^{high} (Pdx1-FI<50, Sox17-FI>50) (dotted lines in Fig. 55B indicate division of these four categories). These cut-off values

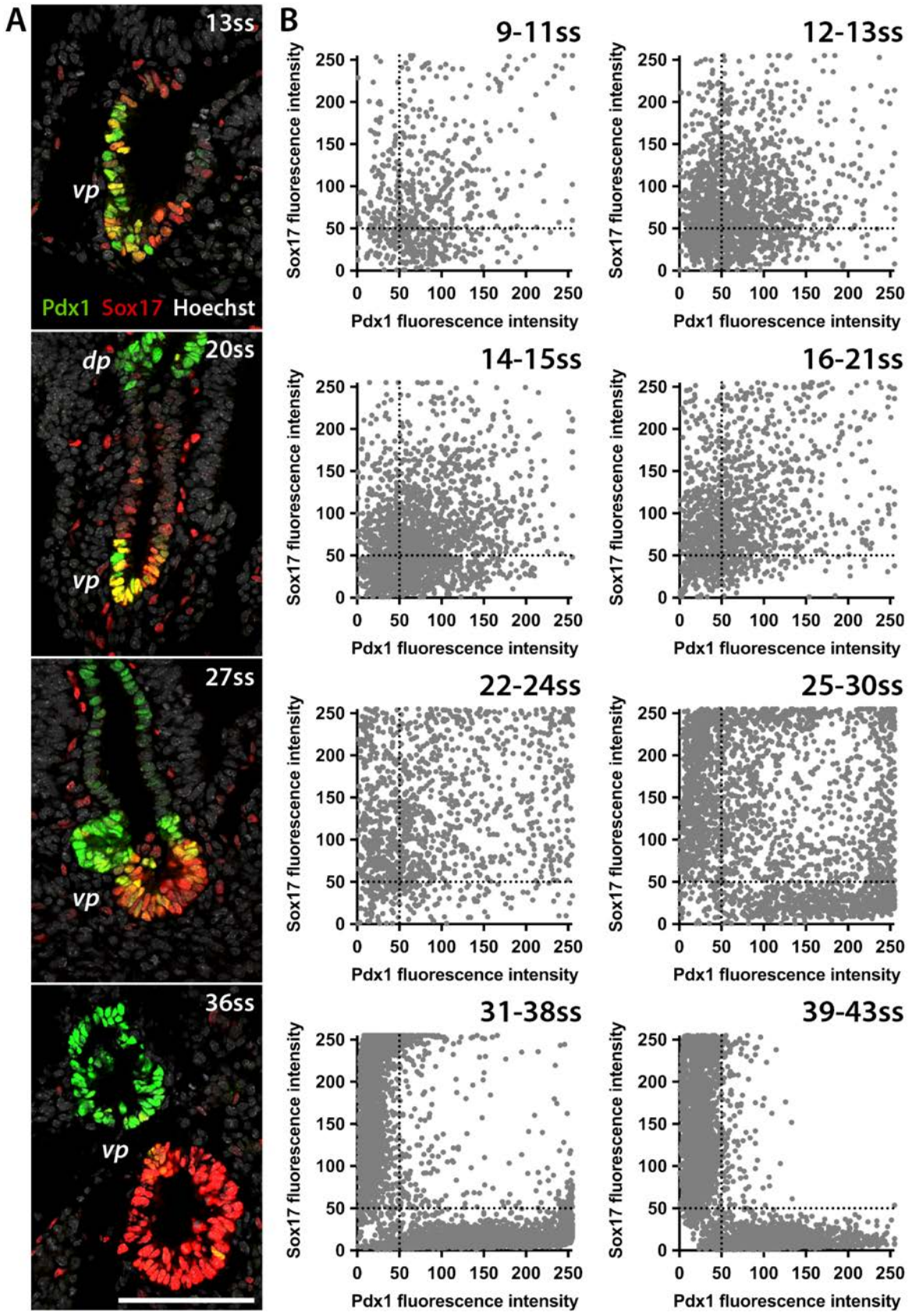
A
13ss
vp
Pdx1 Sox17 Hoechst
dp
20ss
vp
27ss
vp
36ss
vp
B
9-11ss
12-13ss
14-15ss
16-21ss
22-24ss
25-30ss
31-38ss
39-43ss
Sox17 fluorescence intensity
Pdx1 fluorescence intensity
0
50
100
150
200
250

Fig. 55: Establishment of two distinct Sox17$^+$ and Pdx1$^+$ expression domains in the ventral pancreas at E9.75. (A) Representative IF staining of cryosections of E8.75-E10.5 (13-36ss) embryos. Immunostaining of Pdx1 (green) and Sox17 (red) marks the ventral pancreas (*vp*). Tissues are counterstained with Hoechst dye (gray scale). Sox17 and Pdx1 are co-expressed during early ventral pancreatic development but subsequently become restricted to distinct organ subdomains. **(B)** Quantification of IF stained cryosections of E8.5-E11.5 embryos of the indicated somite stages (n=44). Pdx1 and Sox17 fluorescence intensity (FI) in all cells of the respective ventral pancreas (as exemplified in A) were measured. The data plotted show Pdx1 and Sox17 FI values for individual cells. Embryos of similar somite stages were grouped (9-11ss: n=5, 667 cells; 12-13ss: n=7, 1655 cells; 14-15ss: n=8, 1942 cells; 16-21ss: n=6, 1359 cells; 22-24ss: n=5, 1310 cells; 25-30ss: n=6, 2664 cells; 31-38ss: n=4, 4263 cells; 39-43ss: n=3, 3960 cells). At early somite stages (9-24ss), Pdx1 and Sox17 are co-expressed in the majority of ventral pancreatic cells, albeit with considerable heterogeneity in expression levels. At later somite stages (25-43ss), Sox17 and Pdx1 become increasingly restricted in their expression patterns and eventually form two mutually exclusive pools of ventral pancreatic cells. Only a small fraction of ventral pancreatic cells continues to co-express both markers. The transition between these two conditions of Pdx1/Sox17 expression occurs between 25ss and 30ss. (scale bar: 100μm)

were chosen to specifically gate the distinct subpopulations I observed at later developmental time points (31-43ss). Then, I plotted the average cell count for each population (Fig. 56B) or its % fraction of the ventral pancreatic cells (Fig. 56C) against the average somite stage of the respective group of embryos from which these data were obtained.

Analyzing the time-dependent changes in average cell count and % fraction, I detected distinct trends in the individual subpopulations that recapitulated the separation of the ventral pancreas into two subdomains (Figs. 55, 56). For the Pdx1^{low}-Sox17^{high} population, I saw a continuous increase in cell count and % fraction over time, while the Pdx1^{high}-Sox17^{low} population first showed a slight decrease in both parameters (until 23ss) but increased strongly at later somite stages. Cell counts for the Pdx1^{high}-Sox17^{high} population increased steadily until about 27ss, at which point they declined again, while the Pdx1^{low}-Sox17^{low} population followed the opposite trend by decreasing in cell counts until about 27ss and slightly increasing again at later somite stages. As for the % fraction of the Pdx1^{high}-Sox17^{high} population, I observed high levels until about 23ss, whereupon the % fraction of this population declined dramatically. Instead, the % fraction of the Pdx1^{low}-Sox17^{low} population declines slightly from 10ss towards 27ss and remains fairly constant afterwards.

In conclusion, my examination of subpopulations in the ventral pancreas highlighted the distinct developmental dynamics in this tissue during its early morphogenesis (E8.5-11.5). I observed that the ventral pancreas between E8.5-9.75 consisted of a homogenous Pdx1$^+$ Sox17$^+$ cell population. As development progressed, expression levels of Pdx1 and Sox17

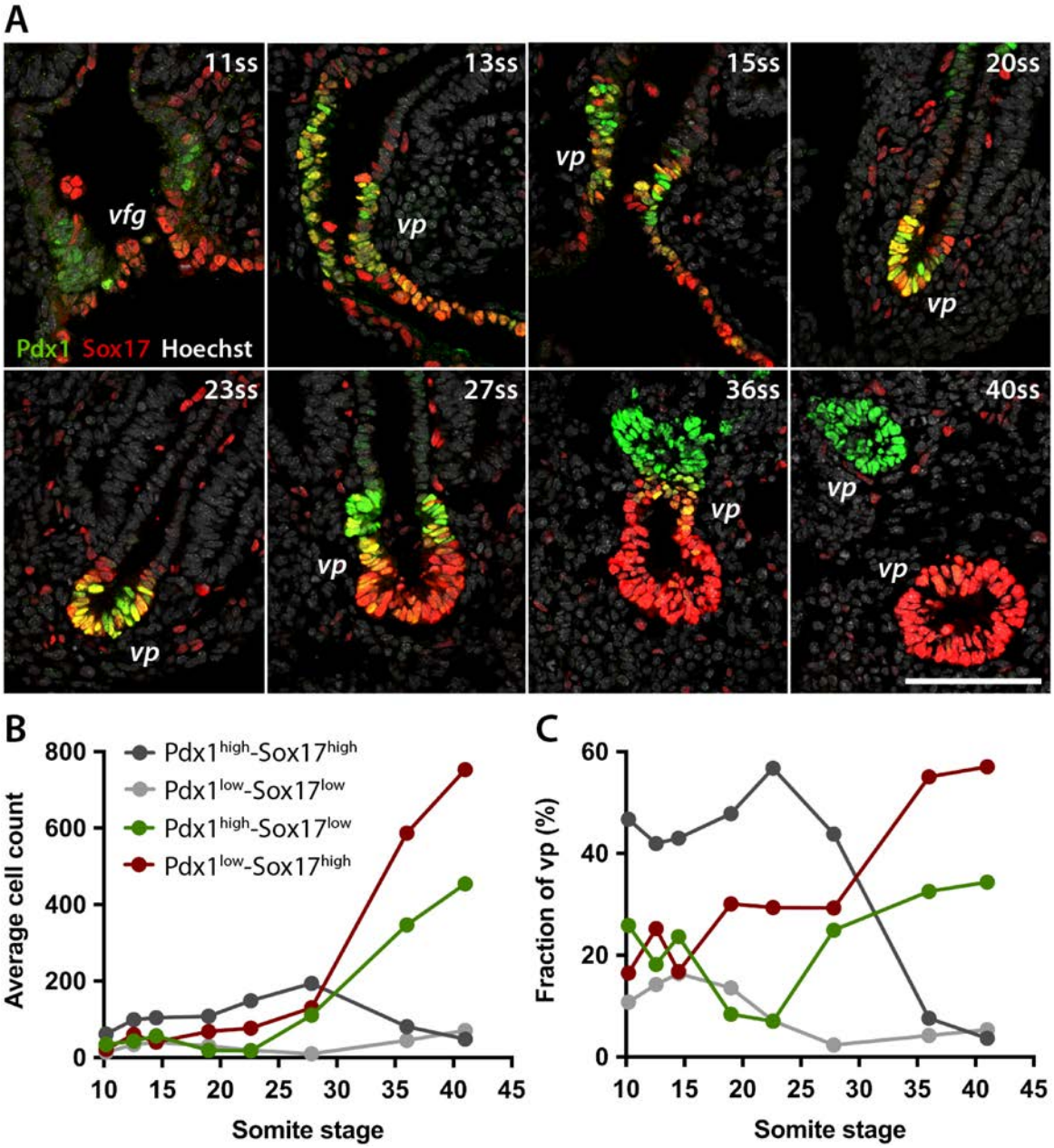

Fig. 56: Sox17 and Pdx1 expression levels show distinct trends during ventral pancreatic development. (A) Representative IF staining of cryosections of E8.5-E11.0 (11-40ss) embryos. Immunostaining of Pdx1 (green) and Sox17 (red) marks the ventral pancreas (*vp*). Tissues are counterstained with Hoechst dye (gray scale). Sox17 and Pdx1 are co-expressed during early ventral pancreatic development in the ventral foregut (vfg) and ventral pancreas (11-23ss) but subsequently become restricted to distinct domains in the ventral pancreas (27-40ss). **(B, C)** Quantification of ventral pancreatic subpopulations during development shows distinct behavioural trends. Fluorescence intensity (FI) data shown in Fig. 55B were used for categorizing ventral pancreatic subpopulations according to Pdx1^{high}-Sox17^{high} (Pdx1-FI>50, Sox17-FI >50), Pdx1^{low}-Sox17^{low} (Pdx1-FI<50, Sox17-FI<50), Pdx1^{high}-Sox17^{low} (Pdx1-FI>50, Sox17-FI<50), or Pdx1^{low}-Sox17^{high} (Pdx1-FI<50, Sox17-FI>50) (dotted lines in Fig 55B indicate division of subpopulations). Average cell count of subpopulations in ventral pancreas at indicated somite stages (B) and fraction of subpopulations in % of total ventral pancreatic cells at the indicated somite stages (C) are given. (scale bar: 100μm)

generally increased but became restricted to distinct subpopulations. At E10.5-11.5 the majority of ventral pancreatic cells were characterized by mutually exclusive expression of either Pdx1^{high} or Sox17^{high}. Interestingly, the population marked by Sox17^{high} expression was shown to harbor progenitors of the gallbladder and common bile duct[150,151], while the Pdx1^{high} population primarily contributes to the future pancreas[13,138,150]. Still, a relatively consistent percentage of ventral pancreatic cells co-expressed Pdx1^{low} and Sox17^{low} throughout the analyzed developmental time window. In addition, despite the massive decrease in the Pdx1^{high}-Sox17^{high} population from 23ss onwards, a small percentage of these cells persisted in the ventral pancreas at E11.5. These two populations (Pdx1^{low}-Sox17^{low}, Pdx1^{high}-Sox17^{high}) represent interesting candidates for a multipotent progenitor domain that may ultimately acquire either pancreatic (Pdx1^{high}-Sox17^{-}), biliary (Pdx1^{-}-Sox17^{high}), or a hepatic fate (Pdx1^{-}-Sox17^{-}).

4. Discussion

In my thesis, I explored the dynamics of lineage acquisition by hepato-pancreatic progenitors during early mouse development. My lineage tracing analyses document a degree of cell fate plasticity in early dorsal and ventral pancreatic progenitors not appreciated before. I discovered that a subset of early dorsal pancreatic progenitors retains the capacity to acquire a gastric fate even after receiving initial pro-pancreatic stimuli. The degree of plasticity observed in the ventral pancreatic progenitors, both in terms of developmental timing and diversity of cell fates, even exceeds that of the dorsal pancreas. Specifically, I provided evidence that the bipotent nature of the ventral foregut endoderm is retained in ventral pancreatic cells at E9.5, which contribute to several distinct ventral foregut derivatives.

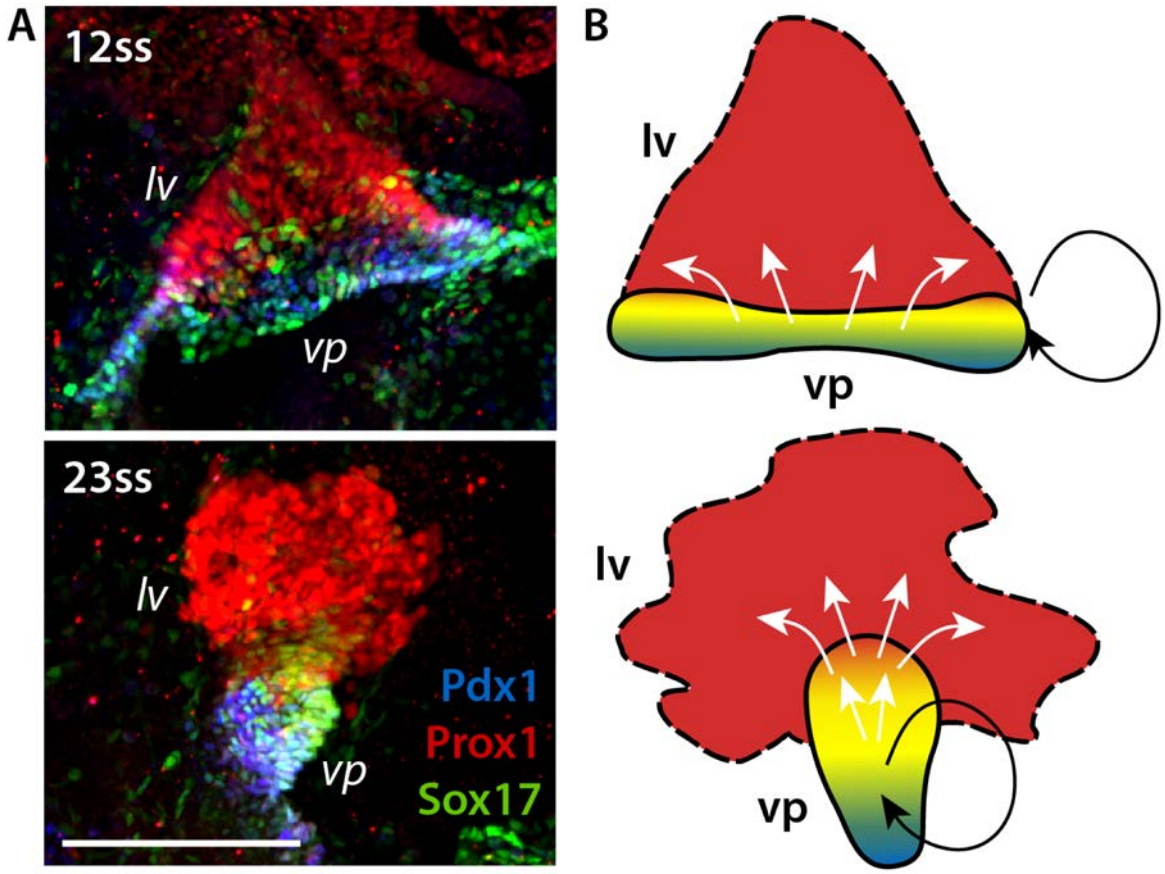

Fig. 57: Ventral pancreatic cells remain in a multipotent state during organogenesis and contribute to the hepatic bud. (A) Representative WMIF of E8.75 and E9.5 (12ss and 23ss) mouse embryos. Immunostaining of Prox1 (red) marks liver (*lv*), while co-immunostaining of Prox1, Pdx1 (blue), and Sox17 (green) marks ventral pancreas (*vp*). **(B)** Schematics of the proposed dynamics of hepatic and ventral pancreatic organogenesis at 12ss and 23ss are depicted. The models show the liver bud in red and the ventral pancreatic bud in a gradient from blue to orange, representing putative distinct ventral pancreatic cell populations. Black arrows indicate self-renewing proliferation while white arrows indicate the contribution of ventral pancreatic cells to the hepatic bud. (scale bar: 100μm)

Based on these data, I propose a novel concept in hepato-pancreatic organogenesis (Fig. 57). According to my concept, cells in the ventral pancreas start to acquire pancreatic identity during organogenesis, but at least a subset of these cells remains in a multipotent non-committed state. Once exposed to proper cues, multipotent cells in the ventral pancreatic domain can contribute to a multitude of adult tissues, including pancreas but also gallbladder, common duct, and liver. As a consequence, the ventral pancreas provides a constant flux of cells contributing to the growing liver bud and it fuels progenitor pools for pancreatic and biliary tissues. This concept has biological significance as it provides an initial boost to early liver growth and allows proper formation of different hepato-pancreatic tissues in a time- and tissue-specific manner.

4.1 Hepato-pancreatic lineage commitment shows high degree of plasticity

The concepts of cell fate commitment and plasticity have been a major focus in developmental biology and stem cell research. Deciphering the mechanisms underlying commitment and plasticity is deemed essential to establish protocols for efficient differentiation of progenitor cells to specific cell types or for lineage reprogramming of one terminally differentiated cell type into another. This field of research has gained particular interest in the light of current efforts to develop regenerative therapies for degenerative diseases targeting liver and pancreas.

Studies aimed at defining progenitor populations and characterizing their commitment to a specific cell lineage often focus on the identification of marker genes specific for the cell population of interest. However, in recent years it has become increasingly obvious that seemingly homogeneous cell populations expressing lineage-specific markers actually show considerable heterogeneity with respect to their epigenetic landscape, gene expression profiles, and signaling environment. This fact has also been shown for dorsal and ventral pancreatic organ domains[228,229]. It is reasonable to assume that a similar level of heterogeneity also exists with respect to cell fate plasticity within a seemingly homogeneous progenitor population.

In the ventral foregut, commitment to hepatic or pancreatic lineages was thought to occur around E8.5 and to be accompanied by the expression of lineage-specific transcription factors or markers, namely albumin for the hepatic and Pdx1 for the pancreatic endoderm[13,27,56,123]. The results of my thesis question the assumption that the initial expression of a lineage-specific transcription factor, such as Pdx1, already represents an irreversible lineage commitment in hepato-pancreatic specification. The ability of both dorsal (Figs. 32, 33, 35) and ventral organ rudiments (Figs. 45-47) to contribute to a multitude of cell types, even at later developmental stages, suggests that lineage commitment in the mouse foregut is more plastic than previously thought. Conceptually, the initiation of lineage-specific gene expression in the ventral and dorsal foregut may represent an initial step towards lineage commitment rather than its conclusion. Subsequent transcriptional or chromatin-remodeling events are required to stabilize the lineage commitment. This concept would be in line with the idea that early lineage-specific transcription factors act as pioneer factors, which alter the epigenetic landscape of a cell and drive the expression of more lineage-specific target genes[230–232].

The lineage tracing experiments presented in my thesis also document that early dorsal pancreatic progenitors, which fail to converge on the embryonic midline to receive additional pro-pancreatic stimuli, are able to contribute to the posterior dorsal stomach (Figs. 32, 33, 35). A lineage relationship between pancreatic and gastric cells has not been proposed so far. However, in support of my conclusions, the stomach harbors entero-endocrine cells that share key transcriptional regulators with pancreatic endocrine cells, such as Pax6 and Ngn3 (Fig. 34)[206–208]. In addition, gastric endocrine cells encompass glucagon- and somatostatin-producing cells, which are otherwise almost exclusively found in the pancreas and intestine[208]. My hypothesis about a close lineage relationship between dorsal pancreatic and gastric cell types is also in line with a recent publication by Ariyachet *et al.*[233]. These authors established gastric endocrine cells as an adequate cellular source for lineage reprogramming into pancreatic progenitors and subsequent differentiation into functional β-cells. Interestingly, only gastric but not intestinal endocrine cells could be successfully reprogrammed, again underlining the lineage relationship between pancreatic and gastric cells that I uncovered in my thesis work.

My current results do not provide evidence that the entero-endocrine population in the stomach may be exclusively descended from dorsal pancreatic progenitors. Still, the contribution of dorsal pancreatic progenitors to the production of this specialized gastric cell type is an exciting observation that warrants further investigation.

4.2 The ventral pancreatic domain remains in a multipotent state

In my thesis, the remarkable plasticity of pancreatic organ domains was explored in more detail with respect to the ventral pancreas. Using lineage tracing experiments and quantitative analysis of tissue dynamics, I experimentally proved previous hypotheses that the ventral foregut contains multipotent progenitors of liver, ventral pancreas, and the biliary system. I also documented that cell fate plasticity is retained in ventral pancreatic cells until much later time points in organogenesis (Figs. 45-47) than previously thought[5,6,8,178].

Initial evidence for the existence of a bipotent progenitor domain in the ventral foregut giving rise to liver and ventral pancreas, was provided in 2001 in two studies published by the group of Ken Zaret[5,6]. The authors performed experiments in mouse foregut explants to dissect specification events leading to the formation of hepato-pancreatic organ domains. The main conclusions drawn by the authors were that the pancreatic fate is the default fate of the ventral foregut and that FGF[5] and BMP[6] signals from the developing heart and septum transversum mesenchyme induce hepatic identity instead of pancreatic fate in the ventral foregut. In addition, the group of Didier Stainier performed lineage tracing experiments in the foregut endoderm of zebrafish embryos using a photo-inducible fluorescent labeling approach[9]. The authors documented bipotent progenitor cells contributing to liver and ventral pancreas during early somite stages in the foregut and they identified BMP2 signals from the lateral plate mesoderm as crucial for the subsequent segregation of hepatic and ventral pancreatic cell types.

To further characterize the origin of dorsal and ventral hepato-pancreatic tissues, the group of Kimberley Tremblay performed fate mapping experiments in the mouse[8]. Dye labeling was used to mark cells in the ventral or dorsal foregut of *ex vivo* cultured mouse embryos. These

studies suggested that the ventral foregut contains both hepatic and ventral pancreatic progenitors, while dorsal pancreatic progenitors arise from a distinct domain in the dorsal foregut. The authors also proposed a distinct regionalization of hepatic and ventral pancreatic progenitors within the ventral foregut, with ventral pancreatic progenitors residing in the lateral sides of the anterior intestinal portal (AIP)[8].

Comparing these published studies to my work on ventral foregut morphogenesis *in vivo*, I confirmed that the endodermal region identified to give rise to liver and ventral pancreas in fact corresponds to a population of Prox1$^+$ cells in the ventral foregut (Figs. 20, 26, 27), as first described by Burke *et al.*[126]. I also observed that the lateral sides of the AIP were the first regions in the foregut to express Pdx1, corroborating the assumption that they primarily contribute to the ventral pancreas (Fig. 20). Although I identified the same population of hepato-pancreatic progenitors as Angelo *et al.*[8], my findings suggest a broader developmental potential of this population. Specifically, Angelo *et al.* proposed that terminal lineage segregation into hepatic and ventral pancreatic progenitor domains had occurred by E8.75. By contrast, I documented that even after initial acquisition of pancreatic identity, the ventral pancreas retains the bipotent potential of the ventral foregut at least until E9.5 and contributes to the hepatic bud (Figs. 18, 37, 45-47).

One explanation for this apparent discrepancy may be the experimental system used for analysis by Angelo *et al*.[8] In particular, the use of dye labeling in *ex vivo* cultured embryos may be less accurate as compared to my *in vivo* genetic lineage tracing approach, which allows precise labeling of individual cells in their physiological context[179–181]. By employing genetic lineage tracing, I was indeed able to quantify the dynamics of hepato-pancreatic lineage segregation *in vivo*. I ascertained the unique bipotent nature of the ventral pancreatic organ domain by showing sustained cell fate plasticity in this cell population and their contribution to the hepatic lineage from E8.5 to E10.5 (Figs. 18, 37, 45-47).

By performing quantitative analysis of IF stainings of ventral pancreatic tissues, I documented the separation of the ventral pancreatic domain into two distinct subpopulations during late organogenesis (E10.5-E11.5) characterized by the exclusive expression of Sox17 or Pdx1 (Figs. 54-56). These two domains represent cells increasingly committed to the pancreatic (Pdx1$^+$)

or biliary fate ($Sox17^{+}$). In addition, I showed that two further subpopulations existed, namely $Pdx1^{high}$-$Sox17^{high}$ and $Pdx1^{low}$-$Sox17^{low}$ (Figs. 55, 56). Of note, all four subpopulations co-expressed the hepato-pancreatic marker Prox1. The $Pdx1^{high}$-$Sox17^{high}$ and $Pdx1^{low}$-$Sox17^{low}$ cell populations may represent interesting candidates for multipotent progenitor domains, in which cell fate plasticity is maintained, as they show concurrent expression of markers that become increasingly lineage-restricted as development progresses (Pdx1, Sox17, Prox1). However, whether both populations or only one of them is responsible for the remarkable cell fate plasticity in the ventral pancreas is as yet not clear.

The existence of a $Sox17^{+}$ and a $Pdx1^{+}$ subpopulation in the ventral foregut was first documented by work of the group of James Wells[150]. Using transgenic mouse models, the authors provided evidence for the essential role of Sox17 in separating distinct organ lineages within the ventral foregut and they showed the contribution of $Sox17^{+}$ cells to the gallbladder and biliary system. Similar results were also shown by Uemura *et al.*[151]. While essentially corroborating these previous studies, my thesis work offers several novel and different perspectives. Firstly, I performed a more detailed time-course analysis of Pdx1 and Sox17 expression in the ventral pancreas as compared to previous studies. Thereby, my data indicate that the definitive separation of the ventral pancreatic domain into a $Sox17^{+}$ and a $Pdx1^{+}$ subpopulation occurs around 25-30ss (Fig. 55), later than hypothesized by Spence *et al*.[150] and Uemura *et al*.[151] (E9.0).

Secondly, by measuring fluorescence intensities in all ventral pancreatic cells individually, I documented the existence of two additional distinct double-positive cell populations ($Pdx1^{high}$-$Sox17^{high}$ and $Pdx1^{low}$-$Sox17^{low}$) throughout organogenesis (E8.5-E11.5) (Figs. 55, 56). These two cell populations have been missed in earlier work by others. Thirdly, by using various lineage tracing approaches, I documented that the ventral pancreatic domain not only harbors the potential for pancreatic or biliary development but contributes to hepatic expansion as well (Figs. 45-47). Further experimental proof for my findings may entail clonal labeling of a single ventral foregut progenitor cell followed by analysis of this cell's contribution to liver, gallbladder and ventral pancreas.

4.3 Balancing bipotency versus terminal differentiation of ventral pancreatic progenitors

A still open question is how the balance between maintaining cell fate plasticity and establishing pancreatic identity is regulated in the ventral pancreatic domain. Assuming the character of a stem cell compartment, cell fate plasticity in the ventral pancreas is probably regulated by the niche environment. Previous studies identified FGF signals from the heart mesoderm[5] and BMP signals originating from mesenchyme surrounding the hepatic bud as essential pro-hepatic signals[6]. Recent work from the Spagnoli laboratory. has shown that the Robo-Slit signaling pathway provides important pro-pancreatic cues to the ventral pancreatic organ domain (Figs. 48-52)[148]. Thus, a complex interplay between FGF, BMP, and the Robo-Slit pathways likely plays a major role in regulating the balance between cell fate plasticity and pancreatic identity at early developmental stages.

Specifically, dominance of the FGF and BMP pathways may induce differentiation towards a hepatic fate, while dominance of the Robo-Slit pathway likely promotes continued commitment to the pancreatic lineage. In addition, further signaling factors, including FGF10[96,145,146] and members of the hedgehog family[117,234–237], as well as non-canonical Wnt signals[147] have been implicated in the regulation of these processes as well. However, the precise actions of these signaling cues on the regulation of cell fate plasticity and pancreatic identity, as well as their interplay, still require further investigation. In addition, the putative niche of the ventral pancreatic bud undergoes distinct time-dependent changes, which are concurrent with the separation of the ventral pancreatic domain into a $Sox17^+$ and a $Pdx1^+$ subpopulation.

While the Notch target Hes-1 is known to be implicated in the establishment of Sox17 and Pdx1 expression domains in the ventral pancreatic bud[150,221,222], the endoderm-intrinsic mechanisms and extrinsic mesoderm-derived signals driving this process are poorly understood. Further dissection of the signaling pathways active within the ventral pancreatic domain is required to elucidate the exact nature of the signaling context involved in maintaining plasticity or promoting hepatic versus biliary versus pancreatic lineage

commitment. This dissection may be achieved by quantitative assessment of immuno-stainings for signaling pathway components, single-cell RNA-sequencing approaches, and/or genetic mouse models.

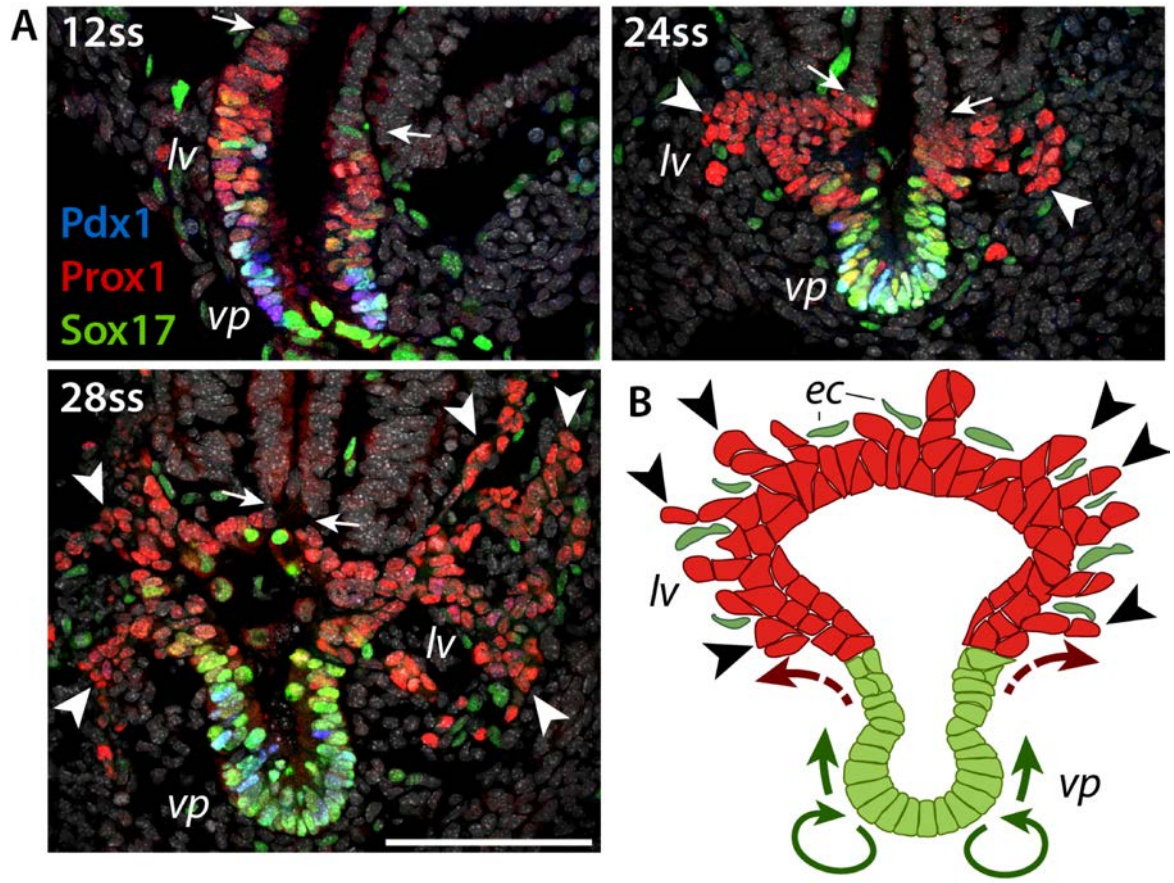

Fig. 58: Ventral pancreatic cells may be passively extruded into the liver bud. (A) Representative IF staining of cryosections of E8.75-E10.0 (12-28ss) mouse embryos. Immunostaining of Prox1 (red) marks liver, whereas co-immunostaining of Prox1, Pdx1 (blue), and Sox17 (green) marks ventral pancreas. Tissues are counterstained with Hoechst dye (gray scale). Arrowheads indicate hepatic chords, while arrows highlight the boundary between liver and gut tube at different stages of separation of liver and ventral pancreas from the gut tube. **(B)** Schematic representation of a putative mechanism leading to the passive extrusion of ventral pancreatic cells into the liver bud. Proliferation in the ventral pancreatic bud (green cells) increases the mechanical pressure within the bud and pushes cells anteriorly (indicated by green arrows) towards the hepatic organ domain (red cells). A second process may be the formation of hepatic chords (red cells in between endothelial cells (*ec*, olive cells), see arrowheads). Leading cells at the tip of the hepatic chords may exert mechanical forces transmitted through mechano-coupling along cell-cell connections, thereby pulling cells from the neighboring ventral pancreatic epithelium anteriorly towards the hepatic bud (process indicated by red arrows). (scale bar: 100μm)

As the ventral pancreatic niche likely provides pro-pancreatic signals, the question arises how cells leave this compartment to receive alternative cues to adopt a different cell fate. Conceptually, ventral pancreatic cells may actively migrate or be passively pushed out of a pro-pancreatic and into a pro-hepatic environment. Ventral pancreatic cells are part of a

pseudostratified epithelial bud with a strong apical-basal polarity, as documented by apical accumulation of F-actin (Fig. 51D) and a thick basal lamina (Fig. 51C). Such a highly organized epithelial structure might hamper active migration. Thus, passive extrusion of ventral pancreatic cells into the hepatic organ domain seems more likely. Such a process of passive transition of progenitor cells from the ventral pancreatic domain into the liver bud might be facilitated by the close proximity of the two organ rudiments throughout organogenesis (Fig. 58A). Both organs, liver and ventral pancreas, are collectively separating from the gut tube and form continuous epithelial structures until late organogenesis stages (E10.5-11.5). The epithelial connection of liver and ventral pancreas may allow ventral pancreatic cells at the interface of the two organ buds to easily move into the hepatic bud, potentially as a result of two alternative processes outlined in Fig. 58B.

As one process, cell proliferation in the ventral pancreas may increase the mechanical pressure within the bud and push cells anteriorly towards the hepatic organ domain (Fig. 58B). A similar process is described for the intestinal epithelium, where stem cells in the intestinal crypt are displaced from their spatially restricted niche as a result of proliferation within the stem cell compartment[184,238,239]. After leaving the stem cell niche, the cells become transiently amplifying cells and undergo several rounds of cell division. This process generates tension within the intestinal epithelium and pushes cells along the entire length of the intestinal villus[239]. During this process progenitor cells adopt a fully matured intestinal cell identity and replace cells at the tip of the villus, which are shed into the gut lumen[239].

A second process facilitating the movement of ventral pancreatic cells into the liver may be the formation of the hepatic chords (Fig. 58B). As liver cells collectively migrate into the septum transversum mesenchyme, leading cells at the tip of the hepatic chords may exert mechanical forces transmitted through mechano-coupling along cell-cell connections throughout the hepato-pancreatic epithelium. The transmitted mechanical forces may pull cells from the neighboring ventral pancreatic epithelium anteriorly towards the hepatic bud. Although the process of mechano-coupling along cell-cell contacts has not been documented for hepatic cell migration so far, similar processes have been described in vertebrate blood vessel sprouting[240,241] and during the development of the tracheal system in *Drosophila*[242,243].

4.4 Biological significance of bipotency in the ventral pancreas

The ventral foregut, specifically the ventral pancreatic domain, gives rise to different organs of the gastro-intestinal tract, including liver, gallbladder, common duct, and pancreas (Fig. 59). This fact is remarkable considering that the ventral pancreatic domain at E8.75 is only comprised of 100-200 cells (Fig. 22). In my thesis work, I documented that the multipotent nature of the ventral foregut is retained in the ventral pancreatic domain until late stages of organogenesis (Figs. 18, 37, 45-47). Likely, retaining such a multipotent state is key to enable a proper response of ventral pancreatic cells to a variety of inductive signaling cues that can promote hepatic, biliary, or pancreatic fate.

A similar situation has been described in the pre-gastrulation mouse epiblast. Work by the group of Miguel Torres has documented that the pluripotent nature of epiblast cells is rigorously controlled by myc-driven cell competition to eliminate cells undergoing aberrant differentiation prior to gastrulation[244,245]. This process effectively assures that all epiblast cells remain in a pluripotent state in which they are able to properly respond to signaling cues during gastrulation.

My hypothesis that maintenance of a multipotent state in ventral pancreatic cells is a key element in ventral foregut development is supported by studies investigating the role of signaling pathways or transcription factors during development of the ventral foregut in general, or hepatic, biliary, or pancreatic development in particular. These studies often observed simultaneous phenotypes in several of these tissues. For instance, genetic ablation of *Sox17* or *Hes-1* in the mouse ventral foregut resulted in gallbladder agenesis and ectopic pancreatic tissue in the common duct[150,221,222]. In addition, overexpression of Sox17 in pancreatic buds caused pancreatic hypoplasia and the appearance of ectopic ductal tissue in duodenum and stomach[150]. Consistently, Robo1/2 KO mouse embryos documented severe ventral pancreas hypoplasia accompanied by aberrant induction of hepatic cell fate within the ventral pancreatic organ domain (Figs. 48-52).

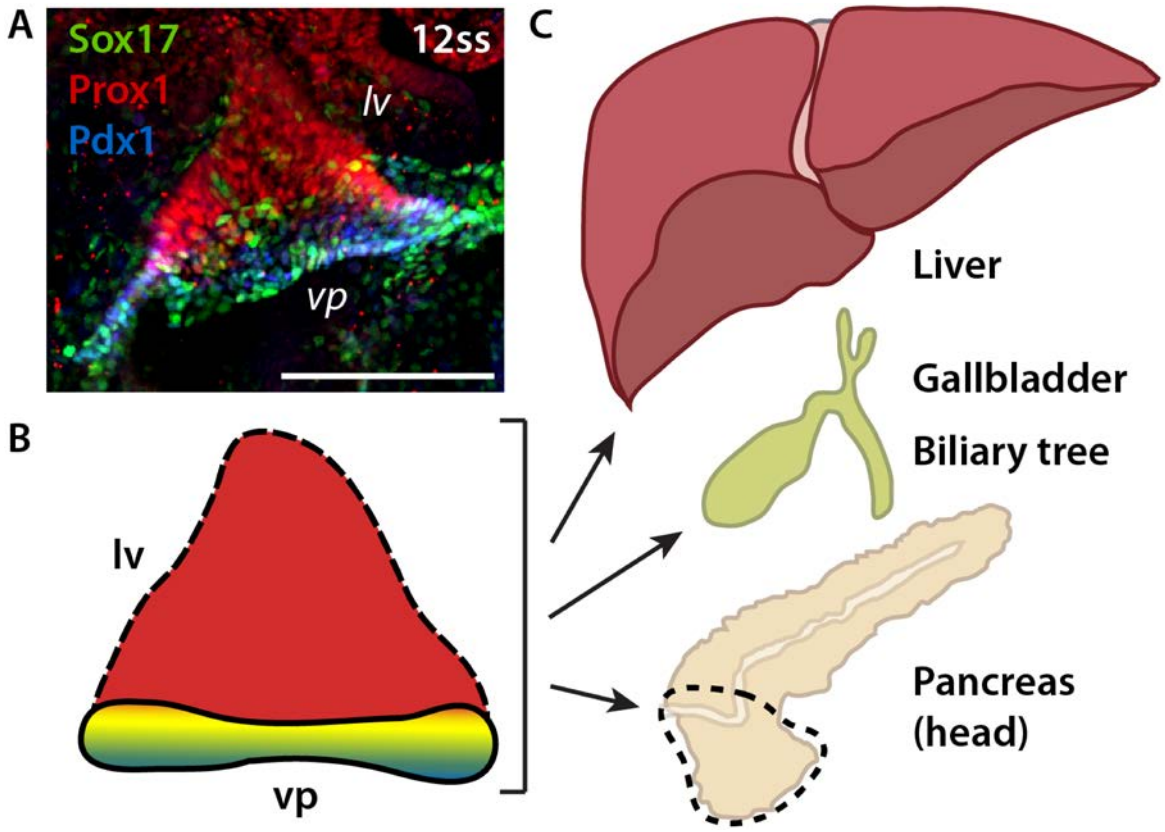

Fig. 59: Ventral foregut derivatives. (A) Representative WMIF of the ventral foregut region of an E8.75 (12ss) mouse embryo. Immunostaining of Prox1 (red) marks the hepatic domain (*lv*), co-immunostaining of Prox1, Pdx1 (blue), and Sox17 (green) marks the ventral pancreatic domain (*vp*). **(B)** Schematic representation of the ventral foregut at E8.75 (12ss). The hepatic organ domain is shown in red and the ventral pancreatic organ domain in a gradient from blue to orange, indicating putative distinct ventral pancreatic cell populations. **(C)** Schematic representation of the adult organs originating from the ventral foregut domain. The ventral foregut gives rise to liver, gallbladder, biliary tree, and head of the pancreas (circled by a dotted line). (scale bar: 100μm)

Other factors, whose genetic ablation in the mouse foregut results in concurrent phenotypes in several ventral foregut derivatives, include Hhex[45,113,246], Hnf1β[247], and HNF-6[248]. Intriguingly, similar multi-organ phenotypes are also observed in human genetic syndromes, such as Martínez-Frías syndrome[249], Mitchell-Riley syndrome[250], as well as a number of other congenital human defects[251–255]. Most of these disorders are caused by autosomal recessive genetic defects of unknown etiology. They usually present a combination of gallbladder agenesis, intestinal atresia, duodenal malrotation, and pancreatic hypoplasia. In some cases, including the Mitchell-Riley syndrome, patients also suffer from neonatal diabetes[250,251]. Potentially, gene defects altering the multipotent state of the ventral foregut or impairing the maintenance of this multipotent state in ventral pancreatic cells may underlie these congenital malformations.

A surprising finding of my studies was the fact that extended cell fate plasticity in the ventral pancreatic domain allows for a constant flux of ventral pancreatic cells to contribute to the growing liver bud (Figs. 46, 47, 57). Conceptually, this contribution may serve to support early hepatic growth. Indeed, during organogenesis the liver grows dramatically as demonstrated by the approximately 20-fold increase in cell counts of the hepatic bud between E8.75 and E10.75 (Fig. 22). Conceivably, the hepatic organ rudiment may require the support of ventral pancreatic cells to achieve this exceptional growth rate. As tissues during this developmental stage tend to grow exponentially, even a small number of ventral pancreatic cells adopting a hepatic cell fate can achieve a significant contribution to liver growth. A comparable situation has been described in heart development in the chick embryo[204]. A proliferative growth center posterior to the heart tube, termed the secondary heart field[256], has been identified and shown to contribute cells to the myocardium to support the early growth of the developing heart[204].

An intriguing question is whether this hepatic cell population of ventral pancreatic origin serves a particular biological role in the adult liver. As documented in Fig. 47C, Pdx1-Cre lineage-traced ventral pancreatic cells can differentiate into both hepatocytes and bile duct cells. Although I did not determine the contribution of ventral pancreatic cells to these cell populations quantitatively, I did not observe a particular bias for differentiation towards hepatocytes or bile duct cells. Still, further characterization of this cell population with respect to transcriptional or signaling signatures would be of great value in specifying its biological function in the adult liver. As of now, it is reasonable to assume that under normal physiological conditions liver cells of ventral pancreatic origin are functionally indistinguishable from other hepatic cell types. However, the situation may be different during liver regeneration following injury or disease.

Most tissues with a high cell turnover, such as the skin[257], the intestine[239], or the mammary gland[186,258], harbor an identifiable stem cell compartment that continually gives rise to more differentiated cell types. These stem cell compartments are responsible for maintaining the regenerative potential of the respective tissues. By contrast, regeneration in the liver following tissue destruction is primarily driven by dedifferentiated hepatic cells, which re-

enter the cell cycle[11,35,46,259]. In this model, terminally differentiated hepatic cells undergo dedifferentiation towards a progenitor-like stage, proliferate until they have expanded sufficiently to restore the destroyed hepatic tissue, and subsequently differentiate again into either hepatocytes or bile duct cells[11,35,46,259].

Given the remarkable extend of cell fate plasticity demonstrated by hepatic cells of ventral pancreatic origin in my thesis work, it is tempting to speculate that these cells might be particularly prone to dedifferentiation and subsequent proliferation in the context of liver regeneration. Further analysis using partial hepatectomy in mice with genetically labeled liver cells, using Pdx1-Cre and H2B-GFP transgenes, may be an experimental approach to query whether liver cells of ventral pancreatic origin define the high regenerative potential of hepatic tissues.

4.5 Relevance for cell-based therapies

In recent years, major efforts have been focused on developing cell-based therapies for the treatment of DM. The overall aim of these approaches is to replace the destroyed or dysfunctional β-cell population in the diabetic patient with *in vitro* generated β-cells that are able to produce insulin and restore systemic glucose homeostasis[2–4,55]. A major advance towards the *in vitro* generation of β-cells was described in 2006 by D'Amour *et al.*[52]. The authors employed growth factor signals similar to those governing the differentiation of endodermal progenitors towards the pancreatic lineage *in vivo*, to differentiate hESCs into pancreatic hormone-expressing endocrine cells[52].

Significant improvement of this initial protocol has been achieved in recent years by adapting each individual steps of differentiation to better recreate the current understanding of pancreas and β-cell development[2–4,13]. Knowledge gained from developmental studies helped to improve the reliability of the differentiation protocols and the maturity of the generated β-cells[53,260–262]. Considerable efforts are currently being focused on optimizing these differentiation protocols to be used with human iPSCs[54,263,264]. The use of patient-derived iPSCs will eliminate ethical and immunological concerns related to the use of hESCs. However,

the generation of iPSCs from patient-derived fibroblasts still involves transfection with constructs encoding for pluripotency factors that may act as oncogenes[263]. Until safer protocols for reprogramming of iPSCs are available, their therapeutic application remains problematic due to their oncogenic potential.

An alternative approach to the therapeutic use of pluripotent stem cells is the reprogramming of differentiated patient cells to β-cells *in vitro*. The success of such reprogramming strategies depends on the transcriptional and epigenetic similarities as well as on the developmental relationship of the donor cell type with the cell type to be generated. Reprogramming strategies for the generation of β-cells have been suggested and some are already under investigation for α-cells[265,266], acinar cells[267,268], and gastric entero-endocrine cells[233]. However, all these cell types have properties rendering them unsuitable for widespread therapeutic use. For example, pancreatic and gastric cell types suggested for reprogramming strategies are often rare and reside in tissues which are surgically difficult to access. Also, these cell types have typically low inherent regenerative properties necessitating the need for other sources for reprogramming strategies.

Obviously, the liver would be a much more suitable therapeutic cell source. It has a common developmental origin with the ventral pancreas. It is surgically easily accessible and has an inherently high potential for self-regeneration[4,269]. Work by the Spagnoli laboratory has already documented that murine hepatic cells can be successfully reprogrammed towards the pancreatic lineage *in vitro* and *in vivo* by overexpression of the transcriptional regulator TGF-β induced factor homeobox 2 (TGIF2)[10]. This study provides proof-of-concept for the therapeutic potential of cells derived from liver biopsies of diabetic patients by dedifferentiating them to a common hepato-pancreatic progenitor state, followed by differentiation to β-cells. In addition, retroviral overexpression of master regulators of β-cell development was used to reprogram mouse liver cells towards β-like-cell in several other studies, further supporting the idea of the liver as a source of pancreatic β-cells for regenerative therapies[270–274].

Now, results from my thesis work may provide important new information for the refinement of protocols for reprogramming of liver cells into pancreatic β-cells. I document that a

multipotent cellular state is maintained in ventral pancreatic cells for a significant time period during organogenesis (Figs. 18, 37, 45-47). The observed plasticity between ventral pancreatic and hepatic cells *in vivo* reinforces the idea that a conversion of hepatic cells towards the multipotent ventral pancreatic cellular state is possible.

Also, work from colleagues in the Spagnoli laboratory and myself identified the Robo-Slit signaling pathway as a potent gatekeeper of pancreatic identity in the ventral foregut (Figs. 48-52)[148]. Thus, it is likely that manipulation of this pathway may be necessary for the successful dedifferentiation of adult hepatic cells towards a multipotent ventral pancreatic state. Ultimately, patient-derived hepatocytes reprogrammed towards a state similar to that of multipotent ventral pancreatic cells may be an ideal cell population for further differentiation to functional, mature β-cells. Further dissection of the transcriptional regulatory networks and signaling pathways underlying the fate segregation of hepato-pancreatic progenitors *in vivo* in the mouse and *in vitro* in human cells, will greatly enhance the success of reprogramming approaches for regenerative therapies in diabetes.

5. Abbreviations

AIP	Anterior intestinal portal
A-P	Anterior-posterior
approx.	Approximately
arm	Armenian
BAC	Bacterial artificial chromosome
BMP	Bone morphogenetic protein
Brachy	Brachyury
BrdU	Bromodeoxyuridine
BSA	Bovine serum albumin
bw	Body weight
cCas3	Cleaved caspase 3
Cdx	Caudal type homeobox
CFP	Cyan fluorescent protein
CI	Confidence interval
CK19	Cytokeratin 19
Cre	Cre recombinase
da	Dorsal aorta
DE	Definitive endoderm
DM	Diabetes mellitus
DNA	Deoxyribonucleic acid
Dox	Doxycycline
D-V	Dorso-ventral
dp	Dorsal pancreas
duo	Duodenum
E	Embryonic day
ec	Endothelial cell
ect	Ectoderm
Ecad	E-cadherin
EDTA	Ethylenediaminetetraacetic acid
EGFP	Enhanced green fluorescent protein
EHF	Early headfold stage
end	Endoderm

Eomes	Eomesodermin
ESC	Embryonic stem cell
FBS	Fetal bovine serum
FGF	Fibroblast growth factor
FI	Fluorescence intensity
Foxa2	Forkhead box A2
GFP	Green fluorescent protein
H2B	Histone 2B
Hes1	Hairy and enhancer of split 1
hESC	Human embryonic stem cells
Hhex	Hematopoietically-expressed homeobox protein
HS	Horse serum
ht	Heart
ICM	Inner cell mass
IF	Immunofluorescence
IGF1	Insulin-like growth factor 1
IgG	Immunoglobulin G
IP	Intraperitoneal
iPSC	Induced pluripotent stem cell
Isl1	Islet-1
IV	Intravenous
IRES	Internal ribosome entry site
KO	Knockout
lv	Liver
mCFP	membrane-associated cyan fluorescent protein
mER	Murine estrogen receptor
mes	Mesoderm
MMP	Matrix metalloproteinase
nc	Notochord
nGFP	nuclear green fluorescent protein
Ngn3	Neurogenin 3
Nkx6.1	Nkx6 homeobox 1
nt	Neural tube
P	Postnatal day

pan	Pancreas
Pax6	Paired box protein 6
PBS	Phosphate buffered saline
PCR	Polymerase chain reaction
Pbx1	Pre-B-cell leukemia transcription factor 1
Pdx1	Pancreatic duodenal homeobox 1
PFA	Paraformaldehyde
pH3	Phospho-histone 3
PIP	Posterior intestinal portal
PP	Pancreatic polypeptide
Prox1	Prospero homeox 1
PS	Primitive streak
Ptf1a	Pancreas-specific transcription factor 1a
R26R	Rosa26 locus
RA	Retinoic acid
rn	Remnant of the node
RNA	Ribonucleic acid
Robo	Roundabout receptor
ROI	Region-of-interest
rtTA	Reverse tetracycline-controlled transactivator
RFP	Red fluorescent protein
SDS	Sodium-dodecyl sulfate
Shh	Sonic hedgehog
Sox	Sex-determining region on Y box protein
spm	Splanchnic mesoderm
ss	Somite stage
SST	Somatostatin
st	Stomach
STM	Septum transversum mesenchyme
TAM	Tamoxifen
TetO	TetO operator sequence
TF	Transcription factor
Tg	Transgene
TGFβ	Transforming growth factor β

TGIF	TGFβ induced factor homeobox 2
vfg	Ventral foregut
vol	Volume
vp	Ventral pancreas
WMIF	Wholemount immunofluorescence staining
Wnt	Wingless-related integration site family
wt	Weight
WT	Wildtype
YFP	Yellow fluorescent protein

6. References

1. Edlund, H. Pancreatic organogenesis--developmental mechanisms and implications for therapy. *Nat. Rev. Genet.* **3**, 524–532 (2002).
2. Ellis, C., Ramzy, A. & Kieffer, T. J. Regenerative medicine and cell-based approaches to restore pancreatic function. *Nat. Rev. Gastroenterol. Hepatol.* **14**, 612–628 (2017).
3. Gangaram-Panday, S. T., Faas, M. M. & de Vos, P. Towards stem-cell therapy in the endocrine pancreas. *Trends Mol. Med.* **13**, 164–173 (2007).
4. Zaret, K. S. & Grompe, M. Generation and regeneration of cells of the liver and pancreas. *Science* **322**, 1490–1494 (2008).
5. Deutsch, G., Jung, J., Zheng, M., Lóra, J. & Zaret, K. S. A bipotential precursor population for pancreas and liver within the embryonic endoderm. *Dev. Camb. Engl.* **128**, 871–881 (2001).
6. Rossi, J. M., Dunn, N. R., Hogan, B. L. & Zaret, K. S. Distinct mesodermal signals, including BMPs from the septum transversum mesenchyme, are required in combination for hepatogenesis from the endoderm. *Genes Dev.* **15**, 1998–2009 (2001).
7. Tremblay, K. D. & Zaret, K. S. Distinct populations of endoderm cells converge to generate the embryonic liver bud and ventral foregut tissues. *Dev. Biol.* **280**, 87–99 (2005).
8. Angelo, J. R., Guerrero-Zayas, M.-I. & Tremblay, K. D. A fate map of the murine pancreas buds reveals a multipotent ventral foregut organ progenitor. *PloS One* **7**, e40707 (2012).
9. Chung, W.-S., Shin, C. H. & Stainier, D. Y. R. Bmp2 signaling regulates the hepatic versus pancreatic fate decision. *Dev. Cell* **15**, 738–748 (2008).
10. Cerdá-Esteban, N. *et al.* Stepwise reprogramming of liver cells to a pancreas progenitor state by the transcriptional regulator Tgif2. *Nat. Commun.* **8**, 14127 (2017).
11. Duncan, A. W., Dorrell, C. & Grompe, M. Stem cells and liver regeneration. *Gastroenterology* **137**, 466–481 (2009).
12. Shih, H. P., Wang, A. & Sander, M. Pancreas organogenesis: from lineage determination to morphogenesis. *Annu. Rev. Cell Dev. Biol.* **29**, 81–105 (2013).
13. Spagnoli, F. M. From endoderm to pancreas: a multistep journey. *Cell. Mol. Life Sci. CMLS* **64**, 2378–2390 (2007).
14. Pan, F. C. & Wright, C. Pancreas organogenesis: from bud to plexus to gland. *Dev. Dyn. Off. Publ. Am. Assoc. Anat.* **240**, 530–565 (2011).
15. Ober, E. A. & Lemaigre, F. P. Development of the liver: Insights into organ and tissue morphogenesis. *J. Hepatol.* **68**, 1049–1062 (2018).
16. Walter, T. J., Sparks, E. E. & Huppert, S. S. 3-dimensional resin casting and imaging of mouse portal vein or intrahepatic bile duct system. *J. Vis. Exp. JoVE* e4272 (2012). doi:10.3791/4272

17. Morales-Navarrete, H. *et al.* A versatile pipeline for the multi-scale digital reconstruction and quantitative analysis of 3D tissue architecture. *eLife* **4**, (2015).
18. Abdel-Misih, S. R. Z. & Bloomston, M. Liver anatomy. *Surg. Clin. North Am.* **90**, 643–653 (2010).
19. Si-Tayeb, K., Lemaigre, F. P. & Duncan, S. A. Organogenesis and development of the liver. *Dev. Cell* **18**, 175–189 (2010).
20. Hata, M. *et al.* Establishment of a hepatocytic epithelial cell line from the murine fetal liver capable of promoting hemopoietic cell proliferation. *J. Cell. Physiol.* **154**, 381–392 (1993).
21. Kinoshita, T. *et al.* Hepatic differentiation induced by oncostatin M attenuates fetal liver hematopoiesis. *Proc. Natl. Acad. Sci. U. S. A.* **96**, 7265–7270 (1999).
22. Raynaud, P., Carpentier, R., Antoniou, A. & Lemaigre, F. P. Biliary differentiation and bile duct morphogenesis in development and disease. *Int. J. Biochem. Cell Biol.* **43**, 245–256 (2011).
23. Lemaigre, F. P. Development of the biliary tract. *Mech. Dev.* **120**, 81–87 (2003).
24. Slack, J. M. Developmental biology of the pancreas. *Dev. Camb. Engl.* **121**, 1569–1580 (1995).
25. Pandol, S. J. *The Exocrine Pancreas*. (Morgan & Claypool Life Sciences, 2010).
26. Röder, P. V., Wu, B., Liu, Y. & Han, W. Pancreatic regulation of glucose homeostasis. *Exp. Mol. Med.* **48**, e219 (2016).
27. Gittes, G. K. Developmental biology of the pancreas: a comprehensive review. *Dev. Biol.* **326**, 4–35 (2009).
28. Brissova, M. *et al.* Assessment of human pancreatic islet architecture and composition by laser scanning confocal microscopy. *J. Histochem. Cytochem. Off. J. Histochem. Soc.* **53**, 1087–1097 (2005).
29. Katsuura, G., Asakawa, A. & Inui, A. Roles of pancreatic polypeptide in regulation of food intake. *Peptides* **23**, 323–329 (2002).
30. Wierup, N., Svensson, H., Mulder, H. & Sundler, F. The ghrelin cell: a novel developmentally regulated islet cell in the human pancreas. *Regul. Pept.* **107**, 63–69 (2002).
31. Kieffer, T. J. & Habener, J. F. The glucagon-like peptides. *Endocr. Rev.* **20**, 876–913 (1999).
32. Dimitriadis, G., Mitrou, P., Lambadiari, V., Maratou, E. & Raptis, S. A. Insulin effects in muscle and adipose tissue. *Diabetes Res. Clin. Pract.* **93 Suppl 1**, S52-59 (2011).
33. Irfan, A. & Ahmed, I. Could Stem Cell Therapy be the Cure in Liver Cirrhosis? *J. Clin. Exp. Hepatol.* **5**, 142–146 (2015).
34. NVSS - Mortality Data. (2018). Available at: https://www.cdc.gov/nchs/nvss/deaths.htm. (Accessed: 21st November 2018)
35. Michalopoulos, G. K. Liver Regeneration. *J. Cell. Physiol.* **213**, 286–300 (2007).
36. Brown, R. S. Hepatitis C and liver transplantation. *Nature* **436**, 973–978 (2005).

37. Weir, G. C. & Bonner-Weir, S. Islet β cell mass in diabetes and how it relates to function, birth, and death. *Ann. N. Y. Acad. Sci.* **1281**, 92–105 (2013).
38. Tabish, S. A. Is Diabetes Becoming the Biggest Epidemic of the Twenty-first Century? *Int. J. Health Sci.* **1**, V–VIII (2007).
39. IDF diabetes atlas - Home. Available at: http://www.diabetesatlas.org/. (Accessed: 21st November 2018)
40. Pociot, F. & Lernmark, Å. Genetic risk factors for type 1 diabetes. *Lancet Lond. Engl.* **387**, 2331–2339 (2016).
41. Nolan, C. J., Damm, P. & Prentki, M. Type 2 diabetes across generations: from pathophysiology to prevention and management. *Lancet Lond. Engl.* **378**, 169–181 (2011).
42. Schwitzgebel, V. M. Many faces of monogenic diabetes. *J. Diabetes Investig.* **5**, 121–133 (2014).
43. Klupa, T., Skupien, J. & Malecki, M. T. Monogenic models: what have the single gene disorders taught us? *Curr. Diab. Rep.* **12**, 659–666 (2012).
44. Fajans, S. S., Bell, G. I. & Polonsky, K. S. Molecular mechanisms and clinical pathophysiology of maturity-onset diabetes of the young. *N. Engl. J. Med.* **345**, 971–980 (2001).
45. Bort, R., Signore, M., Tremblay, K., Martinez Barbera, J. P. & Zaret, K. S. Hex homeobox gene controls the transition of the endoderm to a pseudostratified, cell emergent epithelium for liver bud development. *Dev. Biol.* **290**, 44–56 (2006).
46. Michalopoulos, G. K. & DeFrances, M. C. Liver regeneration. *Science* **276**, 60–66 (1997).
47. Seymour, P. A. *et al.* SOX9 is required for maintenance of the pancreatic progenitor cell pool. *Proc. Natl. Acad. Sci. U. S. A.* **104**, 1865–1870 (2007).
48. Stanger, B. Z., Tanaka, A. J. & Melton, D. A. Organ size is limited by the number of embryonic progenitor cells in the pancreas but not the liver. *Nature* **445**, 886–891 (2007).
49. Dor, Y., Brown, J., Martinez, O. I. & Melton, D. A. Adult pancreatic beta-cells are formed by self-duplication rather than stem-cell differentiation. *Nature* **429**, 41–46 (2004).
50. Butler, P. C., Meier, J. J., Butler, A. E. & Bhushan, A. The replication of beta cells in normal physiology, in disease and for therapy. *Nat. Clin. Pract. Endocrinol. Metab.* **3**, 758–768 (2007).
51. Docherty, K., Bernardo, A. S. & Vallier, L. Embryonic stem cell therapy for diabetes mellitus. *Semin. Cell Dev. Biol.* **18**, 827–838 (2007).
52. D'Amour, K. A. *et al.* Production of pancreatic hormone-expressing endocrine cells from human embryonic stem cells. *Nat. Biotechnol.* **24**, 1392–1401 (2006).
53. Rezania, A. *et al.* Reversal of diabetes with insulin-producing cells derived in vitro from human pluripotent stem cells. *Nat. Biotechnol.* **32**, 1121–1133 (2014).

54. Toyoda, T. *et al.* Cell aggregation optimizes the differentiation of human ESCs and iPSCs into pancreatic bud-like progenitor cells. *Stem Cell Res.* **14**, 185–197 (2015).
55. Nir, T. & Dor, Y. How to make pancreatic beta cells--prospects for cell therapy in diabetes. *Curr. Opin. Biotechnol.* **16**, 524–529 (2005).
56. Zorn, A. M. & Wells, J. M. Vertebrate endoderm development and organ formation. *Annu. Rev. Cell Dev. Biol.* **25**, 221–251 (2009).
57. Tam, P. P. L. & Gad, J. M. Gastrulation of the mouse embryo. in *Gastrulation: From Cells to Embryo* (Cold Spring Harbor Laboratory Press, 2004).
58. Tam, P. P. L. & Loebel, D. A. F. Gene function in mouse embryogenesis: get set for gastrulation. *Nat. Rev. Genet.* **8**, 368–381 (2007).
59. Grapin-Botton, A. & Melton, D. A. Endoderm development: from patterning to organogenesis. *Trends Genet. TIG* **16**, 124–130 (2000).
60. Viotti, M., Foley, A. C. & Hadjantonakis, A.-K. Gutsy moves in mice: cellular and molecular dynamics of endoderm morphogenesis. *Philos. Trans. R. Soc. Lond. B. Biol. Sci.* **369**, (2014).
61. Bedzhov, I., Graham, S. J. L., Leung, C. Y. & Zernicka-Goetz, M. Developmental plasticity, cell fate specification and morphogenesis in the early mouse embryo. *Philos. Trans. R. Soc. Lond. B. Biol. Sci.* **369**, (2014).
62. Beddington, R. S. & Robertson, E. J. Axis development and early asymmetry in mammals. *Cell* **96**, 195–209 (1999).
63. Gardner, R. L. Origin and differentiation of extraembryonic tissues in the mouse. *Int. Rev. Exp. Pathol.* **24**, 63–133 (1983).
64. Lu, C. C., Brennan, J. & Robertson, E. J. From fertilization to gastrulation: axis formation in the mouse embryo. *Curr. Opin. Genet. Dev.* **11**, 384–392 (2001).
65. Shen, M. M. Nodal signaling: developmental roles and regulation. *Dev. Camb. Engl.* **134**, 1023–1034 (2007).
66. D'Amour, K. A. *et al.* Efficient differentiation of human embryonic stem cells to definitive endoderm. *Nat. Biotechnol.* **23**, 1534–1541 (2005).
67. Clements, D., Friday, R. V. & Woodland, H. R. Mode of action of VegT in mesoderm and endoderm formation. *Dev. Camb. Engl.* **126**, 4903–4911 (1999).
68. Green, J. B. & Smith, J. C. Graded changes in dose of a Xenopus activin A homologue elicit stepwise transitions in embryonic cell fate. *Nature* **347**, 391–394 (1990).
69. Stainier, D. Y. R. A glimpse into the molecular entrails of endoderm formation. *Genes Dev.* **16**, 893–907 (2002).

70. Arnold, S. J., Hofmann, U. K., Bikoff, E. K. & Robertson, E. J. Pivotal roles for eomesodermin during axis formation, epithelium-to-mesenchyme transition and endoderm specification in the mouse. *Dev. Camb. Engl.* **135**, 501–511 (2008).
71. Bjornson, C. R. R. *et al.* Eomesodermin is a localized maternal determinant required for endoderm induction in zebrafish. *Dev. Cell* **9**, 523–533 (2005).
72. Dufort, D., Schwartz, L., Harpal, K. & Rossant, J. The transcription factor HNF3beta is required in visceral endoderm for normal primitive streak morphogenesis. *Dev. Camb. Engl.* **125**, 3015–3025 (1998).
73. Hudson, C., Clements, D., Friday, R. V., Stott, D. & Woodland, H. R. Xsox17alpha and -beta mediate endoderm formation in Xenopus. *Cell* **91**, 397–405 (1997).
74. Kanai-Azuma, M. *et al.* Depletion of definitive gut endoderm in Sox17-null mutant mice. *Dev. Camb. Engl.* **129**, 2367–2379 (2002).
75. Lunde, K., Belting, H.-G. & Driever, W. Zebrafish pou5f1/pou2, homolog of mammalian Oct4, functions in the endoderm specification cascade. *Curr. Biol. CB* **14**, 48–55 (2004).
76. Reim, G., Mizoguchi, T., Stainier, D. Y., Kikuchi, Y. & Brand, M. The POU domain protein spg (pou2/Oct4) is essential for endoderm formation in cooperation with the HMG domain protein casanova. *Dev. Cell* **6**, 91–101 (2004).
77. Watt, A. J., Zhao, R., Li, J. & Duncan, S. A. Development of the mammalian liver and ventral pancreas is dependent on GATA4. *BMC Dev. Biol.* **7**, 37 (2007).
78. Germain, S., Howell, M., Esslemont, G. M. & Hill, C. S. Homeodomain and winged-helix transcription factors recruit activated Smads to distinct promoter elements via a common Smad interaction motif. *Genes Dev.* **14**, 435–451 (2000).
79. Hart, A. H. *et al.* Mixl1 is required for axial mesendoderm morphogenesis and patterning in the murine embryo. *Dev. Camb. Engl.* **129**, 3597–3608 (2002).
80. Tam, P. P. L. *et al.* Sequential allocation and global pattern of movement of the definitive endoderm in the mouse embryo during gastrulation. *Dev. Camb. Engl.* **134**, 251–260 (2007).
81. Latinkić, B. V. *et al.* The Xenopus Brachyury promoter is activated by FGF and low concentrations of activin and suppressed by high concentrations of activin and by paired-type homeodomain proteins. *Genes Dev.* **11**, 3265–3276 (1997).
82. Mizoguchi, T., Izawa, T., Kuroiwa, A. & Kikuchi, Y. Fgf signaling negatively regulates Nodal-dependent endoderm induction in zebrafish. *Dev. Biol.* **300**, 612–622 (2006).
83. Poulain, M., Fürthauer, M., Thisse, B., Thisse, C. & Lepage, T. Zebrafish endoderm formation is regulated by combinatorial Nodal, FGF and BMP signalling. *Dev. Camb. Engl.* **133**, 2189–2200 (2006).

84. Viotti, M., Nowotschin, S. & Hadjantonakis, A.-K. SOX17 links gut endoderm morphogenesis and germ layer segregation. *Nat. Cell Biol.* **16**, 1146–1156 (2014).
85. Franklin, V. *et al.* Regionalisation of the endoderm progenitors and morphogenesis of the gut portals of the mouse embryo. *Mech. Dev.* **125**, 587–600 (2008).
86. Lawson, K. A., Meneses, J. J. & Pedersen, R. A. Cell fate and cell lineage in the endoderm of the presomite mouse embryo, studied with an intracellular tracer. *Dev. Biol.* **115**, 325–339 (1986).
87. Grapin-Botton, A. Endoderm specification. in *StemBook* (Harvard Stem Cell Institute, 2008).
88. Wells, J. M. & Melton, D. A. Vertebrate endoderm development. *Annu. Rev. Cell Dev. Biol.* **15**, 393–410 (1999).
89. Chawengsaksophak, K., de Graaff, W., Rossant, J., Deschamps, J. & Beck, F. Cdx2 is essential for axial elongation in mouse development. *Proc. Natl. Acad. Sci. U. S. A.* **101**, 7641–7645 (2004).
90. Kinkel, M. D., Eames, S. C., Alonzo, M. R. & Prince, V. E. Cdx4 is required in the endoderm to localize the pancreas and limit beta-cell number. *Dev. Camb. Engl.* **135**, 919–929 (2008).
91. Martinez Barbera, J. P. *et al.* The homeobox gene Hex is required in definitive endodermal tissues for normal forebrain, liver and thyroid formation. *Dev. Camb. Engl.* **127**, 2433–2445 (2000).
92. Chen, Y. *et al.* Retinoic acid signaling is essential for pancreas development and promotes endocrine at the expense of exocrine cell differentiation in Xenopus. *Dev. Biol.* **271**, 144–160 (2004).
93. Kumar, M., Jordan, N., Melton, D. & Grapin-Botton, A. Signals from lateral plate mesoderm instruct endoderm toward a pancreatic fate. *Dev. Biol.* **259**, 109–122 (2003).
94. Stafford, D. & Prince, V. E. Retinoic acid signaling is required for a critical early step in zebrafish pancreatic development. *Curr. Biol. CB* **12**, 1215–1220 (2002).
95. Bayha, E., Jørgensen, M. C., Serup, P. & Grapin-Botton, A. Retinoic acid signaling organizes endodermal organ specification along the entire antero-posterior axis. *PloS One* **4**, e5845 (2009).
96. Dessimoz, J., Opoka, R., Kordich, J. J., Grapin-Botton, A. & Wells, J. M. FGF signaling is necessary for establishing gut tube domains along the anterior-posterior axis in vivo. *Mech. Dev.* **123**, 42–55 (2006).
97. Haremaki, T., Tanaka, Y., Hongo, I., Yuge, M. & Okamoto, H. Integration of multiple signal transducing pathways on Fgf response elements of the Xenopus caudal homologue Xcad3. *Dev. Camb. Engl.* **130**, 4907–4917 (2003).
98. Goessling, W. *et al.* APC mutant zebrafish uncover a changing temporal requirement for wnt signaling in liver development. *Dev. Biol.* **320**, 161–174 (2008).

99. McLin, V. A., Rankin, S. A. & Zorn, A. M. Repression of Wnt/beta-catenin signaling in the anterior endoderm is essential for liver and pancreas development. *Dev. Camb. Engl.* **134**, 2207–2217 (2007).
100. Wills, A., Dickinson, K., Khokha, M. & Baker, J. C. Bmp signaling is necessary and sufficient for ventrolateral endoderm specification in Xenopus. *Dev. Dyn. Off. Publ. Am. Assoc. Anat.* **237**, 2177–2186 (2008).
101. Tiso, N., Filippi, A., Pauls, S., Bortolussi, M. & Argenton, F. BMP signalling regulates anteroposterior endoderm patterning in zebrafish. *Mech. Dev.* **118**, 29–37 (2002).
102. Li, Y. *et al.* Sfrp5 coordinates foregut specification and morphogenesis by antagonizing both canonical and noncanonical Wnt11 signaling. *Genes Dev.* **22**, 3050–3063 (2008).
103. Ho, C. Y., Houart, C., Wilson, S. W. & Stainier, D. Y. A role for the extraembryonic yolk syncytial layer in patterning the zebrafish embryo suggested by properties of the hex gene. *Curr. Biol. CB* **9**, 1131–1134 (1999).
104. Zorn, A. M., Butler, K. & Gurdon, J. B. Anterior endomesoderm specification in Xenopus by Wnt/beta-catenin and TGF-beta signalling pathways. *Dev. Biol.* **209**, 282–297 (1999).
105. Thomas, P. Q., Brown, A. & Beddington, R. S. Hex: a homeobox gene revealing peri-implantation asymmetry in the mouse embryo and an early transient marker of endothelial cell precursors. *Dev. Camb. Engl.* **125**, 85–94 (1998).
106. Sherwood, R. I., Chen, T.-Y. A. & Melton, D. A. Transcriptional dynamics of endodermal organ formation. *Dev. Dyn. Off. Publ. Am. Assoc. Anat.* **238**, 29–42 (2009).
107. Horb, M. E. Patterning the endoderm: the importance of neighbours. *BioEssays News Rev. Mol. Cell. Dev. Biol.* **22**, 599–602 (2000).
108. Horb, M. E. & Slack, J. M. Endoderm specification and differentiation in Xenopus embryos. *Dev. Biol.* **236**, 330–343 (2001).
109. Kimura, W., Yasugi, S., Stern, C. D. & Fukuda, K. Fate and plasticity of the endoderm in the early chick embryo. *Dev. Biol.* **289**, 283–295 (2006).
110. Kimura, W., Yasugi, S. & Fukuda, K. Regional specification of the endoderm in the early chick embryo. *Dev. Growth Differ.* **49**, 365–372 (2007).
111. Jung, J., Zheng, M., Goldfarb, M. & Zaret, K. S. Initiation of mammalian liver development from endoderm by fibroblast growth factors. *Science* **284**, 1998–2003 (1999).
112. Jørgensen, M. C. *et al.* An illustrated review of early pancreas development in the mouse. *Endocr. Rev.* **28**, 685–705 (2007).

113. Bort, R., Martinez-Barbera, J. P., Beddington, R. S. P. & Zaret, K. S. Hex homeobox gene-dependent tissue positioning is required for organogenesis of the ventral pancreas. *Dev. Camb. Engl.* **131**, 797–806 (2004).
114. Orci, L. Macro- and micro-domains in the endocrine pancreas. *Diabetes* **31**, 538–565 (1982).
115. Kim, S. K., Hebrok, M. & Melton, D. A. Notochord to endoderm signaling is required for pancreas development. *Dev. Camb. Engl.* **124**, 4243–4252 (1997).
116. Kim, S. K. & Hebrok, M. Intercellular signals regulating pancreas development and function. *Genes Dev.* **15**, 111–127 (2001).
117. Hebrok, M., Kim, S. K., St Jacques, B., McMahon, A. P. & Melton, D. A. Regulation of pancreas development by hedgehog signaling. *Dev. Camb. Engl.* **127**, 4905–4913 (2000).
118. Molotkov, A., Molotkova, N. & Duester, G. Retinoic acid generated by Raldh2 in mesoderm is required for mouse dorsal endodermal pancreas development. *Dev. Dyn. Off. Publ. Am. Assoc. Anat.* **232**, 950–957 (2005).
119. Wang, Z., Dollé, P., Cardoso, W. V. & Niederreither, K. Retinoic acid regulates morphogenesis and patterning of posterior foregut derivatives. *Dev. Biol.* **297**, 433–445 (2006).
120. Duester, G. Retinoic acid synthesis and signaling during early organogenesis. *Cell* **134**, 921–931 (2008).
121. Calmont, A. *et al.* An FGF response pathway that mediates hepatic gene induction in embryonic endoderm cells. *Dev. Cell* **11**, 339–348 (2006).
122. Serls, A. E., Doherty, S., Parvatiyar, P., Wells, J. M. & Deutsch, G. H. Different thresholds of fibroblast growth factors pattern the ventral foregut into liver and lung. *Dev. Camb. Engl.* **132**, 35–47 (2005).
123. Zorn, A. M. Liver development. in *StemBook* (Harvard Stem Cell Institute, 2008).
124. Ober, E. A., Field, H. A. & Stainier, D. Y. R. From endoderm formation to liver and pancreas development in zebrafish. *Mech. Dev.* **120**, 5–18 (2003).
125. Gualdi, R. *et al.* Hepatic specification of the gut endoderm in vitro: cell signaling and transcriptional control. *Genes Dev.* **10**, 1670–1682 (1996).
126. Burke, Z. & Oliver, G. Prox1 is an early specific marker for the developing liver and pancreas in the mammalian foregut endoderm. *Mech. Dev.* **118**, 147–155 (2002).
127. Sosa-Pineda, B., Wigle, J. T. & Oliver, G. Hepatocyte migration during liver development requires Prox1. *Nat. Genet.* **25**, 254–255 (2000).
128. Wang, J. *et al.* Prox1 activity controls pancreas morphogenesis and participates in the production of 'secondary transition' pancreatic endocrine cells. *Dev. Biol.* **286**, 182–194 (2005).

129. Kumar, M. & Melton, D. Pancreas specification: a budding question. *Curr. Opin. Genet. Dev.* **13**, 401–407 (2003).
130. Duncan, S. A. Mechanisms controlling early development of the liver. *Mech. Dev.* **120**, 19–33 (2003).
131. Margagliotti, S. *et al.* Role of metalloproteinases at the onset of liver development. *Dev. Growth Differ.* **50**, 331–338 (2008).
132. Margagliotti, S. *et al.* The Onecut transcription factors HNF-6/OC-1 and OC-2 regulate early liver expansion by controlling hepatoblast migration. *Dev. Biol.* **311**, 579–589 (2007).
133. Papoutsi, M. *et al.* Gene regulation by homeobox transcription factor Prox1 in murine hepatoblasts. *Cell Tissue Res.* **330**, 209–220 (2007).
134. Matsumoto, K., Yoshitomi, H., Rossant, J. & Zaret, K. S. Liver organogenesis promoted by endothelial cells prior to vascular function. *Science* **294**, 559–563 (2001).
135. Jacquemin, P. *et al.* An endothelial-mesenchymal relay pathway regulates early phases of pancreas development. *Dev. Biol.* **290**, 189–199 (2006).
136. Lammert, E., Cleaver, O. & Melton, D. Induction of pancreatic differentiation by signals from blood vessels. *Science* **294**, 564–567 (2001).
137. Yoshitomi, H. & Zaret, K. S. Endothelial cell interactions initiate dorsal pancreas development by selectively inducing the transcription factor Ptf1a. *Dev. Camb. Engl.* **131**, 807–817 (2004).
138. Offield, M. F. *et al.* PDX-1 is required for pancreatic outgrowth and differentiation of the rostral duodenum. *Dev. Camb. Engl.* **122**, 983–995 (1996).
139. Guz, Y. *et al.* Expression of murine STF-1, a putative insulin gene transcription factor, in beta cells of pancreas, duodenal epithelium and pancreatic exocrine and endocrine progenitors during ontogeny. *Dev. Camb. Engl.* **121**, 11–18 (1995).
140. Jonsson, J., Carlsson, L., Edlund, T. & Edlund, H. Insulin-promoter-factor 1 is required for pancreas development in mice. *Nature* **371**, 606–609 (1994).
141. Wessells, N. K. & Cohen, J. H. Early Pancreas Organogenesis: Morphogenesis, Tissue Interactions, and Mass Effects. *Dev. Biol.* **15**, 237–270 (1967).
142. Burlison, J. S., Long, Q., Fujitani, Y., Wright, C. V. E. & Magnuson, M. A. Pdx-1 and Ptf1a concurrently determine fate specification of pancreatic multipotent progenitor cells. *Dev. Biol.* **316**, 74–86 (2008).
143. Krapp, A. *et al.* The bHLH protein PTF1-p48 is essential for the formation of the exocrine and the correct spatial organization of the endocrine pancreas. *Genes Dev.* **12**, 3752–3763 (1998).
144. Golosow, N. & Grobstein, C. Epitheliomesenchymal interaction in pancreatic morphogenesis. *Dev. Biol.* **4**, 242–255 (1962).

145. Bhushan, A. *et al.* Fgf10 is essential for maintaining the proliferative capacity of epithelial progenitor cells during early pancreatic organogenesis. *Dev. Camb. Engl.* **128**, 5109–5117 (2001).
146. Dong, P. D. S. *et al.* Fgf10 regulates hepatopancreatic ductal system patterning and differentiation. *Nat. Genet.* **39**, 397–402 (2007).
147. Rodríguez-Seguel, E. *et al.* Mutually exclusive signaling signatures define the hepatic and pancreatic progenitor cell lineage divergence. *Genes Dev.* **27**, 1932–1946 (2013).
148. Escot, S., Willnow, D., Naumann, H., Di Francescantonio, S. & Spagnoli, F. M. Robo signalling controls pancreatic progenitor identity by regulating Tead transcription factors. *Nat. Commun.* **9**, 5082 (2018).
149. Zaret, K. S. Genetic programming of liver and pancreas progenitors: lessons for stem-cell differentiation. *Nat. Rev. Genet.* **9**, 329–340 (2008).
150. Spence, J. R. *et al.* Sox17 regulates organ lineage segregation of ventral foregut progenitor cells. *Dev. Cell* **17**, 62–74 (2009).
151. Uemura, M. *et al.* Expression and function of mouse Sox17 gene in the specification of gallbladder/bile-duct progenitors during early foregut morphogenesis. *Biochem. Biophys. Res. Commun.* **391**, 357–363 (2010).
152. Weinstein, M. *et al.* Smad proteins and hepatocyte growth factor control parallel regulatory pathways that converge on beta1-integrin to promote normal liver development. *Mol. Cell. Biol.* **21**, 5122–5131 (2001).
153. Suksaweang, S. *et al.* Morphogenesis of chicken liver: identification of localized growth zones and the role of beta-catenin/Wnt in size regulation. *Dev. Biol.* **266**, 109–122 (2004).
154. Monga, S. P. S. *et al.* Beta-catenin antisense studies in embryonic liver cultures: role in proliferation, apoptosis, and lineage specification. *Gastroenterology* **124**, 202–216 (2003).
155. Micsenyi, A. *et al.* Beta-catenin is temporally regulated during normal liver development. *Gastroenterology* **126**, 1134–1146 (2004).
156. Michalopoulos, G. K., Bowen, W., Nussler, A. K., Becich, M. J. & Howard, T. A. Comparative analysis of mitogenic and morphogenic effects of HGF and EGF on rat and human hepatocytes maintained in collagen gels. *J. Cell. Physiol.* **156**, 443–452 (1993).
157. Sergi, C., Kahl, P. & Otto, H. F. Contribution of Apoptosis and Apoptosis-Related Proteins to the Malformation of the Primitive Intrahepatic Biliary System in Meckel Syndrome. *Am. J. Pathol.* **156**, 1589–1598 (2000).
158. Clotman, F. *et al.* Control of liver cell fate decision by a gradient of TGF beta signaling modulated by Onecut transcription factors. *Genes Dev.* **19**, 1849–1854 (2005).

159. Clotman, F. & Lemaigre, F. P. Control of hepatic differentiation by activin/TGFbeta signaling. *Cell Cycle Georget. Tex* **5**, 168–171 (2006).
160. Tan, X. *et al.* Beta-catenin deletion in hepatoblasts disrupts hepatic morphogenesis and survival during mouse development. *Hepatol. Baltim. Md* **47**, 1667–1679 (2008).
161. Piper, K. *et al.* Novel SOX9 expression during human pancreas development correlates to abnormalities in Campomelic dysplasia. *Mech. Dev.* **116**, 223–226 (2002).
162. Lioubinski, O., Müller, M., Wegner, M. & Sander, M. Expression of Sox transcription factors in the developing mouse pancreas. *Dev. Dyn. Off. Publ. Am. Assoc. Anat.* **227**, 402–408 (2003).
163. Lee, Y.-H. & Saint-Jeannet, J.-P. Sox9, a novel pancreatic marker in Xenopus. *Int. J. Dev. Biol.* **47**, 459–462 (2003).
164. Akiyama, H. *et al.* Osteo-chondroprogenitor cells are derived from Sox9 expressing precursors. *Proc. Natl. Acad. Sci. U. S. A.* **102**, 14665–14670 (2005).
165. Sussel, L. *et al.* Mice lacking the homeodomain transcription factor Nkx2.2 have diabetes due to arrested differentiation of pancreatic beta cells. *Dev. Camb. Engl.* **125**, 2213–2221 (1998).
166. Chiang, M.-K. & Melton, D. A. Single-cell transcript analysis of pancreas development. *Dev. Cell* **4**, 383–393 (2003).
167. Sander, M. *et al.* Homeobox gene Nkx6.1 lies downstream of Nkx2.2 in the major pathway of beta-cell formation in the pancreas. *Dev. Camb. Engl.* **127**, 5533–5540 (2000).
168. Oster, A., Jensen, J., Edlund, H. & Larsson, L. I. Homeobox gene product Nkx 6.1 immunoreactivity in nuclei of endocrine cells of rat and mouse stomach. *J. Histochem. Cytochem. Off. J. Histochem. Soc.* **46**, 717–721 (1998).
169. Oster, A. *et al.* Rat endocrine pancreatic development in relation to two homeobox gene products (Pdx-1 and Nkx 6.1). *J. Histochem. Cytochem. Off. J. Histochem. Soc.* **46**, 707–715 (1998).
170. Henseleit, K. D. *et al.* NKX6 transcription factor activity is required for alpha- and beta-cell development in the pancreas. *Dev. Camb. Engl.* **132**, 3139–3149 (2005).
171. Pedersen, J. K. *et al.* Endodermal expression of Nkx6 genes depends differentially on Pdx1. *Dev. Biol.* **288**, 487–501 (2005).
172. Villasenor, A., Chong, D. C., Henkemeyer, M. & Cleaver, O. Epithelial dynamics of pancreatic branching morphogenesis. *Dev. Camb. Engl.* **137**, 4295–4305 (2010).
173. Petzold, K. M., Naumann, H. & Spagnoli, F. M. Rho signalling restriction by the RhoGAP Stard13 integrates growth and morphogenesis in the pancreas. *Dev. Camb. Engl.* **140**, 126–135 (2013).
174. Kesavan, G. *et al.* Cdc42-mediated tubulogenesis controls cell specification. *Cell* **139**, 791–801 (2009).

175. Landsman, L. *et al.* Pancreatic Mesenchyme Regulates Epithelial Organogenesis throughout Development. *PLoS Biol.* **9**, (2011).
176. Hibsher, D., Epshtein, A., Oren, N. & Landsman, L. Pancreatic Mesenchyme Regulates Islet Cellular Composition in a Patched/Hedgehog-Dependent Manner. *Sci. Rep.* **6**, 38008 (2016).
177. Guo, T., Landsman, L., Li, N. & Hebrok, M. Factors Expressed by Murine Embryonic Pancreatic Mesenchyme Enhance Generation of Insulin-Producing Cells From hESCs. *Diabetes* **62**, 1581–1592 (2013).
178. Miki, R. *et al.* Fate maps of ventral and dorsal pancreatic progenitor cells in early somite stage mouse embryos. *Mech. Dev.* **128**, 597–609 (2012).
179. Blanpain, C. & Simons, B. D. Unravelling stem cell dynamics by lineage tracing. *Nat. Rev. Mol. Cell Biol.* **14**, 489–502 (2013).
180. Kretzschmar, K. & Watt, F. M. Lineage tracing. *Cell* **148**, 33–45 (2012).
181. Buckingham, M. E. & Meilhac, S. M. Tracing cells for tracking cell lineage and clonal behavior. *Dev. Cell* **21**, 394–409 (2011).
182. Srinivas, S. *et al.* Cre reporter strains produced by targeted insertion of EYFP and ECFP into the ROSA26 locus. *BMC Dev. Biol.* **1**, 4 (2001).
183. Abe, T. *et al.* Establishment of conditional reporter mouse lines at ROSA26 locus for live cell imaging. *Genes. N. Y. N 2000* **49**, 579–590 (2011).
184. Snippert, H. J. *et al.* Intestinal crypt homeostasis results from neutral competition between symmetrically dividing Lgr5 stem cells. *Cell* **143**, 134–144 (2010).
185. Kumar, M. E. *et al.* Defining a mesenchymal progenitor niche at single cell resolution. *Science* **346**, 1258810 (2014).
186. Rios, A. C., Fu, N. Y., Lindeman, G. J. & Visvader, J. E. In situ identification of bipotent stem cells in the mammary gland. *Nature* **506**, 322–327 (2014).
187. Heintz, N. Gene expression nervous system atlas (GENSAT). *Nat. Neurosci.* **7**, 483 (2004).
188. Gong, S. *et al.* A gene expression atlas of the central nervous system based on bacterial artificial chromosomes. *Nature* **425**, 917–925 (2003).
189. Gong, S., Yang, X. W., Li, C. & Heintz, N. Highly efficient modification of bacterial artificial chromosomes (BACs) using novel shuttle vectors containing the R6Kgamma origin of replication. *Genome Res.* **12**, 1992–1998 (2002).
190. Long, H. *et al.* Conserved roles for Slit and Robo proteins in midline commissural axon guidance. *Neuron* **42**, 213–223 (2004).
191. Grieshammer, U. *et al.* SLIT2-mediated ROBO2 signaling restricts kidney induction to a single site. *Dev. Cell* **6**, 709–717 (2004).

192. Theiler, K. *The House Mouse: Atlas of Embryonic Development.* (Springer-Verlag, 1989).
193. Downs, K. M. & Davies, T. Staging of gastrulating mouse embryos by morphological landmarks in the dissecting microscope. *Dev. Camb. Engl.* **118**, 1255–1266 (1993).
194. Geyer, S. H. *et al.* A staging system for correct phenotype interpretation of mouse embryos harvested on embryonic day 14 (E14.5). *J. Anat.* **230**, 710–719 (2017).
195. Hama, H. *et al.* Scale: a chemical approach for fluorescence imaging and reconstruction of transparent mouse brain. *Nat. Neurosci.* **14**, 1481–1488 (2011).
196. Preibisch, S., Saalfeld, S. & Tomancak, P. Globally optimal stitching of tiled 3D microscopic image acquisitions. *Bioinformatics* **25**, 1463–1465 (2009).
197. Husson, F., Josse, J. & Pagès, J. Principal component methods-hierarchical clustering-partitional clustering : why would we need to choose for visualizing data ? in (2010).
198. (PDF) A Review of Clustering Techniques and Developments. *ResearchGate* doi:http://dx.doi.org/10.1016/j.neucom.2017.06.053
199. Park, E. J. *et al.* System for tamoxifen-inducible expression of cre-recombinase from the Foxa2 locus in mice. *Dev. Dyn. Off. Publ. Am. Assoc. Anat.* **237**, 447–453 (2008).
200. Pourquié, O. Vertebrate somitogenesis. *Annu. Rev. Cell Dev. Biol.* **17**, 311–350 (2001).
201. Saga, Y. & Takeda, H. The making of the somite: molecular events in vertebrate segmentation. *Nat. Rev. Genet.* **2**, 835–845 (2001).
202. Tam, P. P. The control of somitogenesis in mouse embryos. *J. Embryol. Exp. Morphol.* **65 Suppl**, 103–128 (1981).
203. Sanders, E. J., Varedi, M. & French, A. S. Cell proliferation in the gastrulating chick embryo: a study using BrdU incorporation and PCNA localization. *Dev. Camb. Engl.* **118**, 389–399 (1993).
204. van den Berg, G. *et al.* A caudal proliferating growth center contributes to both poles of the forming heart tube. *Circ. Res.* **104**, 179–188 (2009).
205. Perl, A.-K. T., Wert, S. E., Nagy, A., Lobe, C. G. & Whitsett, J. A. Early restriction of peripheral and proximal cell lineages during formation of the lung. *Proc. Natl. Acad. Sci. U. S. A.* **99**, 10482–10487 (2002).
206. Jenny, M. *et al.* Neurogenin3 is differentially required for endocrine cell fate specification in the intestinal and gastric epithelium. *EMBO J.* **21**, 6338–6347 (2002).
207. Kim, T.-H. & Shivdasani, R. A. Stomach development, stem cells and disease. *Dev. Camb. Engl.* **143**, 554–565 (2016).
208. Solcia, E., Rindi, G., Buffa, R., Fiocca, R. & Capella, C. Gastric endocrine cells: types, function and growth. *Regul. Pept.* **93**, 31–35 (2000).
209. Richardson, D. S. & Lichtman, J. W. Clarifying Tissue Clearing. *Cell* **162**, 246–257 (2015).

210. Benninger, R. K. P. & Piston, D. W. Two-Photon Excitation Microscopy for the Study of Living Cells and Tissues. *Curr. Protoc. Cell Biol. Editor. Board Juan Bonifacino Al* **0 4**, Unit-4.1124 (2013).
211. Lescroart, F. *et al.* Early lineage restriction in temporally distinct populations of Mesp1 progenitors during mammalian heart development. *Nat. Cell Biol.* **16**, 829–840 (2014).
212. Hingorani, S. R. *et al.* Preinvasive and invasive ductal pancreatic cancer and its early detection in the mouse. *Cancer Cell* **4**, 437–450 (2003).
213. Blockus, H. & Chédotal, A. Slit-Robo signaling. *Development* **143**, 3037–3044 (2016).
214. Brose, K. & Tessier-Lavigne, M. Slit proteins: key regulators of axon guidance, axonal branching, and cell migration. *Curr. Opin. Neurobiol.* **10**, 95–102 (2000).
215. Vogler, G. & Bodmer, R. Cellular Mechanisms of Drosophila Heart Morphogenesis. *J. Cardiovasc. Dev. Dis.* **2**, 2–16 (2015).
216. Mommersteeg, M. T. M., Yeh, M. L., Parnavelas, J. G. & Andrews, W. D. Disrupted Slit-Robo signalling results in membranous ventricular septum defects and bicuspid aortic valves. *Cardiovasc. Res.* **106**, 55–66 (2015).
217. Mommersteeg, M. T. M. *et al.* Slit-roundabout signaling regulates the development of the cardiac systemic venous return and pericardium. *Circ. Res.* **112**, 465–475 (2013).
218. Zhao, J. & Mommersteeg, M. T. M. Slit–Robo signalling in heart development. *Cardiovasc. Res.* **114**, 794–804 (2018).
219. Strickland, P., Shin, G. C., Plump, A., Tessier-Lavigne, M. & Hinck, L. Slit2 and netrin 1 act synergistically as adhesive cues to generate tubular bi-layers during ductal morphogenesis. *Dev. Camb. Engl.* **133**, 823–832 (2006).
220. Macias, H. *et al.* SLIT/ROBO1 signaling suppresses mammary branching morphogenesis by limiting basal cell number. *Dev. Cell* **20**, 827–840 (2011).
221. Fukuda, A. *et al.* Ectopic pancreas formation in Hes1 -knockout mice reveals plasticity of endodermal progenitors of the gut, bile duct, and pancreas. *J. Clin. Invest.* **116**, 1484–1493 (2006).
222. Sumazaki, R. *et al.* Conversion of biliary system to pancreatic tissue in Hes1-deficient mice. *Nat. Genet.* **36**, 83–87 (2004).
223. Jensen, J. *et al.* Control of endodermal endocrine development by Hes-1. *Nat. Genet.* **24**, 36–44 (2000).
224. Turque, N., Plaza, S., Radvanyi, F., Carriere, C. & Saule, S. Pax-QNR/Pax-6, a paired box- and homeobox-containing gene expressed in neurons, is also expressed in pancreatic endocrine cells. *Mol. Endocrinol. Baltim. Md* **8**, 929–938 (1994).

225. Jensen, J. *et al.* Independent development of pancreatic alpha- and beta-cells from neurogenin3-expressing precursors: a role for the notch pathway in repression of premature differentiation. *Diabetes* **49**, 163–176 (2000).
226. Kim, S. K. *et al.* Pbx1 inactivation disrupts pancreas development and in Ipf1-deficient mice promotes diabetes mellitus. *Nat. Genet.* **30**, 430–435 (2002).
227. Grapin-Botton, A., Majithia, A. R. & Melton, D. A. Key events of pancreas formation are triggered in gut endoderm by ectopic expression of pancreatic regulatory genes. *Genes Dev.* **15**, 444–454 (2001).
228. Larsen, H. L. *et al.* Stochastic priming and spatial cues orchestrate heterogeneous clonal contribution to mouse pancreas organogenesis. *Nat. Commun.* **8**, 605 (2017).
229. Li, L.-C. *et al.* Single-cell transcriptomic analyses reveal distinct dorsal/ventral pancreatic programs. *EMBO Rep.* (2018). doi:10.15252/embr.201846148
230. Iwafuchi-Doi, M. & Zaret, K. S. Cell fate control by pioneer transcription factors. *Dev. Camb. Engl.* **143**, 1833–1837 (2016).
231. Mayran, A. & Drouin, J. Pioneer transcription factors shape the epigenetic landscape. *J. Biol. Chem.* **293**, 13795–13804 (2018).
232. Zaret, K. S., Lerner, J. & Iwafuchi-Doi, M. Chromatin Scanning by Dynamic Binding of Pioneer Factors. *Mol. Cell* **62**, 665–667 (2016).
233. Ariyachet, C. *et al.* Reprogrammed Stomach Tissue as a Renewable Source of Functional β Cells for Blood Glucose Regulation. *Cell Stem Cell* **18**, 410–421 (2016).
234. Kim, S. K. & Melton, D. A. Pancreas development is promoted by cyclopamine, a hedgehog signaling inhibitor. *Proc. Natl. Acad. Sci. U. S. A.* **95**, 13036–13041 (1998).
235. Hebrok, M. Hedgehog signaling in pancreas development. *Mech. Dev.* **120**, 45–57 (2003).
236. Hebrok, M., Kim, S. K. & Melton, D. A. Notochord repression of endodermal Sonic hedgehog permits pancreas development. *Genes Dev.* **12**, 1705–1713 (1998).
237. Litingtung, Y., Lei, L., Westphal, H. & Chiang, C. Sonic hedgehog is essential to foregut development. *Nat. Genet.* **20**, 58–61 (1998).
238. Ritsma, L. *et al.* Intestinal crypt homeostasis revealed at single-stem-cell level by in vivo live imaging. *Nature* **507**, 362–365 (2014).
239. Clevers, H. The Intestinal Crypt, A Prototype Stem Cell Compartment. *Cell* **154**, 274–284 (2013).
240. Friedl, P. & Gilmour, D. Collective cell migration in morphogenesis, regeneration and cancer. *Nat. Rev. Mol. Cell Biol.* **10**, 445–457 (2009).
241. Haeger, A., Wolf, K., Zegers, M. M. & Friedl, P. Collective cell migration: guidance principles and hierarchies. *Trends Cell Biol.* **25**, 556–566 (2015).

242. Caussinus, E., Colombelli, J. & Affolter, M. Tip-cell migration controls stalk-cell intercalation during Drosophila tracheal tube elongation. *Curr. Biol. CB* **18**, 1727–1734 (2008).
243. Ribeiro, C., Ebner, A. & Affolter, M. In vivo imaging reveals different cellular functions for FGF and Dpp signaling in tracheal branching morphogenesis. *Dev. Cell* **2**, 677–683 (2002).
244. Clavería, C., Giovinazzo, G., Sierra, R. & Torres, M. Myc-driven endogenous cell competition in the early mammalian embryo. *Nature* **500**, 39–44 (2013).
245. Díaz-Díaz, C. *et al.* Pluripotency Surveillance by Myc-Driven Competitive Elimination of Differentiating Cells. *Dev. Cell* **42**, 585-599.e4 (2017).
246. Hunter, M. P. *et al.* The homeobox gene Hhex is essential for proper hepatoblast differentiation and bile duct morphogenesis. *Dev. Biol.* **308**, 355–367 (2007).
247. Coffinier, C. *et al.* Bile system morphogenesis defects and liver dysfunction upon targeted deletion of HNF1beta. *Dev. Camb. Engl.* **129**, 1829–1838 (2002).
248. Clotman, F. *et al.* The onecut transcription factor HNF6 is required for normal development of the biliary tract. *Dev. Camb. Engl.* **129**, 1819–1828 (2002).
249. Martínez-Frías, M. L. *et al.* Tracheoesophageal fistula, gastrointestinal abnormalities, hypospadias, and prenatal growth deficiency. *Am. J. Med. Genet.* **44**, 352–355 (1992).
250. Mitchell, J. *et al.* Neonatal diabetes, with hypoplastic pancreas, intestinal atresia and gall bladder hypoplasia: search for the aetiology of a new autosomal recessive syndrome. *Diabetologia* **47**, 2160–2167 (2004).
251. Ashraf, A., Abdullatif, H., Hardin, W. & Moates, J. M. Unusual case of neonatal diabetes mellitus due to congenital pancreas agenesis. *Pediatr. Diabetes* **6**, 239–243 (2005).
252. Chappell, L. *et al.* A further example of a distinctive autosomal recessive syndrome comprising neonatal diabetes mellitus, intestinal atresias and gall bladder agenesis. *Am. J. Med. Genet. A.* **146A**, 1713–1717 (2008).
253. Galán-Gómez, E., Sánchez, E. B., Arias-Castro, S. & Cardesa-García, J. J. Intrauterine growth retardation, duodenal and extrahepatic biliary atresia, hypoplastic pancreas and other intestinal anomalies: further evidence of the Martínez-Frías syndrome. *Eur. J. Med. Genet.* **50**, 144–148 (2007).
254. Heij, H. A. & Niessen, G. J. Annular pancreas associated with congenital absence of the gallbladder. *J. Pediatr. Surg.* **22**, 1033 (1987).
255. Martinoli, S., Schmitt, H. E. & Allgöwer, M. [An unusual triad: gall bladder agenesis, annular pancreas and portal anomaly]. *Helv. Chir. Acta* **46**, 767–770 (1980).
256. Kelly, R. G. The second heart field. *Curr. Top. Dev. Biol.* **100**, 33–65 (2012).

257. Blanpain, C. & Fuchs, E. Epidermal Stem Cells of the Skin. *Annu. Rev. Cell Dev. Biol.* **22**, 339–373 (2006).
258. Visvader, J. E. & Stingl, J. Mammary stem cells and the differentiation hierarchy: current status and perspectives. *Genes Dev.* **28**, 1143–1158 (2014).
259. Thorgeirsson, S. S. Hepatic stem cells in liver regeneration. *FASEB J. Off. Publ. Fed. Am. Soc. Exp. Biol.* **10**, 1249–1256 (1996).
260. Rezania, A. *et al.* Maturation of human embryonic stem cell-derived pancreatic progenitors into functional islets capable of treating pre-existing diabetes in mice. *Diabetes* **61**, 2016–2029 (2012).
261. Kroon, E. *et al.* Pancreatic endoderm derived from human embryonic stem cells generates glucose-responsive insulin-secreting cells in vivo. *Nat. Biotechnol.* **26**, 443–452 (2008).
262. Pagliuca, F. W. *et al.* Generation of functional human pancreatic β cells in vitro. *Cell* **159**, 428–439 (2014).
263. Maehr, R. *et al.* Generation of pluripotent stem cells from patients with type 1 diabetes. *Proc. Natl. Acad. Sci. U. S. A.* **106**, 15768–15773 (2009).
264. Loh, K. M. *et al.* Efficient endoderm induction from human pluripotent stem cells by logically directing signals controlling lineage bifurcations. *Cell Stem Cell* **14**, 237–252 (2014).
265. Collombat, P. *et al.* The ectopic expression of Pax4 in the mouse pancreas converts progenitor cells into alpha and subsequently beta cells. *Cell* **138**, 449–462 (2009).
266. Thorel, F. *et al.* Conversion of adult pancreatic alpha-cells to beta-cells after extreme beta-cell loss. *Nature* **464**, 1149–1154 (2010).
267. Baeyens, L. *et al.* Transient cytokine treatment induces acinar cell reprogramming and regenerates functional beta cell mass in diabetic mice. *Nat. Biotechnol.* **32**, 76–83 (2014).
268. Zhou, Q., Brown, J., Kanarek, A., Rajagopal, J. & Melton, D. A. In vivo reprogramming of adult pancreatic exocrine cells to beta-cells. *Nature* **455**, 627–632 (2008).
269. Heinrich, C., Spagnoli, F. M. & Berninger, B. In vivo reprogramming for tissue repair. *Nat. Cell Biol.* **17**, 204–211 (2015).
270. Akinci, E. *et al.* Reprogramming of various cell types to a beta-like state by Pdx1, Ngn3 and MafA. *PloS One* **8**, e82424 (2013).
271. Yang, Y., Akinci, E., Dutton, J. R., Banga, A. & Slack, J. M. W. Stage specific reprogramming of mouse embryo liver cells to a beta cell-like phenotype. *Mech. Dev.* **130**, 602–612 (2013).
272. Banga, A., Akinci, E., Greder, L. V., Dutton, J. R. & Slack, J. M. W. In vivo reprogramming of Sox9+ cells in the liver to insulin-secreting ducts. *Proc. Natl. Acad. Sci. U. S. A.* **109**, 15336–15341 (2012).
273. Ferber, S. *et al.* Pancreatic and duodenal homeobox gene 1 induces expression of insulin genes in liver and ameliorates streptozotocin-induced hyperglycemia. *Nat. Med.* **6**, 568–572 (2000).

274. Wang, A. Y., Ehrhardt, A., Xu, H. & Kay, M. A. Adenovirus transduction is required for the correction of diabetes using Pdx-1 or Neurogenin-3 in the liver. *Mol. Ther. J. Am. Soc. Gene Ther.* **15**, 255–263 (2007).

7. Publications

Escot, S., Willnow, D., Naumann, H., Di Francescantonio, S. & Spagnoli, F. M. Robo signalling controls pancreatic progenitor identity by regulating Tead transcription factors. *Nat. Commun.* **9**, 5082 (2018).

8. Acknowledgements

Firstly, I would like to thank my supervisor Dr. Francesca M. Spagnoli for giving me the opportunity to work in her laboratory on this exciting project. I would like to express my immense gratitude for her constant support, advice, and commitment to my work.

I would like to thank Prof. Dr. Köhrle for his critical evaluation of this thesis document as well as for his advice during my PhD committee meetings. I also wish to thank Dr. Niccolo Zampieri for his evaluation of my work during my PhD committee meetings.

I wish to thank the Berlin Institute of Health that provided funding for my PhD thesis work. Additionally, I wish to thank the TransCard PhD program for giving me the opportunity to present and discuss my work in seminars and for providing funding for me to attend international conferences.

I would like to thank my collaboration partners Dr. Uwe Benary and Dr. Jana Wolf for the stimulating scientific discussions and the exciting possibility to jointly generate a mathematical model of hepato-pancreatic development.

I wish to express my gratitude to Anca Margineanu for her guidance during establishing multicolor reporter imaging and for her valuable scientific input into data acquisition and processing.

I want to thank the entire Spagnoli laboratory, present and past members in Berlin and London, for the wonderful experience of working with such dedicated researchers and of enjoing this unique collegial working environment. I would like to specifically thank Sophie Escot for her mentorship during my Master's thesis and the great opportunity to work together on the Robo-Slit project.

Last but not least, I want to thank my family. Without their support and affection my work would not have been possible.